General Disclaimer

One or more of the Following Statements may affect this Document

- This document has been reproduced from the best copy furnished by the organizational source. It is being released in the interest of making available as much information as possible.

- This document may contain data, which exceeds the sheet parameters. It was furnished in this condition by the organizational source and is the best copy available.

- This document may contain tone-on-tone or color graphs, charts and/or pictures, which have been reproduced in black and white.

- This document is paginated as submitted by the original source.

- Portions of this document are not fully legible due to the historical nature of some of the material. However, it is the best reproduction available from the original submission.

THERMAL ANALYSIS OF THE VERTICAL BRIDGMAN SEMICONDUCTOR CRYSTAL GROWTH TECHNIQUE

by

THOMAS JOHN JASINSKI

S.M. in Mechanical Engineering
Massachusetts Institute of Technology (1978)

B.S. in Mechanical Engineering
University of Detroit (1975)

SUBMITTED TO THE DEPARTMENT OF MECHANICAL ENGINEERING
IN PARTIAL FULFILLMENT OF THE REQUIREMENTS
FOR THE DEGREE OF

DOCTOR OF PHILOSOPHY IN
MECHANICAL ENGINEERING

at the

MASSACHUSETTS INSTITUTE OF TECHNOLOGY

December 1982

Signature of Author _____
Department of Mechanical Engineering
December 22, 1982

Certified by _____
Warren M. Rohsenow
Thesis Supervisor

Accepted by _____
Warren M. Rohsenow
Chairman, Departmental Graduate Committee

THERMAL ANALYSIS OF THE VERTICAL BRIDGMAN SEMICONDUCTOR CRYSTAL GROWTH TECHNIQUE

by

THOMAS JOHN JASINSKI

Submitted to the Department of Mechanical Engineering on December 22, 1982, in partial fulfillment of the requirements for the degree of Doctor of Philosophy in Mechanical Engineering.

ABSTRACT

The quality of semiconductor crystals grown by the vertical Bridgman technique is strongly influenced by the axial and radial variations of temperature within the charge. The present work examines the relationship between the thermal parameters of the vertical Bridgman system and the thermal behavior of the charge.

Thermal models are developed which are capable of producing results expressable in analytical form and which can be used without recourse to extensive computer work for the preliminary thermal design of vertical Bridgman crystal growth systems. These models include the effects of thermal coupling between the furnace and the charge, charge translation rate, charge diameter, thickness and thermal conductivity of the confining crucible, thermal conductivity change and liberation of latent heat at the growth interface, and infinite charge length. The hot and cold zone regions, considered to be at spatially uniform temperatures, are separated by a "gradient control" region which provides added thermal design flexibility for controlling the temperature variations near the growth interface.

One-dimensional thermal models show that the thermal coupling between the furnace and the charge and the change in thermal conductivity at the growth interface are the primary factors influencing the axial temperature gradients near the interface. The effect of the crucible is analytically described in a way which does not compromise the simplicity of the one-dimensional models; its effect is to reduce the thermal coupling between the charge and the furnace. Criteria for the neglect of charge translation rate, charge length and liberation of latent heat are developed.

Two-dimensional models show that the interface shape is primarily affected by thermal conditions near the growth interface. Heat transfer to or from the charge near the interface is shown to provide a means for altering the interface shape. The combined effects of a crucible and the liberation of latent heat and/or conductivity change at the growth interface produce radial temperature variations at the growth interface. For the growth of semiconductors, this effect leads to an adverse interface curvature and remains an unresolved problem inherent to the Bridgman technique.

Thesis Supervisor: W. M. Rohsenow
Title: Professor of Mechanical Engineering

ACKNOWLEDGMENTS

The work described in this thesis was performed for the research efforts of Prof. August Witt in the Department of Materials Science and Engineering. He has long recognized that a collaborative effort among those in the fields of crystal growth and transport processes is essential for the improvement of crystal growth techniques. His promotion of such efforts not only has provided for my involvement in the present research, but places him as a leader in the crystal growing community.

The assistance afforded by my doctoral committee, Profs. B. B. Mikic, R. A. Brown, and especially, the committee chairman, W. M. Rohsenow, is sincerely appreciated.

I would like to acknowledge Javier Valenzuela for having provided an insight which had important implications for the development of this work.

The support of my family was needed and was always there.

Norm Decker, je ne te dérangerai plus, merci. Tu me manqueras.

I also wish to express my gratitude to the National Aeronautics and Space Administration (Materials Processing in Space Division, Grant No. NSG 7645) for their financial support of this study.

TABLE OF CONTENTS

page

LIST OF FIGURES

page

LIST OF TABLES

page

NOMENCLATURE

A	cross sectional area; without subscript denotes the charge cross sectional area
A_i	i = 1 to 5; coefficients in the concentric fin equations (c.f., eq. [6.1])
Bi	Biot number, hD/k
C_o	dopant concentration in the melt
c_p	specific heat; without subscript denotes the specific heat of the charge
d	diffusion coefficient of the dopant in the melt
D	diameter; without subscript denotes the diameter of the charge
D_{in}	diameter of the inner charge fin (c.f., Fig. 6.2)
$D_1/2$	radial location for the temperature of the inner charge fin in the concentric fin model (c.f., Fig. 6.2)
$D_2/2$	radial location for the temperature of the outer charge fin in the concentric fin model (c.f., Fig. 6.2)
$D_3/2$	radial location for the crucible temperature in the concentric fin model (c.f., Fig. 6.2)
$\mathcal{F}_{f,cr}$	radiation surface heat exchange factor between the furnace and the crucible (c.f., eq. [C.4])
g	dimensional axial gradient G/D
G	average charge/crucible axial temperature gradient at the growth interface
h	heat transfer coefficient
h_c	conduction heat transfer coefficient across the furnace cavity gap
h_r	radiation heat transfer coefficient across the furnace cavity gap
ΔH_{sl}	latent heat of solidification
$I_L(\zeta)$	function defined by eq. [7.11a]
$I_S(\zeta)$	function defined by eq. [7.11b]
I''	electric current per unit cross sectional area

k	thermal conductivity; without subscript denotes the thermal conductivity f the charge
K	k_{cr}/k
K_o	equilibrium partition ratio of the phase diagram
L	length of a portion of the charge
L_p	length of the pull rod
L_{mfp}	mean free path length of a molecule of the gas in the furnace cavity gap
m_L	slope of the liquidus of the phase diagram
N	radius of curvature of an isotherm in number of charge radii
p	pressure of the gas in the furnace cavity gap
P	surface area per unit length of the charge
Pe	Peclet number; $VDk/(\rho c_p) = VD/\alpha$
q''	heat transfer to the surface of the charge per unit surface area of the charge
r	radial coordinate
R	growth rate of the crystal, or thermal resistance between adjacent fins
R_G	$k_G A_G/kA$
R_G^*	$R_G/[1 + K_S(\delta^2 - 1)]$
R_H	$\Delta H_{sl}/c_p(T_{f,H} - T_{f,C})$
R_H^*	$R_H/[1 + K_S(\delta^2 - 1)]$
R_K	k_L/k_S
R_K^*	$[R_K + K_S(\delta^2 - 1)]/[1 + K_S(\delta^2 - 1)]$
R_α	α_{cr}/α
Se	Seebeck coefficient
t	time
t_{gap}	gap width between the furnace and the crucible
T	temperature

V lowering rate of the charge

w eigenvalues of the fin equations used in the various thermal models

z axial coordinate measured from the center of the gradient zone

z_ϕ axial distance between the locations of an isotherm at the center and surface of the charge

z_p axial distance from the end of the charge/pull rod boundary

Greek symbols

α thermal diffusivity; without subscript denotes the thermal diffusivity of the charge

δ D_{cr}/D

ϵ surface emissivity

ζ dimensionless axial coordinate, z/D

ζ_c axial location of the cold end of the charge

ζ_H axial location of the hot end of the charge

ζ_i axial location of the growth interface

ζ_p dimensionless axial distance from the end of the charge/pull rod boundary, z_p/D_p

ζ_ϕ dimensionless distance between the axial locations of an isotherm at the center and surface of the charge, z_ϕ/D

ζ_∞ "infinite" charge length (c.f., section 5.5)

η latent heat parameter defined in eq. [5.12]

θ dimensionless temperature determined from one-dimensional models, $(T - T_{f,C})/(T_{f,H} - T_{f,C})$

θ_i dimensionless solidification temperature

λ dimensionless length of a portion of the charge, L/D

λ_p dimensionless length of the pull rod, L_p/D_p

μ $\lambda_G/2$

ρ dimensionless radial coordinate, r/D, or mass density

σ Stefan-Boltzmann constant, 5.729×10^{-8} W/m^2-K^4

τ dimensionless time, $t/(D/V)$

Φ dimensionless temperature determined from two-dimensionless models, $(T - T_{f,C})/(T_{f,H} - T_{f,C})$

Φ_Δ $(\Phi_{out} - \Phi_{in})/2$

ϕ average charge/crucible temperature at a particular axial location (c.f., eq. [4.21]) or, when considering the gradient zone annulus, the average charge/crucible/gradient zone annulus temperature (c.f., eq. [6.17])

ψ parameter defined by eq. [5.16]

Subscripts

C cold zone

cp boundary condition to be used at the cold end of the charge accounting for the effect of the pull rod

cr crucible

end ends of the charge

f furnace

G gradient zone or gradient zone annulus

H hot zone

i growth interface

in inner charge fin

loc charge properties or boundary conditions at a particular axial location

m mean cross sectional charge temperature

out outer charge fin

p pull rod

s surface of the charge

Superscripts

' denotes alternative dimensionless formulation (c.f., eq. [4.3b]) or axial derivative in eqs. [6.3] and [6.4]

* represents effective values of Bi, Pe, R_K, R_H, and R_G, accounting for the presence of the crucible in the moving fin model

** effective Biot number accounting for the radial thermal resistance of the charge in addition to the crucible (c.f., eq. [4.14])

+ values of K and δ which maximize Bi^*

1. INTRODUCTION

The basic material property requirements of semiconductors used for advanced electronic devices are:

(1) absence of grain and twin boundaries (single crystal)

(2) low crystal defect density

(3) uniform distribution of the dopant

(4) minimized contamination by electrically active elements

Numerous techniques exist for the production of semiconductors in single crystal form (c.f., [1,2]). The choice of a technique for a particular application is dictated by the inherent physical and chemical properties of the semiconductor and the desired resultant electronic properties [3]. Increasingly stringent requirements for the electronic properties of semiconductor crystals necessitate the modification and refinement of conventional growth techniques.

Growth from the melt describes several techniques used for the production of bulk crystals by the controlled transformation of a liquid into a solid of high degree of crystalline perfection. The majority of bulk, single crystal semiconductors is currently grown from the melt. The commonly used melt growth techniques are depicted in Fig. 1.1. In each case, growth of a single crystal is initiated by partial melting of a seed crystal; continued growth of the crystal occurs by the relative motion of the charge (crystal and melt) through the thermal boundary conditions imposed by the apparatus.

Each of the melt-growth techniques has advantages and shortcomings. The Czochralski technique (Fig. 1.1a), for example, has relatively high

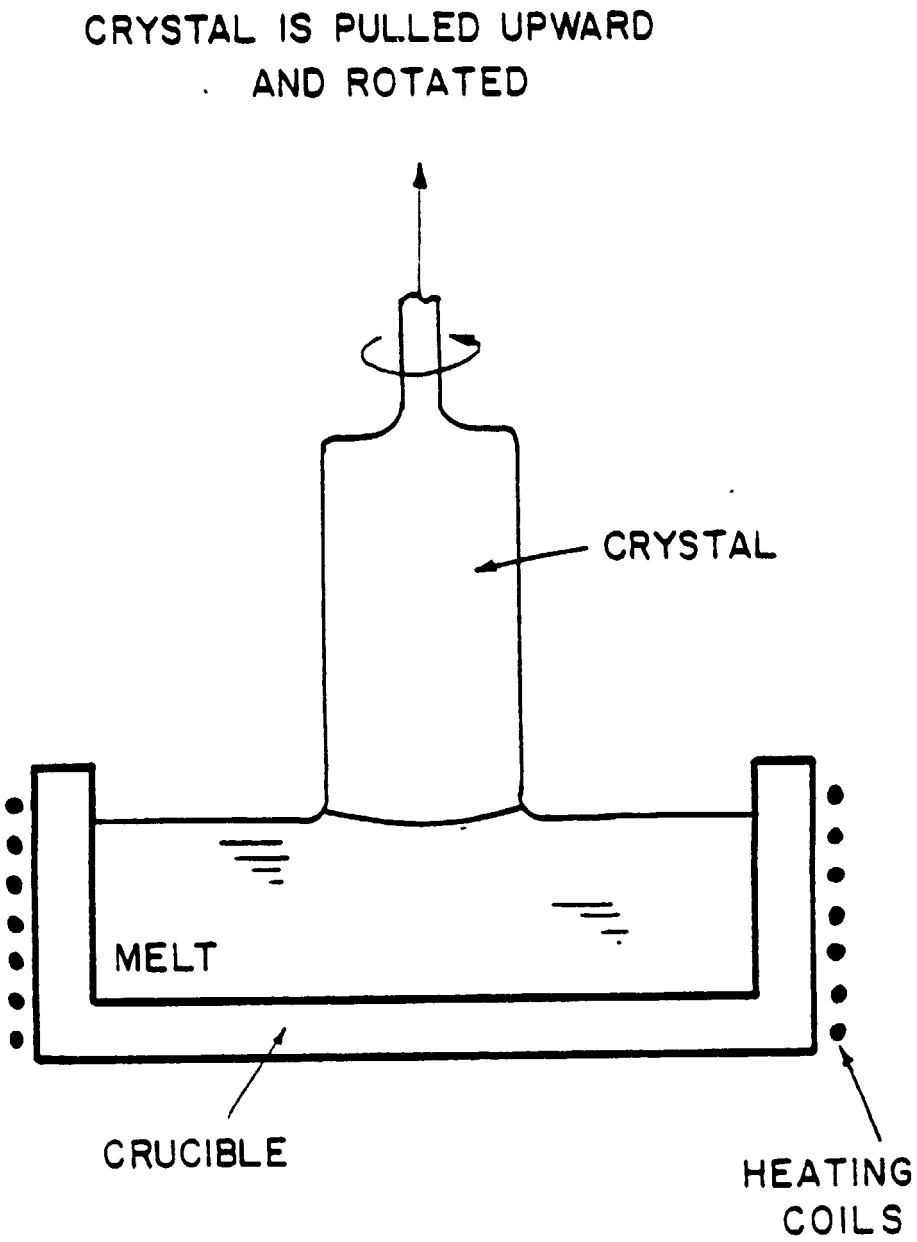

Fig. 1.1a: Sketches of the commonly used melt growth techniques: Czochralski.

rates of production and can produce crystals with a low defect density. Axial and radial segregation of the dopant is typically significant, however, due to the effects of time-varying, natural convective fluid flow in the melt. Also, precaution must be taken to prevent depletion of volatile elements from the melt.

Crystals grown by the float-zone technique (Fig. 1.1b) are relatively free from contamination since the melt is uncontained; radial segregation of the dopant is appreciable, however, due to the strong two-dimensional thermal field near the growth interface and the resulting natural convective fluid flow.

Use of a sealed crucible in the vertical Bridgman technique (Fig. 1.1c) provides a simple means of minimizing the depletion of volatile elements from the melt. (The crucible used in the horizontal Bridgman technique is typically open.) Crystals grown by the Bridgman techique, however, have high defect densities generally attributed to mechanical stresses associated with the confining crucible. The boundary between the growth interface and the crucible also provides sites for heterogeneous nucleation of crystal grains which can prevent single crystal growth. Further, although the vertical Bridgman configuration is relatively stable for natural convective fluid flow (the melt is heated from above), radial segregation of the dopant in Bridgman grown crystals has not been demonstrated to be consistently superior to that in crystals produced by other melt-growth techniques.

It is evident that heat transfer is involved in the phase transformation at the crystal/melt (growth) interface and it is now understood that thermal phenomena greatly affect the quality of melt-grown crystals. Basic thermal considerations have not, however, been adequately applied in the

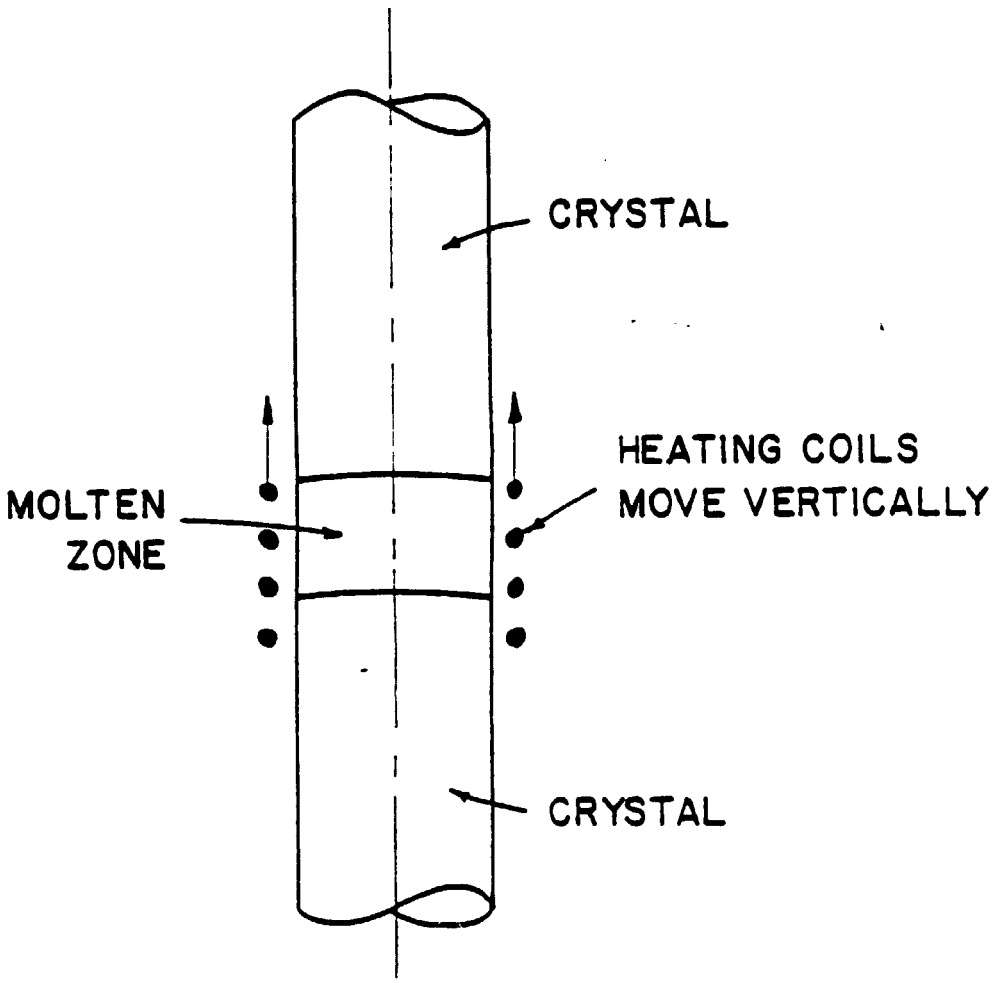

Fig. 1.1b: Sketches of the commonly used melt growth techniques: float-zone.

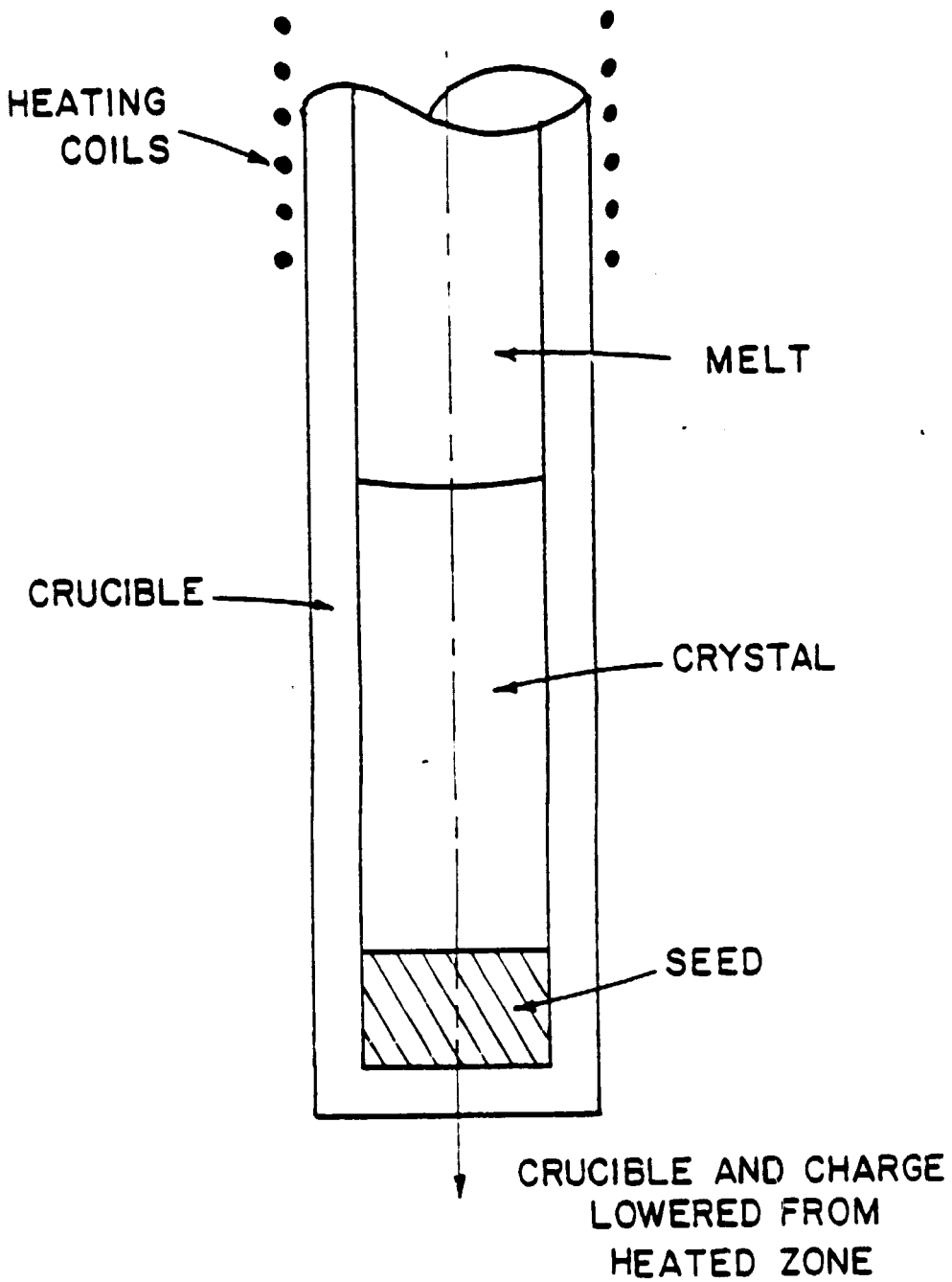

Fig. 1.1c: Sketches of the commonly used melt growth techniques: vertical Bridgman.

analysis or design of melt-growth apparatus. There is, therefore, a strong motivation for a reassessment of the inherent capabilities of the various melt-growth techniques from the point of view of improved thermal design.

Compared to other melt-growth techniques, the thermal configuration of the vertical Bridgman technique offers several features that appear advantageous for semiconductor crystal growth:

(1) The thermal boundary conditions associated with the furnace are relatively simple and axisymmetric.

(2) The furnace configuration is readily adaptable to thermal design changes deemed necessary to accommodate the growth of different semiconductor materials with varying thermal properties.

(3) Natural thermal convection in the melt is reduced since the melt is heated from above and is completely enclosed by the crucible.

For these reasons a combined analytical and experimental program is being conducted to investigate the potential for improvement in the thermal design of the vertical Bridgman crystal growth technique. The present work is the analytical portion of this program. The methodology of the analysis if to develop simplified thermal models which are capable of showing the governing parametric behavior of the growth system. Particular emphasis is given to obtaining approximate analytical expressions which easily demonstrate the interaction among the thermal parameters.

Thermal requirements for satisfactory melt-growth are shown in section 2.1 to depend on both axial and radial temperature variations within the

charge. One-dimensional (i.e., axial temperature variations only) and two-dimensional thermal models are formulated in Chapters 4 and 6 respectively. The temperature field within the charge obtained from the models is then used to evaluate the effects of the thermal parameters from the viewpoint of satisfying the thermal requirements (Chapters 5 and 7).

2. SCOPE OF THE THERMAL ANALYSIS

A combined analytical and experimental program for the improvement of semiconductor crystal growth by the vertical Bridgman technique is being undertaken in the Department of Materials Science and Engineering. The analysis presented in this thesis comprises the analytical portion of this program.

The objective of the thermal analysis is to identify and provide an understanding of the thermal characteristics of semiconductor crystal growth by the vertical Bridgman technique; in this way, problems likely to be encountered, and the means for their possible reslolution, are expected to be identified. To perform this task requires, of course, an adequate knowledge of the effects of the principal thermal parameters. Models are formulated to ascertain these effects with special emphasis directed towards obtaining results which can be presented in analytical form and can therefore be used without recourse to extensive computer work. Design alternatives suggested by the thermal analysis are to be evaluated in the experimental program.

Section 2.1 points out that the behavior of the axial and radial temperature gradients near the growth interface is of primary importance in determining the quality of crystals grown by the Bridgman technique. The results of the thermal analysis are therefore discussed in this context. Chapters 4 and 5 deal with the axial temperature distribution of the charge and Chapters 6 and 7 treat radial temperature variations within the charge.

2.1 THERMAL REQUIREMENTS FOR BRIDGMAN CRYSTAL GROWTH

The electronic properties of a crystal grown by a melt-growth technique depend strongly upon the temperature distribution near the growth interface during solidification. The thermal requirements leading to the growth of high quality semiconductor crystals by the vertical Bridgman technique are: (1) that the axial temperature gradient at the growth interface is greater than a critical value and (2) that the radial temperature gradients near the growth interface produce an interface shape which is slightly concave toward the solid (Fig. 2.1).

2.1.1 Axial Temperature Gradient At The Growth Interface

During solidification, a concentration boundary layer of the dopant is generated in the melt in advance of the growth interface. Within this boundary layer the solidification temperature varies in accordance with the phase diagram. The phenomenon termed constitutional supercooling occurs when the sensible temperature in the melt is less than the local solidification temperature [4]. Under such conditions the morphology of the interface becomes unstable and it is difficult to maintain single crystal growth [5,6,7]. If the concentration boundary layer in the melt is diffusion dominated (i.e., neglecting natural convective fluid flow), the axial temperature gradient in the melt at the interface required to prevent constitutional supercooling is [8]:

$$\left(\frac{dT}{dz}\right)_{min} = C_o m_L \left(1 - \frac{1}{K_o}\right) \frac{R}{d} \qquad [2.1]$$

where: R = growth rate

m_L = slope of the liquidus of the phase diagram

where: C_o = concentration of dopant in the melt

K_o = equilibrium partition ratio of the phase diagram

d = diffusion coefficient of the dopant in the melt

Equation [2.1] indicates that the axial gradient criteria is, to a certain extent, controlled by the crystal grower. By decreasing the lowering rate, V, the growth rate, R, likewise decreases [9,10,11] and the axial gradient criteria becomes less restrictive.

The axial gradient criteria is less restrictive in the presence of a convective component to the mass transfer of dopant near the interface [4]. The axial gradient requirement given by eq. [2.1] represents, therefore, an upper limit.

2.1.2 Shape of the Growth Interface

Heterogeneous nucleation can occur at the boundary between the growth interface and the crucible. When allowed to grow, crystal grains initiated by such nucleation destroy single crystal growth. These unwanted crystal grains do not propagate into the single crystal, however, if the interface is concave toward the crystal as shown in Fig. 2.1. It is desired, therefore, that radial temperature variations within the charge near the growth interface produce an interface which is slightly concave toward the solid.

The shape of the interface is also a factor concerning the radial segregation of the dopant in the solidified charge. For the special case of a diffusion dominated concentration boundary layer at the growth interface, analysis shows [12,13] that the radial mass transfer of the dopant decreases with interface curvature. Thus, to achieve a desired level of radial segregation under such conditions, it is only required that

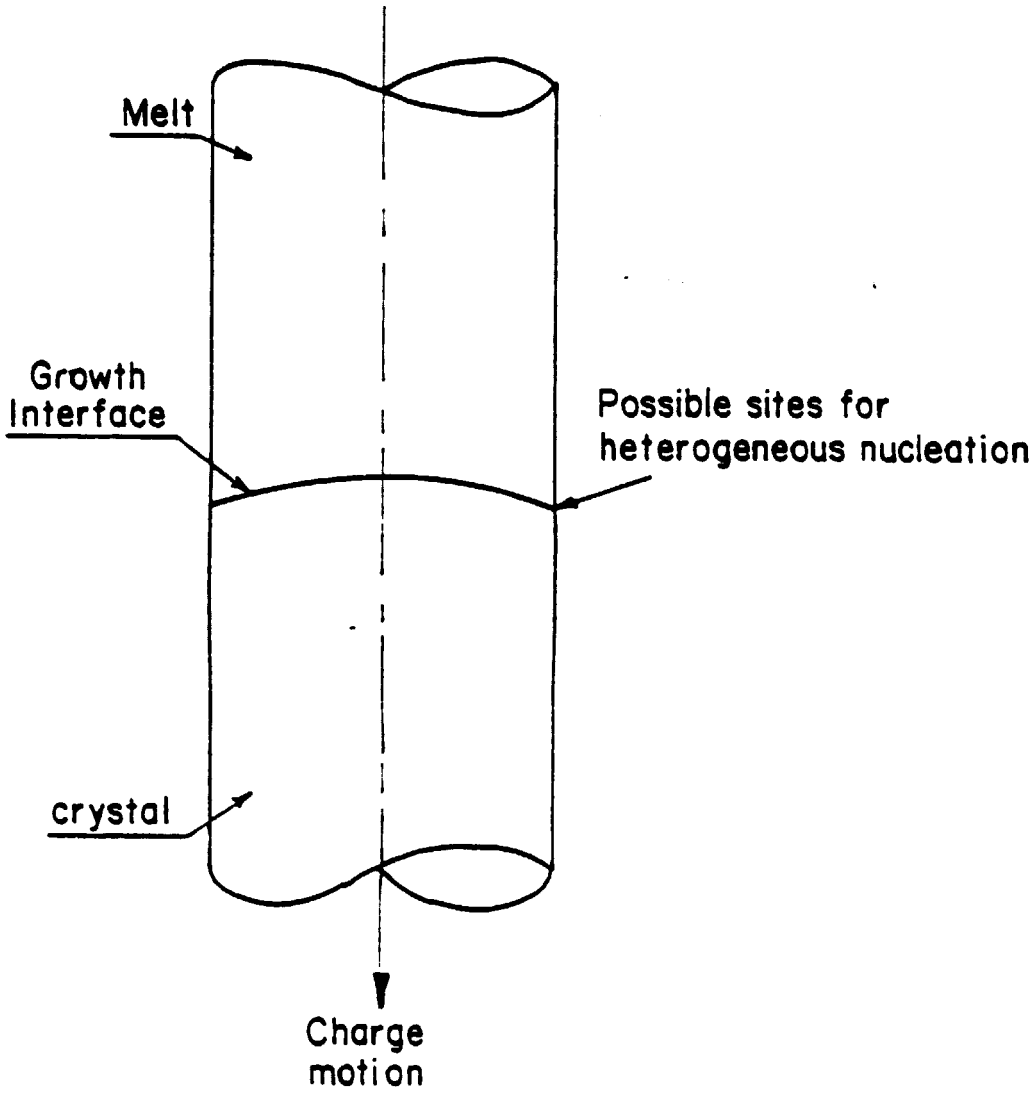

Fig. 2.1: Desired growth interface shape for single crystal growth.

the interface curvature be reduced to an appropriate level. For dilutely doped semiconductors, even in the presence of radial segregation, the interface is very nearly an isotherm. The interface shape criteria therefore translates into a thermal criteria -- the interface isotherm should be nearly flat. That is, heat transfer near the interface should be nearly one-dimensional.

Cases of practical significance occur in which the assumptions leading to the flat interface criteria discussed above are not valid. For example, the theoretical studies of Chang [14] and Chang and Brown [15] show that natural convective fluid flows may have a significant effect on the radial segregation of the dopant while having only a minor effect on the temperature distribution in the charge for melts which have small Prandtl numbers. Under these conditions a flat growth interface is not directly correlated with satisfactory radial segregation of the dopant. Also, in systems which exhibit a large separation of the liquidus and solidus (e.g., HgCdTe), the interface shape is coupled to the radial segregation of the dopant as well as the radial variation of the temperature in the vicinity of the interface. Such cases as these require a detailed analysis of the mass, momentum and heat transfer within the charge in order to predict the radial segregation.

Dopant mass transfer is not within the scope of the present thermal analysis. The behavior of isotherm shapes to be described in subsequent chapters may therefore be correlated to radial segregation behavior only for the special case of dilutely doped, diffusion dominated systems. When these ideal conditions are not approximated, results from the present analysis are nevertheless expected to describe the thermal behavior of the

charge and may thus be used in conjunction with analyses which consider mass transfer of the dopant (e.g., [14,15]) to aid in understanding the manner in which radial segregation is affected by the thermal parameters of the Bridgman growth system.

2.2 THE THERMAL MODEL

The two-dimensional temperature field in the solidifying charge is described by partial differential equations subject to complex boundary conditions. The solution of these equations may be effected by standard numerical techniques (e.g., finite difference or finite element methods). Numerical solution methods preclude, however, the description of results in simple analytical form. The present work emphasizes the development of approximate models which lead to analytical results. The increased accuracy of more exact numerical formulations is not considered warranted at the present time for the following reasons:

(1) Thermal property values (e.g., thermal conductivity of the melt, emissivities of the furnace wall and crucible) are often not well known and introduce uncertainty into the results of any thermal analysis.

(2) The development of approximate thermal models itself leads to a better understanding of the thermal behavior of the Bridgman system.

(3) Approximate results presented in analytical form and indicating the primary thermal behavior of the Bridgman system are more conveniently used to evaluate the effects of various furnace design alternatives.

The present work models the vertical Bridgman configuration being constructed for the experimental portion of the program. The experimental apparatus, described in section 2.2.1, contains the features basic to all vertical Bridgman growth systems; therefore, results obtained in this work can be used in a qualitative manner for any vertical Bridgman furnace configuration. It is necessary, of course, that simplifying approximations be made in the development of any thermal model; the thermal effects incorporated in and excluded from the present models are outlined in Section 2.2.2.

2.2.1 The Experimental Vertical Bridgman Crystal Growth System

Vertical Bridgman crystal growth denotes the solidification of a molten charge, contained in a chemically inert crucible, by its descent from a hot to a cold environment. In conventional Bridgman growth (Fig. 1.1c) the hot environment is a tube furnace of varying design and the cold environment is the surroundings (e.g. the laboratory). The present work formulates a thermal model of a system, currently under construction, which incorporates several modifications of a conventional Bridgman system. There are two objectives for these modifications:

(1) To permit flexibility for controlling the thermal environment exposed to the charge. In this way, through the adjustment of design and operation parameters, the system is expected to provide for a wide range of axial temperature gradients, and radial temperature gradients which lead to interface shapes ranging from convex to concave.

(2) To permit the formulation of more accurate thermal models of the system, particularly in describing the thermal boundary

conditions exposed to the charge. In this way, the thermal analysis is expected to provide more applicable results.

The experimental Bridgman system is depicted in Fig. 2.2. The cold environment is a separate furnace whose temperature can be independently controlled. Stockbarger [16] first introduced a separate furnace for the cold environment which was separated from the hot furnace by a simple radiation shield as a means for increasing the axial temperature gradient at the growth interface. In the present system, heat pipes are used for the hot and cold furnaces. The temperature boundary condition is therefore uniform in both the axial and circumferential directions. The gap between the heat pipes and the charge can be made smaller in order to simplify the description of radiant heat transfer and also, if desired, to obtain significant heat transfer by thermal conduction. Between the heat pipes is a "gradient control" region in which the growth interface is to be located. Chang and Wilcox [17] suggested the use of an adiabatic gradient control region as a means of reducing the curvature of isotherms near the growth interface. The present work considers the thermal design of the gradient control region as a design variable. It is anticipated that judicious design of heat transfer between the gradient control region and the charge will assist in obtaining the requisite control over the interface shape.

2.2.2 Effects Incorporated In and Excluded From the Thermal Models

The following thermal parameters, considered to be of primary importance in determining the thermal characteristics of Bridgman crystal growth, are included in the thermal models of Chapters 4 and 6:

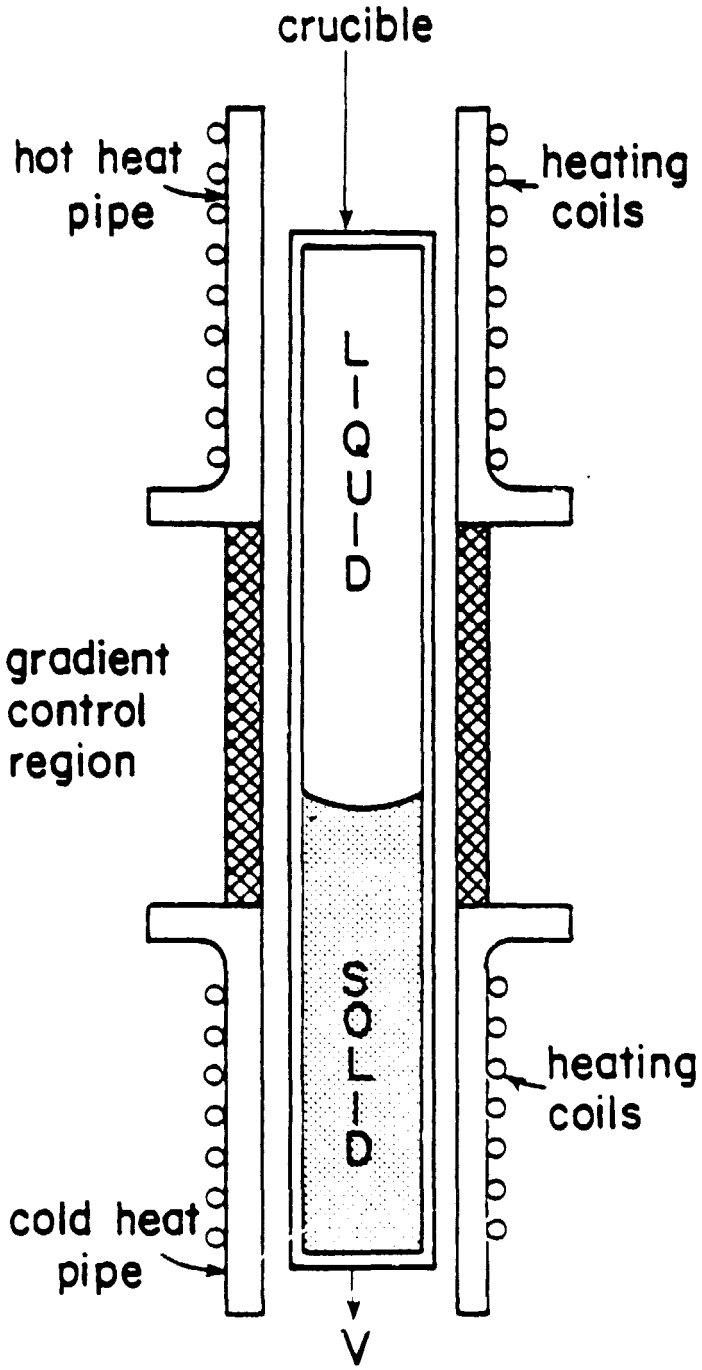

Fig. 2.2: The experimental vertical Bridgman crystal growth system.

(1) **Thermal coupling between the charge and the heat pipe furnace.**

Thermal communication between the charge and the furnace is due to both radiation and conduction heat transfer. The radiative contribution strongly depends on the values of surface emissivities which are oftentimes not accurately known. The conductive contribution is determined by the thickness of the gap between the charge and furnace and the conductivity of the gas in the gap. Thus, evacuating the gas from the gap can eliminate the conduction heat transfer. Appendix C discusses the quantitative evaluation of typical heat transfer coefficients associated with both modes of heat transfer across the gap.

(2) **Thermal design of the gradient zone region.**

The gradient zone portion of the furnace is modelled as an annular ring between the hot and cold heat pipes. Changes in the thermal conductivity and thickness of the annular ring are expected to alter the distribution of heat transfer to the charge and, as a consequence, the shape of the isotherms within the gradient zone.

(3) **Thermal conductivity of the charge and the ratio, R_K, between the melt and crystal conductivities.**

For semiconductors, the melt conductivity is greater than that in the solid, i.e., $R_K > 1$.

(4) **Generation of latent heat at the growth interface.**

(5) **Thickness and thermal conductivity of the crucible.**

(6) **Lowering rate of the charge.**

Lowering rates for typical semiconductor crystal growth range from 0.1 μm/s to 10 μm/s.

(7) **Length of the charge and its position in the furnace.**

(8) **Diameter of the charge.**

Several effects have not been included in the thermal models. The excluded effects are of relatively small importance for typical crystal growth situations or do not contribute to the primary thermal behavior of the Bridgman growth system; it is therefore considered that the increased complexity of thermal models that would be required for inclusion of these effects is not warranted. The excluded effects are:

(1) **Natural convection in the melt.**

The temperature field in the charge is not greatly affected by natural convective fluid flow during typical vertical Bridgman growth of semiconductors (i.e., materials with a small Prandtl number) [14,15].

(2) **Transients.**

All models are quasi-steady; i.e., the transient terms of the heat balance equations are assumed negligible. This assumption is normally valid due to the small lowering rates used in typical Bridgman growth. (Appendix E provides a brief discussion of temperature transients.)

(3) **Thermal coupling between the furnace and the charge.**

Thermal coupling between the charge and the furnace is described in the present work by a heat transfer coefficient, h. The heat transfer coefficient varies with position due, for example, to temperature dependent radiation heat transfer. The present thermal models assume that the heat transfer coefficient is constant within the hot furnace, cold furnace and gradient control region. Since the expected maximum spatial variation of h within a furnace zone is approximately a factor of 2, it is considered that the variation of h is of secondary importance compared to the overall thermal coupling described by a suitable average value. Additionally, the hot and cold zone furnace temperatures are assumed to be uniform reflecting the heat pipe action. The lengths ot the furnace zones are assumed infinite. (Appendix D develops a criterion for the validity of this assumption).

(4) **Constant thermal properties.**

Except for the change in thermal conductivity at the growth interface, all thermal properties are assumed independent of temperature.

3. LITERATURE SURVEY

A number of thermal analyses of Bridgman-type crystal growth systems have been reported in the literature in recent years [9-11,17-28]. They can be classified according to the type of analysis which was performed, as shown below in Table 3.1:

TYPE OF THERMAL ANALYSIS	REFERENCES
One-Dimensional (axial temperature variations only)	9-11, 17-23
Two-Dimensional (axial and radial temperature variations)	17, 24-28
Dimensional Variables	10, 11, 18-20, 25, 27, 28
Nondimensional Variables	9, 17, 21-24, 26
Analytical Results	17, 22, 23
Numerical Results (i.e., computer generated results)	9-11, 18-21, 24-28

Table 3.1: Current literature containing thermal analysis of Bridgman-type crystal growth systems.

3.1 ONE-DIMENSIONAL ANALYSES

All of the one-dimensional models describe the axial temperature distribution of a solidifying charge by equations similar to those used by Davis [18]. In these models, the charge is analogous to a fin moving through spatially varying boundary conditions. The equations for a moving

fin are found in many heat transfer texts [e.g., 29,30]. The principal results obtained through a one-dimensional analysis are the axial temperature gradient at the growth interface and the axial position of the growth interface.

In conjuction with his model, Davis [18] obtained experimental results by solidifying lead-tin alloys at various growth rates and hot and cold zone furnace temperatures. Good correlation between experimental and calculated results demonstrated the usefulness of one-dimensional models for predicting the axial temperature distribution of the charge. Further experimental verification of one-dimensional modeling has been provided by Clyne [10,11] who solidified aluminum at various lowering rates.

The differences among the one-dimensional analyses listed in Table 3.1 concern several factors. The most apparent distinction is the type of system which is modeled. Some works deal with the furnace configurations of experimental growth systems employed for the growth of specific metals or metal alloys (Pb-Sn [18], Al [10,19], Ag-Si [20]); others treat idealized furnace boundary conditions without reference to a specific charge material [9,17,21,22,23]. The former analyses, being limited to specific charge materials, primarily analyze the effects of furnace and operation parameters such as the thermal coupling between the charge and furnace, position of the charge within the furnace, and lowering rate. The latter models are nondimensional and their results are more readily applied to an extended variety of growth systems.

The one-dimensional analyses differ also with regard to the solution technique. Several employ finite difference or finite element methods [10,11,19-21]; others carry out analytical solutions which are sufficiently complicated to require computer evaluation of the resulting expressions

[9,18,22,23]. Only Chang and Wilcox [17] and Sukanek [23] have been able to present results in simple analytical form. Generally, the shift from numerical to analytical methods occurs as the modeling of the growth system becomes more idealized.

Finally, differences among the one dimensional analyses also pertain to the specific effects incorporated into the thermal models: inclusion of the crucible [10,11,18,20], generation of latent heat at the growth interface [10,11,17,28,21-23], unequal melt and crystal thermal conductivities [9-11,18-23], gradient control region [10,11,18,22,23,26], lowering rate of the charge [10,11,17,18,21-23], and temperature transients [10,11,21].

The majority of the one-dimensional models are concerned with the relationship between the position of the charge within the furnace and either the axial temperature gradient at the growth interface or the axial position of the growth interface. Chang and Wilcox [17] demonstrate that the interface position changes as the end of the charge approaches the region between the hot and cold zone furnaces. Their results suggest that larger Biot numbers (see Section 5.2) and longer charge lengths tend to maintain a stationary interface location. Riquet and Durand [9] extend the results of Chang and Wilcox [17]. They show the manner in which the growth and lowering rates differ during a solidification experiment and indicate how the furnace temperatures should be varied with time in order to keep the interface location stationary. Sukanek [23] offers a simple criterion under which growth and lowering rates will be nearly equal during solidification of a significant portion of the charge (see Section 5.5).

3.2 TWO-DIMENSIONAL ANALYSES

Two-dimensional thermal models are employed in order to obtain the interface shape. The difference between the one- and two-dimensional models is the incorporation of radial temperature variations. This addition, however, makes the solution significantly more complex. Chang and Wilcox [17] used a highly idealized system (no crucible, gradient zone, or generation of latent heat, and equal thermal conductivites of crystal and melt) and obtained a solution in the form of two Fourier-Bessel infinite series. Evaluation of these series was carried out by computer. Sen and Wilcox [24], Fu and Wilcox [26], El-Mahallaway and Farag [25] and Domanski et al [27] used finite difference methods. Jones et al [28] used an electrical analogue model whose solution was also obtained by computer.

A series of outstanding publications by Wilcox et al [17,24,26] demonstrate the usefulness of nondimensional variables in order to describe the thermal characteristics of a Bridgman growth system. Their results present two- dimensional isotherms in a solidifying charge for different values of several of these nondimensional variables. The effects of thermal coupling between the charge and the furnace (represented by the Biot number) and the lowering rate (Peclet number) was thus determined by Chang and Wilcox [17]. A significant conclusion is that the shape of the solidification isotherm depends strongly on its axial location within the furnace. Although not including a gradient control region in their thermal model, Chang and Wilcox [17] suggested the use of an insulating gradient control region in order to reduce isotherm curvature near the interface. Fu and Wilcox [26] later demonstrated the validity of this concept for a system which did not consider a crucible, latent heat, and conductivity change at the growth interface. Sen and Wilcox [24] showed

the effect of crucible conductivity on the isotherm shape for various Biot numbers; they also found that the thermal conductivity of the crucible should be close to that of the charge in order to maintain large axial temperature gradients in the gradient zone.

El-Mahallawy and Farag [25] calculated the two-dimensional temperature distribution in a solidifying Al-Al_3Ni eutectic grown under various conditions, including an abrupt change in the inner diameter of the crucible along the axial direction. Several comparisons of calculated results with experimental data showed good agreement.

3.3 EVALUATION OF THE LITERATURE

The cited literature provides a valuable background for further thermal analysis of Bridgman-type growth systems. In particular, the nondimensional formulation of Wilcox et al [17,24,26] identifies the significant combinations of thermal properties and system parameters which govern the thermal behavior of the system. Taken in part or as a whole, however, the previous work has not yet led to a systematic approach for Bridgman furnace design. The areas found deficient are:

(1) Several important effects have not been studied, have been analyzed only in simple systems or have been addressed only for systems with specific thermal property values. For example, a general treatment of the behavior of radial temperature gradients near the growth interface is not available; only the case of a perfectly insulating gradient zone has received attention; generation of latent heat has been included only in one-dimensional models without

crucibles; the effects of unequal thermal conductivities of the crystal and the melt, and crucible thickness have been considered only for systems of specific property values . It is difficult to draw general conclusions regarding these effects.

(2) Conclusions drawn from those analyses which did not use a nondimensional formulation are difficult to extend to systems of different parameter values.

(3) As seen in Table 3.1, all results, excepting parts of [17,22,23], have been determined by computation. The presentation of these results is necessarily in graphical form and their interpretation quickly becomes awkward when several effects are acting simultaneously. In this respect, results presented in simple analytical form are more desirable.

4. THE ONE-DIMENSIONAL THERMAL MODEL

The axial temperature distribution of a solidifying charge determines two important characteristics of a particular growth experiment:

(1) the axial temperature gradient in the melt at the growth interface. This must be greater than a critical value in order to prevent constitutional supercooling (c.f., section 2.1.1).

(2) the axial location of the growth interface. In addition to strongly influencing the interface shape, the temporal sequence of interface locations indicates the growth rate (as opposed to the lowering rate).

Since neither of these factors pertains to radial temperature variations within the charge, the common approach has been to determine the axial temperature distribution through a one-dimensional thermal model, i.e., neglecting the radial temperature variations. Such models neglect the radial thermal resistance within the charge compared to the thermal resistance between the charge and the furnace. The ratio of internal to external thermal resistance is expressed by the Biot number, Bi. A one-dimensional model is therefore valid for sufficiently small Bi (c.f., section 4.2.3).

The one-dimensional thermal model developed in this chapter posesses several unique features. The crucible and the radial thermal resisitance of the charge are accounted for in a way which readily demonstrates their effects on the axial temperature distribution without compromising the

simplicity afforded by the one-dimensional modeling. Additionally, small lowering rates common in semiconductor crystal growth is recognized to lead to simple analytical results from the one-dimensional model. Such results are used in Chapter 5 to demonstrate the effects of the various parameters of the Bridgman growth system on the axial temperature distribution of the charge.

4.1 THE MOVING FIN APPROACH

A heat balance performed on a slice of the charge of infinitesmal length in the axial direction results in eq. [4.1] (see section 4.2.1) for the axial temperature distribution of the charge. The heat balance points out that the amount of heat conducted through the charge in the axial direction, and hence the axial temperature gradient in the charge, depends directly on the amount of heat transferred to the charge in the hot furnace and from the charge in the cold furnace. Factors which affect the radial transfer of heat to or from the surface of the charge are therefore expected to affect the axial temperature distribution of the charge.

The one-dimensional thermal model is initially developed in section 4.2.1 neglecting the crucible and the radial thermal resistance within the charge. The charge is, in this case, analogous to a fin moving through the spatially varying boundary conditions imposed by the furnace. The crucible, however, may provide a significant radial thermal resistance between the surface of the charge and the furnace boundary conditions. Further, a large Biot number indicates that the internal radial thermal resistance of the charge affects the radial heat exchange with the charge. These effects are approximated in sections 4.2.2 and 4.2.3 where it is shown that they can be included in the moving fin model as a modification

of the thermal coupling between the charge and the furnace (i.e., as a modification of the Biot number).

4.2 THE DESCRIBING EQUATIONS FOR THE MOVING FIN MODEL

The factors of concern for the development of a one-dimensional heat transfer model of the modified Bridgman growth system depicted in Fig. 2.2 are shown in Fig. 4.1. The hot and cold heat pipes comprise the hot and cold zones; the region between them is called the gradient zone. The length of the charge is broken down into L_H, L_G, and L_C within the hot, gradient and cold zones respectively. The charge is lowered through the furnace with a velocity V, has crystal and melt portions with different thermal conductivities, and has a crystal-melt interface which generates latent heat. A crucible provides containment for the charge.

The thermal model makes the assumptions described in section 2.2.2. Additionally, the gradient zone is assumed adiabatic (i.e., $h_G = 0$) in the one-dimensional model; this assumption is relaxed for the two-dimensional model of Chapter 6.

4.2.1 The Charge

With the assumption of negligible radial thermal resistance within the charge, and neglecting the crucible, the charge is analogous to the moving thin rod treated by Carslaw and Jaeger [29]; the equation describing the axial temperature distribution is:

$$k_{loc} A \frac{\partial^2 T_m}{\partial z^2} - \rho_{loc} c_{p,loc} V A \frac{\partial T_m}{\partial z} + P q''_{loc} - \rho_{loc} c_{p,loc} A \frac{\partial T_m}{\partial t} = 0 \qquad [4.1]$$

where: A = cross sectional area of the charge

P = surface area per unit length of the charge

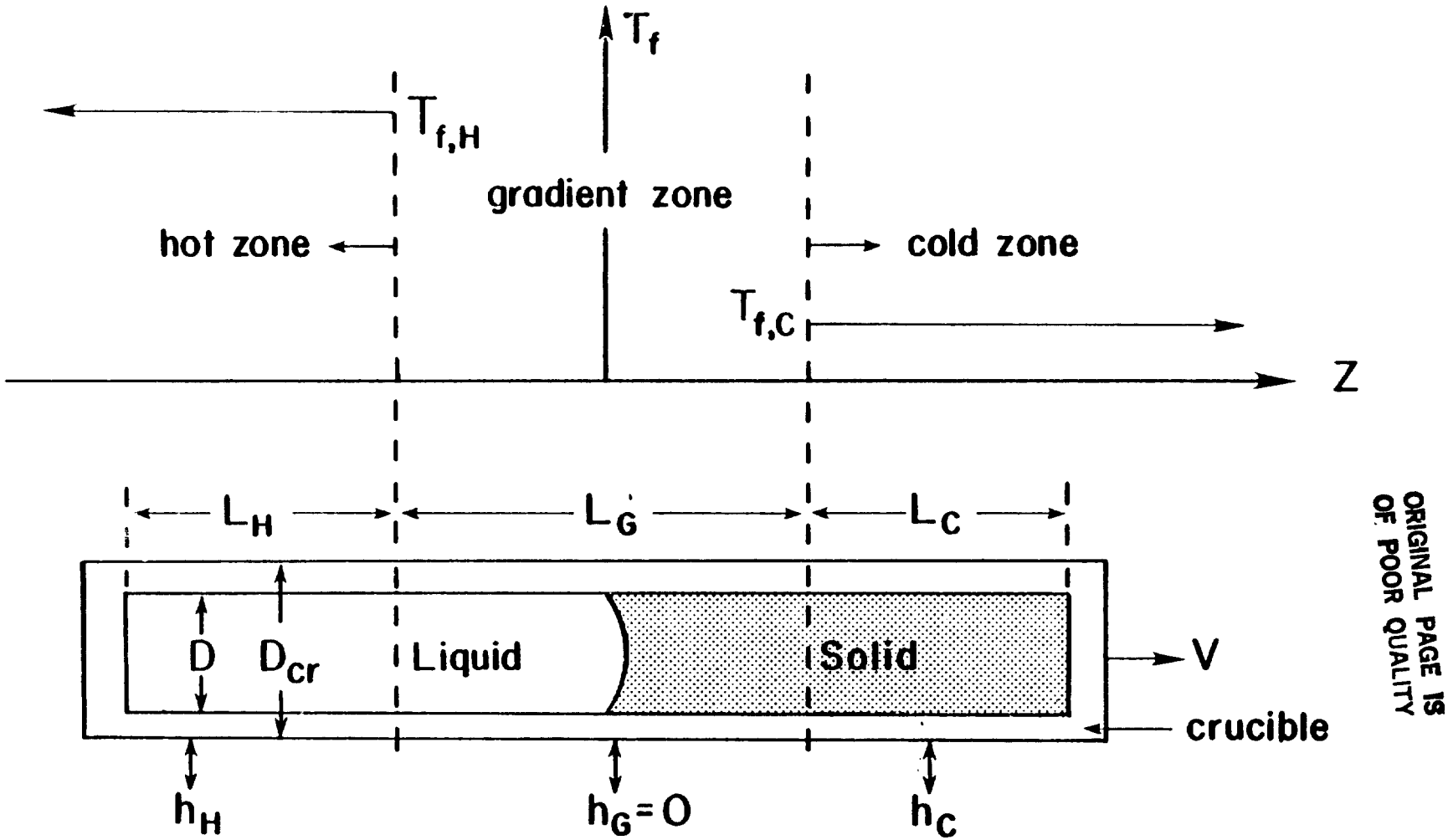

Fig. 4.1: One-dimensional thermal model of the charge, crucible and furnace.

where: Z = axial coordinate measured from the center of the gradient zone

k = thermal conductivity

ρ = mass density

c_p = specific heat

t = time

Subscript "loc" serves to distinguish boundary conditions or charge properties of a particular furnace zone.

T_m denotes the area-averaged charge temperature as a function of Z. The first term of equation [4.1] represents axial conduction of heat within the charge and the second term represents axial convection of heat due to motion of the charge at velocity V. The factor q" in the third term accounts for radial heat transfer to the surface of the charge, per unit surface area of the charge. The final term represents heat storage due to temperature transients at fixed axial location, Z. According to assumption 3 in section 2.2.2, q" is given by:

$$q''_{loc} = h_{loc}\left(T_{f,loc} - T_m\right) \qquad [4.2]$$

where: h = heat transfer coefficient between the furnace and the charge

T_f = furnace temperature

Substituting eq. [4.2] into eq. [4.1], neglecting the transient term according to assumption 2 in section 2.2.2, and nondimensionalizing the resulting expression, yields:

$$\frac{d^2\theta_m}{d\zeta^2} - Pe_{loc}\frac{d\theta_m}{d\zeta} + 4Bi_{loc}\left(\theta_{f,loc} - \theta_m\right) = 0 \qquad [4.3a]$$

An equivalent nondimensional form of eq. [4.3a] is:

$$\frac{d^2\theta_m}{d(\zeta')^2} - Pe'_{loc}\frac{d\theta_m}{d\zeta'} + (\theta_{f,loc} - \theta_m) = 0 \qquad [4.3b]$$

where: $\zeta' \equiv \zeta\left(2\sqrt{Bi_{loc}}\right)$

$$Pe'_{loc} \equiv Pe_{loc} / \left(2\sqrt{Bi_{loc}}\right)$$

Equation [4.3b] has one fewer parameter than eq. [4.3a] but the axial coordinate, ζ', is less physical since the Biot number is included in its definition.

4.2.2 The Crucible

In Bridgman growth a charge is confined in a crucible which, depending on conditions, varies in dimension and composition. Containment of the charge typically tends to decrease axial temperature gradients (Sen and Wilcox [24]). A crucible of low thermal conductivity lowers the axial gradient by adding thermal resistance between the charge and furnace, thereby decreasing the thermal coupling between the charge and the furnace; one of high thermal conductivity lowers these gradients by conducting heat transferred from the furnace axially within the crucible rather than within the charge.

The domain of eq. [4.3] is considered to be the charge only and the crucible is not explicitly included. However, a model of the heat transfer within the crucible approximates its effect on q" of eq. [4.1] which is then expressed through modified Biot and Peclet numbers.

Several previous one-dimensional models [18,22,23] have included the crucible only as a radial resistance between the furnace and the charge.

The present model for the crucible includes axial conduction as well as radial resistance by solving in an approximate manner the heat conduction equation for the temperature distribution of the crucible:

$$\frac{1}{r}\frac{\partial}{\partial r}\left(r\frac{\partial T_{cr}}{\partial r}\right) + \frac{\partial^2 T_{cr}}{\partial z^2} - \frac{V}{\alpha_{cr}}\frac{\partial T_{cr}}{\partial z} = 0 \qquad [4.4]$$

where: r = radial coordinate

α = thermal diffusivity, $k/\rho c_p$

Subscript "cr" denotes the crucible.

The first term of eq. [4.4] accounts for the radial thermal resistance of the crucible, while the second term accounts for the axial conduction of heat within the crucible.

The principal assumptions involved in utilizing eq. [4.4] are that, at each axial location of the crucible, $\partial T_{cr}/\partial z$ and $\partial^2 T_{cr}/\partial z^2$ are independent of the radial coordinate r and equal to dT_m/dz and d^2T_m/dz^2 of the charge. (See section 4.4.1 for a discussion of these approximations.) The first term of eq. [4.4] can then be integrated to yield a radial distribution of T_{cr} in terms of the axial gradients in the charge. The boundary conditions at the crucible surfaces are:

$$h_{loc}\left(T_{f,loc} - T_{cr}\right) = k_{cr}\frac{\partial T_{cr}}{\partial z} \qquad \text{(at the outer crucible surface)} \qquad [4.5a]$$

$$T_{cr} = T_m \qquad \text{(at the inner crucible surface)} \qquad [4.5b]$$

The heat transfer coefficient in eq. [4.5a] is between the furnace and the outer crucible surface. Equation [4.5b] assumes that the crucible and the

charge are in contact. The radial heat flow to the charge in eq. [4.1], q", is related to the radial distribution of T_{cr} by:

$$q''_{loc} = k_{cr} \frac{\partial T_{cr}}{\partial r} \qquad \text{(at the inner crucible surface)} \qquad [4.6]$$

The heat flow given by eq. [4.6] is substituted for q" in the third term of eq. [4.1]. When nondimensionalized, the resulting expression has the same form as eq. [4.3] if Bi and Pe are replaced by their respective "effective" values, Bi* and Pe*:

$$\frac{Bi^*_{loc}}{\delta Bi_{loc}} = \frac{1}{1 + \delta Bi_{loc}\left[\frac{1}{4}(\delta^2-1) - \frac{1}{2}\ln\delta\right] + K_{loc}(\delta^2-1) + \frac{\delta Bi_{loc}\ln\delta}{2K_{loc}}} \qquad [4.7]$$

$$\frac{Pe^*_{loc}}{Pe_{loc}} = \frac{1 + \frac{\delta Bi_{loc}}{R_{\alpha,loc}}\left[\frac{1}{4}(\delta^2-1) - \frac{1}{2}\ln\delta\right] + \frac{K_{loc}}{R_{\alpha,loc}}(\delta^2-1) + \frac{\delta Bi_{loc}\ln\delta}{2K_{loc}}}{1 + \delta Bi_{loc}\left[\frac{1}{4}(\delta^2-1) - \frac{1}{2}\ln\delta\right] + K_{loc}(\delta^2-1) + \frac{\delta Bi_{loc}\ln\delta}{2K_{loc}}} \qquad [4.8]$$

where: $\delta = D_{cr}/D$

$K_{loc} = k_{cr}/k_{loc}$

$R_{\alpha,loc} = \alpha_{cr}/\alpha_{loc}$

The relationship between the effective Biot number and the conductivity ratio K is shown in Fig. 4.2 for $\delta = 1.25$ and various Bi. It is seen that Bi* is significantly reduced by both low and high values of K, especially for larger Bi. In section 5.2 it is shown that increasing Bi* tends to increase the axial gradient at the growth interface. The conductivity ratio, K^+, which maximizes Bi* for given δ and Bi can be obtained from eq. [4.7]:

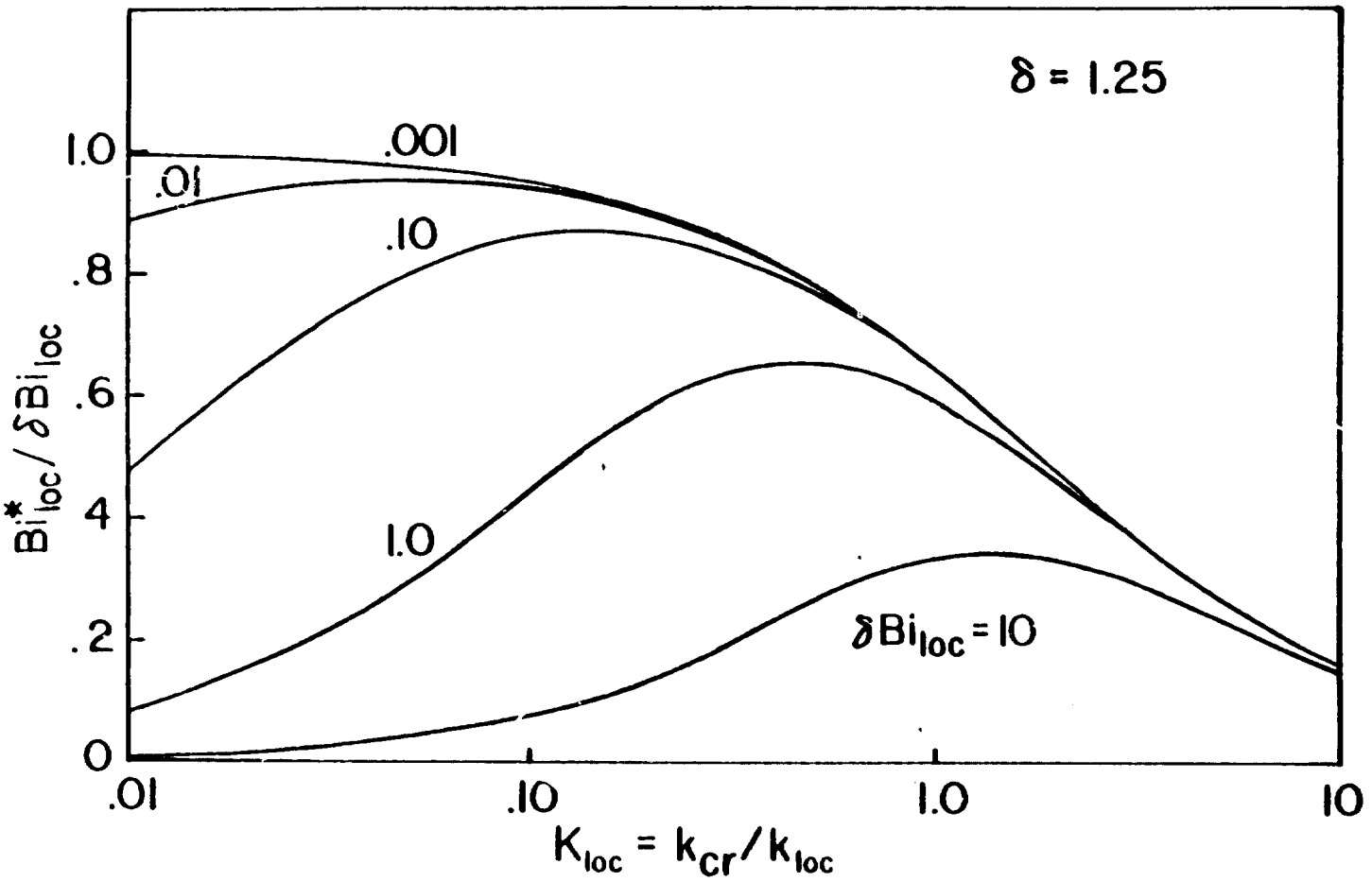

Fig. 4.2: The effect of the thermal conductivity of the crucible on the effective Biot number, Bi^*, for $\delta = 1.25$.

$$K_{loc}^{+} = \left[\frac{\delta Bi_{loc} \ln\delta}{2(\delta^2-1)}\right]^{1/2} \qquad [4.9]$$

For typical values of Bi and δ, the conductivity ratio providing the maximum effective Biot number is found to lie between 0.1 and 1.0.

It is sometimes possible to increase Bi^* by increasing the thickness of the crucible (i.e., by increasing δ). This effect is similar to the "critical radius of insulation" effect whereby a wire which is conducting electricity may be able to dissipate more heat to its surroundings with a layer of insulation on its surface [30]. For the charge/crucible system, an increase in δ increases the charge surface area exposed to heat transfer with the furnace. If this effect more than offsets the opposing effects of increased radial resistance and axial conductance of the crucible, then Bi^* increases with δ.

Consider that Bi^* in eq. [4.7] is a function of δ with constant K and Bi. The value of δ which maximizes Bi^*, δ^+, is given by the roots of the following equation:

$$\frac{Bi_{loc}}{2}(\delta^+)^3 + K_{loc}(\delta^+)^2 - \frac{Bi_{loc}}{2}\frac{K_{loc}-1}{K_{loc}}(\delta^+) + (K_{loc}-1) = 0 \qquad [4.10]$$

Equation [4.10] has positive roots greater than unity ($\delta > 1$ when a crucible is present) only when $K < 1/2$ and $Bi < 1/4$. Figure 4.3 plots the values of δ^+ for various K and Bi. It is seen that it is advantageous to have a thicker crucible when Bi is small, but only if K is also small. Figure 4.4 shows the increase in Bi^* when $\delta = \delta^+$ compared to a bare charge (i.e., compared to $\delta = 1$). (It is found that this ratio is not a

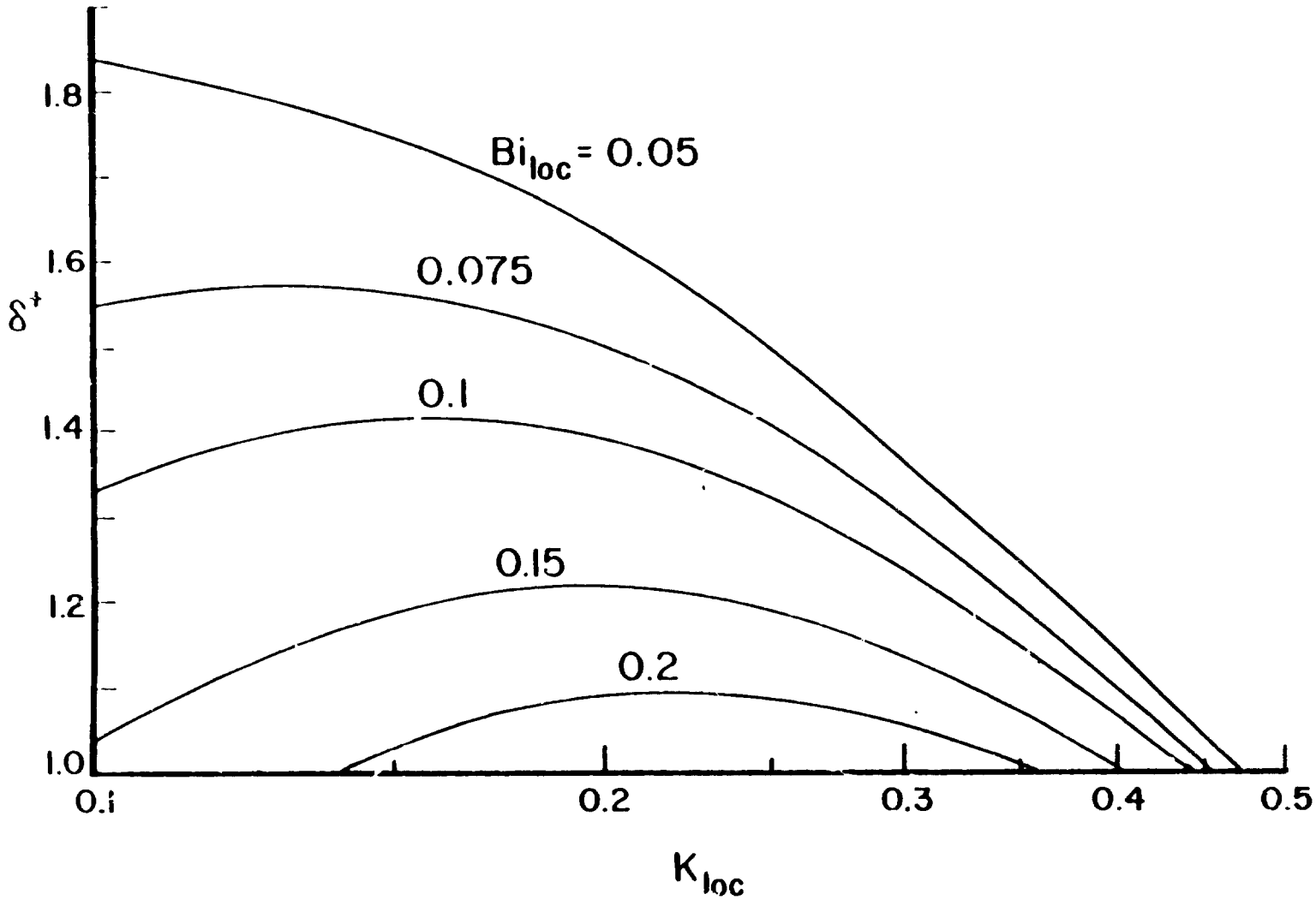

Fig. 4.3: δ^+, the diameter which maximizes Bi^*_{loc} in eq. (4.7), for various K_{loc} and Bi_{loc}.

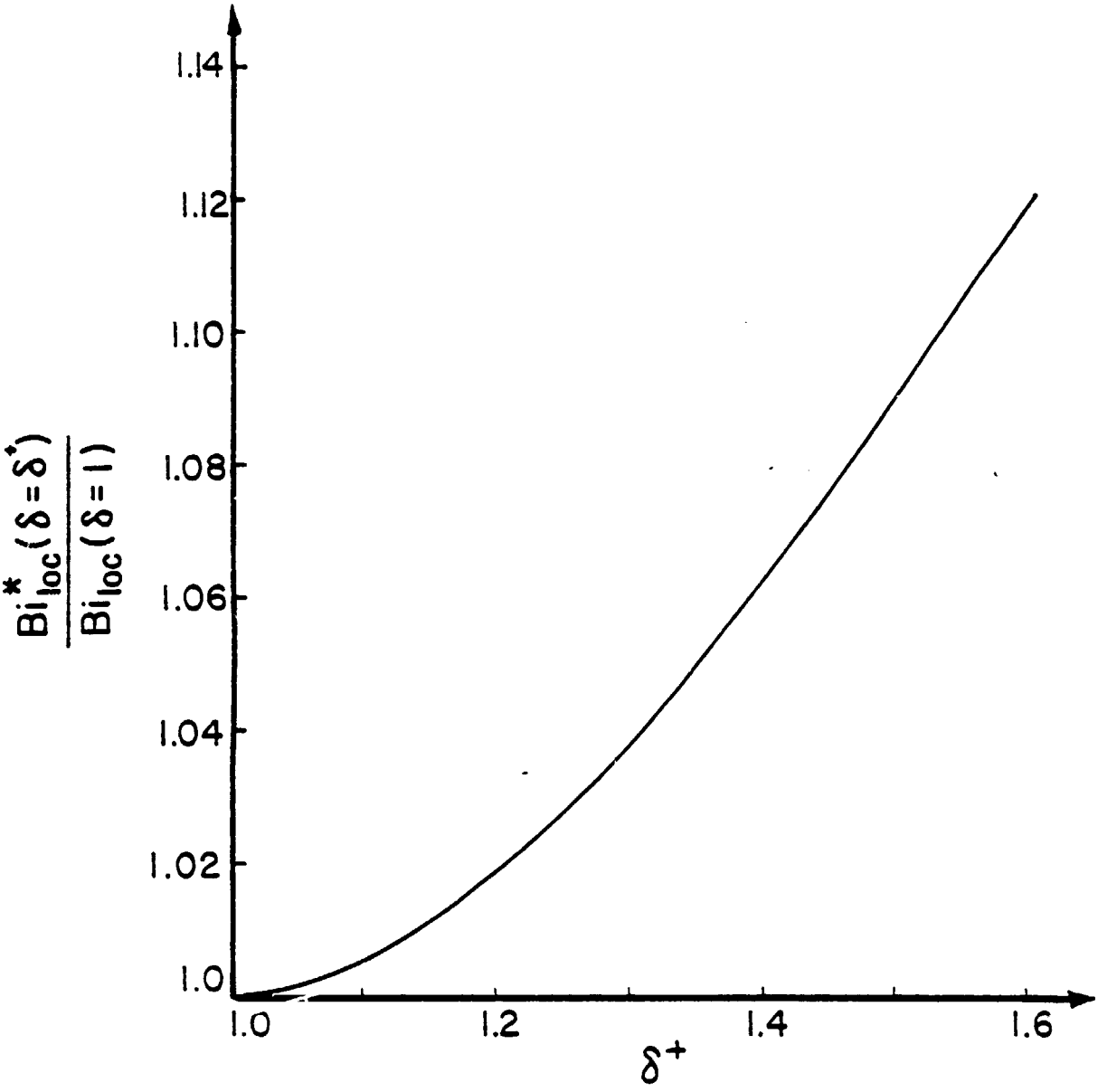

Fig. 4.4: Increase in Bi^*_{loc} caused by using the optimum crucible diameter ratio, δ^+, compared to a charge without a crucible.

strong function of K but correlates well with δ^+.) Accordingly, for those cases where an increase in δ results in an increase in Bi^*, the maximum effect is not large. Therefore, increasing the crucible thickness should not be considered as a viable method for increasing the axial temperature gradients near the growth interface.

4.2.3 Radial Temperature Gradients Within the Charge

Equation [4.1] considers that the temperature within the charge at each axial location is uniform. Presently, radial gradients in the charge are considered insofar as they affect the thermal coupling between the furnace and the charge and thereby the axial temperature distribution.

When radial temperature variations in the charge are taken into consideration, eq. [4.3] assumes the form (see Appendix A):

$$\frac{d^2\theta_m}{d\zeta^2} - Pe^*_{loc}\frac{d\theta_m}{d\zeta} + 4Bi^*_{loc}\left[(\theta_{f,loc} - \theta_m) - (\theta_s - \theta_m)\right] = 0 \qquad [4.11]$$

where: θ_s = surface temperature of the charge, i.e., at $\rho = 1/2$

The term $\theta_s - \theta_m$ in eq. [4.11] accounts for the effect of radial temperature variations within the charge on the q" term of eq. [4.1]. An approximation for $\theta_s - \theta_m$ is obtained by solving in an approximate manner the two-dimensional heat conduction equation in the charge:

$$\frac{1}{\rho}\frac{\partial}{\partial\rho}\left(\rho\frac{\partial\theta}{\partial\rho}\right) + \frac{\partial^2\theta}{\partial\zeta^2} - Pe_{loc}\frac{\partial\theta}{\partial\zeta} = 0 \qquad [4.12]$$

Assuming that the Peclet term is negligible (see section 5.1), and, as in the crucible effect, that $\partial^2\theta/\partial\zeta^2$ is only a weak function of the radial coordinate, ρ, eq. [4.12] can be integrated in the radial direction with

$d^2\theta_m/d\zeta^2$ as a variable. The integration indicates a parabolic variation for the charge temperature at a particular axial location:

$$\theta - \theta_m = -\frac{1}{4}\frac{d^2\theta_m}{d\zeta^2}\left(\rho^2 - \frac{1}{8}\right) \qquad [4.13a]$$

and:

$$\theta_s - \theta_m = -\frac{1}{32}\frac{d^2\theta_m}{d\zeta^2} \qquad [4.13b]$$

Combining eqs. [4.11] and [4.13b] leads to a new effective Biot number, Bi^{**}, replacing Bi in the third term of eq. [4.3a], which accounts for radial temperature gradients within the charge as well as within the crucible:

$$Bi^{**}_{loc} = \frac{Bi^{*}_{loc}}{1 + Bi^{*}_{loc}/8} \qquad [4.14]$$

According to eq. [4.14], $Bi^{**} = Bi^{*}$ for $Bi^{*} \ll 8$; i.e., the radial thermal resistance within the charge does not affect the axial temperature distribution. Equation [4.14] indicates also that the maximum value that Bi^{**} can attain is 8 when Bi^{*} is very large. The internal radial resistance of the charge thus limits the degree to which axial temperature gradients can be increased by an augmentation of the thermal coupling between the charge and the furnace.

The validity of eq. [4.14] may be tested by comparing the axial temperature distributions for a system whose internal thermal resistance in the radial direction is considered (1) exactly through the use of a two-dimensional model and (2) through the use of eq. [4.14]. A stationary fin

(without crucible) of infinite length provides a simple system for which analytical results for both models are readily available (see Fig. 4.5). In order to consider the most extreme case, the heat transfer coefficient at the surface of the fin is taken to be infinite; for these conditions, Bi^* is infinite and $Bi^{**} = 8$. In this case, the expression for the cross sectional area-averaged temperature for the two-dimensional fin is [31]:

$$\theta_{m,2D}(\zeta) = \theta_o \sum_{n=1}^{\infty} \frac{4}{\omega_n^2} \exp(-2\zeta\omega_n) \qquad [4.15]$$

where:

$$J_o(\omega_n) = 0$$

J_o = Bessel function of order zero

and the axial temperature distribution for the one-dimensional fin is [31]:

$$\theta_{m,1D}(\zeta) = \theta_o \exp\left[-2\zeta (Bi^{**})^{-1/2}\right] \qquad [4.16]$$

Equation [4.16] with $Bi^{**} = 8$ is compared to eq. [4.15] in Fig. 4.6 with good results. Equation [4.14] is therefore taken to be a reasonable anaytical approximation for the effect of radial gradients in the charge on the overall axial temperature distribution.

Abrupt changes in surface boundary conditions affect the temperature of the charge more at its surface than at its center. The assumption of constant $\partial^2\theta/\partial\zeta^2$ over the cross section of the charge and, as a consequence, eq. [4.14], are expected to be less valid near such changes in boundary conditions. The moving fin model considers an abrupt change in the heat transfer coefficient at the ends of the gradient zone. Equation [4.14] is least accurate near these locations but becomes increasingly valid with distance into the furnace zones. A further verification of

(a) Two-dimensional model

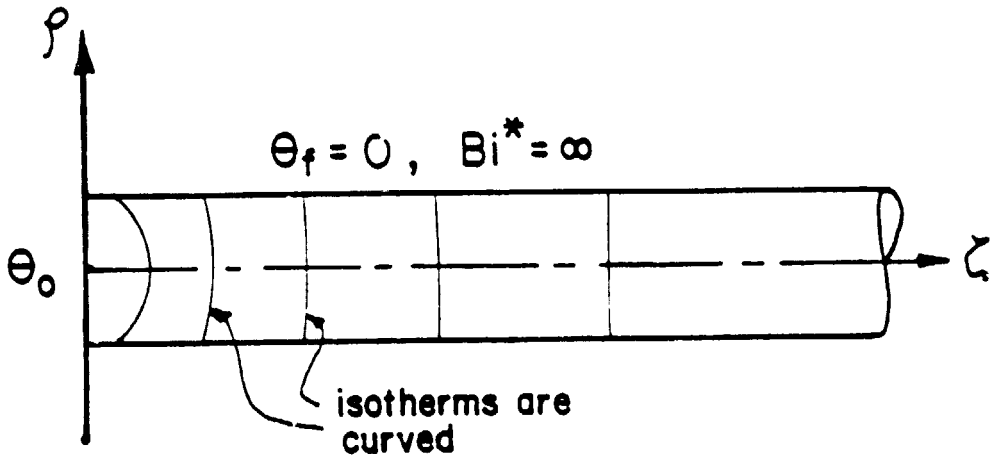

(b) One-dimensional model used with eq.[4.14]

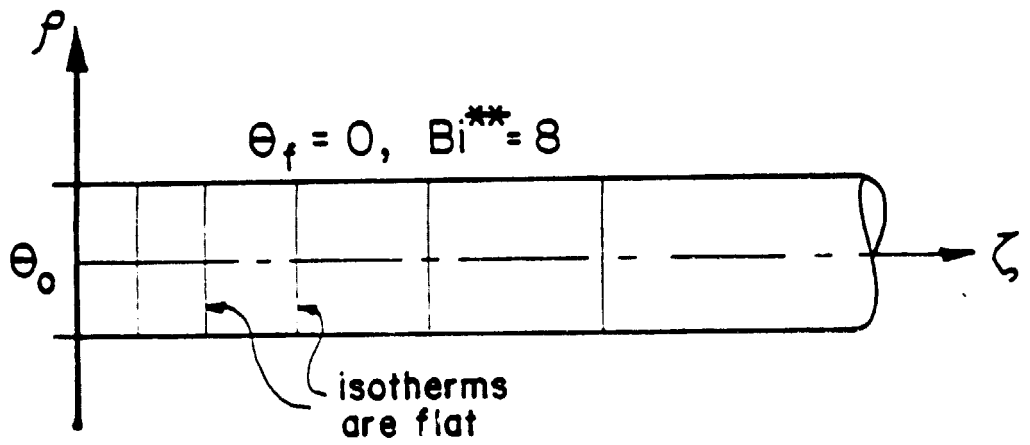

Fig. 4.5: Models of a simple stationary fin used to check the validity of eq. [4.14].

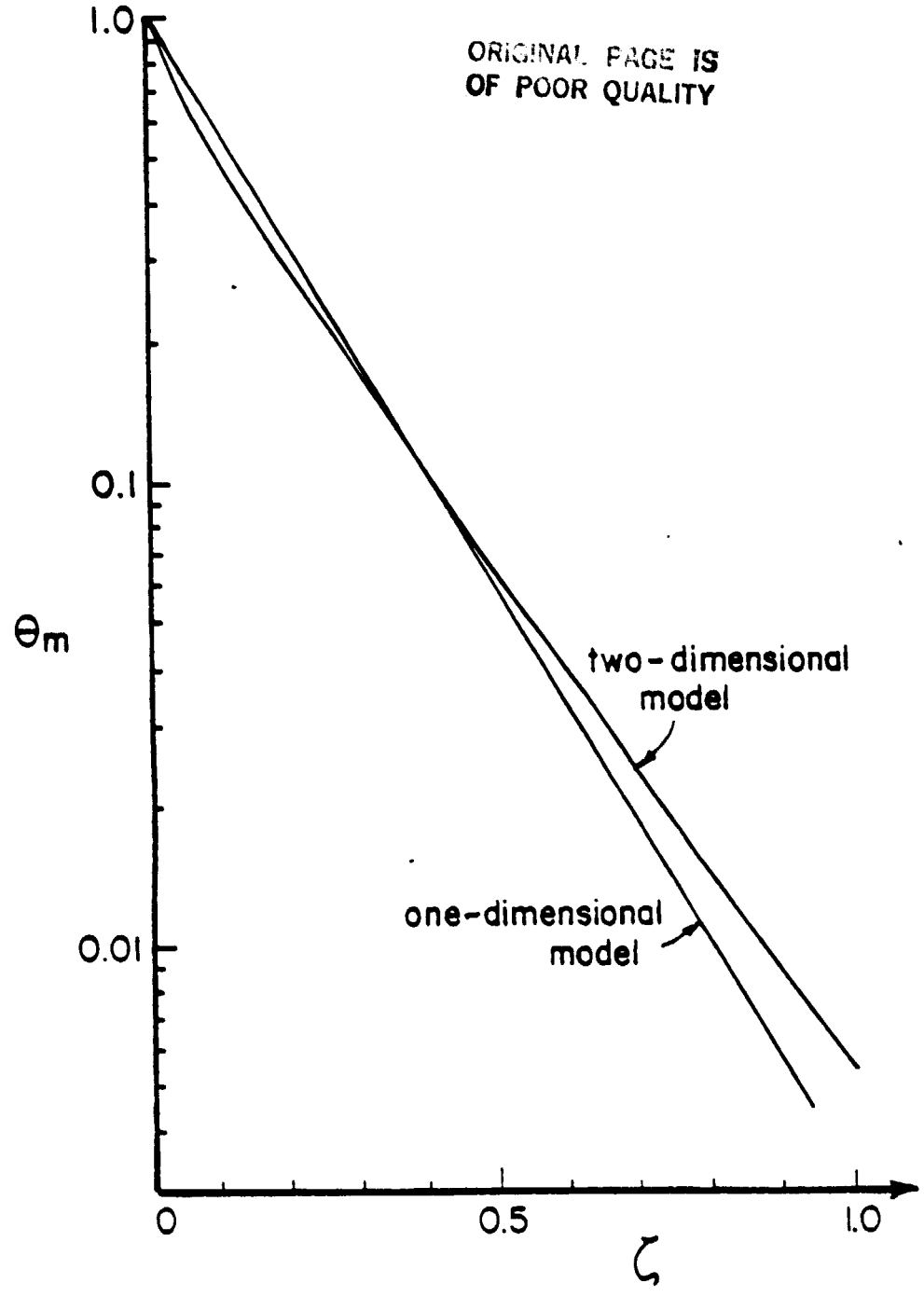

Fig. 4.6: Axial temperature distributions (eqs. [4.15] and [4.16]) for the one- and two-dimensional models of the simple stationary fin used to check the validity of eq. [4.14].

eq. [4.14] obtained for the conditions of an adiabatic gradient zone is provided in section 4.6.

4.3 SOLUTION OF THE MOVING FIN EQUATIONS

Using the results of sections 4.2.2 and 4.2.3 in order to include the effects of the crucible and radial thermal resistance within the charge, eq. [4.3a] becomes:

$$\frac{d^2\theta_m}{d\zeta^2} - Pe^*_{loc}\frac{d\theta_m}{d\zeta} + 4Bi^*_{loc}\left(\theta_{f,loc} - \theta_m\right) = 0 \qquad [4.17]$$

The parameters Pe^*, Bi^{**}, and θ_f are not constant throughout the furnace. According to assumptions 3 and 4 in section 2.2.2, however, they are constant within each of four separate furnace regions: the hot and cold zones and the liquid and solid parts of the gradient zone. (It is assumed that the growth interface is located within the gradient zone.) The solution of eq. [4.17] within each region yields two exponential terms for the homogeneous solution and a particular solution that depends on θ_f. The assumption of uniform hot and cold zone furnace temperatures yields a simple constant for the particular solution in these zones. A particular solution is not needed in the gradient zone since $h_G = 0$.

The constants of integration for the homogeneous solution of eq. [4.17] are found using the boundary conditions of equality of temperature and continuity of heat flux between adjacent regions. The temperature boundary condition is:

$$\theta_{m,j} = \theta_{m,k} \qquad [4.18]$$

where the subscripts "j" and "k" refer to opposite sides of a boundary

between adjacent regions. The flux boundary conditions used in the moving fin model are:

$$\frac{d\theta_{m,j}}{d\zeta} = \frac{d\theta_{m,k}}{d\zeta}$$

between the hot and gradient zones — or — between the gradient and cold zones [4.19]

$$\left[R_K + K_s(\delta^2-1)\right]\left(\frac{d\theta_m}{d\zeta}\right)_L =$$

$$\left[1 + K_s(\delta^2-1)\right]\left(\frac{d\theta_m}{d\zeta}\right)_s + Pe_s R_H$$

at the growth interface [4.20]

Section 4.4.3 explains that the axial gradients in the gradient zone which result from the use of eq. [4.20] should be interpreted as average charge/crucible axial gradients; these average gradients will be denoted by G_L and G_S for the liquid and solid sides of the interface respectively. Unavoidable radial heat transfer between the charge and the crucible near the growth interface causes G_L and G_S to significantly differ from their respective counterparts in the charge, $(d\theta_m/d\zeta)_L$ and $(d\theta_m/d\zeta)_s$. The relevant axial gradient for the supercooling requirement is, however, that in the charge. Evaluation of the difference between G and $d\theta_m/d\zeta$ at the growth interface requires two-dimensional modeling and is therefore considered in Chapter 7.

Boundary conditions at the end of the charge must be applied when the charge length can not be considered infinite (c.f., section 5.5). Appendix D discusses the calculation of approximate Biot numbers for the nondimensional end boundary conditions.

The constants of integration have been determined analytically for systems of infinite charge length; expressions for the axial gradient in

the melt at the interface and for the axial position of the interface of such systems are given in Appendix B. Of special interest are the simplified results obtained for the small lowering rates common to semiconductor crystal growth, eqs. [B.9] and [B.10]. If the complete axial temperature distribution is desired, or if the charge length is not infinite, it is more convenient to determine the constants of integration by computer.

4.4 ASSUMPTIONS IN THE MOVING FIN MODEL

The validity of the primary assumptions employed in the development of the moving fin thermal model of section 4.2 is discussed in this section.

4.4.1 Equal Axial Gradients of the Charge and Crucible

In order to obtain a simple analytical expression for the effect of the crucible thickness and conductivity on the axial temperature distribution of the charge, the crucible model (section 4.2.2) assumes that the first and second axial temperature derivatives in the crucible are independent of the radial coordinate, ρ , and equal to their respective values within the charge. These approximations are motivated by the two-dimensional temperature distributions presented by Wilcox et.al. [24,26]. Sen and Wilcox [24] determined isotherm shapes in a charge/crucible system for various K and Bi by a two-dimensional finite difference computer model under the following simplified conditions: $\delta = 1.25$, $\lambda_G = 0.0$, $Pe = 0.0$, $\lambda_C = \lambda_H = .75$, $R_K = 1.0$, $R_H = 0.0$. The shapes of their numerically computed isotherms indicate that the assumptions are reasonable for values of K greater than about 1/2. As K decreases below 1/2 (e.g., as k_{cr} decreases), increasing radial resistance of the crucible produces a

pronounced radial temperature variation in the crucible; the axial gradients in the crucible are larger than those in the charge near the ends of the hot and cold zone. It is therefore expected that the crucible effect, as described by eqs. [4.7] and [4.8] will be most in error for small values of K.

The temperature distributions of Fu and Wilcox [26] indicate that the radial variation of the axial gradients are most pronounced at the ends of the hot and cold zones, especially for systems without a gradient zone. The absence of a gradient zone in the model of Sen and Wilcox [24] therefore accentuates the error in the approximation for systems with a gradient zone.

The two-dimensional thermal model developed in Chapter 6 does not assume that axial temperature gradients in the charge and crucible are equal. The effect of the crucible on the axial temperature gradients of the charge determined by the two-dimensional model are compared to results given by the one-dimensional model using Bi^{**}. Agreement is good even for values of K as small as 0.1. It is therefore concluded that the effective Biot number provides a reasonable estimate of the crucible effect on the axial temperature distribution of the charge.

4.4.2 Equal Growth and Lowering Rates

The term $Pe_S R_H$ in eq. [4.20] represents the generation of latent heat at the growth interface; the velocity used in Pe_S should therefore be the actual growth rate, R. When the charge length is not infinite, however, the growth rate exceeds the lowering rate, V, [9,11,22]. The present model neglects the difference between V and R under such conditions and uses Pe_S based on the lowering rate V. In this way, the mathematical solution is

simplified since the rate of generation of latent heat then has a known and constant value. On the other hand, if the growth rate, R, were used, the rate of generation of latent heat would not be known a priori or constant.

The assumption that R=V in not exessively restrictive. Riquet and Durand [9] and Sukanek [22] show that the growth rate is most different from the lowering rate when the ends of the charge are passing zone boundaries. When the length of the charge in both the hot and cold zones can be considered infinite (see section 5.5), the growth rate and lowering rate are equal. Further, growth conditions may be such so that the effect of latent heat on the axial temperature profile is negligible (see section 5.4); the error created by the use of V rather than R in Pe_S would then be likewise small. Lastly, if desired, the solution of eq. [4.17] can be modified so that Pe_S in eq. [4.20] is based on R as follows: The axial position of the growth interface for two closely spaced locations of the charge in the furnace is calculated with an initial assumed value of R. The difference in position of the interface for these two locations indicates a growth rate which need not be equal to the original assumed value. The growth rate is accordingly modified and the procedure iterated until convergence is achieved.

4.4.3 Flux Boundary Condition at the Growth Interface

Consider that the charge and crucible temperatures, ϕ_m and ϕ_{cr} respectively, are each represented by a single value at each axial location. (The variable ϕ is used in this work to denote non-dimensional temperatures employed in two-dimensional thermal models.) When $Pe_S R_H \neq 0$ and/or $R_K \neq 0$, the axial gradient in the charge, $d\phi_m/d\zeta$, must undergo an abrupt change at the growth interface. The axial gradient in the crucible,

on the other hand, does not change at the growth interface. Figure 4.7 shows that such conditions lead to a difference between the charge and crucible temperatures as well as their axial temperature gradients. The temperature difference leads to an exchange of heat between the charge and crucible near the growth interface. The relationship between this radial heat transfer and the shape of isotherms is discussed in section 7.3; the present section addresses its effect on the flux boundary condition at the growth interface for the moving fin model, eq. [4.20].

Define an average charge/crucible temperature weighted by their respective axial thermal conductances:

$$\bar{\phi} = \frac{k_{loc} A \phi_m + k_{cr} A_{cr} \phi_{cr}}{k_{loc} A + k_{cr} A_{cr}} \qquad [4.21]$$

k_{loc} is respectively k_L and k_S for the liquid and solid portions of the charge. Nondimensionalizing eq. [4.21] yields:

$$\bar{\phi} = \frac{\phi_m + K_{loc}(\delta^2-1)\,\phi_{cr}}{1 + K_{loc}(\delta^2-1)} \qquad [4.22]$$

Differentiating eq. [4.22] in the liquid and solid yields:

$$G_L \equiv \left(\frac{d\bar{\phi}}{d\zeta}\right)_L = \frac{R_K \left(\frac{d\phi_m}{d\zeta}\right)_L + K_s(\delta^2-1)\left(\frac{d\phi_{cr}}{d\zeta}\right)_L}{R_K + K_s(\delta^2-1)} \qquad [4.23a]$$

$$G_s \equiv \left(\frac{d\bar{\phi}}{d\zeta}\right)_s = \frac{\left(\frac{d\phi_m}{d\zeta}\right)_s + K_s(\delta^2-1)\left(\frac{d\phi_{cr}}{d\zeta}\right)_s}{1 + K_s(\delta^2-1)} \qquad [4.23b]$$

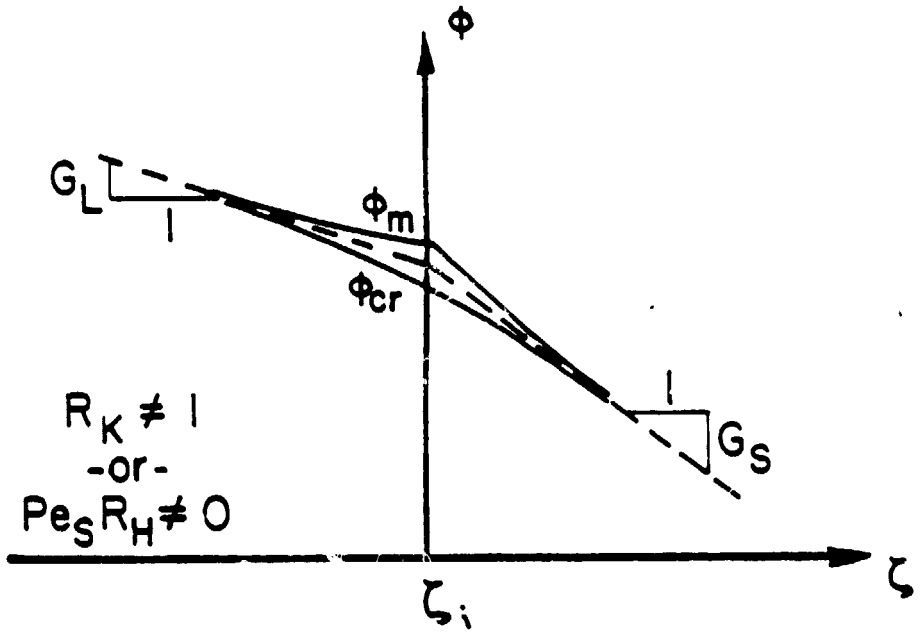

Fig. 4.7: Crucible and mean charge temperature distributions near the interface when $Pe_S R_H \neq 0$ and/or $R_K \neq 1$.

The moving fin model assumes that $B_G = 0$. In this case, there is no heat transfer to or from the surface of the crucible in the gradient zone and G must be invariant in the gradient zone except for a step change at the growth interface. The relationship between G_L and G_S is found by considering the heat flux boundary condition at the growth interface. In nondimensional form:

$$R_K\left(\frac{d\phi_m}{d\zeta}\right)_{L,i} = \left(\frac{d\phi_m}{d\zeta}\right)_{S,i} + Pe_s R_H \qquad [4.24a]$$

$$\left(\frac{d\phi_{cr}}{d\zeta}\right)_{L,i} = \left(\frac{d\phi_{cr}}{d\zeta}\right)_{S,i} \qquad [4.24b]$$

where subscript "i" denotes the interface

By multiplying eq. [4.24b] by $K_s(\delta^2-1)$, adding to eq. [4.24a] and using eqs. [4.23], the following relation is obtained:

$$\left[R_K + K_s(\delta^2-1)\right] G_L = \left[1 + K_s(\delta^2-1)\right] G_S + Pe_s R_H \qquad [4.25]$$

The one-dimensional moving fin model neglects the difference between ϕ_m and ϕ_{cr} ; i.e., $\phi_m = \phi_{cr} = \theta_m$. In this case, eqs. [4.23] show that:

$$G_L = \left(\frac{d\theta_m}{d\zeta}\right)_L \qquad [4.26a]$$

$$G_S = \left(\frac{d\theta_m}{d\zeta}\right)_S \qquad [4.26b]$$

Substituting eqs. [4.26] into eq. [4.25] results in the interface boundary condition used by the moving fin model, eq. [4.20]. These results suggest that the axial temperature gradient in the gradient zone predicted by the

moving fin model, $d\theta_m/d\zeta$, should be interpreted as the average charge/crucible axial gradient, G. The difference between G and $d\phi_m/d\zeta$ is discussed in section 7.3.

4.4.4 Diabatic Gradient Control Region

The moving fin model assumes that there is no heat exchange between the charge and the furnace within the gradient control region; i.e., $h_G = 0$. Chang and Wilcox [17] suggested the use of an adiabatic gradient control region as a means of reducing isotherm curvature near the growth interface. Further motivation for this assumption is that it simplifies the analytical expression of the temperature distribution in the solidifying charge.

A perfectly insulating gradient control region is a conceptual limit and is unobtainable in practice. Radial heat transfer to or from the charge in the gradient zone affects isotherm curvature; the assumption of an adiabatic gradient control region is therefore eliminated in the two-dimensional model described in Chapter 6. The present section formulates a simple model of heat exchange within the gradient control region in order to determine when this heat exchange is negligible with regard to the axial temperature distribution of the charge.

Consider the portion of the furnace in the gradient control region to be an annulus located between and in contact with the hot and cold heat pipes. The gradient zone annulus has conductivity k_G, cross sectional area A_G, and has a temperature, $T_G(Z)$ which depends only on the axial coordinate. Heat exchange between the gradient zone annulus is described by the gradient zone heat transfer coefficient h_G. No heat loss is assumed at the outer diameter of the gradient zone annulus. (This model of the

gradient control region is identical to that used in Chapter 6; c.f., section 6.2 and Figs. 6.1 and 6.2.)

In order to develop a relatively simple expression for the temperature distributions of the charge and gradient zone annulus, the present system is specified by the following parameter values:

1. Equal heat transfer coefficients in the hot and cold zones.
2. Axial convection of heat due to the charge motion is negligible; i.e., Pe is small. (See section 5.1.)
3. The effect of the generation of latent heat is negligible; ($Pe_S R_H = 0$). (See section 5.4.)
4. Equal thermal conductivities of the melt and crystal ($R_K = 1$). With condition 1 above, $Bi_H^{**} = Bi_C^{**}$.
5. Equal charge lengths in the hot and cold zones ($\lambda_H = \lambda_C$).

A system which has the above parameter values is referred to in the present work as a "symmetric" system. The axial temperature distribution of the charge for a symmetric system is:

$$\theta_m(\zeta) + \theta_m(-\zeta) = 1 \qquad [4.27]$$

It is only necessary to consider one-half of a symmetric system, either $\zeta > 0$ or $\zeta < 0$. An additional assumption used in this section is that the charge length is infinite; in this way, the absence of the end

boundary conditions and charge length as thermal parameters simplifies the expressions for the temperature distributions of the charge and gradient zone annulus.

A schematic of the temperature distributions in the charge and gradient zone annulus is shown in Fig. 4.8. Only the cold portion of the symmetric system is shown. At the center of the gradient zone (i.e., at $\zeta = 0$), the assumption of a symmetric system dictates that $\theta_m = \theta_G = 0.5$. The cold end of the gradient zone annulus is at the cold zone heat pipe temperature.

The equation governing the mean charge temperature in the cold zone is adapted from eq. [4.17] assuming that Pe = 0.0:

$$\frac{d^2\theta_m}{d\zeta^2} + 4Bi_c^{**}(\theta_{f,c} - \theta_m) = 0 \qquad [4.28]$$

where: $\zeta \geq \mu \equiv \lambda_G/2$

The charge temperature in the gradient zone is described by eq. [4.28] with Bi_C^{**} replaced by Bi_G^{**} and $\theta_{f,c}$ replaced by θ_G:

$$\frac{d^2\theta_m}{d\zeta^2} + 4Bi_G^{**}(\theta_G - \theta_m) = 0 \qquad [4.29]$$

where: $0 \leq \zeta \leq \mu$

The fin equation for the gradient zone annulus can be derived by noting that the transfer of heat between it and the charge/crucible requires the following relation between the second axial derivatives:

$$\frac{d^2\theta_m}{d\zeta^2}(kA + k_{cr}A_{cr}) = -\frac{d^2\theta_G}{d\zeta^2}(k_G A_G) \qquad [4.30]$$

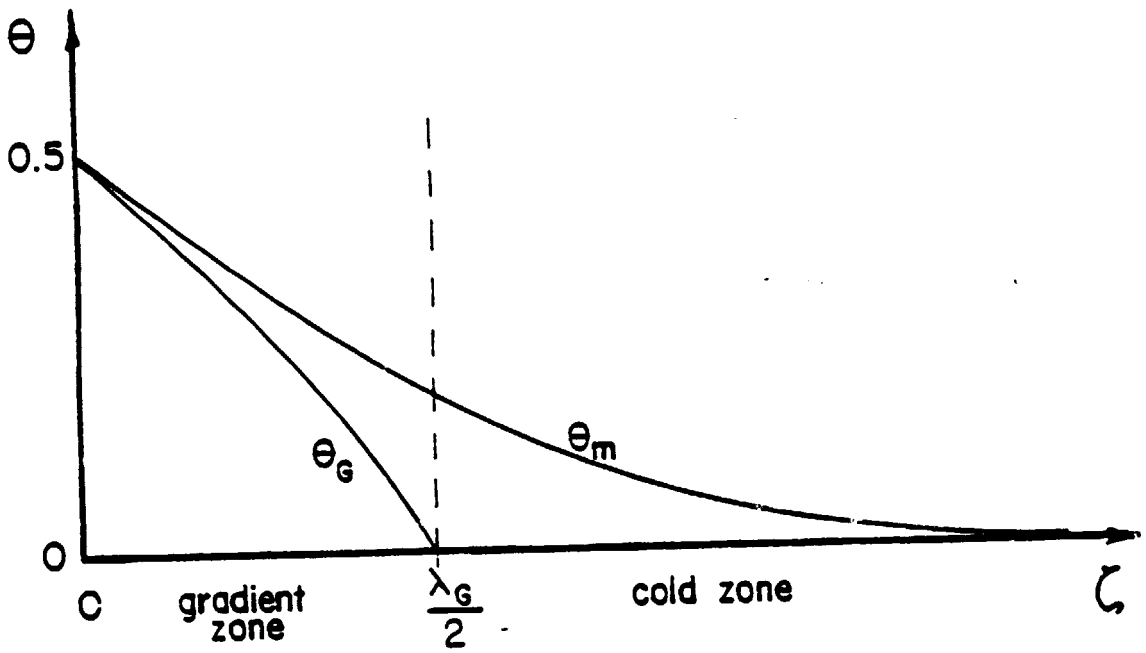

Fig. 4.8: Schematic of the temperature distribution in the charge and gradient zone annulus for a symmetric system when $Bi_G \neq 0$.

(Equation [4.30] assumes that the axial conduction of heat in the crucible is described by the axial derivatives of θ_m .) Substituting eq. [4.30] into eq. [4.29]:

$$\frac{d^2\theta_G}{d\zeta^2} + \frac{1+K_s(\delta^2-1)}{R_{G,S}} \cdot 4Bi_G^{**}(\theta_m - \theta_G) = 0 \qquad [4.31]$$

where: $$K_s(\delta^2-1) = \frac{k_{cr}A_{cr}}{k_s A}$$

$$R_{G,S} = \frac{k_G A_G}{k_s A}$$

$$0 \leq \zeta \leq \mu$$

Equations [4.28], [4.29] and [4.31] are simultaneously solved utilizing the following boundary conditions:

$$\theta_G(0) = 0.5$$

$$\theta_G(\mu) = 0$$

$$\theta_m(0) = 0.5 \qquad [4.32]$$

$$\theta_m(\infty) = 0$$

$$[\theta_m(\mu)]_G = [\theta_m(\mu)]_c$$

$$\left[\frac{d\theta_m(\mu)}{d\zeta}\right]_G = \left[\frac{d\theta_m(\mu)}{d\zeta}\right]_c$$

The resulting distribution for the temperature difference between the charge and gradient zone annulus is:

$$(\theta_m - \theta_G) = \frac{\frac{1}{2}\frac{\sinh(w_G \zeta_o)}{\sinh(w_G \mu)}}{\frac{1}{R_G^* + 1} + \frac{R_G^*}{R_G^* + 1}\frac{\mu w_G}{\tanh(\mu w_G)} + \mu w_m} \qquad [4.33]$$

where: $w_G = 2\left[Bi_G^{**}\left(1 + R_G^{*-1}\right)\right]^{1/2}$

$$w_m = 2\left(Bi_c^{**}\right)^{1/2}$$

$$R_G^* = R_G / \left[1 + K_s(\delta^2 - 1)\right]$$

Equation [4.33] demonstrates that the difference in temperature between the gradient zone annulus and the charge varies exponentionally and decreases more rapidly for larger Bi_G^{**} and smaller R_G^*. A large value of Bi_G^{**} is indicative of effective thermal coupling between the charge and gradient zone annulus. A small value of R_G^* indicates that the gradient zone annulus has a relatively small capacity to conduct heat in the axial direction compared to that of the charge/crucible combination; consequently, any heat transfer to or from the gradient zone annulus serves to rapidly equilibrate θ_G to θ_m.

The importance of heat transfer in the gradient zone compared to that occuring in the hot and cold zones on the axial temperature distribution of the charge is revealed by the expression for the axial temperature gradient in the charge at the center of the gradient zone:

$$2 \cdot G(\zeta = 0) = \frac{\frac{R_G^*}{R_G^* + 1}\left\{w_G\left[\frac{1}{\sinh(\mu w_G)} - \frac{1}{\tanh(\mu w_G)}\right]\right\} - w_m}{\frac{1}{R_G^* + 1} + \frac{R_G^*}{R_G^* + 1}\frac{\mu w_G}{\tanh(\mu w_G)} + \mu w_m} \qquad [4.34]$$

Figure 4.9 shows the variation of $G(\zeta = 0)$ with R_G^* for systems with $Bi_G^{**} = Bi_C^{**}$. When $R_G^* = 0$, the gradient zone does not conduct heat from the hot or cold zones for subsequent exchange to or from the charge; in this case, the gradient zone may be called adiabatic even though $Bi_G \neq 0$. As R_G^* increases, the temperature distribution of the gradient zone annulus becomes increasingly linear providing a temperature difference between it and the charge; the resulting heat exchange increases the axial temperature gradient of the charge. As R_G^* approaches infinity, the heat exchange between the gradient zone annulus and charge is little affected by changes in R_G^* since $\theta_G(\zeta)$ approaches its limiting linear variation.

Figure 4.10 demonstrates the effect of Bi_G^{**} for systems with $R_G^* = 1.0$. The adiabatic gradient zone case is indicated by the curve labeled $Bi_G^{**}/Bi_C^{**} = 0.0$. Heat exchange between the charge and gradient zone annulus becomes increasingly important as Bi_G^{**} increases relative to Bi_C^{**}, resulting in a significant increase in the axial gradient of the charge. In the limit as Bi_G^{**} approaches infinity, the temperature distribution of the charge in the gradient zone varies linearly between the boundary conditions imposed by the hot and cold zone furnace.

The results presented in this section were based on a model which assumed infinite charge length. Further, Figs. 4.9 and 4.10 examined the special case of $\lambda_G = 1.0$. It is expected that the effect of a diabatic gradient zone increases as the relative length of the gradient zone increases (e.g., finite charge length and increasing λ_G). Nevertheless, the results of this section suggest that the gradient zone can be made effectively adiabatic by two design options:

(1) Small R_G. A material of poor thermal conductivity placed

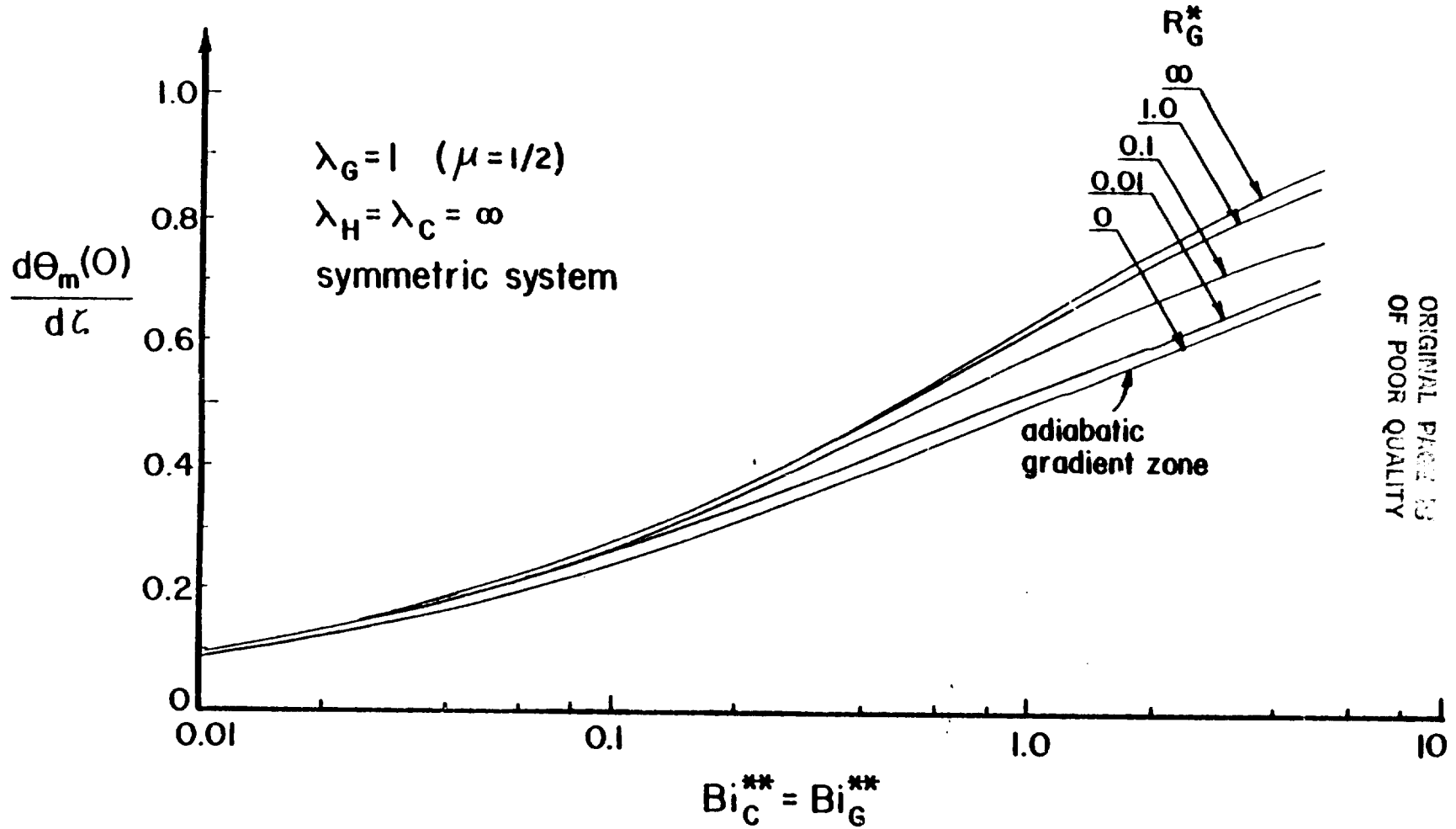

Fig. 4.9: The effect of R_G^* on the axial temperature gradient at the interface for a symmetric system and $Bi_G^{**} = Bi_C^{**}$.

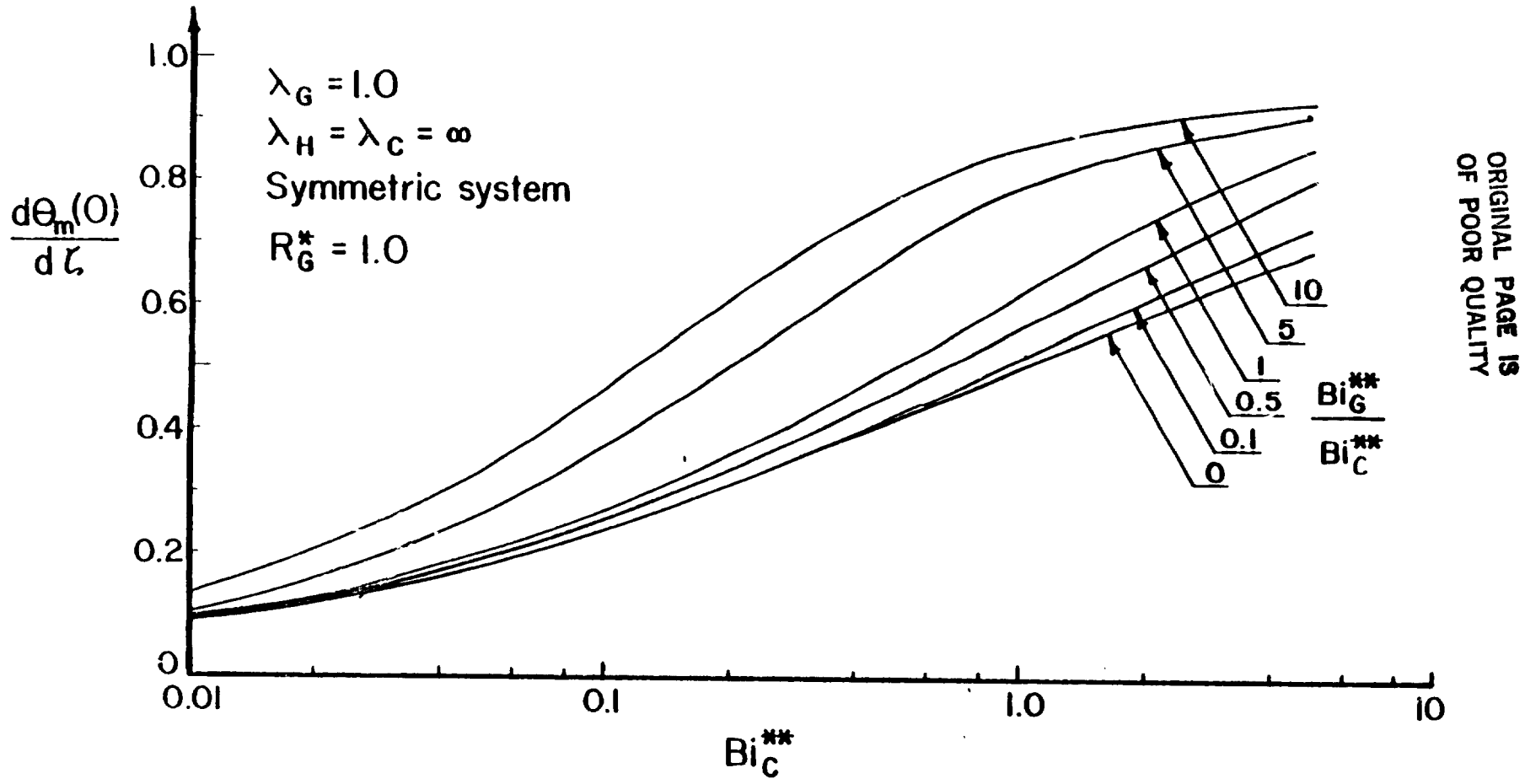

ORIGINAL PAGE IS
OF POOR QUALITY

Fig. 4.10: The effect of Bi_G^{**} on the axial temperature gradient at the interface for a symmetric system and $R_G^* = 1.0$.

between the hot and cold zone furnaces provides for a small value of R_G.

(2) Small Bi_G relative to the Biot numbers in the hot and cold zones. This may be accomplished in systems where the conductive component to the gap heat transfer coefficient is small (see Appendix C) by placing highly reflecting radiation shields between the gradient zone annulus and the charge.

4.5 THERMAL PARAMETERS OF THE MOVING FIN MODEL

The thermal parameters which appear in the moving fin model are summarized in Table 4.1

4.6 COMPARISON WITH THE TWO-DIMENSIONAL RESULTS OF FU AND WILCOX [26]

Results derived from the present one-dimensional model can be compared to similar results of Fu and Wilcox [26] who included radial temperature gradients within the charge in a two-dimensional finite difference model. Figure 3 of their paper presents the radial variation of the axial gradient at the growth interface for systems of infinite charge length in the absence of a crucible. Point values, estimated from the curves of their Fig. 3, were numerically integrated to obtain the average axial gradient over the cross section at the growth interface. These results are compared to the values obtained using eqs. [4.14] and [5.8] for several values of Bi and λ_G in Table 4.2.

Since the model of Fu and Wilcox [26] does not include a crucible, the comparison shown in Table 4.2 tests the validity of eq. [4.14] in accounting for the effect of radial thermal resistance of the charge on the effective Biot number. Considering the approximations required in the derivation of eq. [4.14], the agreement of the data must be taken as

excellent. It is considered, therefore, that eq. [4.14] provides a reasonable correction for the effect of radial temperature variations within the charge on the axial temperature distribution of the charge. (The validity of eq. [4.7] in accounting for the effect of the crucible on the effective Biot number is provided in section 6.3.)

parameter	definition	comments
Bi_H	$h_H D/k_L$	
Bi_C	$h_C D/k_S$	
Pe_S	$VDk_S/\rho c_p$	$Pe_L = Pe_S R_K$
δ	D_{cr}/D	
K_S	k_{cr}/k_S	$K_L = K_S/R_K$
$R_{\alpha,S}$	α_{cr}/α_S	$R_{\alpha,L} = R_{\alpha,S}/R_K$
R_K	k_L/k_S	
R_H	$\Delta H_{sl}/c_p(T_{f,H} - T_{f,C})$	
λ_G	L_G/D	
λ_H	L_H/D	required only if the charge can not be considered infinitely long (c.f., section 4.2.5)
λ_C	L_C/D	
$Bi_{H,end}$	$h_{H,end}D/k_L$	
$Bi_{C,end}$	$h_{C,end}D/k_S$	
ζ_i	z_i/D	only one is independent
θ_i	$\dfrac{(T_i - T_{f,C})}{(T_{f,H} - T_{f,C})}$	

Table 4.1: Thermal parameters in the moving fin model.

	λ_G	$(\partial\theta/\partial\zeta)_{av}$ Fu and Wilcox [26]	G Eqs. [4.14] and [5.8]
Bi = 2 (Bi^{**} = 1.6)	0.0	1.310	1.261
	0.25	0.975	0.961
	0.50	0.778	0.775
Bi = 0.4 (Bi^{**} = 0.38)	0.0	0.616	0.617
	0.5	0.464	0.472

Table 4.2: Axial temperature gradients at the growth interface, G, as obtained through eqs. [4.14] and [5.8], and average axial temperature gradients, $(\partial\theta/\partial\zeta)_{av}$, as determined from the two-dimensional model of Fu and Wilcox [26]. (Symmetric system and no crucible.)

5. THE AXIAL TEMPERATURE DISTRIBUTION OF THE CHARGE

This chapter describes the effects of the thermal parameters of the vertical Bridgman growth system on the one-dimensional thermal behavior of the charge. The presentation of the results emphasizes the thermal requirements for satisfactory single crystal growth developed in section 2.1 which relate to the axial temperature distribution in the charge: (1) the axial gradient in the liquid at the growth interface (constitutional supercooling) and (2) the axial position of the growth interface (a factor strongly affecting the shape of the interface).

Axial temperature distributions in the charge are calculated by computer using the moving fin model described in Chapter 4. Such results indicate how the interface position (or the nondimensional melt temperature) is affected by the thermal parameters. The axial temperature gradient within the melt in the gradient zone, is studied by utilizing the analytical results presented in Appendix B.

Section 4.4.3 explains that the axial temperature gradient at the interface calculated from the moving fin model must be interpreted as the average of the charge and crucible axial gradients. The variable G is used to denote this average value. The difference between G and the axial temperature gradient in the charge is discussed in section 7.3.

For a particular growth experiment having constant process parameters (e.g., furnace temperature, lowering rate) the temperature of the interface and its location within the furnace are functionally related. Since the shape of the interface strongly depends on its axial location [17,26 and Chapter 7], it is expedient to consider the interface location as the

independent variable. Given the interface location, the thermal model predicts a nondimensional interface temperature, θ_i; the dimensional interface temperature, T_i, is related to the hot and cold zone furnace temperatures and θ_i as follows:

$$T_i = T_{f,C} + \theta_i (T_{f,H} - T_{f,C}) \qquad [5.1]$$

The desired interface location is achieved by adjusting the hot and/or cold zone furnace temperatures so that eq. [5.1] is satisfied.

In consideration of the many variables in the moving fin model, the symmetric system defined in section 4.4.4 is used as a reference against which the effects of individual parameters will be compared.

5.1 PECLET NUMBER EFFECT

The Peclet number expresses the ratio of axial heat transfer in the charge due to the lowering velocity, V, and due to conduction. The effective Peclet number, Pe^*, incorporates the effect of the crucible on the convection term of eq. [4.1a]. The unmodified Peclet number is used to describe the generation of latent heat (eq. [4.20]).

The effect of Pe^* on the axial temperature distribution in an otherwise symmetric system obtained through eq. [4.17] is shown in Fig. 5.1. It is seen that Pe^* tends to increase the temperature of the charge at all locations; the effect is more pronounced as Pe^* increases (e.g., high lowering rate or low thermal conductivity of the charge). As a consequence, in systems with fixed hot and cold zone furnace temperatures (i.e., the nondimensional melting point temperature is constant), the growth interface moves toward the cold zone as Pe^* increases; alternatively, the nondimensional melting point temperature must increase

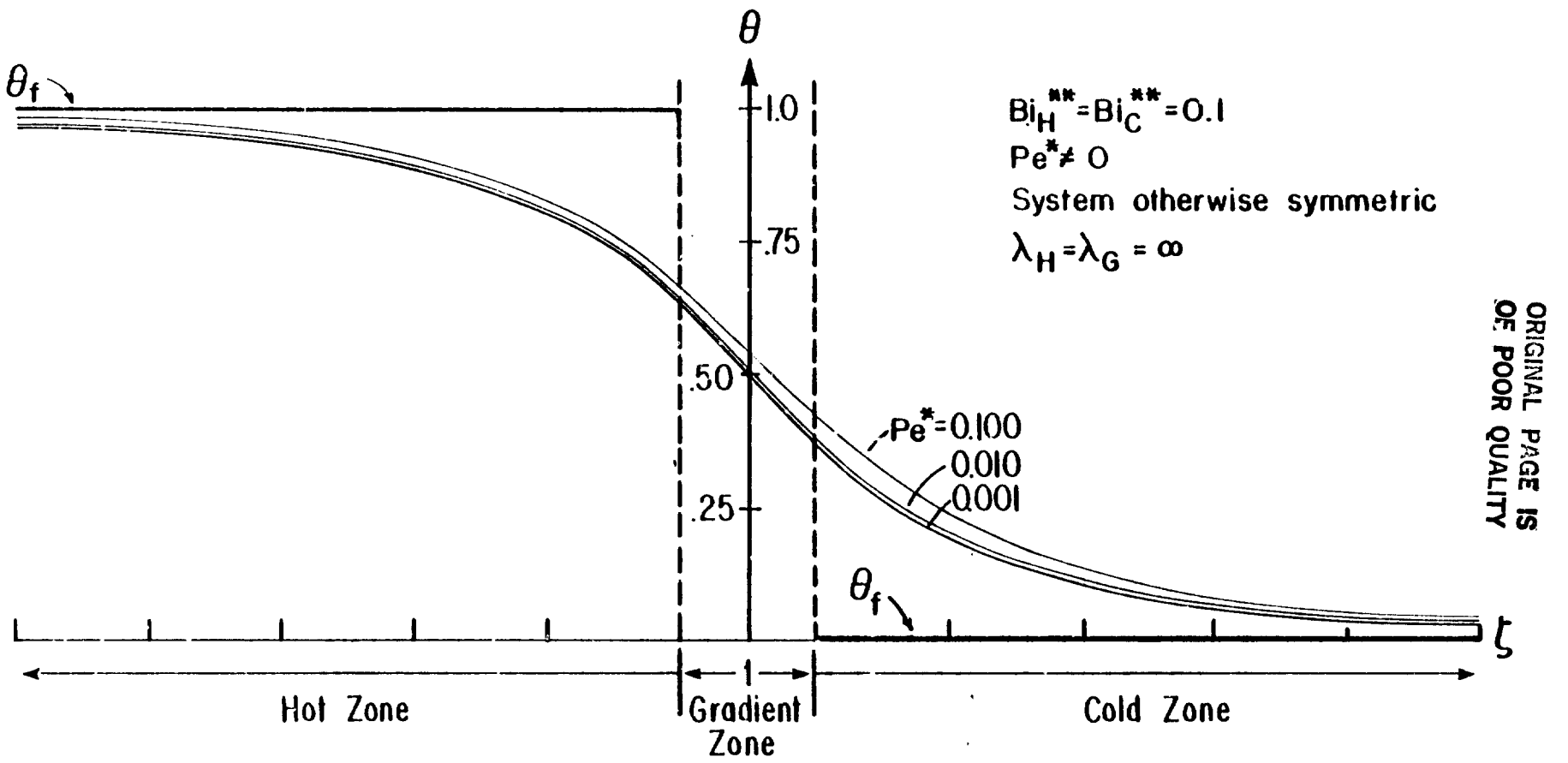

Fig. 5.1: Effect of charge motion on the axial temperature distribution of the charge.

(i.e., one or both of the furnace temperatures must be lowered) if the interface is to remain at the same axial location as Pe^* increases.

Table 5.1 gives expressions for the Peclet number based on solid properties for Ge and CdTe (materials with high and low thermal conductivity, respectively) as a function of lowering rate V and charge diameter D. Using lowering rates common to Bridgman growth experiments (e.g., .1-10 μm/sec), it is seen that the Peclet number is small compared to unity. A test criterion for its relative magnitude is provided through the characteristic roots of eq. [4.17]:

$$w_m = \frac{Pe^*}{2}\left\{1 \pm \left[1 + 16\,\frac{Bi^{**}}{(Pe^*)^2}\right]^{1/2}\right\} \qquad [5.2]$$

Expanding eq. [5.2]:

$$w_m = \frac{Pe^*}{2} \pm 2\,(Bi^{**})^{1/2}\left\{1 + \frac{1}{2}\,\frac{(Pe^*)^2}{16\,Bi^{**}} - \frac{1}{8}\left[\frac{(Pe^*)^2}{16\,Bi^{**}}\right]^2 + \cdots\right\} \qquad [5.3]$$

	α_s	Pe_s
Ge	.097 cm^2/sec	VD/967
CdTe	.011 cm^2/sec	VD/111

α = thermal diffusivity

V measured in μm/sec

D measured in cm

Table 5.1: Magnitude of typical Peclet numbers.

If the following inequality holds, the characteristic values, w_m, are of opposite sign and their sum is equal to Pe^*:

$$\text{if:} \quad \frac{1}{2}\,\frac{(Pe^*)^2}{16\,Bi^{**}} \ll 1 \qquad [5.4]$$

$$\text{then:} \quad w_m = \frac{Pe^*}{2} \pm 2\,(Bi^{**})^{1/2} \qquad [5.5]$$

Further, Pe^* disappears from the characteristic roots under the following conditions:

$$\text{if:} \quad \frac{Pe^*}{4\,(Bi^{**})^{1/2}} \ll 1 \qquad [5.6]$$

$$\text{then:} \quad w_m = \pm 2\,(Bi^{**})^{1/2} \qquad [5.7]$$

Equation [5.6] agrees with Chang and Wilcox [17] who reported that the Peclet effect is stronger for smaller Biot numbers.

If the inequality in eq. [5.6] holds, the Peclet effect is small enough to satisfy the Peclet number criterion for symmetric systems (i.e., Pe=0); in addition, simplified analytical expressions are obtained for the axial gradient within the melt in the gradient zone (Appendix B). Since eq. [5.6] does hold for typical Bridgman growth, the simplified expressions are used in the remainder of this chapter.

Equation [4.20] shows that the generation of latent heat at the growth interface is also dependent on Pe. The charge lowering rate, therefore, has a small effect on the axial temperature distribution if both eq. [5.6] holds and the latent heat effect is small. (Sections 5.4 and 7.3 address

the effect of latent heat on the axial temperature distribution in the charge and on the radial temperature variations near the interface, respectively.)

5.2 BIOT NUMBER EFFECT

The Biot number, through the heat transfer coefficient, h, is a direct measure of the thermal coupling between the charge and the furnace. The effective Biot number, Bi^{**}, incorporates the effects of the crucible and radial temperature gradients within the charge on this thermal coupling. Typical values for the effective Biot number vary from 0.05 for high conductivity materials such as Ge to 5.0 for low conductivity materials such as CdTe. (Appendix C gives approximate values for typical heat transfer coefficients.) Axial temperature profiles for several Bi^{**} are shown in Fig. 5.2. In agreement with the results of Chang and Wilcox [17], it is found that the charge temperature follows more closely the furnace temperature and, as a result, the axial temperature gradient in the gradient zone increases, as Bi^{**} increases.

The expression for the axial gradient near the growth interface presented in Appendix B for infinite charge length can be simplified for symmetric systems:

$$G_L = \frac{-1}{\lambda_G + (Bi^{**})^{-1/2}} \qquad [5.8]$$

The dependence of the axial gradient on Bi^{**}, according to eq. [5.8], is plotted in Fig. 5.3 for various gradient zone lengths, λ_G. The curves show that the dependence of the axial gradient on λ_G becomes stronger with increasing Bi^{**}. It can also be seen (curve $\lambda_G = 0$) that there exists a

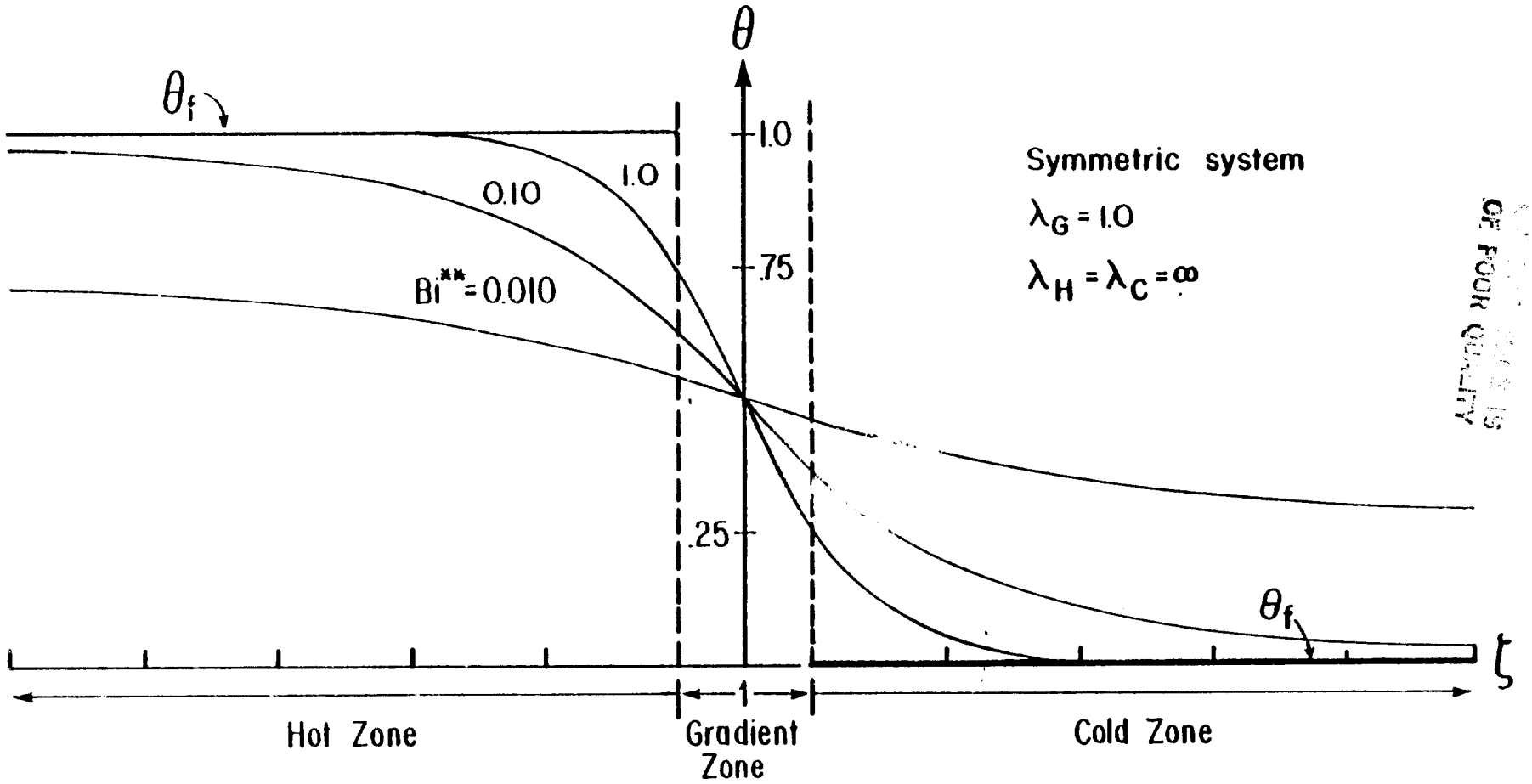

Fig. 5.2: Effect of the thermal coupling between the furnace and the charge on the axial temperature distribution of the charge.

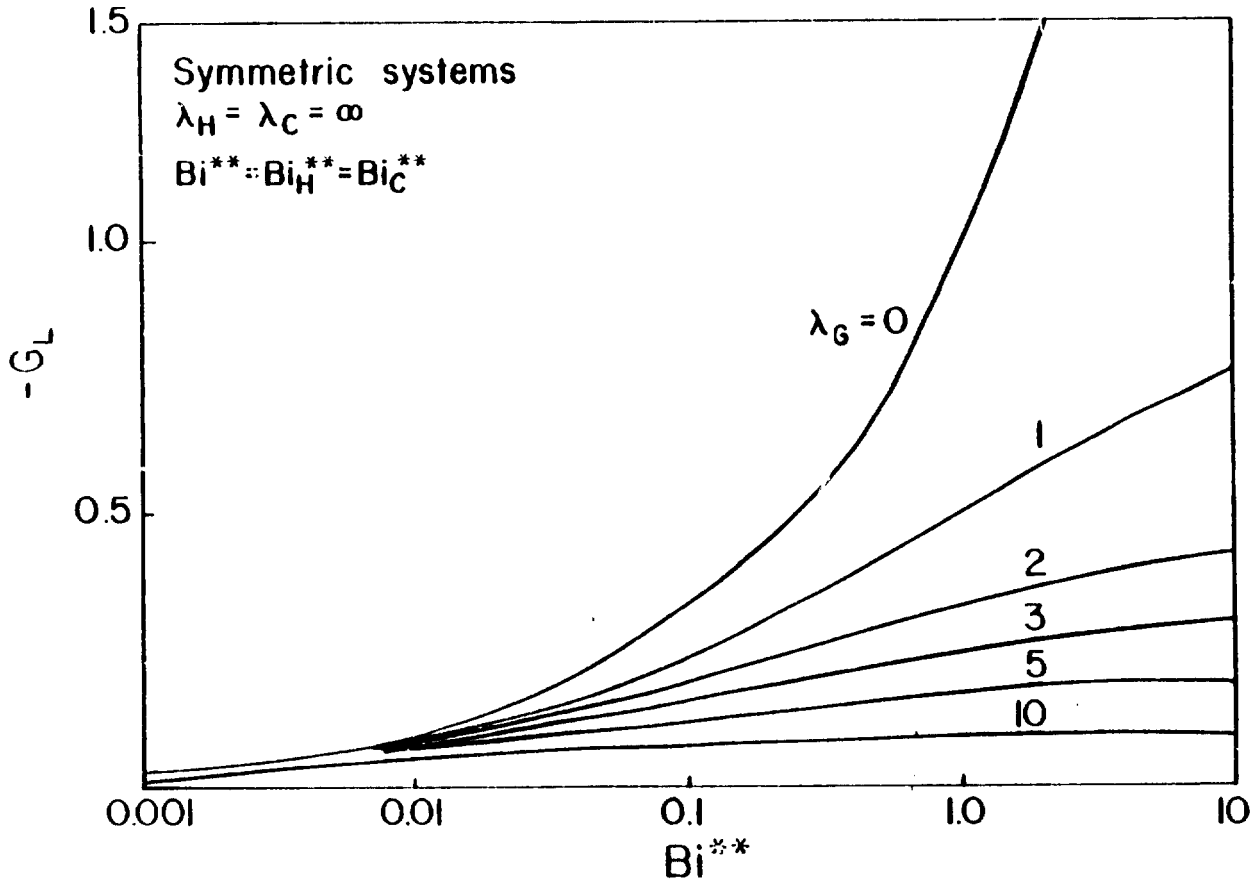

Fig. 5.3: Effect of the gradient zone length and the effective Biot number on the axial temperature gradient in the gradient zone.

minimum Bi^{**} for any desired nondimensional axial gradient.

The Biot numbers of the hot and cold zones are generally not equal due, for example, to the temperature dependence of radiative heat transfer. For such conditions, the zone with the larger effective Biot number more strongly influences the overall temperature level (Fig. 5.4). Compared to the symmetric case where $Bi_H^{**} = Bi_C^{**}$, the charge temperature for asymmetric systems increases when $Bi_H^{**} > Bi_C^{**}$ and decreases when $Bi_C^{**} > Bi_H^{**}$. If the location of the crystal-melt interface for each curve of Fig. 5.4 is considered to be the center of the gradient zone, the effect of unequal Biot numbers appears as a change in nondimensional interface temperature. To retain the interface in a given location requires lowering the hot and/or cold zone furnace temperatures as Bi_H^{**} increases relative to Bi_C^{**}.

The expression for the axial temperature gradient in the gradient zone for a system with infinite length which is symmetric except $h_H \neq h_C$ is:

$$G_L = \frac{-1}{\lambda_G + \frac{1}{2}\left[\left(Bi_H^{**}\right)^{-1/2} + \left(Bi_C^{**}\right)^{-1/2}\right]} \qquad [5.9]$$

Equation [5.9] indicates that the smaller of the effective Biot numbers has a greater effect on decreasing the axial gradient. Efforts to increase axial gradients by adjusting the heat transfer coefficients should therefore first be directed at the zone with the smaller Bi^{**}.

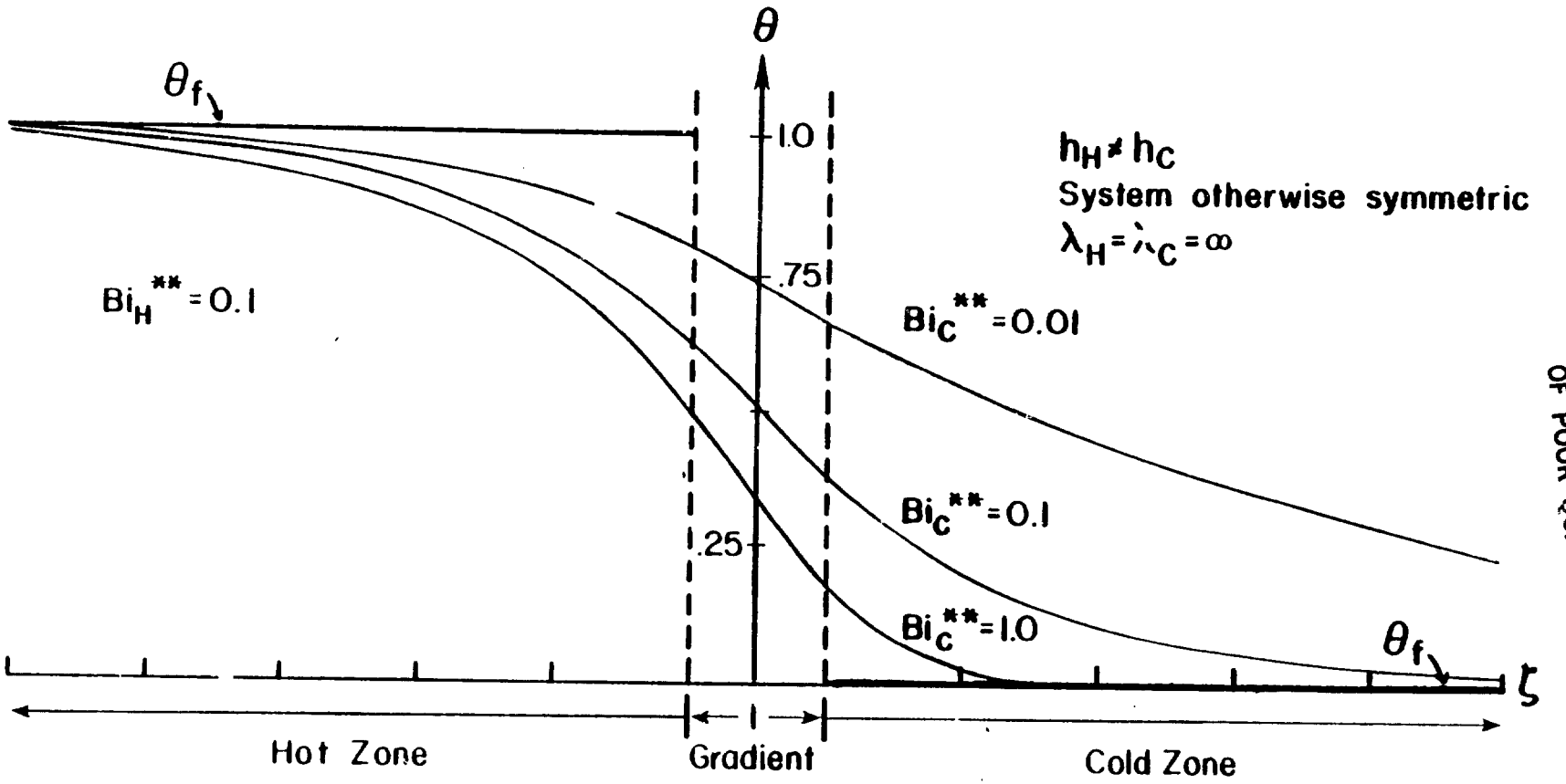

Fig. 5.4: Effect of unequal hot and cold zone Bi^{**} on the axial temperature distribution of the charge.

5.3 EFFECT OF UNEQUAL THERMAL CONDUCTIVITY OF THE CRYSTAL AND THE MELT ($R_K \neq 1$)

R_K expresses the ratio of melt to crystal thermal conductivity. Semiconductors have R_K values greater than unity whereas, for metals, the value of R_K is less than unity. The effect of R_K on the axial temperature distribution in the charge obtained through eq. [4.17] is demonstrated in Fig. 5.5 for systems with $\delta = 1$ and which are otherwise symmetric (i.e., $Bi_H = Bi_C/R_K$). The charge phase with the higher thermal conductivity tends in all instances to have a lower axial gradient because of lower thermal resistance to heat transfer in the axial direction. The axial gradient in the melt near the interface is therefore less than in the crystal for charges with $R_K > 1$.

The expression for the axial gradient in the melt near the growth interface for a system of infinite length which is symmetric except $R_K \neq 1$ is (Appendix B):

$$G_L = \frac{-2}{R_K^* \left[(Bi_c^{**})^{-1/2} + \lambda_G - 2\zeta_i\right] + \left[(Bi_H^{**})^{-1/2} + \lambda_G + 2\zeta_i\right]} \qquad [5.10]$$

A comparison of eqs. [5.4] and [5.10] shows that a value of R_K greater than unity is detrimental to the establishment of large axial gradients in the melt. The axial gradient as a function of R_K according to eq. [5.10] is plotted in Fig. 5.6 for several values of Bi_C. It is found, for example, that this conductivity effect may reduce the gradient in a germanium melt ($R_K = 2.5$) by about 50%.

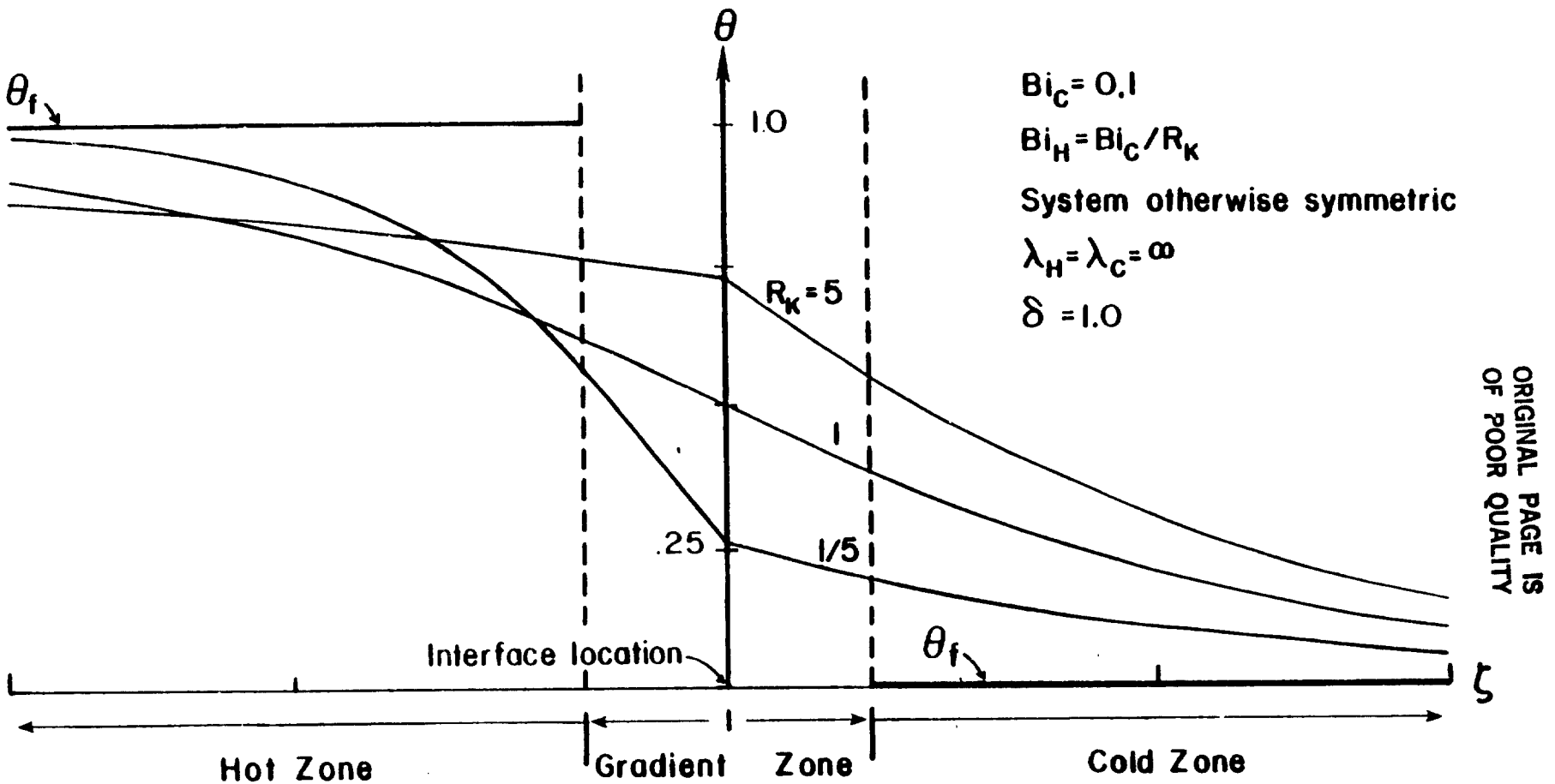

Fig. 5.5: Effect of unequal thermal conductivity of the crystal and the melt on the axial temperature distribution of the charge.

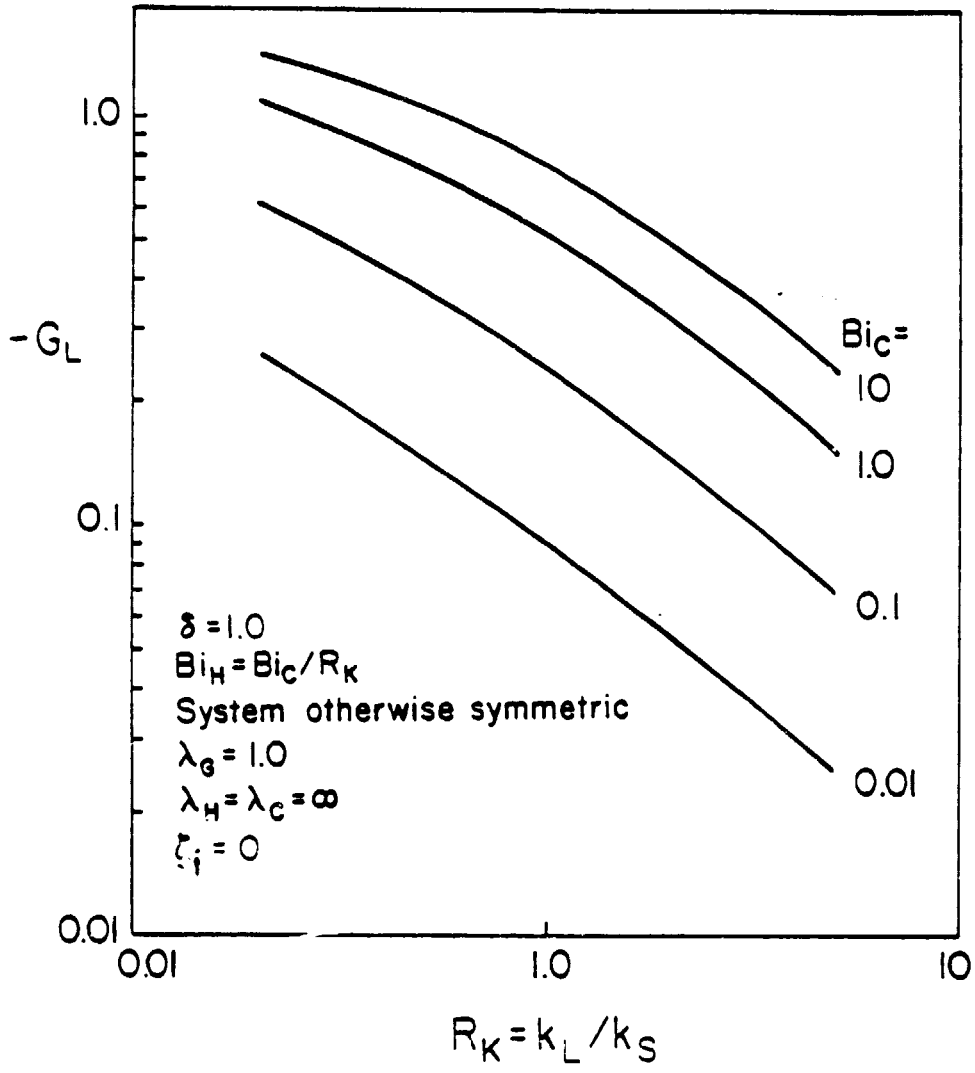

Fig. 5.6: Effect of R_K and Bi on the axial temperature gradient in the melt within the gradient zone (no crucible).

5.4 LATENT HEAT EFFECT

The quantity of latent heat of solidification liberated at the crystal-melt interface is given in nondimensional form by the product $Pe_S R_H$ (eq. [4.20]). The expression for the axial gradient in the melt near the growth interface in a system of infinite length which is symmetric except $Pe_S R_H \neq 0$ is:

$$G_L = \frac{-2 + Pe_s R_H^* \left[(Bi^{**})^{-1/2} + \lambda_G - 2\zeta_i \right]}{2 \left[(Bi^{**})^{-1/2} + \lambda_G \right]} \qquad [5.11]$$

It can be seen that the effect of latent heat on the axial gradient (and also on the axial temperature profile) is small if:

$$\eta \equiv \frac{1}{2} Pe_s R_H^* \left[(Bi^{**})^{-1/2} + \lambda_G - 2\zeta_i \right] \ll 1 \qquad [5.12]$$

Equation [5.12] demonstrates that the effect of latent heat on the axial temperature behavior is larger for smaller Bi^{**} and for larger lowering rates of the charge (Pe_S is proportional to V).

Axial temperature profiles for various values of η are given in Fig. 5.7. It is seen that the generation of latent heat both increases the charge temperature and decreases the axial gradient in the melt; the latent heat effect disappears for small values of η .

(The effect of latent heat and the Peclet number effect described in section 5.1 are coupled through their mutual dependence on the lowering rate, V. In order to isolate the latent heat effect in Fig. 5.7 , Pe is chosen sufficiently small so that eq. [5.6] is satisfied. Such a small value for Pe would normally also eliminate the latent heat effect; i.e., eq. [5.12] would also be satisfied. The values of η in Fig. 5.7 were obtained by choosing appropriately large values of R_H.)

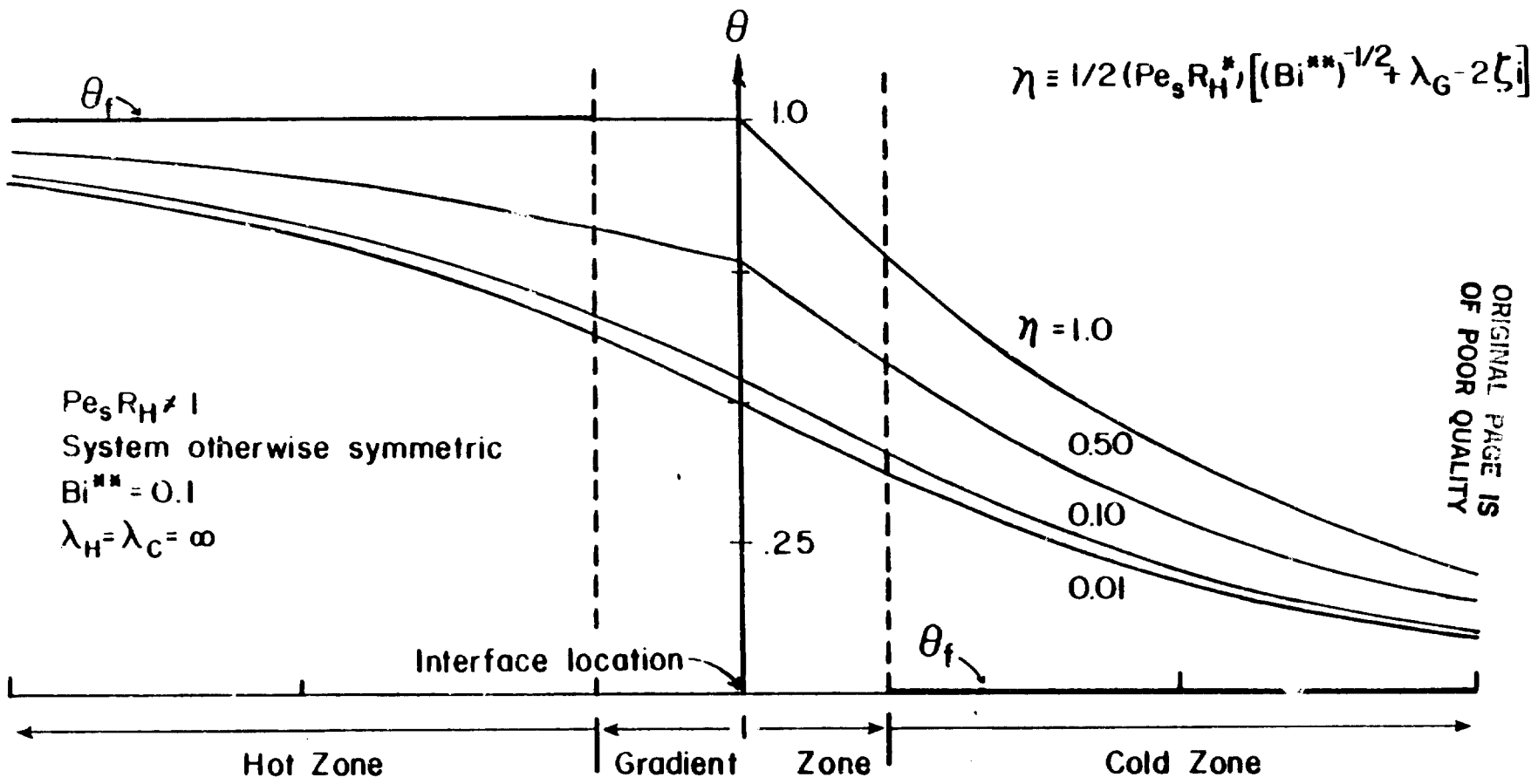

Fig. 5.7: Effect of the generation of latent heat at the growth interface on the axial temperature distribution of the charge.

5.5 "INFINITE" CHARGE LENGTH

When the charge is infinitely long, the temperature field of the charge does not change during growth and, hence, the interface position remains fixed. Figure 5.8 shows the progression of axial temperature profiles as the charge is lowered from the hot zone to the cold zone for charge lengths less then infinite. It can be seen that charge temperatures are displaced toward the hot zone furnace temperature when most of the charge is in the hot zone and vice-versa. Accordingly, to achieve constant interface position for non-infinite charge lengths, the nondimensional solidification temperature, θ_i, must be reduced as the experiment proceeds. At constant θ_i, the growth rate is greater than the lowering rate while the interface moves from the cold to the hot zone.

The contribution from the positive characteristic root, eq. [5.2], to the solution of eq. [4.17] is normally small and is zero for an infinite charge length. The charge thus appears infinite in length when the contribution from the negative root also becomes small, i.e., for large ζ. The temperature change within the hot or cold zone reaches approximately 99% of its total value when $\exp|w_m \zeta| = 0.01$. Using this as a criterion for infinite length:

$$\zeta_\infty = 5/|w_m| \qquad [5.13]$$

where: ζ_∞ = length of charge within the hot or cold zone for charge to appear infinitely long.

If Pe^* is small so that eq. [5.6] is satisfied, the characteristic roots are given by eq. [5.7]. Substituting eq. [5.7] into eq. [5.13]:

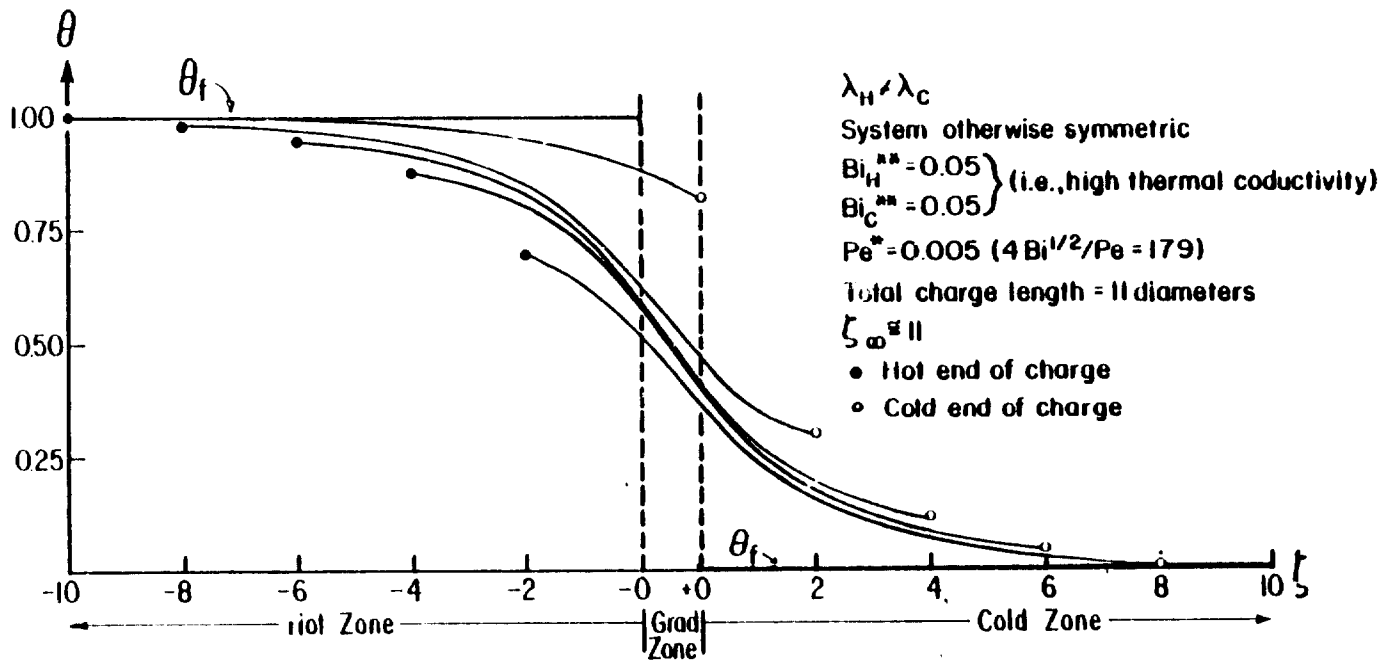

Fig. 5.8: Effect of charge position within the furnace on the axial temperture distribution of the charge.

$$\zeta_\infty = \frac{5}{2} \left(Bi^{**}\right)^{-1/2} \qquad [5.14]$$

which is a useful expression for determining ζ_∞. Equation [5.14] is in agreement with the experimental results of Clyne [11] which suggest that longer charges and higher Biot numbers tend to stabilize the interface position (i.e., the growth rate is equal to the lowering rate).

Results from the one-dimensional numerical model of Riquet and Durand [9] suggest that the growth and lowering rates are equal when the length of charge within the hot and cold zones is about $1.5(Bi^{-1/2})$. This result agrees well with eq. [5.14]; the difference in the constant coefficient is attributed to the choice of criteria defining "infinite" charge length.

When the charge length is not infinite, appropriate boundary conditions must be applied to the ends of the charge. For example, a solid pull rod contacting the crucible at the bottom of the charge can be approximated by treating it as a simple fin exchanging heat with the environment. In this way, a Biot number can be calculated for the end boundary condition. Appendix D describes a method to determine the end boundary condition for some simple end geometries. The curves of Fig. 5.8 have been calculated using the same Biot number for the ends of the charge as for the circumference.

5.6 CHARGE DIAMETER EFFECT

Any change in the charge diameter, D, affects the dimensionless parameters Bi, Pe, ξ, ζ_∞, ζ_i, and λ_q. Further, changes in D may alter the heat transfer coefficients between the furnace and charge as the geometry of the furnace cavity changes. The effect of a change in D is assessed by reevaluating the necessary parameters and then using the

appropriate expressions for the axial gradient. In general, increases in D may either increase or decrease the axial temperature gradient in the gradient zone depending on the corresponding changes in the other parameters.

As an illustrative example, consider a symmetric system of infinite charge length. The appropriate expression for the axial temperature gradient in the gradient zone is given by eq. [5.8]. Since, however, changes in diameter are to be analyzed, it is more informative to compare the axial gradients of eq. [5.8] based on the dimensional axial coordinate, Z:

$$g_L \equiv \left(\frac{d\theta_m}{dZ}\right)_L = \frac{G_L}{D} = \frac{-1}{L_G + D/(Bi^{**})^{1/2}} \qquad [5.15]$$

Defining the variable:

$$\psi \equiv \frac{d\left[D/(Bi^{**})^{1/2}\right]}{dD} \qquad [5.16]$$

Taking L_G as constant, eq. [5.15] shows that the dimensional axial gradient, g_L, increases with D when ψ is negative and vice-versa.

For an increase in D accompanied by a proportional increase in D_{cr}, (i.e., δ remains constant), eqs. [4.7] and [4.14] show that Bi^{**} increases at most linearly with D (assuming that all other thermal parameters are constant). Consequently (using eq. [5.16]), ψ is positive and the dimensional axial gradient, g_L, according to eq. [5.15], decreases as D increases.

The crucible diameter may, on the other hand, remain constant as D

increases. This occurs when increasing the charge diameter within a constant diameter furnace cavity at the expense of the thickness of the crucible. Fig. 5.9 shows the corresponding behavior of ψ for various Bi and K with $\delta = 1.25$. Accordingly, ψ is either positive or negative depending on the values of Bi and K; the axial gradient of eq. [5.15] may therefore increase or decrease with an increase in D.

In summary, the effect of a change in charge diameter on the axial temperature gradient at the growth interface should be examined on a case by case basis.

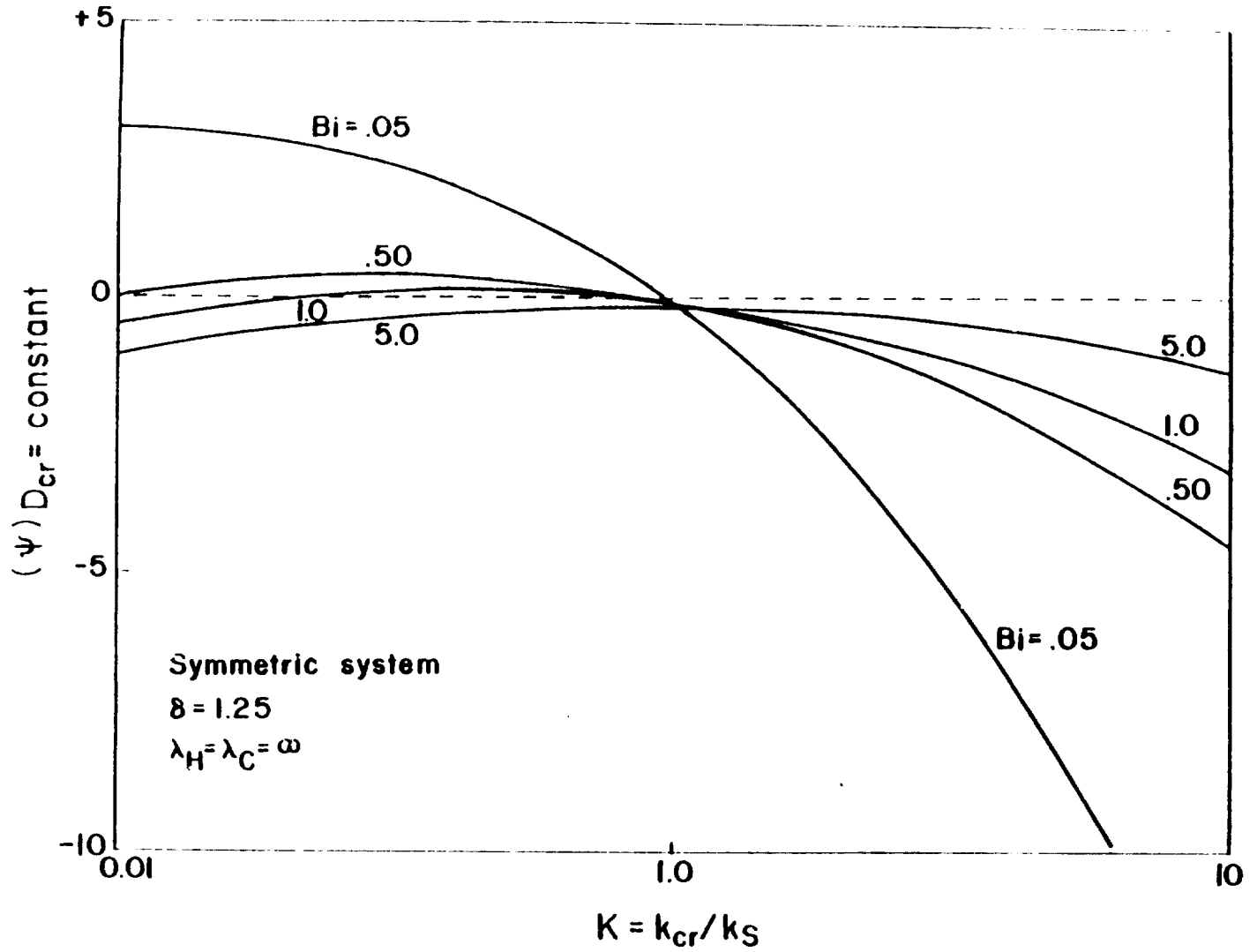

Fig. 5.9: The parameter Ψ (eq. [5.16]) for a symmetric system, δ = 1.25 and constant D_{cr}.

6. THE TWO-DIMENSIONAL THERMAL MODEL

Thermal criteria for satisfactory Bridgman crystal growth include requirements for the shape of the melting temperature isotherm (c.f., section 2.1.2). The one-dimensional model of Chapter 4 does not permit evaluation of the isotherm shape since it neglects radial temperature variations in the charge. Therefore, a two-dimensional model of the Bridgman growth system is developed in this chapter. Results from the two-dimensional model are used in Chapter 7 in order to establish the causes of radial temperature variations within the charge and to study their dependence on the thermal parameters of the Bridgman growth system.

6.1 THE CONCENTRIC FIN APPROACH

The present two-dimensional thermal model of vertical Bridgman growth treats the entire system as a set of coaxial fins. Radial temperature variations are therefore accounted for by differences in the fin temperatures at the same axial location. The model can thus be considered a hybrid between a continuous description in the axial direction and a finite difference description in the radial direction. This approach, rather than a complete finite difference or finite element formulation, is taken for several reasons:

(1) The primary objective of the two-dimensional model is to develop insight into the origin and behavior of radial temperature gradients near the growth interface for the purpose of controlling the shape of this interface through system design. The increased accuracy achievable using a fine grid network in a finite difference or finite element

model is not considered essential for this objective and, furthermore, does not appear warranted for systems for which reliable thermal property data are not yet available. The present model incorporates all the critical thermal effects; it is expected, therefore, to be able to predict the radial gradient behavior at least to first order approximations. (By utilizing enough coaxial fins, the present model should, in principle, be as accurate as a finite difference model.)

(2) The present model is easily implemented on the computer and is a simple extension of the one-dimensional moving fin model developed in Chapter 4.

(3) Even with the simplifications inherent to the concentric fin approach, the added complexity of a two-dimensional formulation necessitates the use of a computer to calculate the two-dimensional temperature distribution of the charge. The concentric fin model can be simplified, however, without loss of pertinent information, to a point which permits presentation of some relevant results in analytical form.

6.2 THE DESCRIBING EQUATIONS FOR THE CONCENTRIC FIN MODEL

The factors of concern for the development of the concentric fin model of the Bridgman growth system depicted in Fig. 2.2 are indicated in Figs. 6.1 and 6.2. The two-dimensional thermal model incorporates the following assumptions in addition to those described in Section 2.2.2:

(1) Radial temperature variations within the charge are accounted for by modeling the charge as two radially distinct fins.

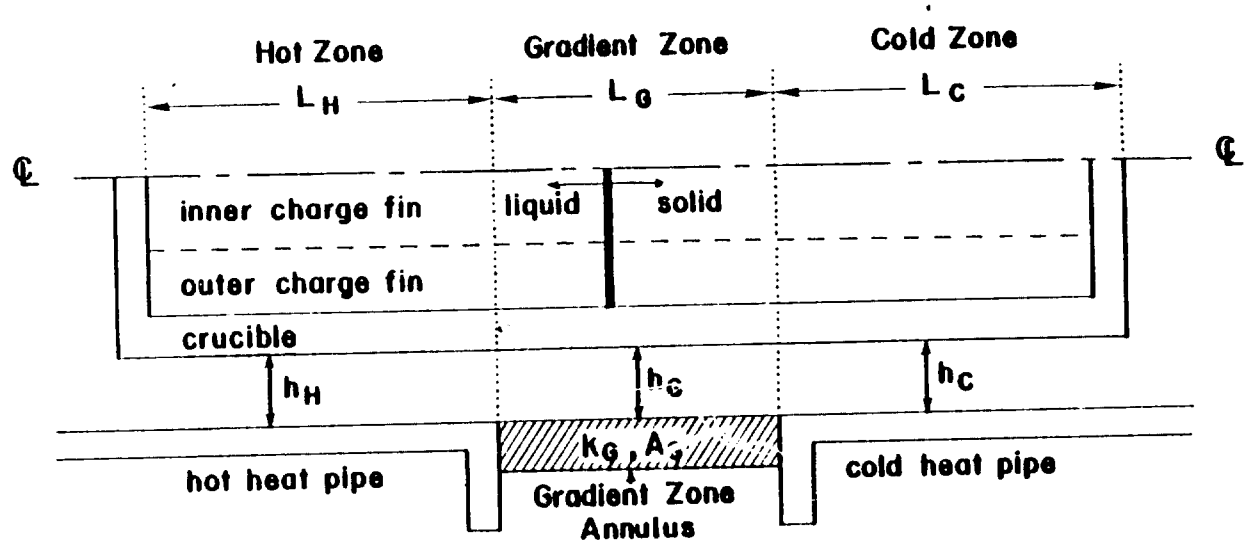

Fig. 6.1: Schematic of the charge, crucible, gradient zone annulus and furnace heat pipes in the concentric fin model.

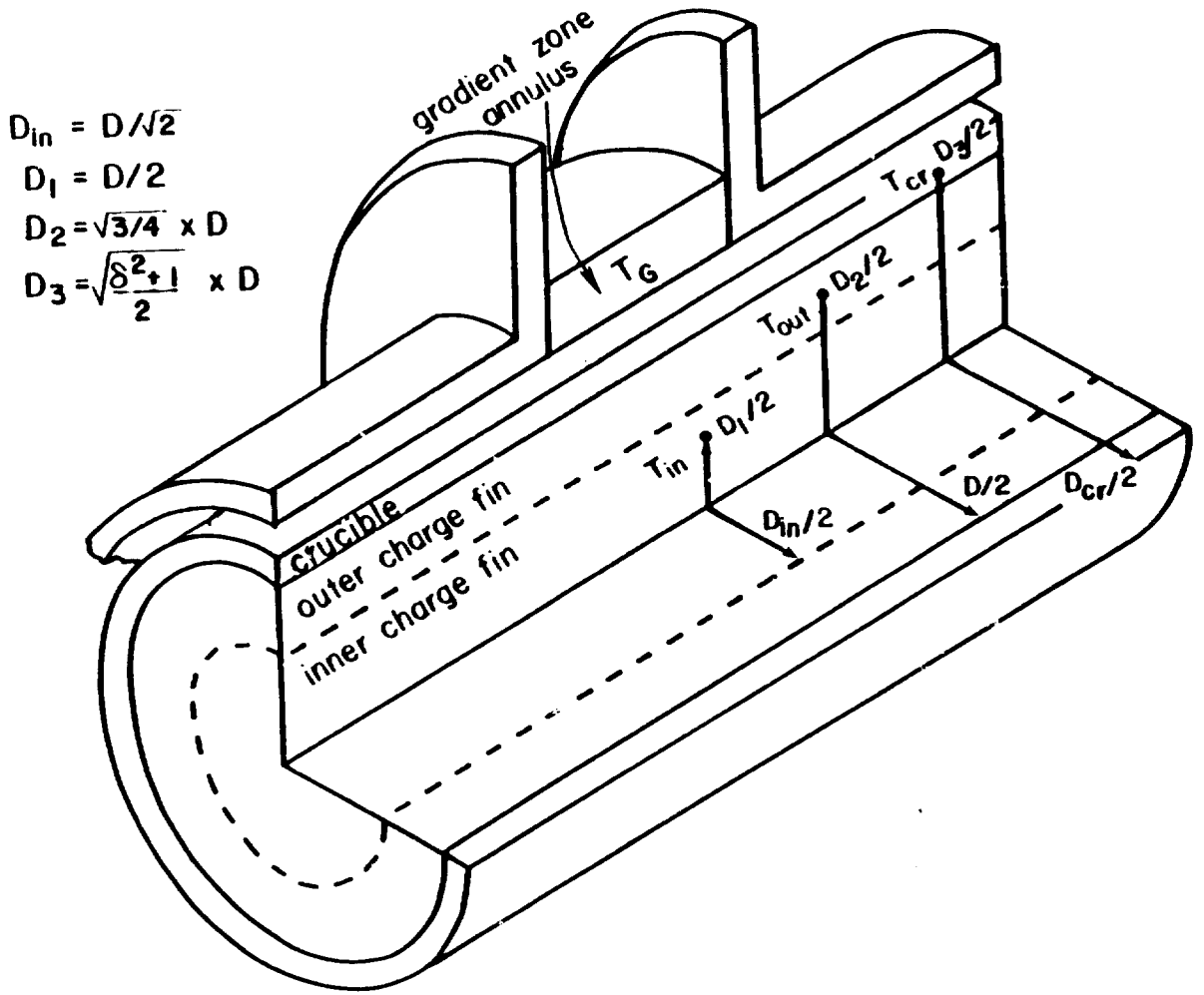

Fig. 6.2: Cut-away sketch of the charge, crucible and gradient zone annulus showing the geometry of the concentric fins.

The inner fin is a cylinder of diameter D_{in} and has an axial temperature distribution $T_{in}(Z)$. The outer fin is an annulus of inner and outer diameters, D_{in} and D, and has an axial temperature distribution $T_{out}(Z)$. The diameter D_{in} is chosen so that the inner and outer fins have equal cross sectional area. The temperature of each charge fin is not considered a function of radius. The difference in temperature between T_{in} and T_{out} is indicative of radial temperature variations within the charge.

(2) The crucible is modeled as a coaxial annular fin in contact with the outer charge fin. The crucible fin temperature, $T_{cr}(Z)$, is not a function of radius.

(3) As opposed to the corresponding assumption in the one-dimensional model, the gradient zone is not adiabatic; i.e., $h_G \neq 0$. This assumption is relaxed in the two-dimensional model so that the effect of radial heat transfer between a non-perfectly insulating gradient zone and the charge can be studied.

(4) The portion of the furnace in the gradient zone is considered to be an annulus of conductivity k_G and cross sectional area A_G located coaxially with the charge and crucible. The temperature of the gradient zone annulus is assumed constant in the radial direction; its axial temperature distribution, $T_G(Z)$, depends on its thermal interaction with the charge and crucible. Temperature boundary conditions are used at the ends of the gradient zone annulus and no heat loss is assumed at its outer diameter. (This model of the gradient zone

annulus was also used in section 4.4.4 in order to determine the effect of a non-perfectly insulating gradient zone on the axial temperature behavior of the charge.)

On the basis of the above assumptions, each of the concentric fins is analogous to the moving thin rod treated by Carslaw and Jaeger [29]; eq. [4.1] (neglecting the transient term by virtue of the quasi-steady assumption) therefore describes the axial temperature distribution within each fin. In the concentric fin model, the q" term of eq. [4.1] accounts for the heat transfer between radially adjacent fins. In Appendix F, this radial heat transfer is approximated resulting in the following set of coupled ordinary differential equations for the axial temperature distribution of the fins:

$$\frac{d^2\phi_m}{d\zeta^2} - Pe_{1\alpha}\frac{d\phi_m}{d\zeta} + A_1(\phi_{cr} - \phi_m - \phi_\Delta) = 0 \qquad [6.1a]$$

$$\frac{d^2\phi_\Delta}{d\zeta^2} - Pe_{1\alpha}\frac{d\phi_\Delta}{d\zeta} + A_1(\phi_{cr} - \phi_m - \phi_\Delta) - A_2\phi_\Delta = 0 \qquad [6.1b]$$

$$\frac{d^2\phi_{cr}}{d\zeta^2} - Pe_{cr}\frac{d\phi_{cr}}{d\zeta} + A_3(\phi_\Delta + \phi_m - \phi_{cr}) + A_4(\phi_f - \phi_{cr}) = 0 \qquad [6.1c]$$

$$\frac{d^2\phi_G}{d\zeta^2} + A_5(\phi_{cr} - \phi_G) = 0 \qquad [6.1d]$$

where: $\phi_m \equiv \frac{1}{2}(\phi_{out} + \phi_{in})$

where: $\phi_\Delta \equiv \frac{1}{2}\left(\phi_{out} - \phi_{in}\right)$

$$Pe_{loc} = VD\rho c_p / k_{loc}$$

$$Pe_{cr} = VD(\rho c_p / k)_{cr}$$

The coefficients A_1, A_2, A_3, A_4, and A_5 depend on the radial thermal resistance between the concentric fins. They are given by:

$$A_1 = \frac{8}{\ln\sqrt{\frac{4}{3}} + \frac{1}{K_{loc}} \cdot \ln\left(\frac{\delta^2+1}{2}\right)^{1/2}} \qquad [6.2a]$$

$$A_2 = \frac{32}{\ln\sqrt{3}} \qquad [6.2b]$$

$$A_3 = \frac{A_1}{K_{loc}(\delta^2-1)} \qquad [6.2c]$$

$$A_4 = \frac{8}{K_{loc}(\delta^2-1)} \cdot \frac{1}{\frac{2}{\delta Bi_{loc}} + \frac{1}{K_{loc}} \ln\left(\frac{2}{1+\delta^{-2}}\right)^{1/2}} \qquad [6.2d]$$

$$A_5 = \frac{A_4 K_{loc}(\delta^2-1)}{R_{G,loc}} \qquad [6.2e]$$

The fin equations for ϕ_{out} and ϕ_{in} have been added to and subtracted from one another in Appendix F in order to produce eqs. [6.1a] and [6.1b] for ϕ_m and ϕ_Δ respectively. Since the cross sectional areas of the inner

and outer charge fins are equal, ϕ_m is interpreted as the mean cross sectional temperature of the charge; ϕ_Δ is a measure of the radial temperature difference within the charge. Within the hot and cold zones, the furnace temperature, $\phi_\pm$, is the temperature of the hot and cold heat pipes, respectively, and eq. [6.1d] for the gradient zone annulus in not needed. Within the gradient zone, $\phi_\pm$ is identified with $\phi_G(\zeta)$ and eq. [6.1d] has no Peclet term since the gradient zone annulus is stationary.

6.3 SOLUTION OF THE CONCENTRIC FIN EQUATIONS

The set of eqs. [6.1] has constant coefficients if a separate set of equations is employed for each axial region of uniform thermal properties and furnace boundary conditions. As in the one-dimensional model, four such axial regions are present in the concentric fin model: the hot and cold zones and the liquid and solid portions of the gradient zone. (It is assumed that the growth interface is in the gradient zone.) The hot and cold zones are therefore described by eqs. [6.1a], [6.1b] and [6.1c]; the two regions within the gradient zone include, in addition, eq. [6.1d], representing the gradient zone annulus.

The solution of eqs. [6.1] within a particular axial region is described in many texts (e.g., [36,37]). The system of p second order differential equations can be changed to an equivalent system of 2p first order differential equations by the definition:

$$\phi' = \frac{d\phi}{d\zeta} \qquad [6.3]$$

Performing this transformation and putting the result in matrix notation,

eqs. [6.1] become:

$$\frac{d\mathbf{X}}{d\zeta} = \mathbf{P}\mathbf{X} + \mathbf{F} \qquad [6.4]$$

where:

$$\mathbf{X} = \begin{bmatrix} \phi_m \\ \phi_\Delta \\ \phi_{cr} \\ \phi'_m \\ \phi'_\Delta \\ \phi'_{cr} \end{bmatrix}$$

(hot and cold zones)

$$\mathbf{X} = \begin{bmatrix} \phi_m \\ \phi_\Delta \\ \phi_{cr} \\ \phi_G \\ \phi'_m \\ \phi'_\Delta \\ \phi'_{cr} \\ \phi'_G \end{bmatrix}$$

(gradient zone)

(Variables in boldface denote matrices.) The elements of **P** and **F** are found by direct substitution. In the gradient zone, **F** is an empty matrix.

The solution to eq. [6.4] is of the form:

$$\mathbf{X} = c_1 \mathbf{E}_1 e^{w_1 \zeta} + c_2 \mathbf{E}_2 e^{w_2 \zeta} + \cdots + c_{2p} \mathbf{E}_{2p} e^{w_{2p} \zeta} + \mathbf{X}_p \qquad [6.5]$$

The values of w are commonly called the eigenvalues of the matrix **P** and the values of **E** are commonly called the eigenvectors of **P**. The eigenvalues and eigenvectors are easily found by standard computer subroutines. The coefficients denoted by c in eq. [6.5] are the unknown constants of integration. $\mathbf{x}_p$ denotes the particular solution of eq. [6.4].

Equation [6.5] is written for each axial region. The hot and cold zones each contribute six unknown constants of integration; the liquid and solid parts of the gradient zone each contribute eight unknown constants of integration. There are, therefore, 28 unknown constants of integration

which must be determined by using boundary conditions of (a) equality of temperature and (b) continuity of flux between corresponding fins of adjacent axial regions as well as (c) heat transfer coefficients at the ends of charges of finite length and (d) imposed temperature boundary conditions at the ends of the gradient zone annulus. Application of the boundary conditions results in a set of 28 simultaneous linear algebraic equations whose unknowns are the required constants of integration. The solution of these simultaneous equations is easily accomplished by standard computer subroutines.

6.4 APPROXIMATION FOR THE GROWTH INTERFACE BOUNDARY CONDITION

The solution of the fin equations requires a trial and error procedure when the extent of each axial region is not initially known. For example, the one-dimensional model of Chapter 4 shows that the interface location, ζ_i, and the interface temperature, θ_i, are functionally related. When θ_i is chosen as the independent variable, ζ_i must be found by iteration (c.f., the analytical results of Appendix B). When ζ_i is taken as the independent variable, the location of the interface boundary conditions is known a priori resulting in a direct solution for θ_i as well as the entire axial temperature distribution.

Figure 6.3 shows that the axial position of the growth interface in the inner and outer charge fins is, in general, not the same; they are the same only when the interface is flat. The correct application of the concentric fin model requires that a separate set of eqs. [6.1] be written for the short region between the axial locations of the interface. In this case, the interface temperature, θ_i, depends on the interface locations of both the inner and outer charge fins, $\zeta_{i,in}$ and $\zeta_{i,out}$ respectively:

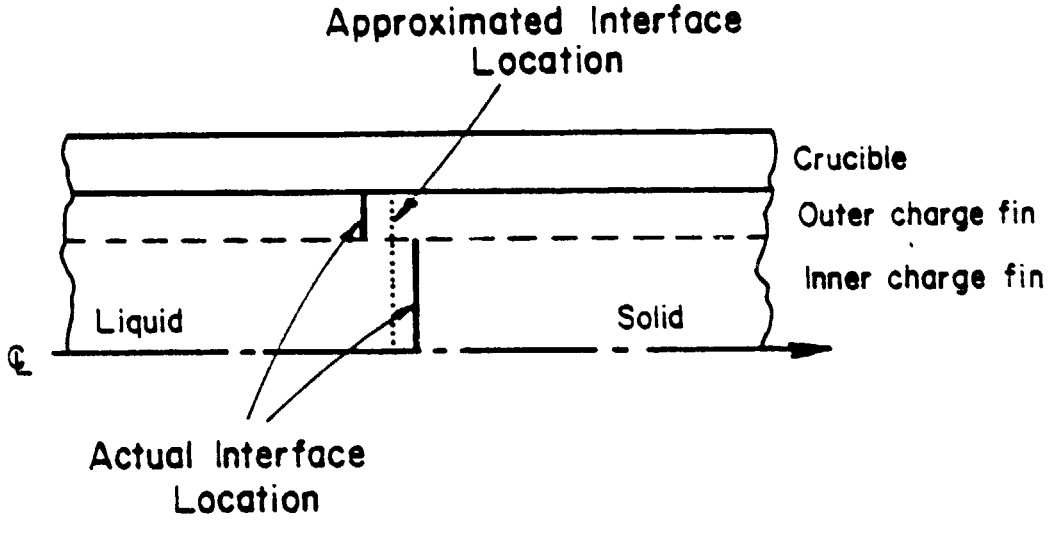

Fig. 6.3: Approximation for the interface boundary conditions used in the concentric fin model.

$$f(\theta_i, \zeta_{i,in}, \zeta_{i,out}) = 0 \qquad [6.6]$$

Since this functional relationship is not known a priori, it is not possible to choose initial values of $\zeta_{i,in}$ and $\zeta_{i,out}$ which satisfy eq. [6.6]; the solution therefore requires an iterative procedure. The present section describes an approximate model of the interface which precludes the use of a trial and error solution for the concentric fin model.

The length of the region separating the interface in the inner and outer charge fins is normally small since it is desired to have an interface of small curvature. The present model neglects this axial region and applies the boundary conditions of the interface at a single axial location for each of the inner and outer charge fins. The axial location of the interface is taken to be the location where the mean charge temperature, ϕ_m, is equal to the interface temperature, θ_i (see Fig. 6.3). In this sense, the axial location where $\phi_m = \theta_i$ denotes an "average" interface position (i.e., between the actual interface positions of the inner and outer charge fins). The value of ϕ_Δ at this location, $\phi_\Delta(\zeta_i)$, is indicative of the curvature of the interface.

The use of the above approximation for the interface boundary condition permits the a priori choice of the "average' interface location and, therefore, the solution for the temperature field in the charge is not a trial and error procedure. The approximation introduces no error if $R_K = 1$ and $Pe_S R_H = 0$ or if the interface is flat. Otherwise, when the interface curvature is small, the error should likewise be small and the predictions of the present model concerning the radial temperature variations in the charge are expected to be correct to a first-order

approximation.

The interface flux boundary conditions, assuming that the melt/crystal conductivity change and the generation of latent heat occur at the same axial location in each of the charge fins, are:

$$R_K \left(\frac{d\phi_m}{d\zeta}\right)_L = Pe_s R_H + \left(\frac{d\phi_m}{d\zeta}\right)_S \qquad [6.7a]$$

$$R_K \left(\frac{d\phi_\Delta}{d\zeta}\right)_L = \left(\frac{d\phi_\Delta}{d\zeta}\right)_S \qquad [6.7b]$$

$$\left(\frac{d\phi_{cr}}{d\zeta}\right)_L = \left(\frac{d\phi_{cr}}{d\zeta}\right)_S \qquad [6.7c]$$

$$\left(\frac{d\phi_G}{d\zeta}\right)_L = \left(\frac{d\phi_G}{d\zeta}\right)_S \qquad [6.7d]$$

where the subscripts "L" and "S" refer to the melt and crystal side of the interface, respectively. Equations [6.7] assume that the growth rate, R, is equal to the lowering rate, V (see section 4.4.2).

6.5 THERMAL PARAMETERS OF THE CONCENTRIC FIN MODEL

The thermal parameters required by the concentric fin model are those necessary for the one-dimensional moving fin model (see Table 4.1) and, additionally, those listed in Table 6.1.

6.6 COMPARISON WITH THE TWO-DIMENSIONAL MODEL OF FU AND WILCOX [26]

The figures of Fu and Wilcox [26] plot the shape of various isotherms within the charge by the use of two-dimensional finite difference computer

parameter	definition	comments
$Bi_{G,S}$	$h_G D/k_S$	$Bi_{G,L} = Bi_{G,S}/R_K$
$R_{G,S}$	$k_G A_G/k_S A$	$R_{G,L} = R_{G,S}/R_K$
Pe_{cr}	$VD(\rho c_p/k)_{cr}$	$Pe_{cr} = Pe_S/R_{\alpha,S}$
$\Phi_G(-\lambda_G/2)$		
$\Phi_G(\lambda_G/2)$		

Table 6.1: Thermal parameters of the concentric fin model, in addition to those listed in Table 4.1.

solutions. Isotherm shapes taken from their paper are used in this section in order to check the results of the present two-dimensional model.

In the figures which follow, the shape of an isotherm is indicated by the axial distance between the location of the isotherm at the center of the charge and the outer diameter of the charge and is denoted by ζ_ϕ. ζ_ϕ is scaled directly from the isotherm plots of Fu and Wilcox [26]; the representative axial location of each isotherm is taken to be the axial location of the isotherm at the diameter D_{in} (c.f., Fig. 6.2). The present model predicts ϕ_Δ and ϕ_m as functions of ζ. In Appendix G, ζ_ϕ is related to ϕ_Δ and ϕ_m through eqs. [G.2] and [G.5]:

$$\zeta_\phi \approx \frac{4\,\phi_\Delta}{d\phi_m/d\zeta} \qquad [6.8]$$

The system modeled by Fu and Wilcox [26] has an adiabatic gradient zone, infinite charge length, and does not include a crucible, generation of latent heat, or change in thermal conductivity at the growth interface. The results of the concentric fin model are therefore obtained using the

following parameter values: $\zeta = 1$, $R_K = 1$, $R_H = 0$, and an adiabatic gradient zone. Four cases, each with different Biot or Peclet numbers, are compared in the graphs of Fig. 6.4; the parameters tested are listed in Table 6.2. It is seen that there is good agreement between the results of the two models. (The apparent scatter in the results taken from Fu and Wilcox [26] is attributed to difficulty in scaling the values of ζ_ϕ from their plotted isotherms.) It is therefore concluded that the present concentric fin model of the charge predicts, at least to first-order approximation, the correct two-dimensional thermal behavior of the charge.

6.7 TEST OF THE EFFECTIVE BIOT NUMBER

The effective Biot number, Bi^{**}, is developed in Sections 4.2.2 and 4.2.3 in order to account for the effects of crucible conductivity and thickness as well as radial temperature variations within the charge on the axial temperature distribution of the charge. Section 4.6 provides a partial verification of the effective Biot number concept by comparing the one-dimensional results of this work, using Bi^{**}, to the results of the two-dimensional model of Fu and Wilcox [26]. This comparison, however, included only the effects of radial temperature gradients within the charge on Bi^{**} since the model of Fu and Wilcox [26] does not provide for a crucible. The present two-dimensional model can be used to verify the quantitative accuracy of Bi^{**}, including the effects of the crucible. For this purpose, a symmetric system with $Bi_G = 0$ and of infinite length is used. The applicable relation for the axial temperature gradient in the gradient zone from the one-dimensional results of Chapter 5 is eq. [5.8]:

$$G_L = \frac{d\theta_m}{d\zeta} = \frac{-1}{\lambda_G + (Bi^{**})^{-1/2}} \qquad [5.8]$$

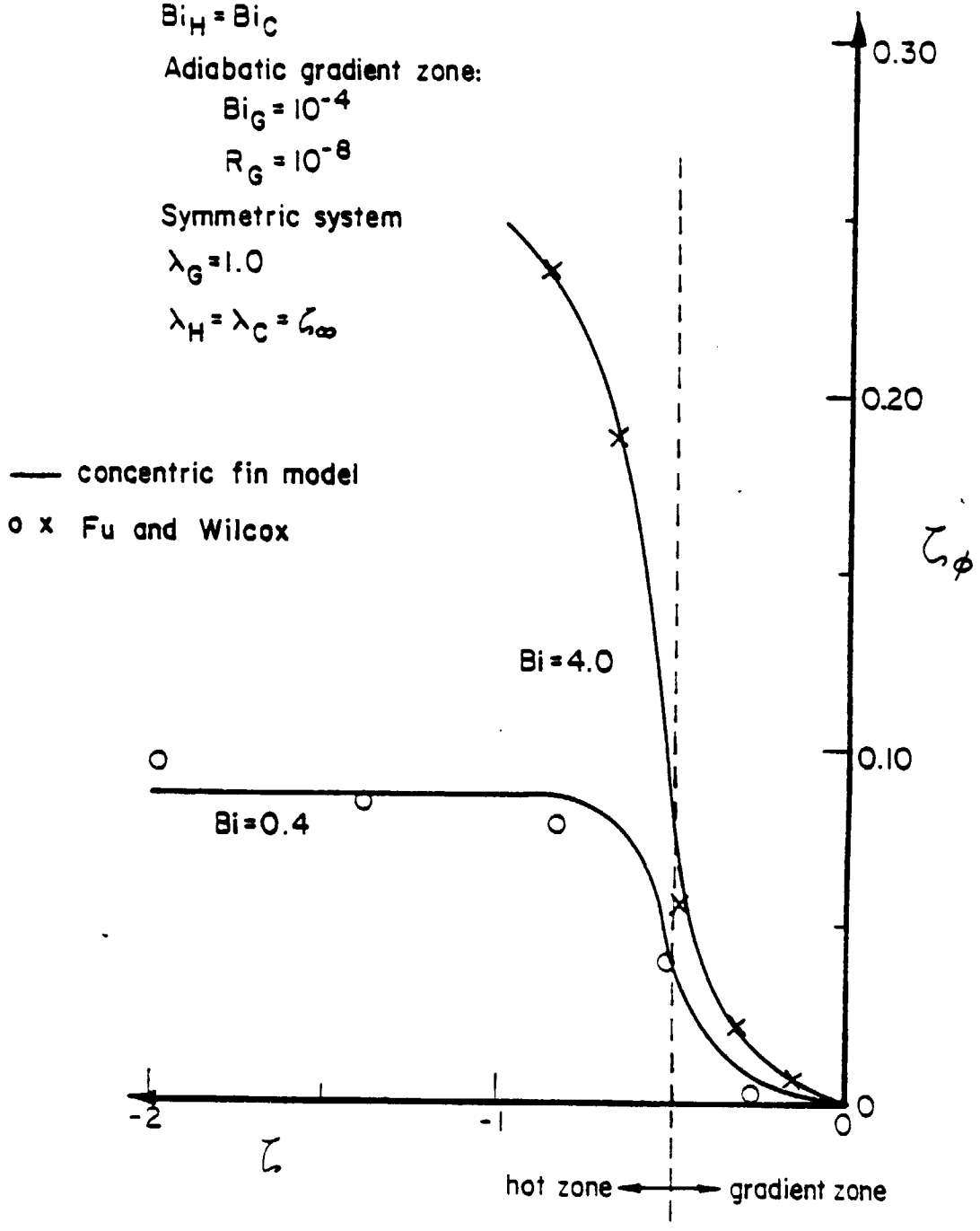

Fig. 6.4a: Comparison of isotherm shapes from the results of the concentric fin model and Fu and Wilcox [26]: Bi = 0.4, 4.0, and Pe = 0.0.

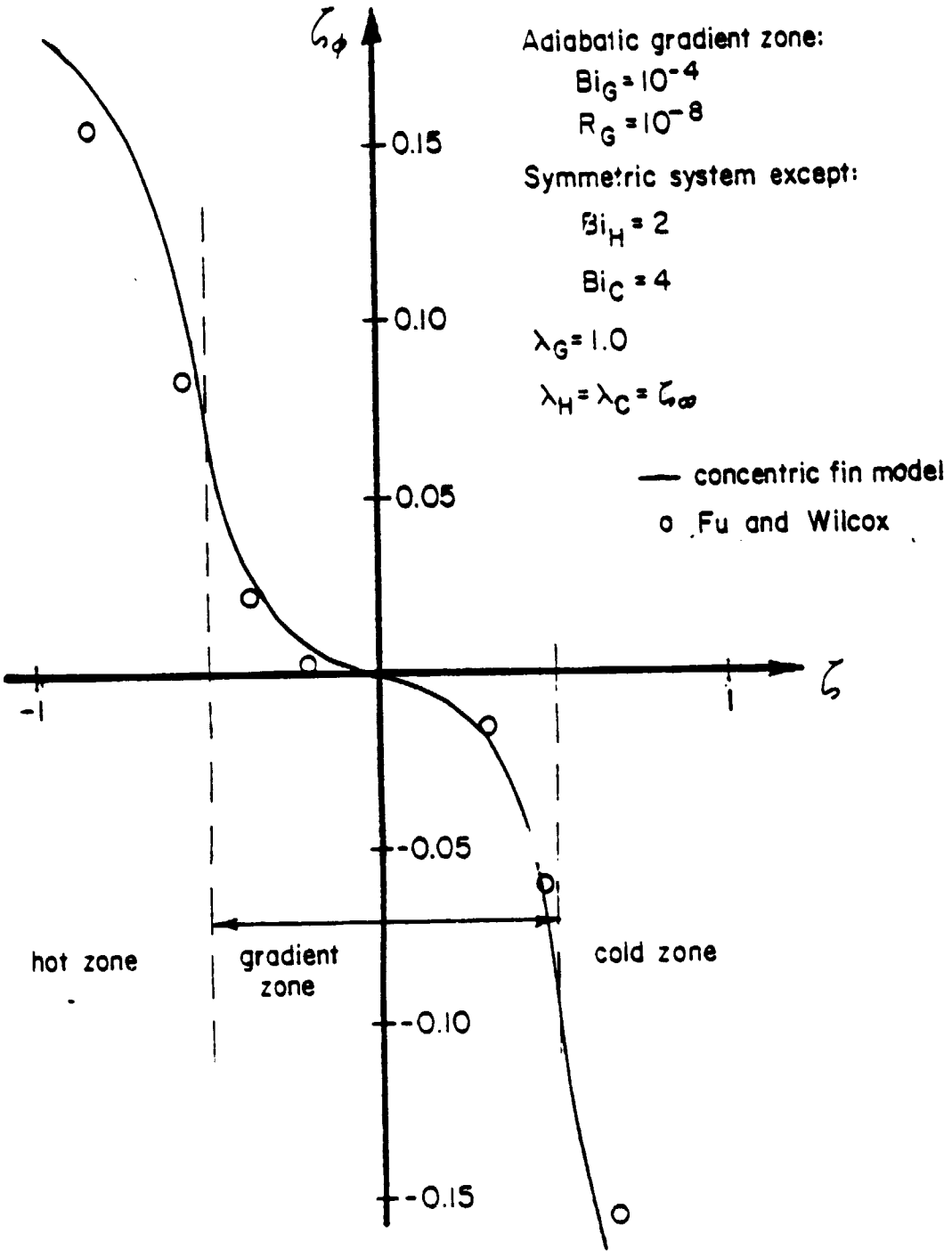

Fig. 6.4b: Comparison of isotherm shapes from the results of the concentric fin model and Fu and Wilcox [26]: Bi_H = 2.0, Bi_C = 4.0, and Pe = 0.0.

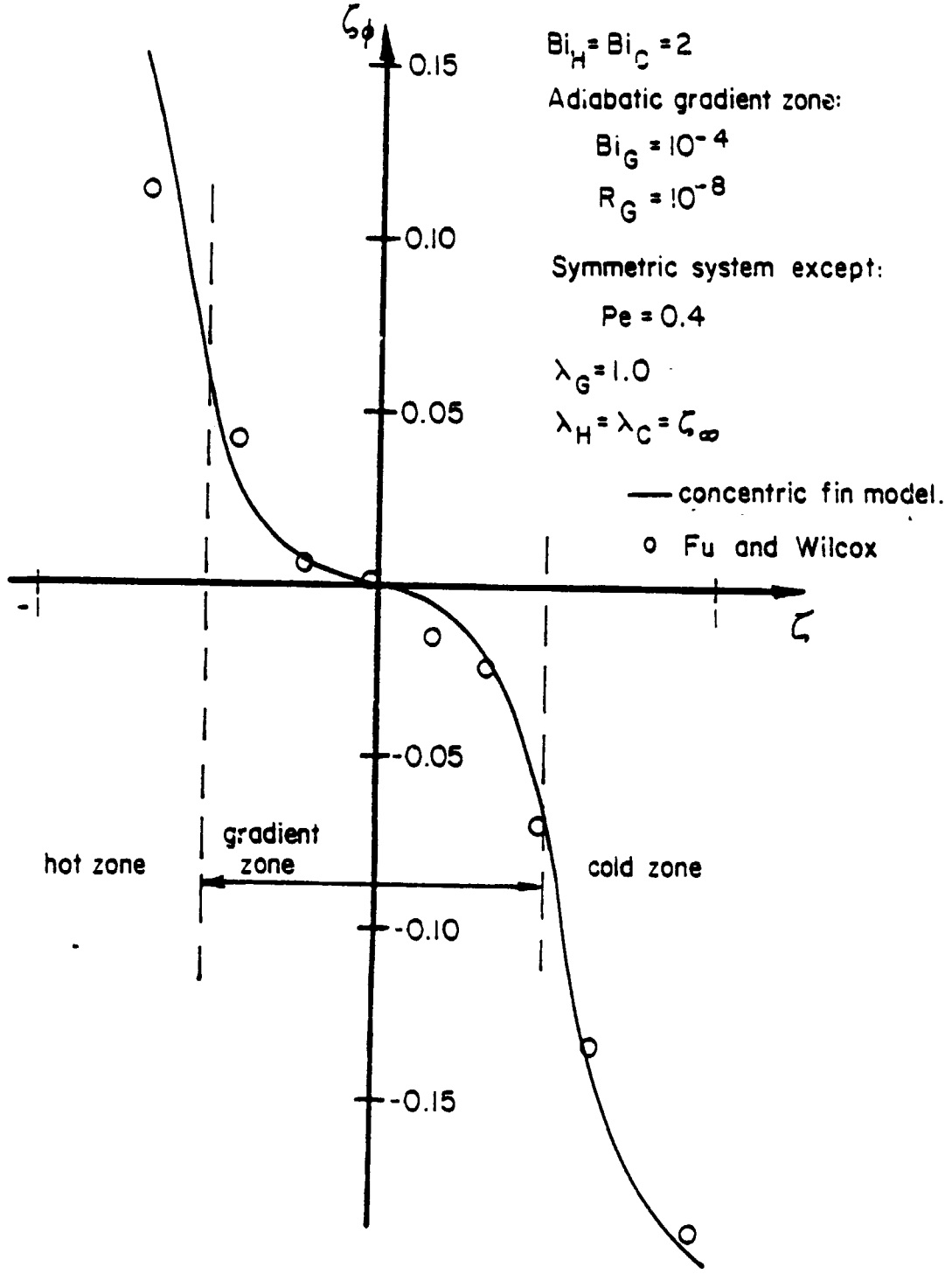

Fig. 6.4c: Comparison of isotherm shapes from the results of the concentric fin model and Fu and Wilcox [26]: Bi = 2.0 and Pe = 0.4.

	Figure from Fu & Wilcox [26]	Bi_H	Bi_C	Pe
Fig. 6.4a	Fig. 4	0.4	0.4	0.0
	Fig. 4	4.0	4.0	0.0
Fig. 6.4b	Fig. 5	2.0	4.0	0.0
Fig. 6.4c	Fig. 7	2.0	2.0	0.4

$\lambda_G = 1.0$ $\quad\quad$ $\delta = 1.0$
$\lambda_H = \lambda_C = \zeta_\infty$ $\quad\quad$ $R_H = 0.0$
$R_K = 1.0$
adiabatic gradient zone

Table 6.2: Parameters used for comparing the results of Fu and Wilcox [26] and the present concentric fin model.

The system used in this comparison is further specified by taking $\lambda_G = 1$ and $\delta = 1.25$.

The axial gradient given by eq. [5.8] is compared in Table 6.3 to that determined by the concentric fin model for several values of Bi and K. It is seen that the agreement is excellent. It is concluded, therefore, that Bi^{**} is an accurate approximation for the effects of the crucible on the heat exchange between the furnace and the charge.

6.8 EIGENVALUES OF THE CONCENTRIC FIN MODEL

The eigenvalues reflect, in a qualitative sense, the thermal interactions among the fins which cause their temperatures to equilibrate in the axial direction. Larger eigenvalues suggest faster equilibration. It is expected that the eigenvalues increase as the ratio of axial to radial thermal resistance increases. As an illustrative example, consider

		one-dimensional model		two-dimensional model
Bi	K	Bi^{**} eqs. [4.7] and [4.14]	$d\theta_m/d\zeta$ eq. [5.8]	$d\theta_m/d\zeta$
1.0	0.1	0.473	-0.407	-0.415
	0.3	0.684	-0.453	-0.459
	1.0	0.660	-0.448	-0.453
	3.0	0.427	-0.395	-0.397
	10.0	0.183	-0.300	-0.299
0.1	0.1	0.103	-0.243	-0.244
	0.3	0.101	-0.241	-0.242
	1.0	0.078	-0.219	-0.219
	3.0	0.046	-0.177	-0.176
	10.0	0.019	-0.120	-0.120

$\delta = 1.25$ $\quad$ Pe = 0.0
$R_K = 1.0$ $\quad$ $\lambda_G = 1.0$
$R_H = 0.0$ $\quad$ $\lambda_H = \lambda_c = \infty$
adiabatic gradient zone

Table 6.3: Testing the effect of the crucible on Bi^{**} by using the concentric fin model.

the moving fin model of Chapter 4; the Biot number expresses the ratio of axial to radial thermal resistance in this case. Equation [5.8] and Fig. 5.2 show that as the Biot number increases, the significant temperature difference in the model, $\theta_f - \theta_m$, decreases more rapidly with distance into the hot and cold zones.

As eq. [6.5] indicates, the eigenvalues only partially express the thermal behavior of the concentric fins. The eigenvectors, E, and the constants of integration, c, combine to determine the importance which each eigenvalue has for each of the fin temperatures. Nevertheless, a study of the parametric behavior of the eigenvalues serves to emphasize the nature of the thermal interactions occuring among the concentric fins.

6.8.1 Hot and Cold Zones

By substituting a solution of the form:

$$\begin{bmatrix} \phi_m \\ \phi_\Delta \\ \phi_{cr} \end{bmatrix} = \begin{bmatrix} c_m \\ c_\Delta \\ c_{cr} \end{bmatrix} e^{w\zeta} \qquad [6.9]$$

into eqs. [6.1], the characteristic equation for the eigenvalues of the hot and cold zones is found to be:

$$\left(w^2 - Pe_{loc}w - A_1\right)\left(w^2 - Pe_{loc}w - A_2\right)\left(w^2 - \frac{Pe_{loc}}{K_{loc}}w - A_1\right)$$

$$- A_3\left(w^2 - Pe_{loc}w\right)\left(w^2 - Pe_{loc}w - A_2\right)$$

$$- A_1\left(w^2 - Pe_{loc}w\right)\left(w^2 - \frac{Pe_{loc}}{K_{loc}}w - A_4\right) = 0 \qquad [6.10]$$

The six roots of equation [6.10] are the eigenvalues of the hot and cold zones. By inspection of eqs. [6.2] which define the coefficients A_1, A_2, A_3, A_4 and A_5, it is seen that the eigenvalues depend on four parameters: δ, K_{loc}, Bi_{loc} and Pe_{loc}.

When $Pe_{loc} = 0$, eq. [6.10] becomes a cubic polynomial in w^2 indicating that the eigenvalues, in this case, appear in pairs of opposite sign. When $Pe_{loc} \neq 0$ but $K_{loc} = 1$, it may be shown by direct substitution that the eigenvalue pairs have the following form:

$$w^+ = a + Pe_{loc} \qquad [6.11a]$$

$$w^- = -a \qquad [6.11b]$$

where: a is a positive number

When $K_{loc} \neq 1$, results suggest that the eigenvalue pairs are separated by a number whose magnitude is of the order Pe_{loc}/K_{loc}:

$$w^+ = a + \varepsilon Pe_{loc}/K_{loc} \qquad [6.12a]$$

$$w^- = -a \qquad [6.12b]$$

where: ε is of order unity

Since the Peclet number is typically small, it is appropriate to study the behavior of the eigenvalue pairs assuming that $Pe = 0$; in this way, the order of the characteristic equation, eq. [6.10], is halved.

Figure 6.5 illustrates the variation of the three eigenvalue pairs as a function of δ with K_{loc} and Bi_{loc} as parameters. The lowest set of curves is seen to vary greatly with Bi_{loc}. Further, the values of the eigenvalues represented by the lowest set of curves is found to be closely

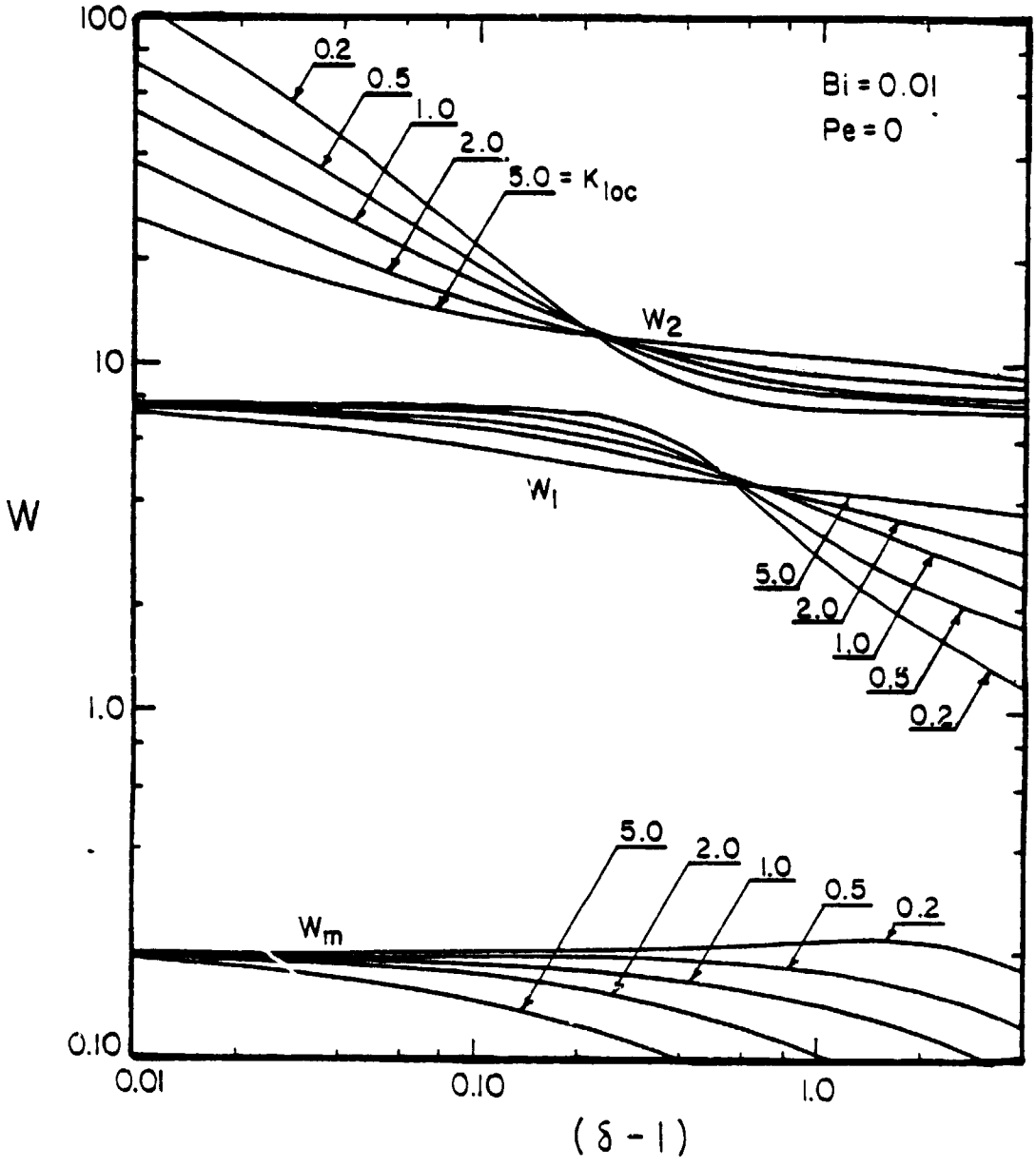

Fig. 6.5a: Eigenvalues for the hot and cold zones, Pe = 0.0 and Bi = 0.01.

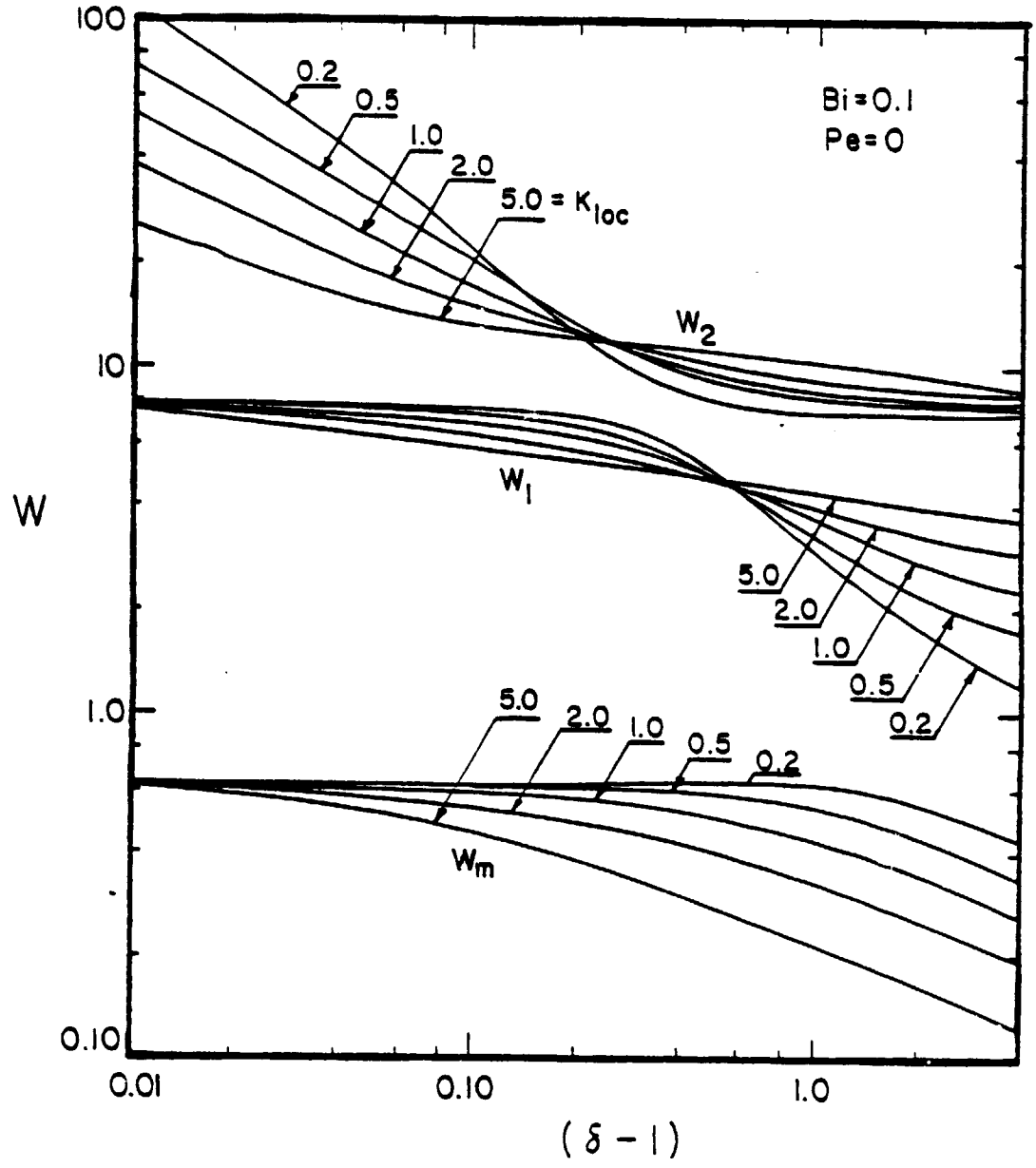

Fig. 6.5b: Eigenvalues for the hot and cold zones, Pe = 0.0 and Bi = 0.1.

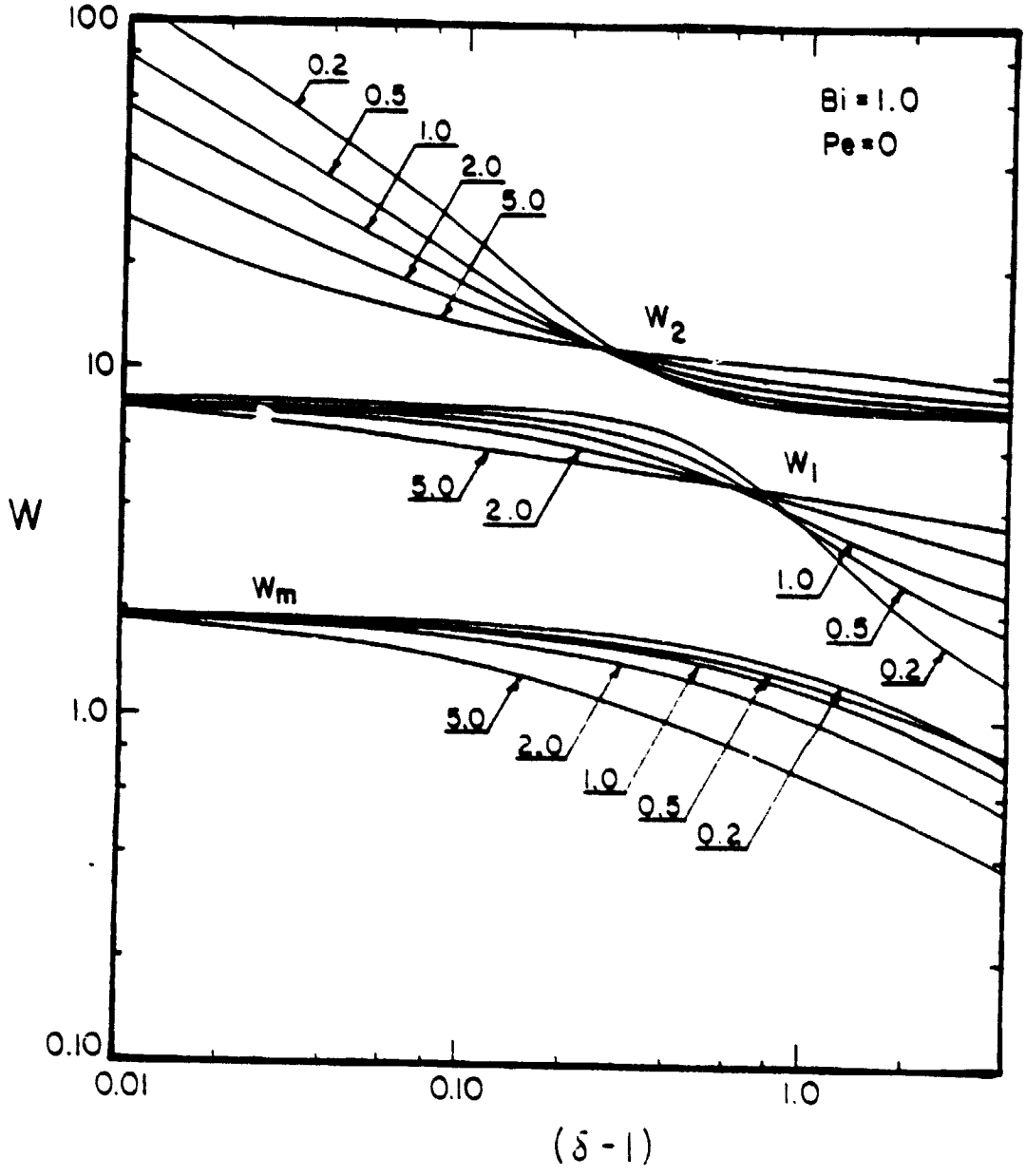

Fig. 6.5c: Eigenvalues for the hot and cold zones, Pe = 0.0 and Bi = 1.0.

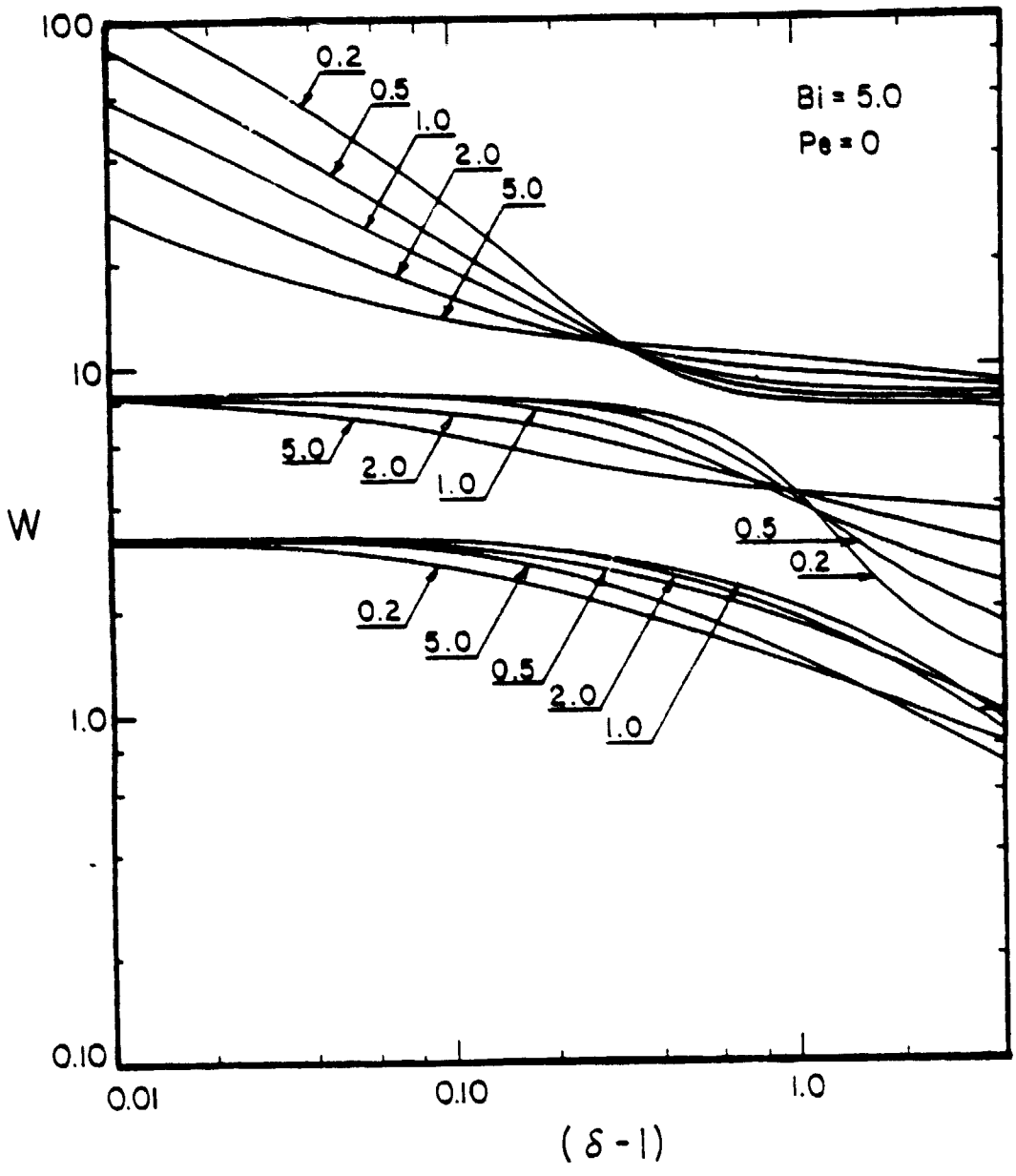

Fig. 6.5d: Eigenvalues for the hot and cold zones, Pe = 0.0 and Bi = 5.0.

predicted by eq. [5.7]:

$$w_m = \pm 2 \left(Bi^{*}_{loc} \right)^{1/2} \qquad [5.7]$$

(The largest difference between the eigenvalues predicted by eq. [5.7] and those in Fig. 6.5 is 26% at $K_{loc} = 0.2$, $\delta = 5$ and $Bi_{loc} = 5.0$; the difference decreases for smaller δ and Bi.) These eigenvalues, therefore, can be associated with the variation of the mean charge temperature and are denoted by w_m. As w_m increases, ϕ_m tends to approach more rapidly the temperature boundary conditions of the furnace.

The eigenvalues represented by the middle and upper set of curves in Fig. 6.5, denoted by w_1 and w_2 respectively, are relatively insensitive to Bi_{loc}. They do exhibit, however, a strong sensitivity to K_{loc} and δ, parameters which describe the thermal interaction between the charge and the crucible.

For the limiting case of $\delta \rightarrow 1$, i.e., no crucible, it is seen that w_1 approaches a constant value (approximately 7.6) independent of δ and K_{loc}. This value is therefore most easily identified with the thermal characteristics of the charge alone. Results derived in section 7.2 indicate that radial temperature gradients in a charge without a crucible attenuate at a rate proportional to $\exp(-7.63\zeta)$. Thus, w_1, is indicative of the rate of decay of ϕ_δ for systems when δ is small. The value of w_2 is very much larger than either w_1 or w_m for small values of δ suggesting that the crucible temperature equilibrates rapidly with the temperature of the outer charge fin.

A second limiting condition is that of large δ. Figure 6.5 shows that w_2 approaches the value of 7.6 as δ increases; further, the approach

to the limiting value takes place at smaller values of δ as K_{loc} decreases. These facts suggest that the charge is, in this case, "insulated" in the sense that heat transfer within the charge is much better than that between the charge and the crucible.

6.8.2 Gradient Zone

The characteristic equation for the eigenvalues in the gradient zone is determined in a manner analogous to that used to develop eq. [6.10]:

$$\left(w^2 - Pe_{loc}w - A_1\right)\left(w^2 - Pe_{loc}w - A_2\right)\left[\left(w^2 - \frac{Pe_{loc}}{K_{loc}}w\right)\left(w^2 - A_5\right) - A_4 w^2\right]$$

$$- A_3\left(w^2 - Pe_{loc}w\right)\left(w^2 - Pe_{loc}w - A_2\right)\left(w^2 - A_5\right)$$

$$- A_1\left(w^2 - Pe_{loc}w\right)\left[\left(w^2 - \frac{Pe_{loc}}{K_{loc}}w\right)\left(w^2 - A_5\right) - A_4 w^2\right] = 0 \qquad [6.13]$$

Equation [6.13] is a polynomial of eighth order in w; there are therefore eight eigenvalues in the gradient zone.

In eq. [6.13], the term of lowest order in w is the linear term:

$$-w\,Pe_{loc}\left[\frac{A_1 A_2 A_5}{K_{loc}} + A_2 A_3 A_5\right] \qquad [6.14]$$

Since there is no term of order zero in w, one of the eigenvalues is zero. Further, when $Pe_{loc} = 0$, eq. [6.14] shows that the linear term disappears; in this case, a second eigenvalue is zero. The solution for the fin temperatures given by eq. [6.5] is valid only when there are no repeated roots. When $Pe_{loc} = 0$, the term which would include the second zero eigenvalue is replaced by a term linear in ζ.

The linear component of equation [6.5] in the gradient zone can be demonstrated by multiplying eq. [6.1a] by $k_{loc}A$, eq. [6.1c] by $k_{cr}A_{cr}$ and eq. [6.1d] by $k_G A_G$ and then adding. With $Pe_{loc} \sim 0$, the result is:

$$\frac{d^2}{d\zeta^2}\left[k_{loc}A\phi_m + k_{cr}A_{cr}\phi_{cr} + k_G A_G \phi_G\right] = 0 \qquad [6.15]$$

or:
$$\frac{d^2\bar{\phi}}{d\zeta^2} = 0 \qquad [6.16]$$

where:
$$\bar{\phi} \equiv \frac{k_{loc}A\phi_m + k_{cr}A_{cr}\phi_{cr} + k_G A_G \phi_G}{k_{loc}A + k_{cr}A_{cr} + k_G A_G} \qquad [6.17]$$

$\bar{\phi}$ is interpreted as an average temperature of the charge/crucible/gradient zone annulus combination. Equation [6.15] results in a linear variation in $\bar{\phi}$ within the gradient zone. The physical interpretation is that there is only internal heat exchange between the fins of the gradient zone; there is no external heat addition or removal to the charge/crucible/gradient zone annulus combination by virtue of the assumption that the gradient zone annulus is adiabatic at its outer circumference. Therefore, neglecting Pe, the axial conduction of heat is constant within the gradient zone. The definition of $\bar{\phi}$ as an average of ϕ_m, ϕ_{cr} and ϕ_G weighted according to their respective axial heat conducting capacities is demonstrated by eq. [6.15] to correctly express the constant total axial heat transfer.

As occurs for the eigenvalues of the hot and cold zones, results show that the eigenvalues of the gradient zone occur in pairs of opposite sign which are separated by a number whose order of magnitude is that of Pe_{loc}/K_{loc} (c.f., eq. [6.12]). The partner of the zero eigenvalue

therefore has a value of order of magnitude Pe_{loc}. Since Pe_{loc} is typically small, the exponential function of eq. [6.5] with this eigenvalue is very nearly linear in the gradient zone.

The additional fourth pair of eigenvalues introduced by the gradient zone annulus within the gradient zone are associated with the rate of equilibration of ϕ_G with ϕ_m. An analytical expression for this eigenvalue based on a symmetric, one-dimensional system was developed in section 4.4.4:

$$w_G = 2 \left\{ Bi^{**}_{G,loc} \left[1 + \left(R^{*}_{G,loc} \right)^{-1} \right] \right\}^{1/2} \qquad [6.18]$$

Table 6.4 compares the values of w_G determined from the concentric fin model and from eq. [6.18]. The comparison is favorable, indicating that this eigenvalue pair of the concentric fin model is correctly associated with the rate of equilibration of ϕ_G and ϕ_m.

The eigenvalue pairs w_1 and w_2 are shown in Section 6.8.1 to be relatively insensitive to conditions external to the charge and crucible. Table 6.5 demonstrates that the additional parameter introduced into eqs. [6.1] by the gradient zone annulus, i.e., R_G, also has a second order effect on these eigenvalues. Therefore, approximations for w_1 and w_2 of the gradient zone may be obtained from Fig. 6.5.

Bi_G	$R_{G,loc}$ = 0.01	0.1	1.0	10.0
0.01	2.452 2.010	.7908 .6633	.2943 .2828	.1810 .2098
0.1	7.729 6.356	2.476 2.098	.9218 .8944	.5663 .6633
1.0	23.22 21.10	7.601 6.63	2.653 2.828	1.644 2.098
10.0	43.34 44.94	14.25 14.83	3.967 6.325	2.742 4.690

key: w_G from concentric fin model
w_G from eq. [6.18]

$Pe_S = 0.001$ $K_{loc} = 1.0$ $R_K = 1.0$

Table 6.4: Comparison of w_G determined from the concentric fin model and from eq. [6.18]

$Bi_{G,loc}$	$R_{G,loc}$ = 0.01	0.1	1.0	10.0
0.01	9.635 4.838	9.635 4.837	9.635 4.837	9.635 4.837
0.1	9.641 4.824	9.637 4.859	9.637 4.854	9.637 4.853
1.0	9.631 4.828	9.686 4.729	9.657 5.054	9.656 5.009
10.0	9.631 4.827	9.577 4.763	9.741 6.255	9.718 5.569

key: w_1 / w_2

$Pe_S = 0.001$ $K_{loc} = 1.0$ $R_K = 1.0$

Table 6.5: The relationship of w_1 and w_2 in the gradient zone to the parameters $Bi_{G,loc}$ and $R_{G,loc}$.

7. RADIAL TEMPERATURE VARIATIONS WITHIN THE CHARGE

Radial temperature variations near the growth interface are shown in this chapter to result from several effects usually present in Bridgman crystal growth. Systems with an adiabatic gradient zone, first studied by Chang and Wilcox [17], addresses only one of these factors. The other factors have not been adequately considered in the literature: non-perfectly insulating gradient zone ($h_G \neq 0$), and thermal conductivity change and/or generation of latent heat at the growth interface in the presence of a crucible. Computer solutions of the concentric fin model are used to graphically illustrate the behavior of the radial temperature variations under the influence of these factors. Special attention is given, however, to the development of approximate analytical expressions which serve to emphasize the functional dependence of the radial temperature variations on the various system parameters.

The variable ϕ_Δ defined by the concentric fin model of Chapter 6, is used to indicate the radial temperature variations within the charge. The results for ϕ_Δ to be shown in the following sections are conveniently approximated to the interface shape by the following relation developed in Appendix G:

$$N \simeq -\frac{1}{16}\frac{(d\phi_m/d\zeta)}{\phi_\Delta} \qquad [7.1]$$

where N is the radius of curvature of an isotherm in number of charge radii at a particular axial location. (N is positive for an interface which is concave toward the crystal as shown in Fig. 2.1.) Accordingly, the degree

of flatness of isotherms is enhanced by large axial temperature gradients ($d\phi_m/d\zeta$) and small radial temperature gradients (ϕ_Δ).

7.1 CAUSES OF RADIAL TEMPERATURE VARIATIONS WITHIN THE GRADIENT ZONE

Subtracting eq. [6.1b] from eq. [6.1a], and assuming that the Peclet term is regligible (c.f., section 5.1), yields:

$$\frac{d^2\phi_\Delta}{d\zeta^2} - A_2\,\phi_\Delta = \frac{d^2\phi_m}{d\zeta^2} \qquad [7.2]$$

The particular solution of eq. [7.2], denoted by ϕ_Δ^P, may be solved by using the appropriate Green's function:

$$G(\zeta, x) = -\frac{1}{2A_2^{1/2}} \exp\left(-A_2^{1/2}|\zeta - x|\right) \qquad [7.3]$$

Using eq. [7.3], the particular solution of eq. [7.2] is:

$$\phi_\Delta^P(\zeta) = -\frac{1}{15.26}\int_{\zeta_H}^{\zeta_c}\left[\frac{d^2\phi_m}{dx^2}\right]\exp(-7.63|\zeta - x|)\,dx \qquad [7.4]$$

where the value of A2 given by eq. [6.2b] has been used, x is a dummy variable of integration, and ζ_c and ζ_H are the axial locations of the cold and hot ends of the charge, respectively. (Note that eq. [7.4] is not the complete solution for ϕ_Δ^P since ϕ_m and ϕ_Δ are not independent by virtue of the coupled nature of the fin equations. Nevertheless, the actual distributions for ϕ_Δ^P and ϕ_m must satisfy eq. [7.4].)

$d^2\phi_m/d\zeta^2$ is non-zero when the combined axial heat conduction within the inner and outer charge fins is not constant with axial position; i.e., when there is heat addition to or removal from the charge. Equation [7.4],

therefore, clearly demonstrates that radial temperature gradients within the charge are caused by heat exchange between the charge and its surroundings. Such heat exchange occurs:

1) if, in the idealized case of no crucible, there is a difference between the temperatures of the outer charge fin and the furnace, and the heat transfer coefficient between them is not zero.
(2) if, when a crucible is present, there is a difference between the temperatures of the crucible and the outer charge fin.

Equation [7.4] expresses ϕ_Δ^P at a particular axial location as the superposed effects of heat transfer to the charge along its entire length. However, the effect of heat transfer to the charge at one location, x, on the radial temperature gradient at another location, ζ, attenuates rapidly with the distance between the two locations, being proportional to the factor $\exp(-7.63|\zeta - x|)$. For example, when $|\zeta - x| = 1$, the value of this exponential function is 0.00049. Therefore, the radial variation in temperature at the location ζ is primarily affected by heat exchange with the charge within the range $\zeta \pm 1$ (i.e., one charge diameter to either side of the given location).

7.1.1 Analysis of Radial Temperature Variations In the Gradient Zone

The total solution for $\phi_\Delta(\zeta)$ includes, in addition to eq. [7.4], the homogeneous part of the solution:

$$\phi_\Delta(\zeta) = C_1 e^{-7.63\zeta} + C_2 e^{7.63\zeta} + \phi_\Delta^P \qquad [7.5]$$

Equation [7.5] is applied separately to each region of the charge of uniform properties; given the assumptions of the concentric fin model, there are two such regions -- the liquid and the solid portions of the charge. The coefficients C_1 and C_2 in eq. [7.5] are found by applying boundary conditions at the ends of the charge and at the growth interface.

Radial temperature variations near the growth interface are of primary concern. Since the interface is assumed to be in the gradient zone, eq. [7.5] is applied, in the remainder of this chapter, only to the gradient zone; i.e., $-\lambda_G/2 \leq \zeta \leq \lambda_G/2$. It is also assumed that there is at least one diameter of charge in both the hot and cold zones:

$$\zeta_H < -(\lambda_G/2 + 1) \qquad [7.6a]$$

$$\zeta_C < (\lambda_G/2 + 1) \qquad [7.6b]$$

As noted earlier, heat exchange with the charge at distances greater than about one diameter from the ends of the gradient zone contribute little to the radial temperature variations in the gradient zone. Equations [7.6] thus permit the limits of integration in eq. [7.5] to be contracted if desired, and further, the effects of the boundary conditions at the ends of the charge on Φ_Δ can be neglected.

When the solid and liquid thermal properties of the charge are equal, i.e., $R_K = 1$, eq. [7.5] need be applied only once to the entire length of the charge. The homogeneous part of the solution disappears under the restrictions of eq. [7.6] and the total solution for $\Phi_\Delta(\zeta)$ within the gradient zone becomes:

$$\Phi_\Delta(\zeta) = -\frac{1}{15.26}\int_{\zeta_H}^{\zeta_c}\left[\frac{d^2\Phi_m}{dx^2}\right]\exp\left(-7.63|\zeta - x|\right)dx \qquad [7.7]$$

where: $-\lambda_G/2 \le \zeta \le \lambda_G/2$

$R_K = 1$

When $R_K \neq 1$, eq. [7.5] must be applied separately to the liquid and solid portions of the charge using the following boundary conditions at the growth interface:

$$\left[\Phi_\Delta(\zeta_i)\right]_L = \left[\Phi_\Delta(\zeta_i)\right]_S \qquad [7.8a]$$

$$R_K\left[\frac{d\Phi_\Delta(\zeta_i)}{d\zeta}\right]_L = \left[\frac{d\Phi_\Delta(\zeta_i)}{d\zeta}\right]_S \qquad [7.8b] \text{ (also eq. [6.7b])}$$

Applying these boundary conditions yields:

$$\left[\Phi_\Delta(\zeta)\right]_L = \frac{2I_S(\zeta_i) + (R_K - 1)I_L(\zeta_i)}{R_K + 1}e^{-7.63(\zeta_i - \zeta)} + I_L(\zeta) \qquad [7.9]$$

where: $-\lambda_G/2 \le \zeta \le \zeta_i$

$$\left[\Phi_\Delta(\zeta)\right]_S = \frac{-(R_K - 1)I_S(\zeta_i) + 2R_K I_L(\zeta_i)}{R_K + 1}e^{-7.63(\zeta - \zeta_i)} + I_S(\zeta) \qquad [7.10]$$

where: $\zeta_i \le \zeta \le \lambda_G/2$

The variables $I_L(\zeta)$ and $I_S(\zeta)$ represent the respective contributions of radial heat exchange with the liquid and solid portions of the charge to the value of Φ_Δ at any axial location ζ within the gradient zone. They are defined as follows:

$$I_L(\zeta) = -\frac{1}{15.26}\int_{\zeta_H}^{\zeta_i}\left[\frac{d^2\phi_m}{dx^2}\right]\exp(-7.63|\zeta-x|)dx \qquad [7.11a]$$

$$I_S(\zeta) = -\frac{1}{15.26}\int_{\zeta_i}^{\zeta_C}\left[\frac{d^2\phi_m}{dx^2}\right]\exp(-7.63|\zeta-x|)dx \qquad [7.11b]$$

The first term in each of eqs. [7.9] and [7.10] represents a contribution to $\phi_\Delta(\zeta)$ which is produced at the growth interface and which attenuates with distance from the interface. This contribution is absent when $R_K = 1$.

The value of ϕ_Δ at the interface, $\phi_\Delta(\zeta_i)$, is determined from either eq. [7.9] or eq. [7.10]:

$$\phi_\Delta(\zeta_i) = \frac{2}{R_K+1}\left[I_S(\zeta_i) + R_K I_L(\zeta_i)\right] \qquad [7.12]$$

An attractive possibility for the quantitative utilization of eqs. [7.9] and [7.10] is to provide $d^2\phi_m/d\zeta^2$ from the results of one-dimensional modeling; that is, to approximate $d^2\phi_m/d\zeta^2$ with $d^2\theta_m/d\zeta^2$. In this way, a two-dimensional temperature distribution is obtained only through these equations and a one-dimensional model. The error in ϕ_Δ calculated in this manner would be due to approximations in (1) the one-dimensional model which estimates $d^2\theta_m/d\zeta^2$ and (2) the concentric fin model which provides eq. [7.2].

One-dimensional models do provide good approximations for the charge mean temperature distribtuion, $\theta_m(\zeta)$. Taking two derivatives of such a distribution in order to obtain a good approximation for $d^2\phi_m/d\zeta^2$ is more likely to be unreliable. Results presented later in this chapter, in fact,

demonstrate that the presence of a crucible produces a distribution of radial heat exchange with the charge which is not predicted by a one-dimensional model; therefore, the use of $\partial^2\phi_m/\partial\zeta^2$ calculated from one-dimensional models is not appropriate for use in eqs. [7.11]. Nevertheless, even in these cases, the Green's function approach developed in this section may be used to obtain a qualitative understanding of the behavior of radial temperature variations within the charge.

7.2 PENETRATION OF RADIAL TEMPERATURE VARIATIONS INTO THE GRADIENT ZONE FROM THE HOT AND COLD ZONES

Heat transfer to the charge in the hot zone and from the charge in the cold zone must occur so that the required axial temperature gradient at the growth interface is obtained. Such heat exchange, according to the results of section 7.1, produces radial temperature variations within the charge which, even within an adiabatic gradient zone, influence the shape of the growth interface.

Fu and Wilcox [26] studied the penetration of radial temperature variations into an adiabatic gradient zone for systems without a crucible through the use of a two-dimensional finite difference model. Isotherm shapes indicate, for various Bi and Pe, that radial temperature variations within the charge in the hot and cold zones attenuate rapidly from the ends of the gradient zone. If the gradient zone is sufficiently long, there exists a region within which the shape of isotherms is quite flat.

7.2.1 Systems Without a Crucible

Figure 7.1 shows the variation of ϕ_Λ in an adiabatic gradient zone, obtained by the concentric fin model of Chapter 6 for systems without a crucible. (Note that the vertical scale of Fig. 7.1 changes from

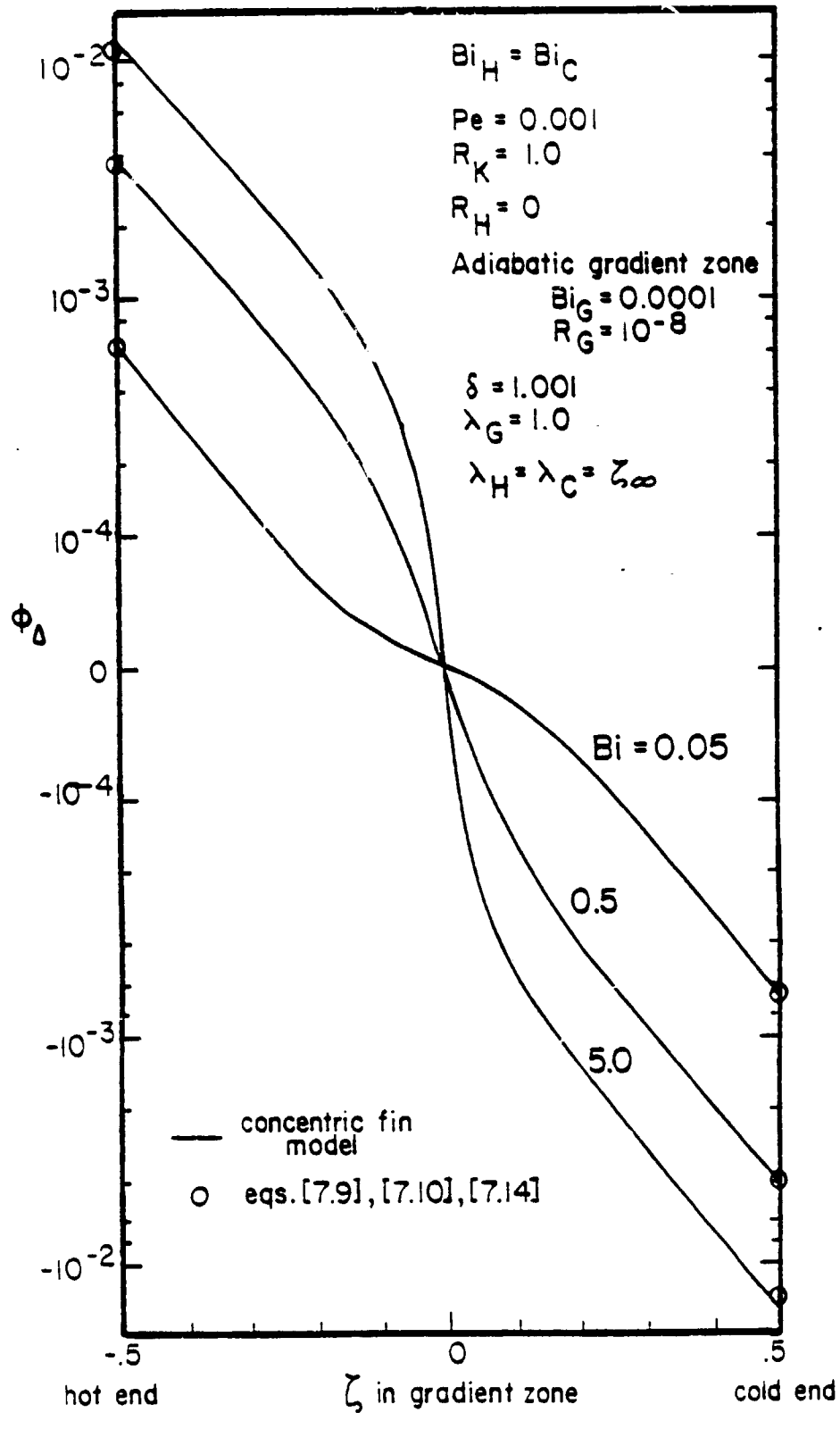

Fig. 7.1: Variation of ϕ_Δ in an adiabatic gradient zone without a crucible. The system is symmetric.

logarithmic to linear at $\pm 10^{-4}$ so that both negative and positive values of Φ_3 may be plotted in the same figure.) Accordingly, it is seen that Φ_3 attenuates at a rate approximately proportional to $\exp(-7.6\,\zeta^*)$ where ζ^* is measured from the ends of the gradient zone. It is also seen that Φ_3 in the gradient zone increases with the Biot number of the hot and cold zones reflecting greater amounts of radial heat transfer to the charge in these zones.

The variation of the radius of curvature of isotherms for the same cases considered in Fig. 7.1 is shown in Fig. 7.2. These curves were calculated using eq. [7.1] along with values of Φ_3 and $d\Phi_m/d\zeta$ determined from the concentric fin model. Accordingly, there is a central region of the gradient zone where the isotherm shapes are quite flat. To obtain an interface which is slightly concave toward the crystal, i.e., small but positive N^{-1}, requires that the interface be located slightly to the hot side of the center of the gradient zone. Also seen in Fig. 7.2 is that isotherms are more curved as Bi increases. Therefore, for the parameter values considered, increasing the Biot number of the hot and cold zones has a greater effect on increasing Φ_3 than upon increasing the axial temperature gradient of the charge in the gradient zone.

The effect of unequal hot and cold zone Biot numbers in an otherwise symmetric system is shown in Fig. 7.3. As the hot zone Biot number increases relative to the constant cold zone Biot number, Φ_3 becomes more positive in the hot portion of the gradient zone. In this region, therefore, isotherm shapes become more concave toward the crystal and the location of the flat isotherm shifts slightly toward the cold zone. The effect of changing thermal conditions in the hot zone attenuates rapidly

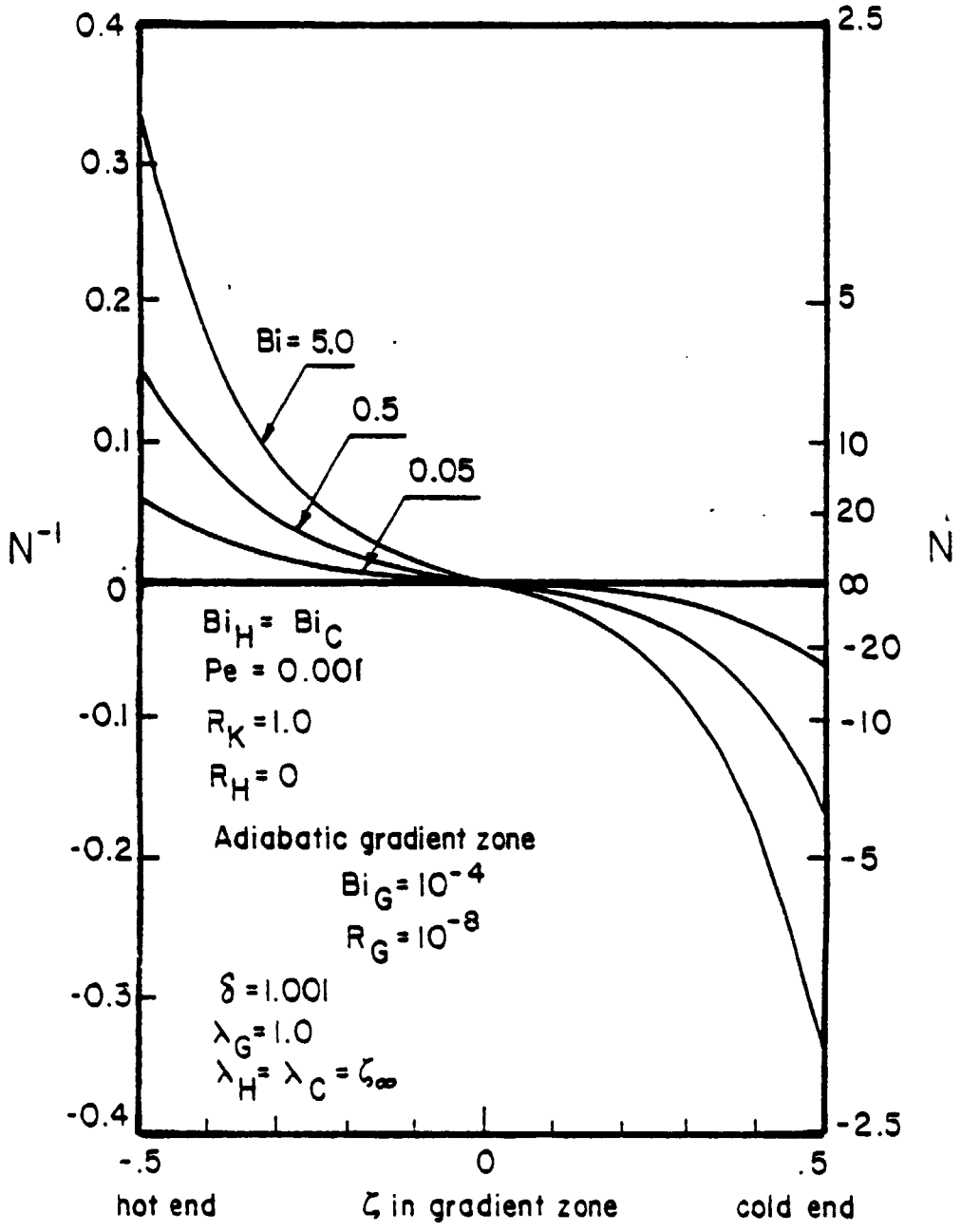

Fig. 7.2: Variation of isotherm shapes for the same cases considered in Figure 7.1.

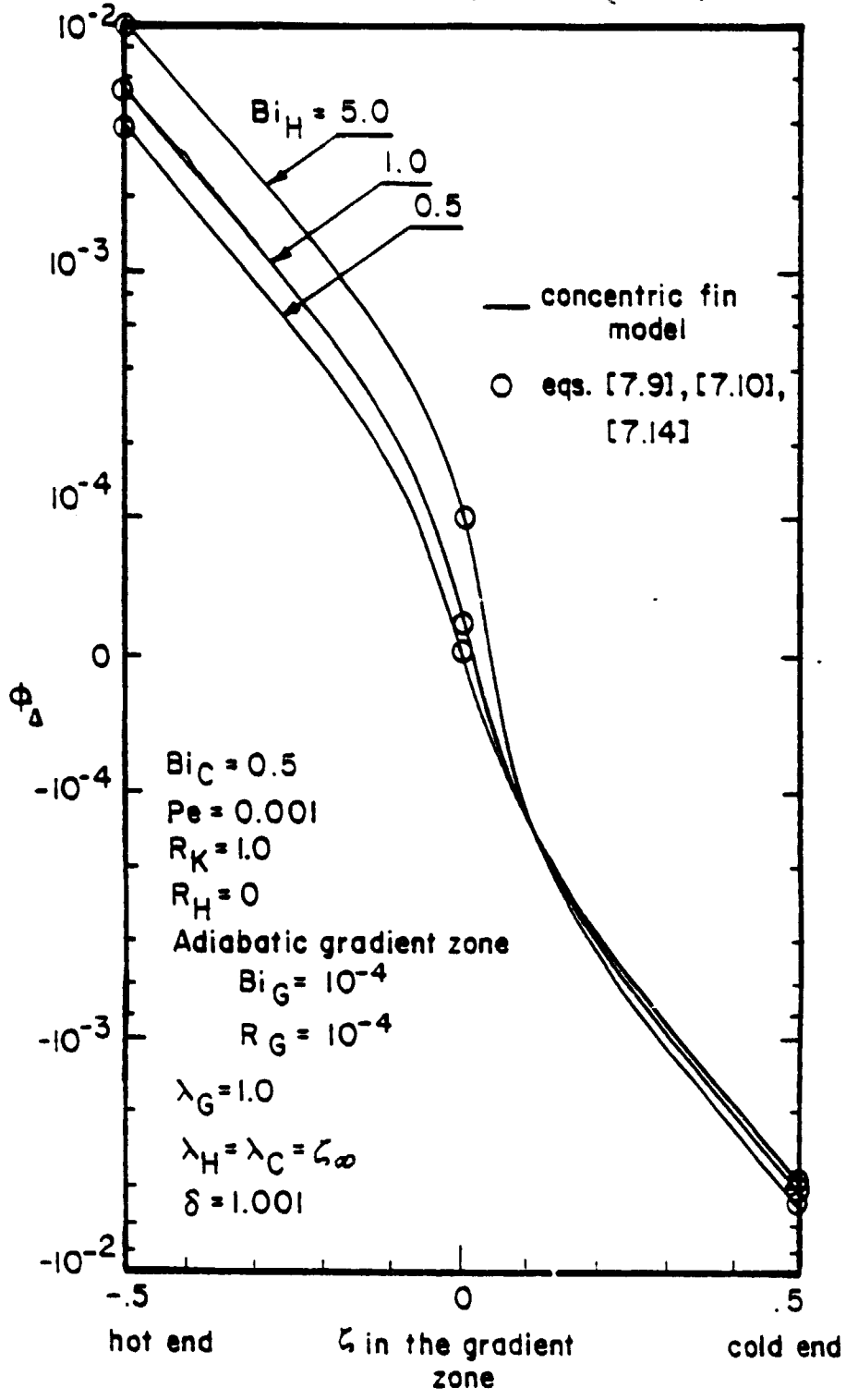

Fig. 7.3: The effect of unequal hot and cold zone Biot numbers on Φ_Δ in an adiabatic gradient zone. The systems are otherwise symmetric.

from the end of the hot zone and affects only slightly the radial temperature variations near the cold end of the gradient zone.

Figure 7.4 shows the variation of ϕ_Δ in systems which are symmetric except $R_K \neq 1$. In the systems considered, the cold zone Biot number remains constant; the hot zone Biot number therefore changes with R_K ($Bi_H = Bi_C/R_K$). As R_K increases, it is seen that ϕ_Δ in the hot part of the gradient zone decreases whereas ϕ_Δ in the cold part of the gradient zone is little affected. This behavior is similar to that of a changing value of Bi_H exhibited in Fig. 7.3. Further, a disturbance appears at the interface which increases as R_K increases and which dies out with distance from the interface. This disturbance represents the first term in eqs. [7.9] and [7.10] where it is shown that it appears only when $R_K \neq 1$.

An analytical expression for the variation of ϕ_Δ in an adiabatic gradient zone may be obtained by using θ_m determined by the moving fin model in order to approximate $d^2\phi_m/d\zeta^2$ in eqs. [7.11]. The charge is assumed infinite in length; in this case, θ_m is described by a simple exponential function in both the hot and cold zones. Further, the Peclet number is assumed small enough to satisfy eq. [5.6]; the argument for the exponential function is then given by w_m in eq. [5.7]. Hence:

hot zone: $\zeta \leq -\lambda_G/2$

$$\theta_m(\zeta) = 1 - [1 - \theta_m(-\lambda_G/2)] \exp[2(Bi_H^{**})^{1/2}(\zeta + \lambda_G/2)] \qquad [7.13a]$$

cold zone: $\zeta \geq \lambda_G/2$

$$\theta_m(\zeta) = \theta_m(\lambda_G/2) \exp[2(Bi_C^{**})^{1/2}(\lambda_G/2 - \zeta)] \qquad [7.13b]$$

Substituting the second derivatives of eqs. [7.13] into eqs. [7.11] and

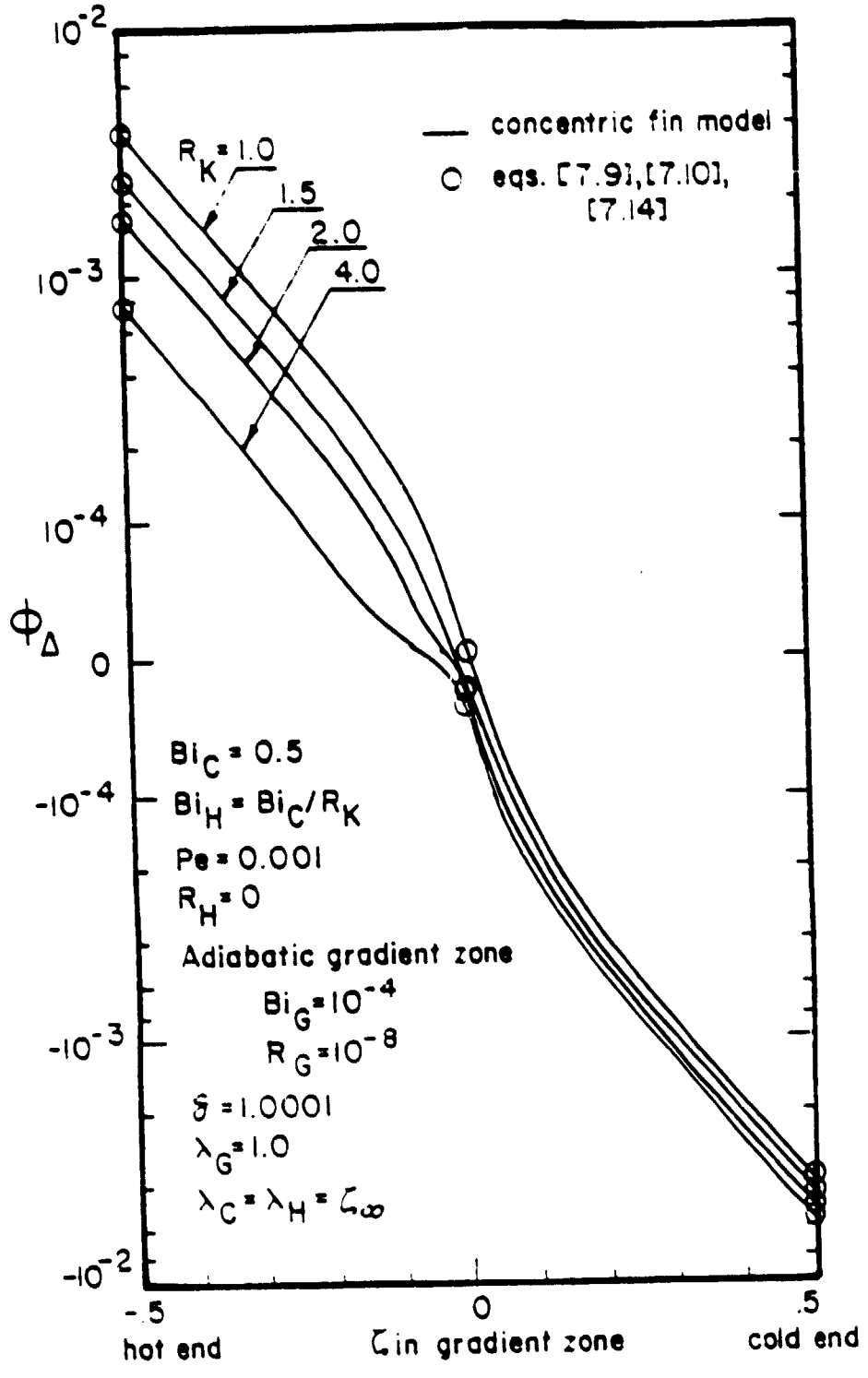

Fig. 7.4: Variation of ϕ_Δ in an adiabatic gradient zone without a crucible. The systems are symmetric except $R_K \neq 1$.

noting that $d^2\theta_m/d\zeta^2 = 0$ in the adiabatic gradient zone, yields:

$$I_L(\zeta) = \frac{Bi_H^{**}\left[1-\theta_m(-\lambda_G/2)\right]}{3.82\left[7.63+2(Bi_H^{**})^{1/2}\right]}\exp\left[-7.63(\zeta+\lambda_G/2)\right] \qquad [7.14a]$$

$$I_s(\zeta) = \frac{Bi_c^{**}\,\theta_m(\lambda_G/2)}{3.82\left[7.63+2(Bi_c^{**})^{1/2}\right]}\exp\left[-7.63(\lambda_G/2-\zeta)\right] \qquad [7.14b]$$

where: $-\lambda_G/2 \le \zeta \le \lambda_G/2$

Equation [7.14a] represents the effect of radial heat transfer between the charge and the furnace in the hot zone on the radial temperature variations in the gradient zone. The effect of the hot zone dies out exponentially with distance from the hot end of the gradient zone at approximately the same rate observed in Fig. 7.1. Equation [7.14b] has an analogous interpretation with regard to heat transfer in the cold zone.

Substituting eqs. [7.14] into eqs. [7.9] and [7.10] produces the desired approximation for ϕ_Δ in the gradient zone due to attenuation of radial gradients from the furnace zones. Evaluating eqs. [7.14] at $\zeta = \zeta_i$ and substituting the result into eq. [7.12] yields ϕ_Δ at the growth interface.

The one-dimensional results required by eqs. [7.14] are the effective Biot numbers and the mean charge temperatures at the hot and cold ends of the gradient zone. For a system with $Bi_G = 0$ and which has a negligible Peclet number, the axial temperature gradient in the gradient zone, G, is constant except for a step change at the growth interface. The temperatures at the ends of the gradient zone are therefore approximated by the following expressions:

$$\theta_m(-\lambda_G/2) = \theta_m(\zeta_i) - G_L \cdot (\lambda_G/2 + \zeta_i) \qquad [7.15a]$$

$$\theta_m(\lambda_G/2) = \theta_m(\zeta_i) + G_S \cdot (\lambda_G/2 - \zeta_i) \qquad [7.15b]$$

where: Pe satisfies eq. [5.6]

$Bi_G = 0$

$-\lambda_G/2 \leq \zeta \leq \lambda_G/2$

The non-dimensional interface temperature, θ_i , is given by eq. [B.10], G_L is given by eq. [B.9], and G_S is related to G_L in eq. [4.25].

The circled points in Figs. 7.1, 7.3, and 7.4 indicate values of ϕ_Δ calculated through the use of eqs. [7.14]. The values of G_L, G_S and θ_i required by eqs. [7.14] have been calculated using eqs. [7.15] as described above. It is seen that the values of ϕ_Δ obtained by the two methods agree very closely indicating that the moving fin model provides a good approximation for $d^2\phi_m/d\zeta^2$ for the systems considered, i.e., those without a crucible and with an adiabatic gradient zone. The largest difference occurs for the largest value of Bi reflecting the slight decrease in accuracy of the effective Biot number as Bi increases.

7.2.2 Systems With a Crucible

The effects of the presence of a crucible on radial temperature variations in an adiabatic gradient zone are shown in Figs. 7.5 and 7.6. The systems examined are symmetric and infinite in length; Fig. 7.5 considers variable δ (with $K = 1$) while Fig. 7.6 considers variable K (with $\delta = 1.5$). The primary effects of the crucible are seen to be a reduction in the value of ϕ_Δ at the ends of the gradient zone and a reduction in the rate at which ϕ_Δ attenuates toward the center of the

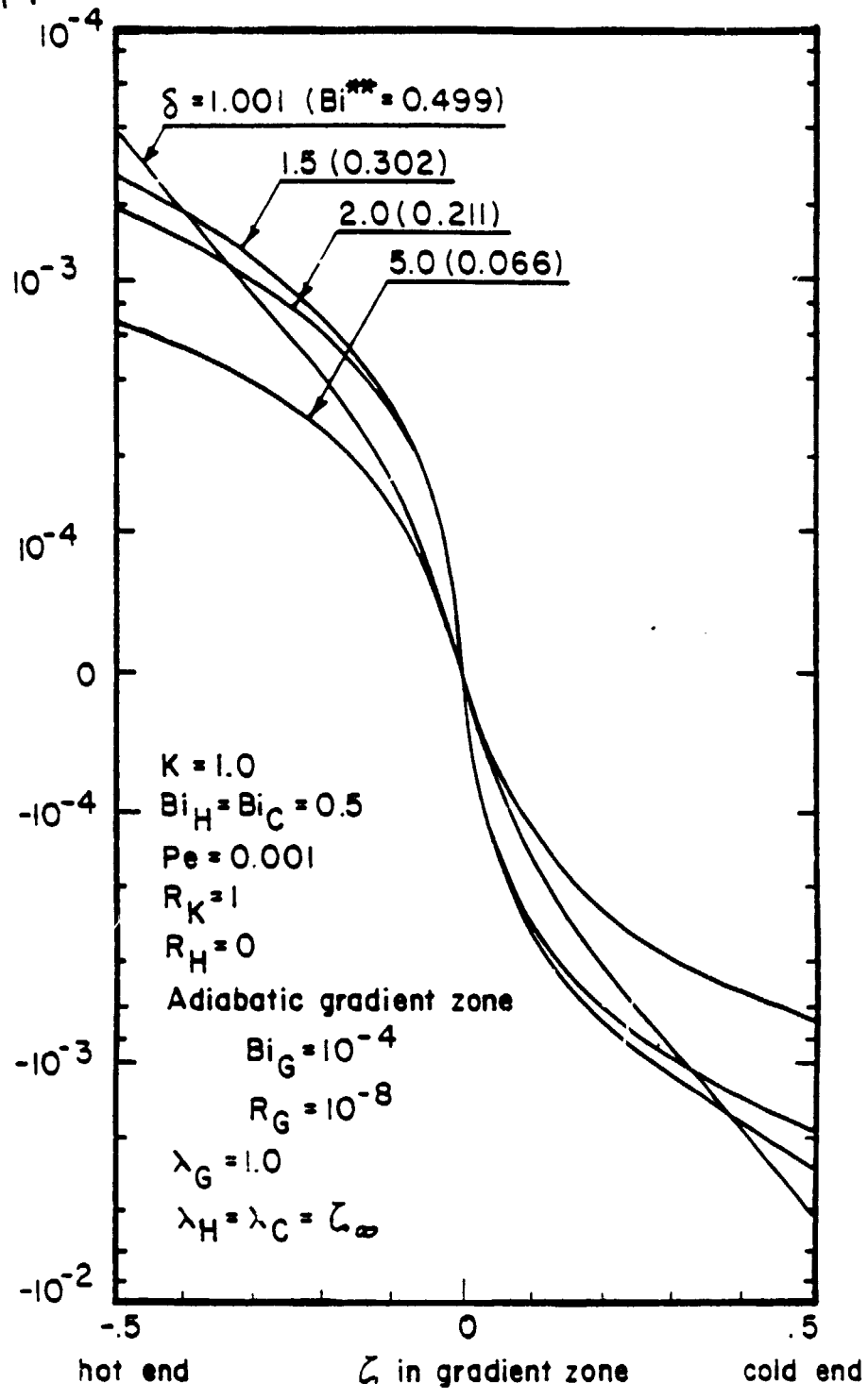

Fig. 7.5: Variation of ϕ_Δ in an adiabatic gradient zone with a crucible. The systems are symmetric with variable diameter ratio δ (K = 1.0).

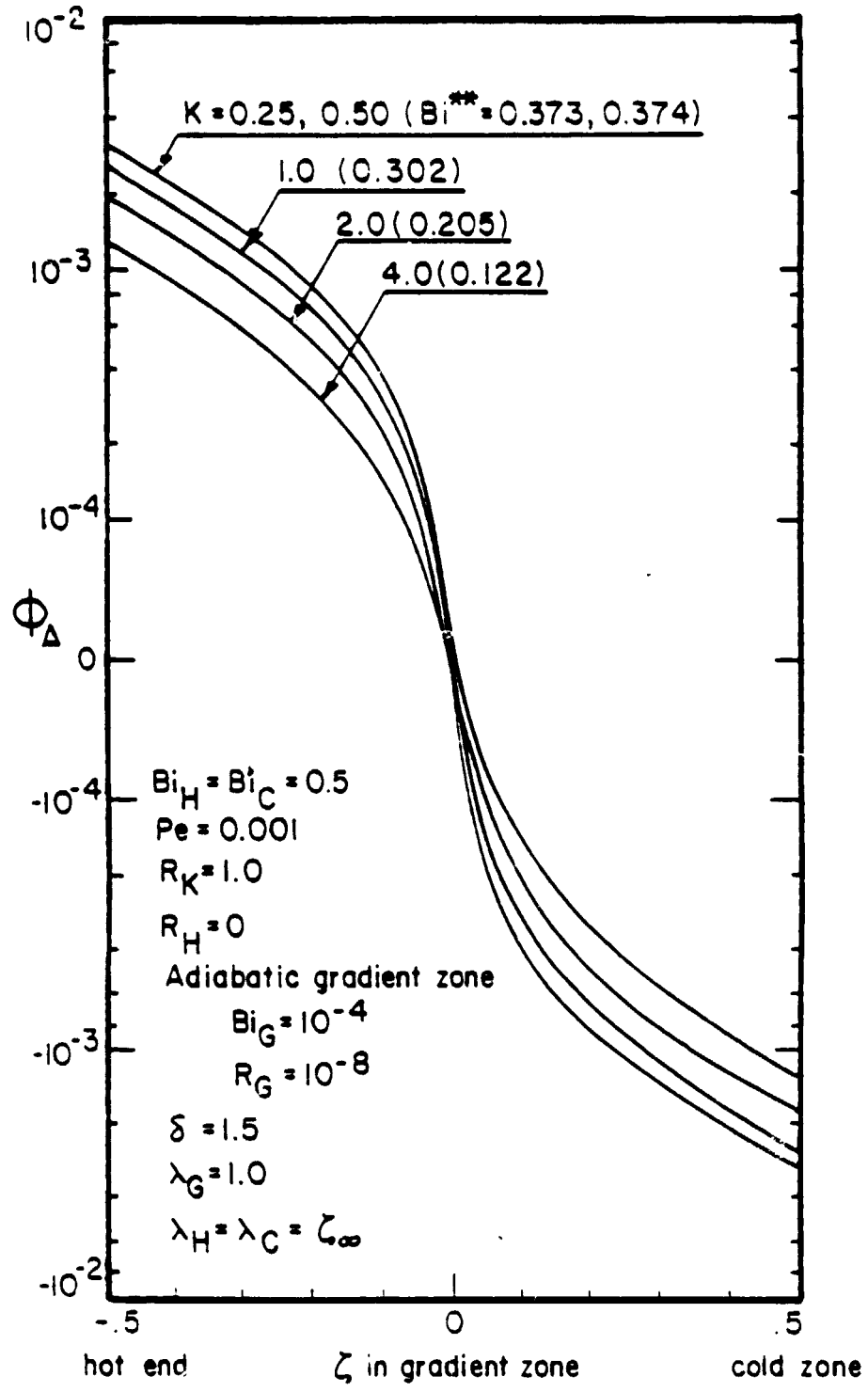

Fig. 7.6: Variation of Φ_Δ in an adiabatic gradient zone with a crucible. The systems are symmetric with variable thermal conductivity K (δ = 1.5).

gradient zone.

The reduction in the value of ϕ_Δ at the ends of the gradient zone when a crucible is present is attributable to the effect of the crucible on the effective Biot number, Bi^{**}. In most cases, the presence of a crucible decreases Bi^{**} compared to a charge without a crucible (c.f., section 4.2.2). A reduction in the heat exchange between the charge and furnace is therefore expected, resulting in decreased radial temperature variations within the charge. The individual curves of Figs. 7.5 and 7.6, labeled with their respective values of Bi^{**}, demonstrate the correlation between $\phi_\Delta(\pm\lambda_c/2)$ and Bi^{**}.

The reduction in the rate of attenuation of ϕ_Δ when a crucible is present results from radial heat exchange between the crucible and the charge near the ends of the gradient zone. Such heat transfer occurs when the crucible and the charge temperatures are not equal. A value of zero for the local Biot number is no longer sufficient to eliminate heat transfer to the charge in the gradient zone.

The variation of $(\phi_{cr} - \phi_m)$ near the hot end of the gradient zone, is shown in Fig. 7.7 for the case of $\delta = 2$ from Fig. 7.5. It is seen that the difference in the crucible and charge temperatures created by heat transfer in the hot zone furnace extends into the adiabatic gradient zone. The resultant effect on radial heat exchange with the charge is indicated by the distribution of $d^2\phi_m/d\zeta^2$ in Fig. 7.8 (lower solid curve). It is seen that $d^2\phi_m/d\zeta^2$ is not zero in the adiabatic gradient zone; the effect of the crucible is to extend radial heat transfer taking place in the hot zone into the gradient zone. Analysis of eqs. [7.11] verifies that this extension of radial heat exchange serves to decrease the apparent rate of attenuation of ϕ_Δ at the ends of the gradient zone.

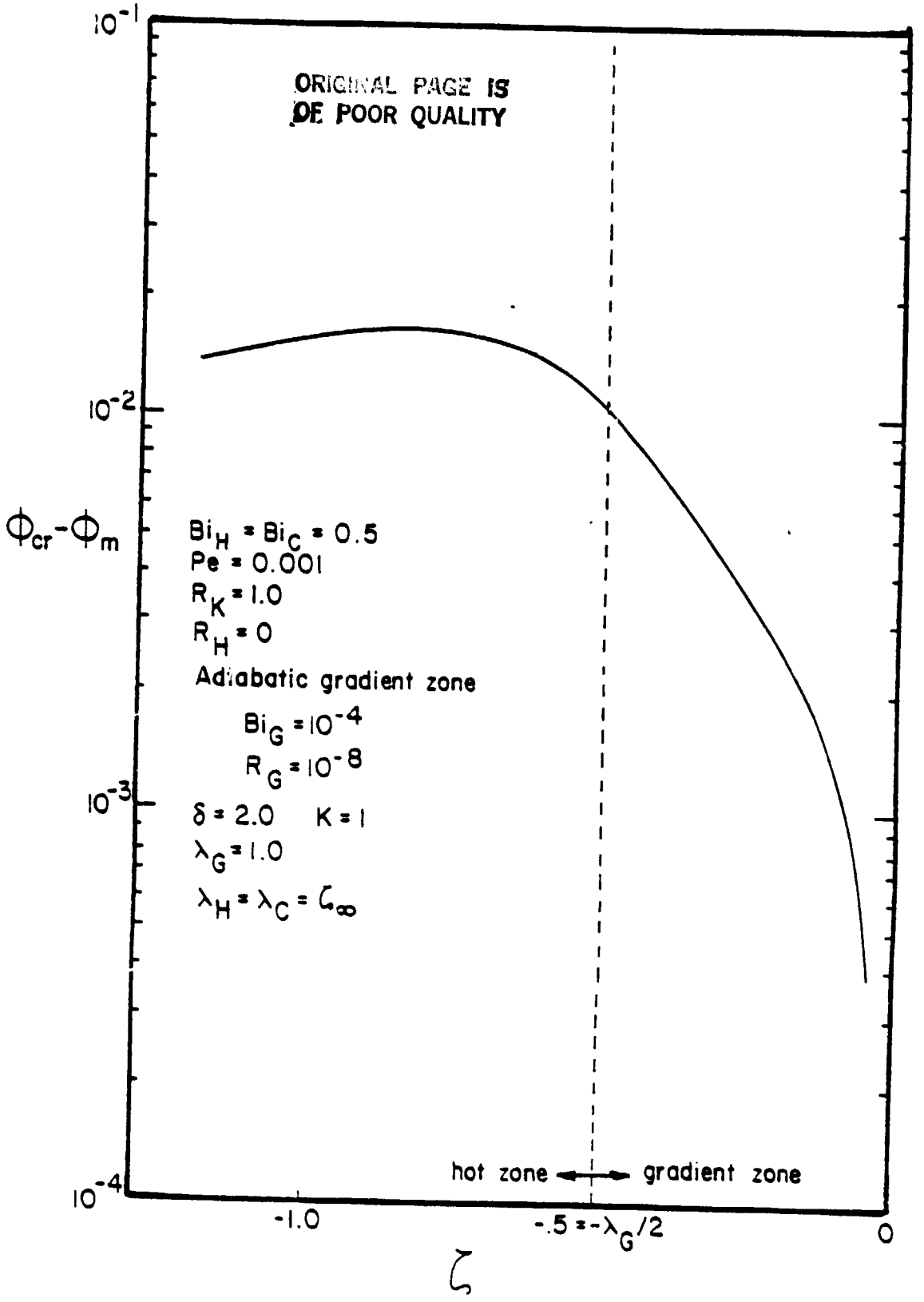

Fig. 7.7: The distribution of $\Phi_{cr} - \Phi_m$ near the hot end of an adiabatic gradient zone, calculated by the concentric fin model.

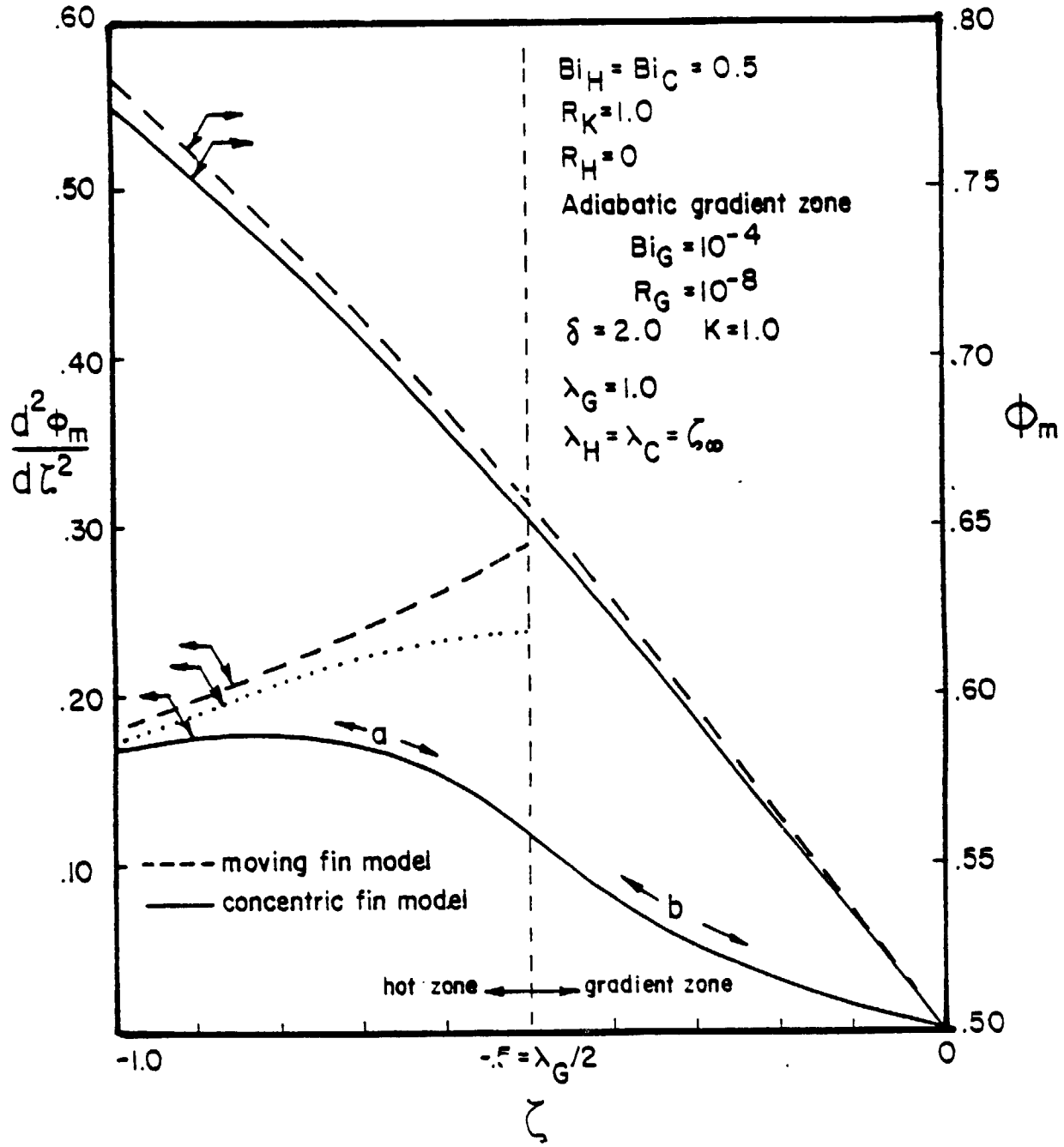

Fig. 7.8: Distributions of ϕ_m and $d^2\phi_m/d\zeta^2$ near the hot end of the gradient zone, calculated by the moving fin and concentric fin models.

Assuming that the Pe term in eq. [4.17] is negligible, the one-dimensional moving fin model of Chapter 4 predicts:

$$\frac{d^2\theta_m}{d\zeta^2} = -4Bi^{**}_{loc}\left(\theta_{F,loc} - \theta_m\right) \qquad [7.16]$$

Since $Bi_G = 0$, the moving fin model predicts that $d^2\theta_m/d\zeta^2 = 0$ in an adiabatic gradient zone, whether a crucible is present or not. The dashed curve of Fig. 7.8 is the distribution of $d^2\theta_m/d\zeta^2$ determined from the moving fin model. The moving fin model is unable to account for the particular nature of radial heat transfer between the charge and crucible caused by the abrupt change in furnace boundary conditions at the ends of the gradient zone. Although the error is of minor consequence in calculating the distribution of θ_m, results from the moving fin model, in particular $d^2\theta_m/d\zeta^2$, are inadaquate to describe the local variation of radial heat transfer near the ends of an adiabatic gradient zone when a crucible is present.

Table 7.1 compares values of ϕ_Δ at the end of the hot zone (i.e., at $\zeta = -\frac{\lambda_G}{2} = -0.5$) calculated by eq. [7.14a] (i.e., with the use of the moving fin model) and by the concentric fin model for the cases shown in Figs. 7.5 and 7.6. It appears that eq. [7.14a] predicts well the qualitative trends as K and δ change as well as being, to a certain degree, quantitatively accurate. This conclusion provides further evidence for the correlation between Bi^{**} and $\phi_\Delta(\pm\lambda_G/2)$ noticed in Figs. 7.5 and 7.6. Such a favorable comparison may seem, however, surprising in view of the limitations in the moving fin model discussed in the preceeding paragraph. This apparent anomoly is explained by a closer examination of the

		moving fin model			$\Phi_\Delta(-\lambda_G/2)$	
K_{loc}	δ	Bi**	$d\theta_m/d\zeta$	$\theta_m(-\frac{\lambda_G}{2})$	eq. [7.14a]	concentric fin model
1.0	1.001	0.471	-0.407	0.703	0.00407	0.00407
1.0	1.5	0.291	-0.350	0.675	0.00284	0.00263
1.0	2.0	0.205	-0.312	0.656	0.00216	0.00193
1.0	5.0	0.0619	-0.199	0.600	0.000797	0.000683
0.25	1.5	0.357	-0.374	0.687	0.00331	0.00318
0.50	1.5	0.356	-0.374	0.687	0.00331	0.00310
2.0	1.5	0.200	-0.309	0.654	0.00212	0.00197
4.0	1.5	0.121	-0.258	0.629	0.00141	0.00132

$Bi = Bi_C = Bi_H = 0.5$

Symmetric system

$\lambda_G = 1.0$

$\lambda_H = \lambda_C = \zeta_\infty$

Table 7.1: Comparison of eq. [7.14] and the concentric fin model to predict Φ_Δ at the end of the gradient zone. The systems are those examined in Figs. 7.5 and 7.6

distributions of $d^2\theta_m/d\zeta^2$ and $d^2\phi_m/d\zeta^2$ shown in Fig. 7.8.

The abrupt change in $d^2\theta_m/d\zeta^2$ predicted by the moving fin model at the end of the gradient zone becomes smoothed out in the distribution of $d^2\phi_m/d\zeta^2$ given by the concentric fin model. The moving fin model overpredicts the radial heat transfer to the charge in the hot zone while underpredicting this heat transfer in the gradient zone. The overpredicted heat transfer in the hot zone contributes to Φ_Δ while the lack of heat transfer in

the gradient zone reduces ϕ_Δ ; if the effects of the two errors in $d^2\theta_m/d\zeta^2$ approximately balance, the moving fin model provides a good estimation of $\phi_\Delta(-\frac{\lambda_G}{2})$. The balance of the two errors is illustrated by the dotted curve in Fig. 7.8 which is plotted by reflecting the section of the curve for $d^2\phi_m/d\zeta^2$ labeled "a" about the axial location $\zeta = -.5 = -\lambda_G/2$ and adding to the section of the same curve labeled "b". If the distribution of $d^2\theta_m/d\zeta^2$ calculated by the moving fin model was to exactly match the dotted curve, the value of $\phi_\Delta(-\lambda_G/2)$ from eq. [7.14a] would equal that given by the concentric fin model. Figure 7.8 shows that these curves, while not exactly coinciding, are nevertheless close. Therefore, the use of the moving fin model approximation for $d^2\phi_m/d\zeta^2$ can be expected to provide a reasonable estimate of ϕ_Δ at the end of an adiabatic gradient zone. Table 7.1 indicates that this conclusion is valid at least over the range of K and δ examined.

7.3 RADIAL TEMPERATURE GRADIENTS GENERATED AT THE GROWTH INTERFACE IN THE PRESENCE OF A CRUCIBLE

The axial temperature gradient in the charge, $d\phi_m/d\zeta$, must undergo an abrupt change at the growth interface when $Pe_S R_H \neq 0$ or when $R_K \neq 1$. (c.f., eq. [6.7a]). The axial gradient in the crucible, on the other hand, does not change at the growth interface. Figure 7.9 shows that such conditions produce a difference between the charge and crucible temperatures at the interface which diminishes with distance from the interface. The exchange of heat between the charge and the crucible which results from this temperature difference has a profound effect on the distribution of ϕ_Δ in the vicinity of the interface.

Figure 7.10 shows the variation of ϕ_Δ in an adiabatic gradient zone for systems which are symmetric except $R_K \neq 1$. The presence of a crucible

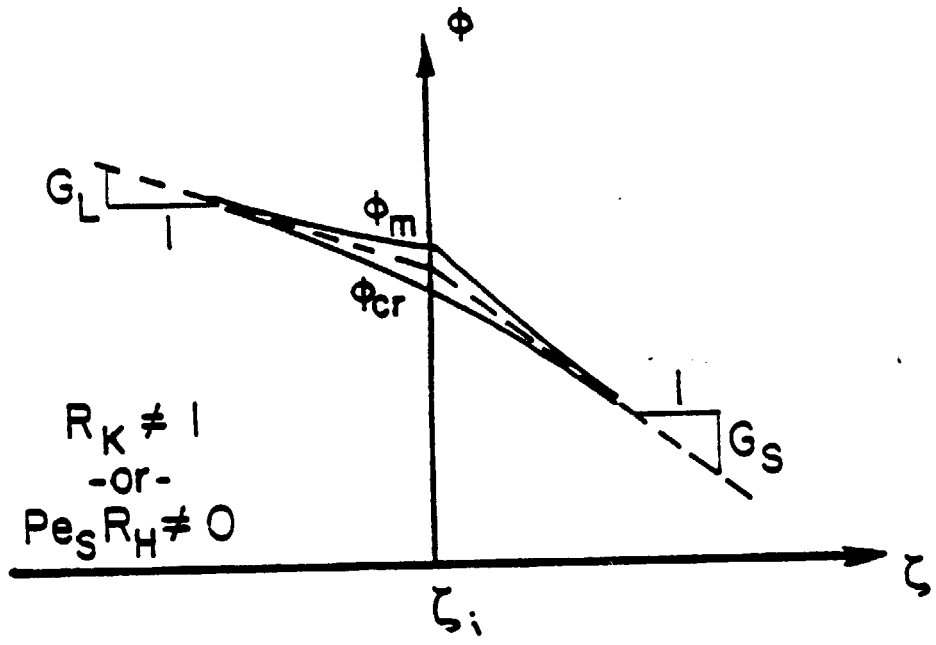

Fig. 7.9: Crucible and mean charge temperature distributions near the interface when $R_K \neq 1$ and/or $Pe_S R_H \neq 0$.

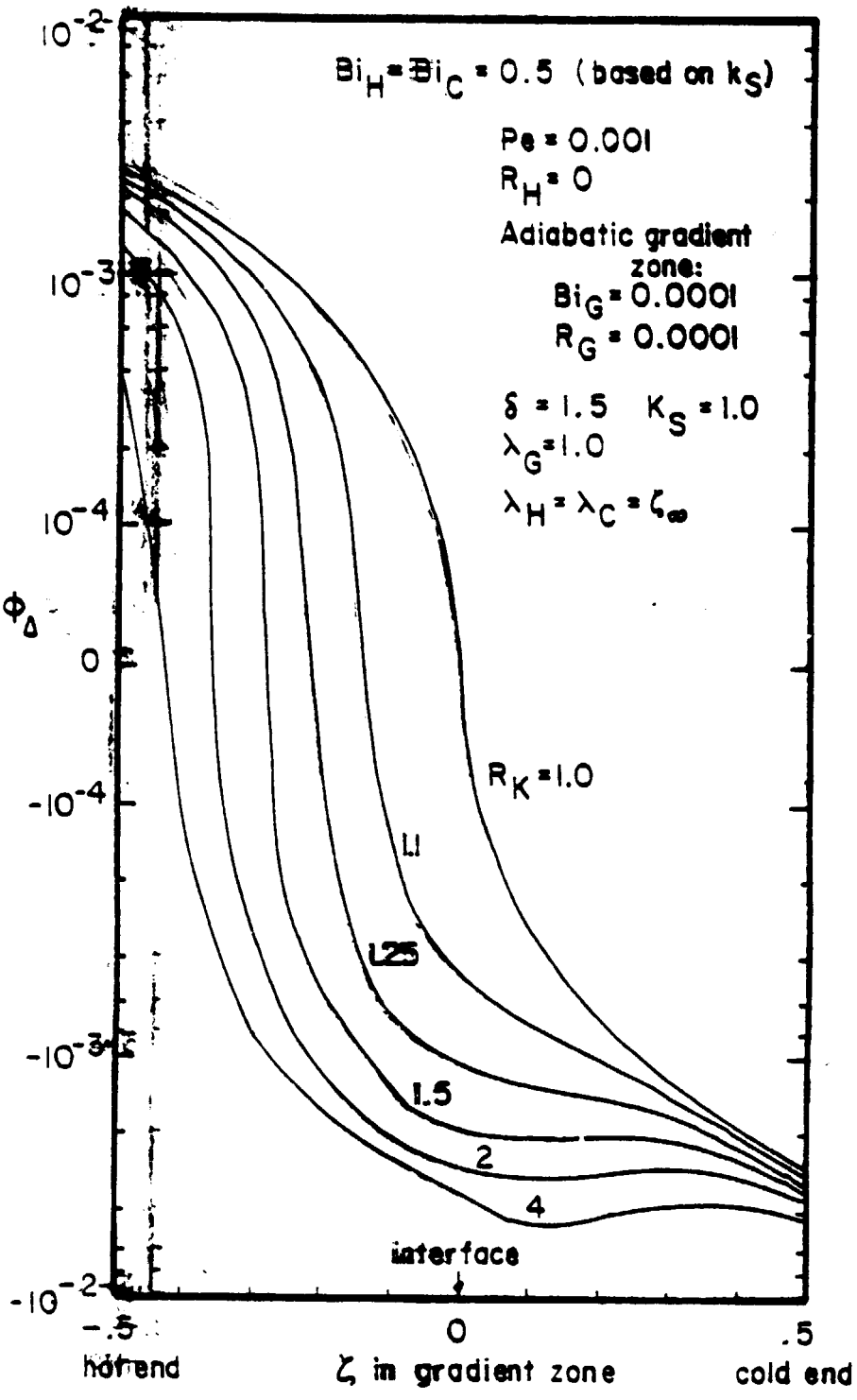

Fig. 7.10: Radial temperature variations generated at the interface when $R_K \neq 1$.

is indicated by a value of 1.5 for the diameter ratio δ. As R_K increases, it is seen that the distribution of ϕ_Δ, and more importantly, the value of ϕ_Δ at the interface, becomes more negative, causing isotherm shapes to be curved in the adverse direction (concave toward the melt). Even a small difference in melt and crystal thermal conductivities (e.g., $R_K = 1.1$ in Fig. 7.10) has a pronounced effect on $\phi_\Delta(\zeta_i)$.

Values of R_K greater than unity, being typical of semiconductors, have been considered in Fig. 7.10. The variation of ϕ_Δ which occurs when R_K is less than unity is similar to that shown in Fig. 7.10 except that the curves would be displaced toward more positive values of ϕ_Δ compared to the symmetric case of $R_K = 1$.

The effect of the generation of latent heat at the growth interface on ϕ_Δ in the gradient zone is shown in Fig. 7.11. The systems considered are symmetric except that $Pe_S R_H \neq 0$. It is seen that as R_H increases, $\phi_\Delta(\zeta_i)$ becomes more negative, similar to the effect of $R_K > 1$ shown in Fig. 7.10.

Although the curves of Fig. 7.11 are plotted with R_H as a parameter, it must be noted that the effect of the generation of latent heat is proportional to the product $Pe_S R_H$. The curves of Fig. 7.11 may also be interpreted as indicating the effects of changing Pe with a constant value of R_H. The value of $Pe_S = 0.05$ used in Fig. 7.11 has been chosen so that $Pe_S R_H$ would be sufficiently large to have an effect on ϕ_Δ for typical values of R_H.

The generation of radial gradients at the interface is due to the presence of a crucible. Figure 7.12 shows the effect of the crucible diameter ratio, δ, on $\phi_\Delta(\zeta)$ for systems which are symmetric except $R_K = 2$. Accordingly, very thin crucibles are required to eliminate the

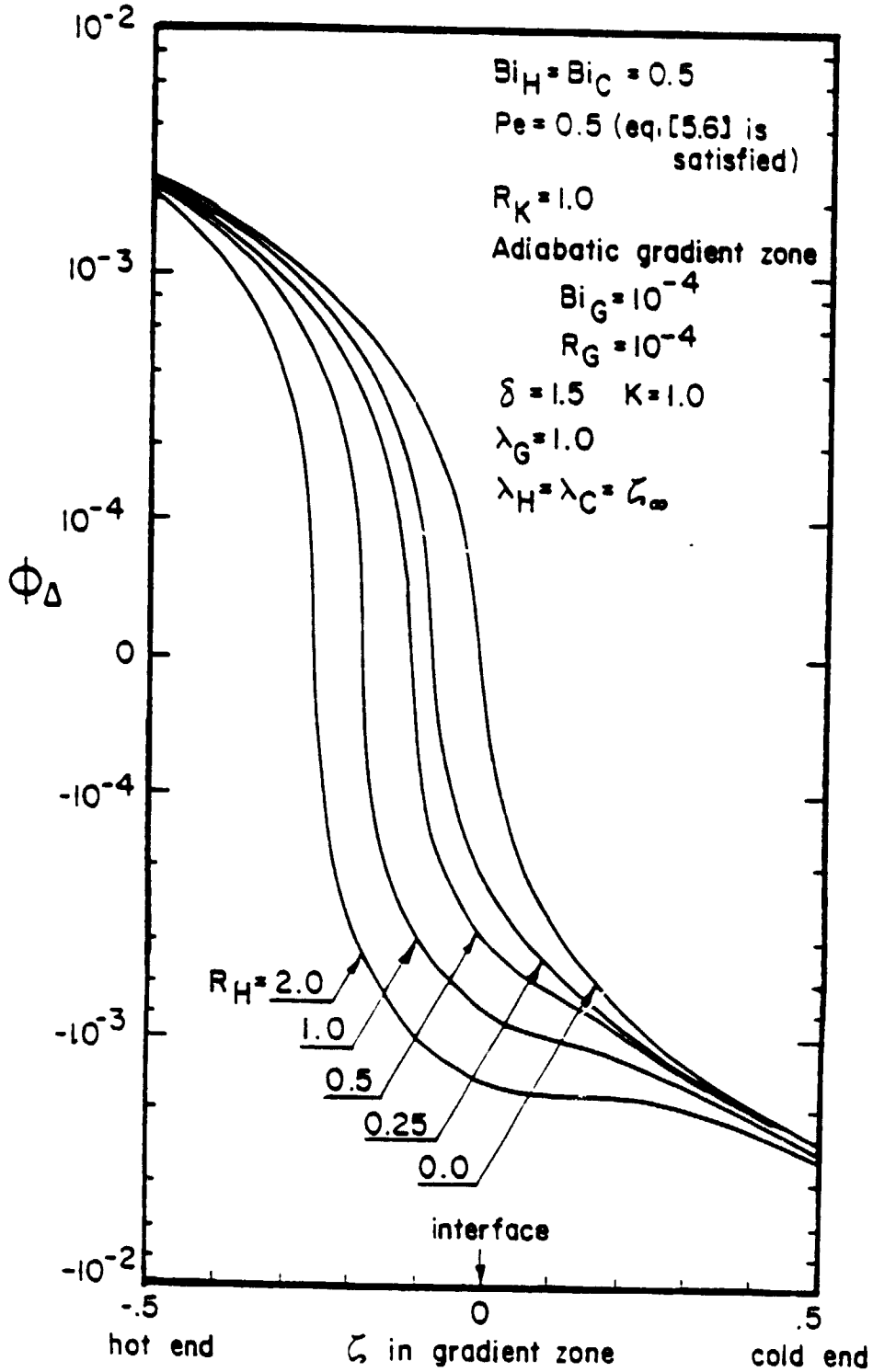

Fig. 7.11: The effect of the generation of latent heat on the radial temperature variations in the gradient zone.

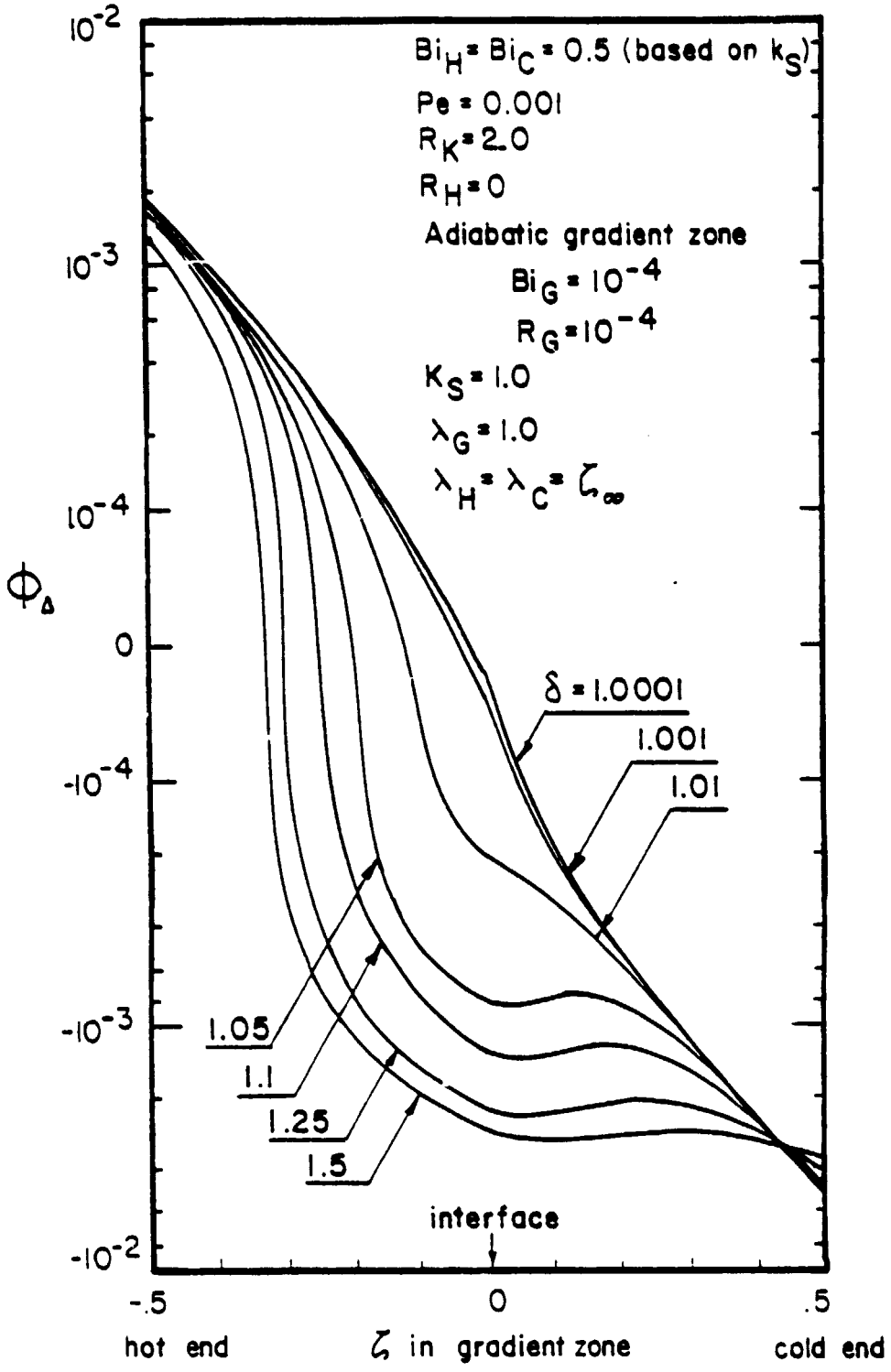

Fig. 7.12: The effect of the thickness of the crucible on the radial temperature variations generated at the interface.

interface effect.

Figure 7.13 shows the effect of changing the location of the interface on the distribution of ϕ_Δ in the adiabatic gradient zone for systems which are symmetric except that $R_K = 2$. As the interface approaches the hot zone, the value of ϕ_Δ at the interface becomes more positive due to the influence of radial temperature variations created in the hot zone (see section 7.2). For the systems considered in Fig. 7.13, however, the dominant factor is clearly the conductivity change at the interface. In general, the importance of radial temperature variations generated at the interface depends on their relative magnitude compared to radial temperature variations created by other effects.

7.3.1 The Two-Fin Thermal Model

In order to obtain from the results of section 7.1 a useful analytical relation which expresses the primary effects of the thermal parameters on the radial temperature variations near the growth interface, a simple and accurate analytical expression for $d^2\phi_m/d\zeta^2$ is necessary. Radial heat exchange between the charge and crucible in the vicinity of the interface is not accounted for in the one-dimensional moving fin model; approximating $d^2\phi_m/d\zeta^2$ by $d^2\theta_m/d\zeta^2$, therefore, is not accurate near the interface when a crucible is present. The concentric fin model is too complex to yield a simple analytical solution for $d^2\phi_m/d\zeta^2$. The present section describes a thermal model of the heat transfer near the interface which provides a simple approximation for $d^2\phi_m/d\zeta^2$.

The new thermal model is equivalent to the concentric fin model described in Chapter 6 except for the following:

(1) The charge is modeled as a single fin as shown in Fig. 7.14.

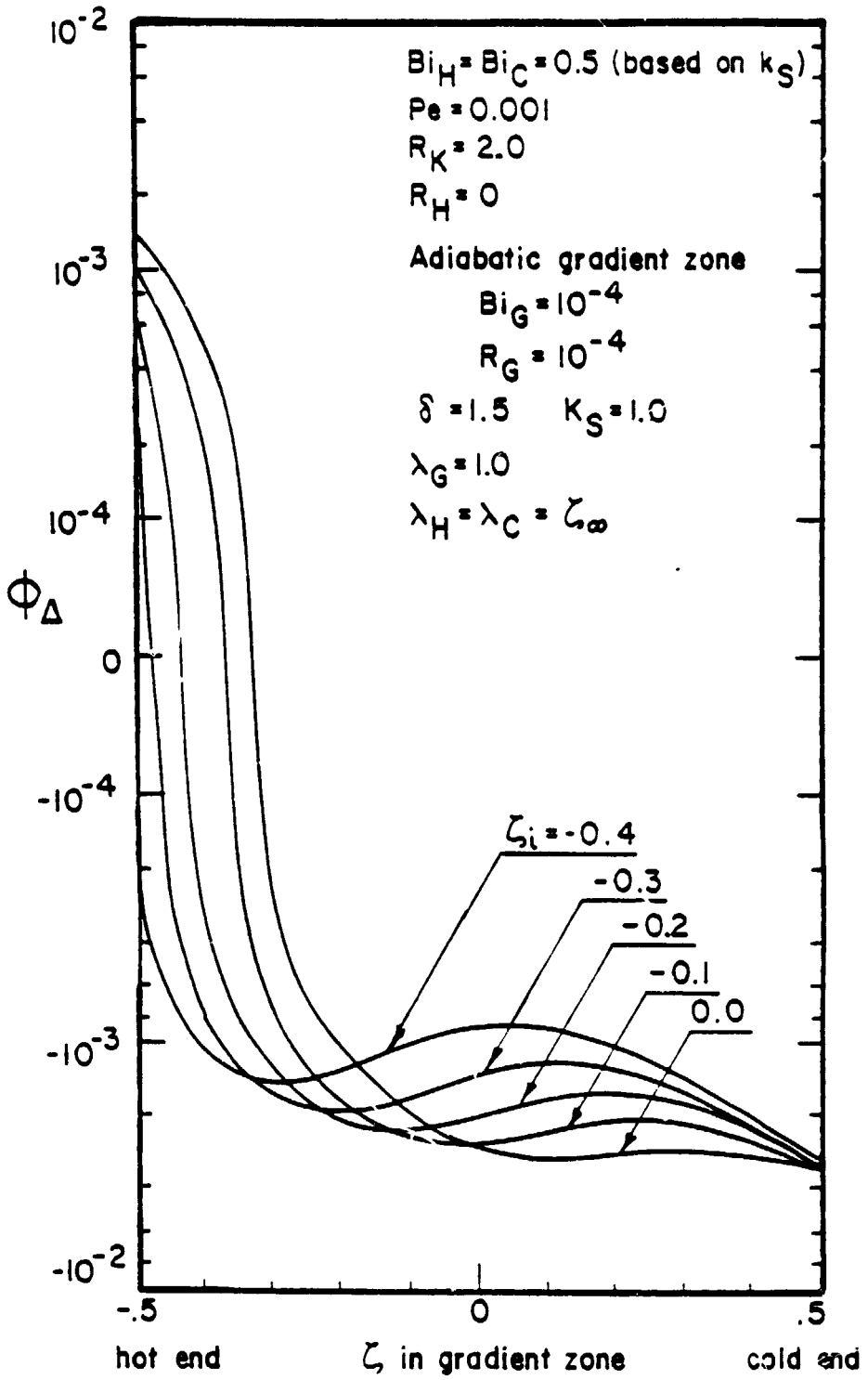

Fig. 7.13: The effect of the interface position on radial temperature variations generated at the interface.

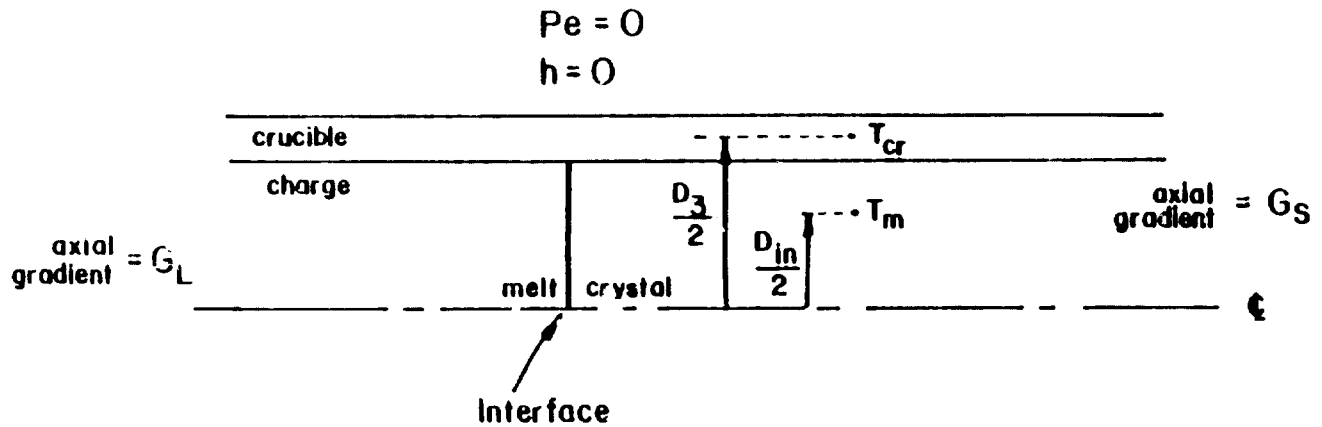

$$D_{in} = D/\sqrt{2}$$

$$D_3 = D\left[\frac{\delta^2+1}{2}\right]^{1/2}$$

Fig. 7.14: The two-fin thermal model.

Since there are only two concentric fins -- the charge and the crucible — the present thermal model is called the "two-fin" thermal model. The representative radial location for the charge temperature is taken as $D_{in}/2$, defined in Fig. 6.2, since this location divides the charge equally with regard to its cross sectional area. The representative radial location for the crucible temperature is again $D_3/2$ (c.f., Fig 6.2).

(2) The Peclet number is assumed negligible.

(3) The gradient zone is assumed adiabatic; hence, the gradient zone annulus is neglected.

(4) Only the region in the vicinity of the interface is modeled. This region extends from the interface, in either direction, at least the distance required for the interface effect to significantly die out. The effect of the remainder of the growth system is included only through imposing the average charge/crucible axial temperature gradients in the gradient zone, G_L and G_S in the solid and liquid respectively. These parameters are obtained from the one-dimensional moving fin model. Radial temperature gradients generated by other factors are neglected.

In accordance with the assumptions listed above, the fin equations for the charge and crucible are:

$$k_{cr} A_{cr} \frac{d^2 T_{cr}}{dz^2} + \frac{T_m - T_{cr}}{R_{mcr,loc}} = 0 \qquad [7.17]$$

$$k_{loc} A \frac{d^2 T_m}{dz^2} + \frac{T_{cr} - T_m}{R_{mcr,loc}} = 0 \qquad [7.18]$$

The thermal resistance, $R_{mcr,loc}$, which defines the thermal coupling between the crucible and the charge, is given by [30]:

$$R_{mcr,loc} = \frac{\ln\sqrt{2}}{2\pi k_{loc}} + \frac{\ln\left(\frac{\delta^2+1}{2}\right)^{1/2}}{2\pi k_{cr}} \qquad [7.19]$$

Define the following non-dimensional temperatures:

$$\bar{\phi} \equiv \frac{k_{loc} A \phi_m + k_{cr} A_{cr} \phi_{cr}}{k_{loc} A + k_{cr} A_{cr}} \qquad [7.20a]$$

$$\phi_{m,cr} \equiv \phi_m - \phi_{cr} \qquad [7.20b]$$

$\bar{\phi}$ is the average charge/crucible temperature weighted by their respective axial thermal conductances. Using eqs. [7.19] and [7.20] in eqs. [7.17] and [7.18], and nondimensionalizing, results in the following form for the two-fin model fin equations:

$$\frac{d^2\bar{\phi}}{d\zeta^2} = 0 \qquad [7.21]$$

$$\frac{d^2\phi_{m,cr}}{d\zeta^2} - W_{loc}^2 \phi_{m,cr} = 0 \qquad [7.22]$$

$$W_{loc}^2 = \frac{8\left[1 + \frac{1}{K_{loc}(\delta^2-1)}\right]}{\ln\sqrt{2} + \frac{1}{K_{loc}} \ln\left(\frac{\delta^2+1}{2}\right)^{1/2}} \qquad [7.23]$$

Equation [7.21] indicates that $\bar{\phi}$ varies linearly in the gradient zone under the present assumptions. This conclusion is also obtained in section 4.4.3 where the axial gradient of $\bar{\phi}$ is also denoted by G_L and G_S in the liquid and solid respectively. Section 4.4.3 also explains that the axial temperature gradients in the gradient zone predicted by the moving fin model should be interpreted as G_L and G_S. The present two-fin model therefore assumes that G_L and G_S are known a priori from the results of the moving fin model.

The solution of eq. [7.22] is:

in the liquid: $\zeta < \zeta_i$

$$(\phi_{m,cr})_L = C_{1L}\exp[-w_L(\zeta_i-\zeta)] + C_{2L}\exp[w_L(\zeta_i-\zeta)] \qquad [7.24a]$$

in the solid: $\zeta > \zeta_i$

$$(\phi_{m,cr})_S = C_{1S}\exp[-w_S(\zeta-\zeta_i)] + C_{2S}\exp[w_S(\zeta-\zeta_i)] \qquad [7.24b]$$

where the coefficients denoted by C are the unknown constants of integration.

The assumptions of the two-fin model require that $\phi_{m,cr} \to 0$ as $\zeta \to \infty$; therefore, $C_{1L} = C_{2S} = 0$. Continuity of temperature at the interface requires $(\phi_{m,cr})_L = (\phi_{m,cr})_S$; therefore $C_{2L} = C_{1S}$. Finally, continuity of flux in the crucible fin at the interface requires $(d\phi_{cr}/d\zeta)_L = (d\phi_{cr}/d\zeta)_S$; this boundary condition yields:

$$C_{1S} = C_{2L} = \frac{G_L - G_S}{\dfrac{w_S}{1+K_S(\delta^2-1)} + \dfrac{R_K w_L}{R_K + K_S(\delta^2-1)}} \qquad [7.25]$$

The difference between G_L and G_S is found from eq. [4.25]:

$$G_L - G_S = \frac{Pe_S R_H - G_L(R_K - 1)}{1 + K_S(\delta^2 - 1)} \qquad [7.26]$$

Substituting these results into eqs. [7.24] produces the solution for $\phi_{m,cr}$:

$$(\phi_{m,cr})_L = C \exp\left[-W_L(\zeta_i - \zeta)\right] \qquad [7.27a]$$

$$(\phi_{m,cr})_S = C \exp\left[-W_S(\zeta - \zeta_i)\right] \qquad [7.27b]$$

where:

$$C = \frac{Pe_S R_H - G_L(R_K - 1)}{\dfrac{W_S}{1 + K_S(\delta^2 - 1)} + \dfrac{R_K W_L}{R_K + K_S(\delta^2 - 1)}} \cdot \frac{1}{1 + K_S(\delta^2 - 1)} \qquad [7.28]$$

The constant C defined by eq. [7.28] includes in the numerator the superposed effects of the generation of latent heat and the change in charge thermal conductivity at the interface. The axial gradient in the liquid, G_L, is always negative; if $R_K > 1$, as is typical of semiconductors, these two effects reinforce each other, causing a larger disturbance at the interface than would occur by either effect acting alone. On the other hand, if $R_K < 1$, it may be possible to eliminate the interface effect by choosing a value for the product $Pe_S R_H$ that would make the numerator of eq. [7.28] equal to zero. This could be accomplished by changing either the lowering rate (thus changing Pe_S) or the temperature difference between the hot and cold zone furnaces (thus changing R_H). Either possibility, however, has potentially harmful side effects on the constitutional supercooling requirement.

7.3.2 Radial Temperature Variations Near the Growth Interface

Substituting eqs. [7.27] into the nondimensional form of eq. [7.18] yields an expression for $d^2\phi_m/d\zeta^2$ due to the heat exchange between the charge and the crucible near the interface:

$$\left[\frac{d^2\phi_m}{d\zeta^2}\right]_L = \frac{W_L K_s(\delta^2-1)}{R_K + K_s(\delta^2-1)} C \exp\left[-W_L(\zeta_i-\zeta)\right] \qquad [7.29a]$$

$$\left[\frac{d^2\phi_m}{d\zeta^2}\right]_S = \frac{W_s K_s(\delta^2-1)}{1 + K_s(\delta^2-1)} C \exp\left[-W_s(\zeta-\zeta_i)\right] \qquad [7.29b]$$

Using eqs. [7.29] in eqs. [7.11] and [7.12] produces the value of ϕ_Δ at the interface due to the interface effect:

$$\phi_\Delta(\zeta_i) = -\frac{C}{7.63}\frac{K_s(\delta^2-1)}{R_K+1}\left[\frac{W_s^2/(W_s+7.63)}{1+K_s(\delta^2-1)} + \frac{W_L^2/(W_L+7.63)}{R_K+K_s(\delta^2-1)}R_K\right] \qquad [7.30]$$

The value of ϕ_Δ at the interface determined by eq. [7.30] is compared to the results shown previously in Figs. 7.10 to 7.13 in Table 7.2. In general, the comparison is favorable, indicating that the two-fin model provides a reasonable approximation for $d^2\phi_m/d\zeta^2$ in the vicinity of the interface. The largest differences occur for those cases which consider effects not included in the two-fin model. For example, the cases considered in Fig. 7.11 use a larger Peclet number, 0.05, compared to that used for the other figures, 0.001, in order to accentuate the liberation of latent heat. The effect of the larger Peclet number, not included in the two-fin model, is to create a more negative value of $\phi_\Delta(\zeta_i)$.

A difference between eq. [7.30] and the results from the concentric fin model is also apparent for the cases of small δ considered in Fig. 7.12.

		$\phi_\Delta(\zeta_i)$		
Figure	variable parameter	concentric fin model	eq. [7.30]	eq. [7.30] plus attenuation effect from eq. [7.9], [7.10], and [7.14]
7.10	R_K = 1.0	.000000	.000000	.000000
	1.1	-.000493	-.000464	-.000464
	1.25	-.00110	-.00114	-.00114
	1.5	-.00186	-.00176	-.00175
	2.0	-.00274	-.00261	-.00260
	4.0	-.00343	-.00330	-.00329
7.11	R_H = 0.0	-.000023	.000000	.000000
	0.25	-.000219	-.000179	-.000179
	0.5	-.000416	-.000358	-.000360
	1.0	-.000810	-.000716	-.000720
	2.0	-.00160	-.00143	-.00144
7.12	δ = 1.0001	-.000021	-.000002	-.000021
	1.001	-.000040	-.000021	-.000039
	1.01	-.000214	-.000183	-.000201
	1.05	-.000818	-.000730	-.000744
	1.1	-.00136	-.00122	-.00123
	1.25	-.00227	-.00207	-.00207
	1.5	-.00274	-.00261	-.00260
7.13	ζ_i = 0.0	-.00274	-.00261	-.00260
	-0.1	-.00245	-.00258	-.00248
	-0.2	-.00210	-.00254	-.00231
	-0.3	-.00166	-.00252	-.00200
	-0.4	-.00108	-.00249	-.00138

The values of G_L and θ_i required for use in eqs. [7.14] and [7.30] are listed in Tables 7.3 and 7.4.

Table 7.2: Comparison of the approximate methods of calculating $\phi_\Delta(\zeta_i)$ to results of the concentric fin model for the cases considered in Figs. 7.10 to 7.13.

This error is attributable to the neglect by the two-fin model of radial gradients generated in the furnace zones. In order to include an approximation of the attenuation effect, the value of $\phi_\Delta(\zeta_i)$ determined by eqs. [7.9], [7.10], and [7.14] is simply added to that determined by eq. [7.30]. The results of this approximation, shown in the last column of Table 7.2, are seen to improve the estimation of $\phi_\Delta(\zeta_i)$ for small values of δ. As δ increases, the contribution to $\phi_\Delta(\zeta_i)$ due to the attenuation effect becomes less important than the radial gradients generated at the interface.

Table 7.2 also demonstrates that eq. [7.30] is unable to account for the effects of the changing interface location on $\phi_\Delta(\zeta_i)$. This error is again attributable to the relative importance at the interface of radial gradients generated in the hot and cold zones compared to those generated at the interface. As the interface approaches the end of the gradient zone, the influence of radial gradients generated in the adjacent furnace zone becomes increasingly important.

The last column of Table 7.2 also provides an approximation for the effect of changing interface location on $\phi_\Delta(\zeta_i)$. This correction to eq. [7.30] has been calculated assuming that the radial gradients generated in the hot and cold zones attenuate at a rate proportional to $\exp(-7.63\zeta)$. The actual rate of attenuation is, however, smaller when a crucible is present (c.f., section 7.2). It is expected that use of the actual rate of attenuation would produce a better correction to eq. [7.30] for the effect of changing interface location. Unfortunately, a simple analytical expression for the attenuation of ϕ_Δ from the ends of the gradient zone in the presence of a crucible is not available.

7.3.3 Correction to the Axial Temperature Gradient In the Liquid At The Growth Interface

The moving fin model predicts the value of $G_L = d\bar{\phi}_L/d\zeta$ for the axial temperature gradient in the liquid at the interface. The constitutional supercooling requirement, however, depends on the value of $(d\phi_m/d\zeta)_L$ at the interface. The difference between these temperature gradients can be approximated from the results of the two-fin model. Differentiating eqs. [7.20] with respect to ζ and solving for $d\phi_m(\zeta_i)/d\zeta$ yields:

$$\left[\frac{d\phi_m(\zeta_i)}{d\zeta}\right]_L = G_L + \frac{K_s(\delta^2-1)}{R_K + K_s(\delta^2-1)}\left[\frac{d\phi_{m,cr}(\zeta_i)}{d\zeta}\right]_L \qquad [7.31]$$

Differentiating eq. [7.27a] with respect to ζ and substituting into eq. [7.31] yields:

$$\left[\frac{d\phi_m(\zeta_i)}{d\zeta}\right]_L = G_L + \frac{K_s(\delta^2-1)}{R_K + K_s(\delta^2-1)} W_L C \qquad [7.32]$$

The second term on the right side of eq. [7.32] is a correction to be applied to G_L in order to account for the effect of radial heat transfer near the interface on the axial gradient in the charge at the interface.

The axial temperature gradient in the liquid at the interface calculated by the moving fin model, G_L, and by eq. [7.32] are compared to results from the concentric fin model in Table 7.3 for the cases considered in Figs. 7.10 to 7.13. It is seen that eq. [7.32] provides an excellent approximation to $\left[d\phi_m(\zeta_i)/d\zeta\right]_L$ even though the correction term may be significant (e.g., large R_K or large R_H). The approximation is most in

		axial temperature gradient in the liquid at the growth interface		
Figure	variable parameter	concentric fin model	moving fin model G_L	eq. [7.32]
7.10	R_K = 1.0	-.351	-.350	-.350
	1.1	-.332	-.340	-.332
	1.25	-.308	-.326	-.307
	1.5	-.275	-.306	-.275
	2.0	-.228	-.272	-.228
	4.0	-.140	-.190	-.140
7.11	R_H = 0.0	-.351	-.350	-.350
	0.25	-.344	-.348	-.344
	0.5	-.338	-.345	-.338
	1.0	-.325	-.339	-.325
	2.0	-.300	-.328	-.300
7.12	= 1.0001	-.251	-.252	-.252
	1.001	-.251	-.252	-.252
	1.01	-.251	-.252	-.251
	1.05	-.249	-.256	-.249
	1.1	-.247	-.260	-.246
	1.25	-.240	-.267	-.239
	1.5	-.228	-.272	-.228
7.13	= 0.0	-.228	-.272	-.228
	-0.1	-.225	-.269	-.225
	-0.2	-.222	-.266	-.223
	-0.3	-.217	-.262	-.220
	-0.4	-.211	-.260	-.217

Table 7.3: Comparison of the approximate methods of calculating $d\phi_m(\zeta_i)/d\zeta$ to results of the concentric fin model for the cases considered in Figs. 7.10 to 7.13.

error as the interface approaches the hot zone (c.f., $\zeta_i = -0.3, -0.4$ in Fig. 7.13) due to the additional influence of radial heat transfer in the hot zone.

7.3.4 Correction To the Interface Temperature

The moving fin model predicts for the interface temperature the average charge/crucible temperature; i.e., θ_i is interpreted as $\bar{\phi}(\zeta_i)$. The difference between $\bar{\phi}(\zeta_i)$ and $\phi_m(\zeta_i)$ found by the two-fin model may be used as a simple correction to the value of θ_i found by the moving fin model:

$$\theta_i - \phi_m(\zeta_i) \simeq \left[\bar{\phi}(\zeta_i) - \phi_m(\zeta_i)\right] \qquad [7.33]$$

Rearranging eqs. [7.20] yields:

$$\left[\bar{\phi}(\zeta_i) - \phi_m(\zeta_i)\right]_L = \frac{-K_s(\delta^2-1)}{R_K + K_s(\delta^2-1)}\,\phi_{m,cr}(\zeta_i) \qquad [7.34a]$$

$$\left[\bar{\phi}(\zeta_i) - \phi_m(\zeta_i)\right]_S = \frac{-K_s(\delta^2-1)}{1 + K_s(\delta^2-1)}\,\phi_{m,cr}(\zeta_i) \qquad [7.34b]$$

Since both $\phi_{m,cr}(\zeta_i)$ and $\phi_m(\zeta_i)$ have the same value in the liquid and solid at the interface, eqs. [7.34] imply that $\bar{\phi}_L(\zeta_i) \neq \bar{\phi}_S(\zeta_i)$; that is, the two-fin model predicts a step change in $\bar{\phi}$ at the interface. This is due to the definition of $\bar{\phi}$ which averages the charge and crucible temperatures according to their respective axial thermal conductances. Since the moving fin model neglects the temperature difference between ϕ_m and ϕ_{cr}, it does not predict this step change in $\bar{\phi}$ at the interface.

In order to approximate the effect of radial heat transfer near the interface on the interface temperature, the correction term within brackets

in eq. [7.33] is taken simply as the arithmetic average of eqs. [7.34a] and [7.34b]. Using eq. [7.27] evaluated at $\zeta = \zeta_i$ yields:

$$\Phi_m(\zeta_i) = \theta_i + \frac{1}{2} C \left[\frac{K_s(\delta^2-1)}{1+K_s(\delta^2-1)} + \frac{K_s(\delta^2-1)}{R_K + K_s(\delta^2-1)} \right] \qquad [7.35]$$

The interface temperature determined by eq. [7.35] is compared to that found from the concentric and moving fin models in Table 7.4 for the cases considered in Figs. 7.10 to 7.13. It is seen that the moving fin model, provides a reasonable estimation to the interface temperature, θ_i, without the correction afforded by eq. [7.35]; this indicates that radial heat transfer at the interface between the charge and the crucible has a relatively small effect on the interface temperature or location. Utilizing the corresponding values of G_L listed in Table 7.3, the moving fin model would mislocate the interface by at most 0.1 charge diameter for the cases considered (c.f., $R_K = 4$ from Fig. 7.10). Results calculated from eq. [7.35], however, compare yet more favorably to those of the concentric fin model.

The largest errors in the estimate of the interface temperature considered by Table 7.4 are attributable to the larger Peclet number used in the cases of Fig. 7.11. Calculating θ_i through the use of the non-zero Peclet number relation, eq. [B.8], increases the accuracy of eq. [7.35]; for the cases considered by Fig 7.11, the difference between θ_i calculated in this way and by the concentric fin model is no more than one digit in the third significant figure.

		temperature of the growth interface		
Figure	variable parameter	concentric fin model	moving fin model (Pe = 0)	eq. [7.35]
7.10	R_K = 1.0	.500	.500	.500
	1.1	.509	.507	.509
	1.25	.522	.518	.522
	1.5	.540	.534	.540
	2.0	.570	.561	.572
	4.0	.648	.634	.651
7.11	R_H = 0.0	.517	.500	.500
	0.25	.522	.504	.505
	0.5	.527	.508	.509
	1.0	.536	.516	.519
	2.0	.554	.532	.537
7.12	δ = 1.0001	.619	.619	.619
	1.001	.619	.618	.618
	1.01	.617	.617	.617
	1.05	.610	.610	.611
	1.1	.603	.602	.604
	1.25	.587	.584	.588
	1.5	.570	.561	.572
7.13	ζ_i = 0.0	.570	.561	.572
	-0.1	.602	.593	.604
	-0.2	.633	.624	.635
	-0.3	.664	.655	.665
	-0.4	.693	.685	.695

The values of G_L required for use in eqs. [7.35] are listed in Table 7.3.

Table 7.4: Comparison of the approximate methods of calculating θ_i to results of the concentric fin model for the cases considered in Figs. 7.10 to 7.13.

7.4 DIABATIC GRADIENT ZONE

Two additional parameters are required by the concentric fin model when heat transfer in the gradient zone is considered: Bi_G and R_G. The Biot number in the gradient zone, Bi_G, indicates the thermal coupling between the gradient zone annulus and the charge. R_G is the ratio of the axial heat conducting capacities of the gradient zone annulus and the charge (c.f., eqs. [6.2]). The one-dimensional model of a diabatic gradient zone developed in section 4.4.4 shows that the gradient zone approaches abiadatic conditions as either Bi_G or R_G approaches zero. Otherwise, the temperature difference between the gradient zone annulus and the charge ($\phi_G - \phi_m$) produces heat transfer which affects axial temperature gradients and also, as shown in this section, radial temperature gradients within the charge.

7.4.1 Results From the Concentric Fin Model

Figures 7.15a, 7.15b, and 7.15c show the variation of ϕ_Δ in a diabatic gradient zone as calculated by the concentric fin model. The systems in these figures are symmetric and do not consider a crucible. Since the systems are symmetric, the curves have been plotted only for the hot side of the gradient zone. Each figure considers a constant Biot number throughout the furnace while the separate curves in each figure consider various values of R_G. The graphs inserted in each figure are axial temperature distributions of ϕ_m and ϕ_G corresponding to the individual curves of ϕ_Δ. As a reference, the distribution of ϕ_Δ in an adiabatic gradient zone (i.e., $Bi_G = 0$) is also included in each figure.

According to Figs. 7.15, the value of R_G significantly affects the distribution of ϕ_Δ in the gradient zone. When R_G is small, heat exchange

$Bi_H = Bi_C = Bi_G = 0.05$

No crucible

Symmetric system

$\lambda_G = 1.0$

$\lambda_H = \lambda_C = \zeta_\infty$

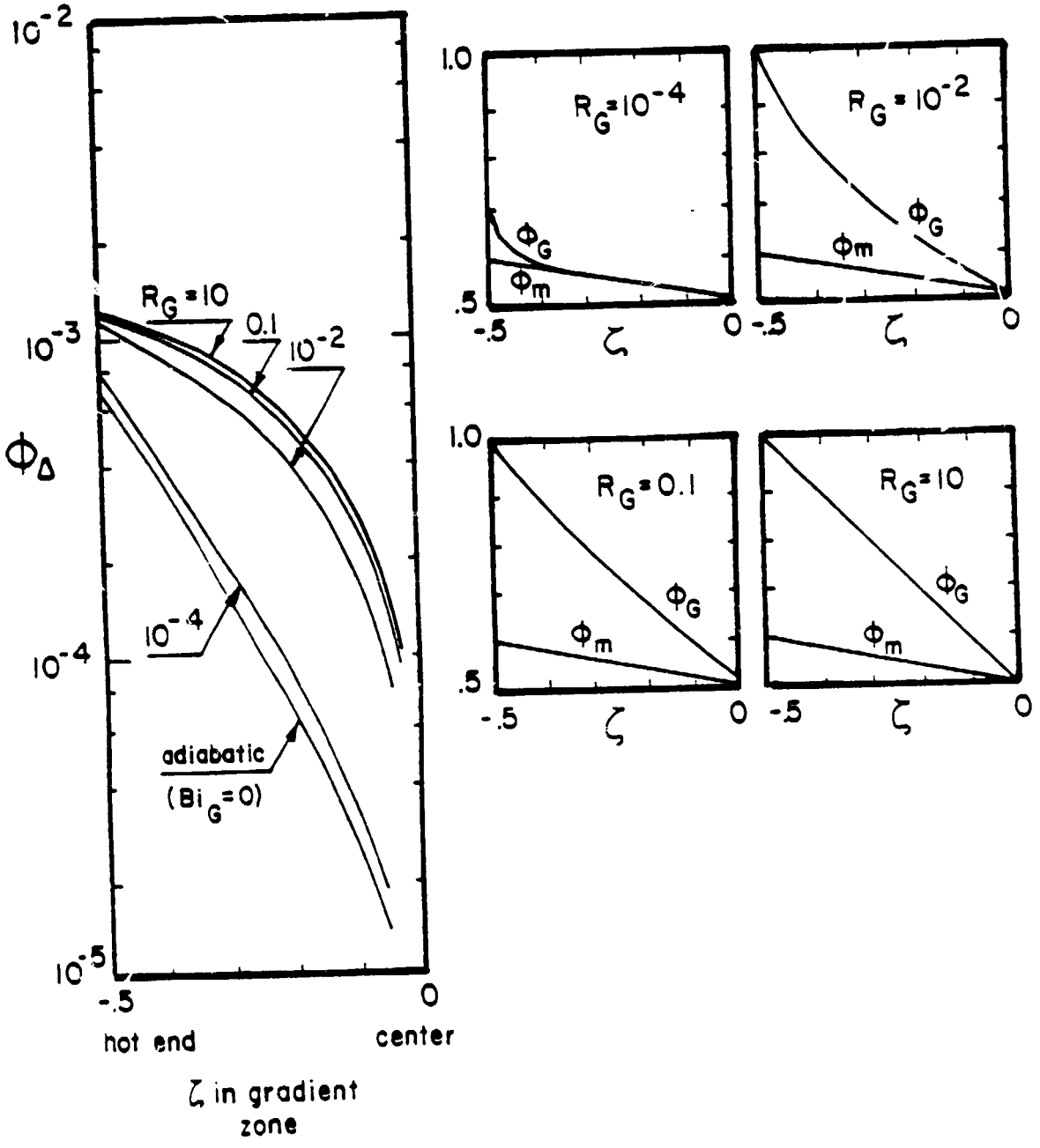

Fig. 7.15a: Φ_Δ, Φ_m and Φ_G in a diabatic gradient zone with no crucible and a symmetric system: Bi = 0.05.

$Bi_H = Bi_C = Bi_G = 0.5$

No crucible

Symmetric system

$\lambda_G = 1.0$

$\lambda_H = \lambda_C = \zeta_\infty$

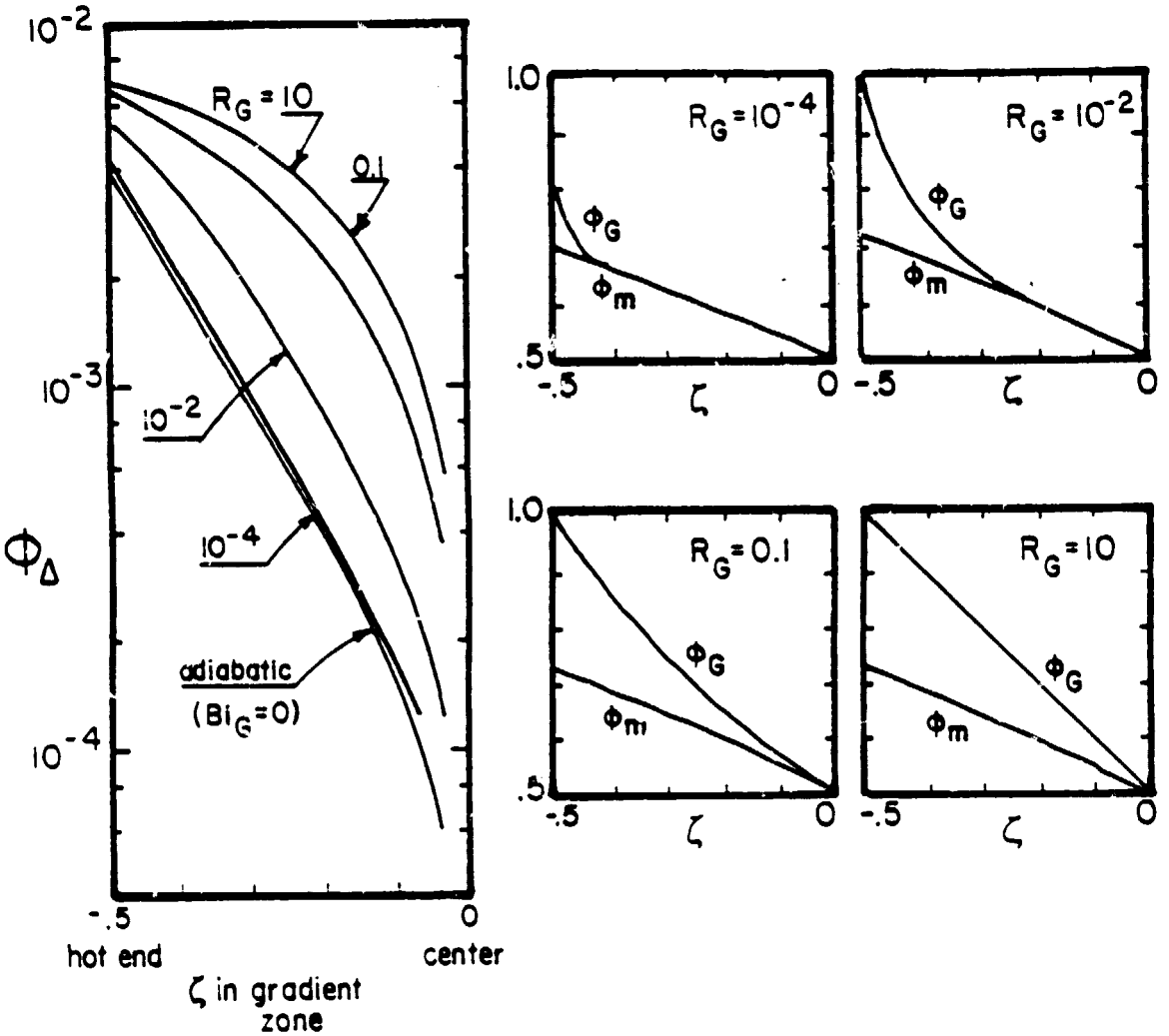

Fig. 7.15b: Φ_Δ, Φ_m and Φ_G in a diabatic gradient zone with no crucible and a symmetric system: Bi = 0.5.

$Bi_H = Bi_C = Bi_G = 5.0$

No crucible

Symmetric system

$\lambda_G = 1.0$

$\lambda_H = \lambda_C = \zeta_\infty$

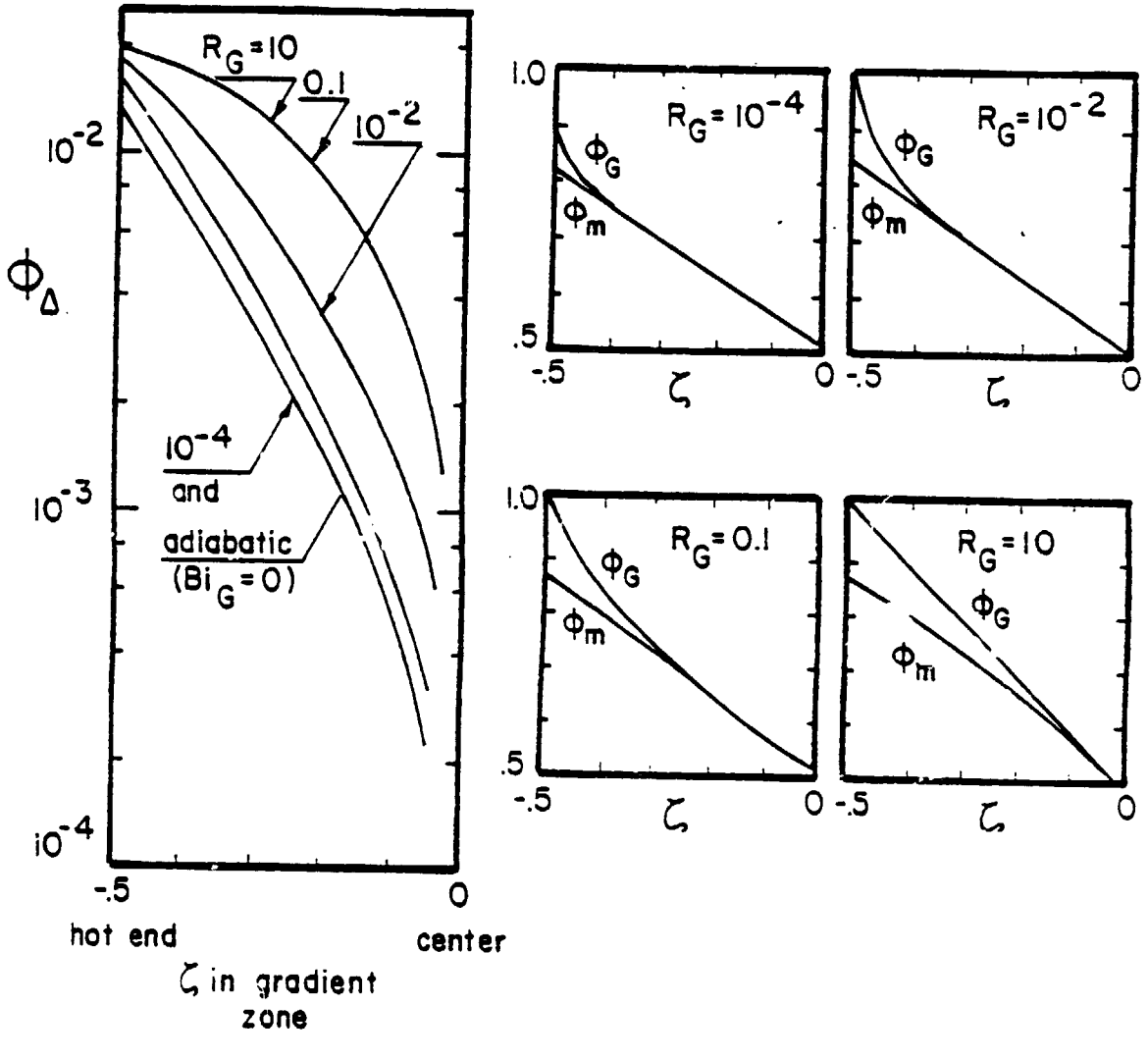

Fig. 7.15c: Φ_Δ, Φ_m and Φ_G in a diabatic gradient zone with no crucible and a symmetric system: Bi = 5.0.

between the charge and the gradient zone annulus occurs only near the ends of the gradient zone; toward the center of the gradient zone ϕ_G is nearly equal to ϕ_m. In such cases, the distribution of ϕ_Δ is only slightly altered from that in the corresponding system with an adiabatic gradient zone. As R_G increases, the temperature difference $\phi_G - \phi_m$ is more pronounced and increases the radial heat transfer to the charge; as a consequence, ϕ_Δ increases as well. For sufficiently large values of R_G, ϕ_G is approximately linear; further increases in R_G do not affect either $\phi_G - \phi_m$ or ϕ_Δ but serve only to conduct more heat from the hot to the cold zone furnaces through the gradient zone annulus.

Figure 7.16 demonstrates the effect of increasing Bi_G for systems which have a linear variation of ϕ_G as calculated by the concentric fin model. A linear variation of ϕ_G has been obtained by choosing a large value of R_G (i.e., R_G=1000). Increasing Bi_G has a slight effect on the axial temperature distribution in the gradient zone, tending to reduce the driving force for radial heat transfer in the gradient zone, $\phi_G - \phi_m$. This effect, however, is more than offset by the augmented thermal coupling between the charge and gradient zone annulus represented by the larger value of Bi_G. As shown in Fig. 7.16, the result is that ϕ_Δ increases with Bi_G. The curve for Bi_G = 5 shows, for example, that ϕ_Δ increases, rather than attenuates, from the end of the gradient zone when the gradient zone Biot number is greater than that in the furnace zones.

Figure 7.17 shows that the effect of heat transfer in the gradient zone when a crucible is present is similar to those systems examined above without a crucible. (The system considered in Fig. 7.17 is analogous to that of Fig. 7.15b except for the presence of a crucible.)

$Bi_H = Bi_C = 1.0$

No crucible

Symmetric system

Φ_G linear: $R_G = 10^3$

$\lambda_G = 1.0$

$\lambda_H = \lambda_C = \zeta_\infty$

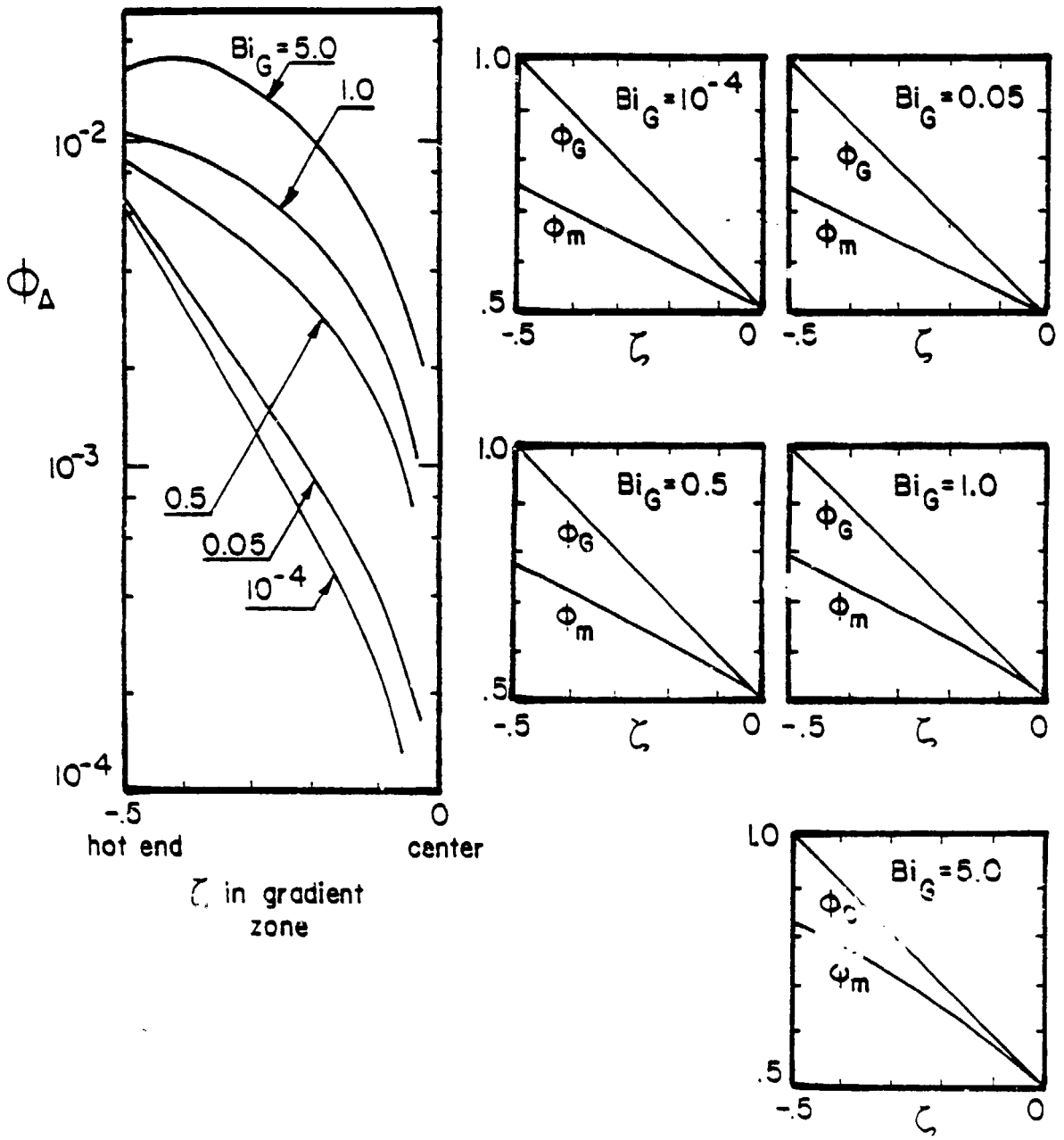

Fig. 7.16: Φ_Δ, Φ_m and Φ_G in a diabatic gradient zone for increasing Bi_G. No crucible, symmetric system and linear Φ_G.

$Bi_H = Bi_C = Bi_G = 0.5$

$\delta = 1.5 \quad K_S = 1.0$

Symmetric system

$\lambda_G = 1.0$

$\lambda_H = \lambda_C = \zeta_\infty$

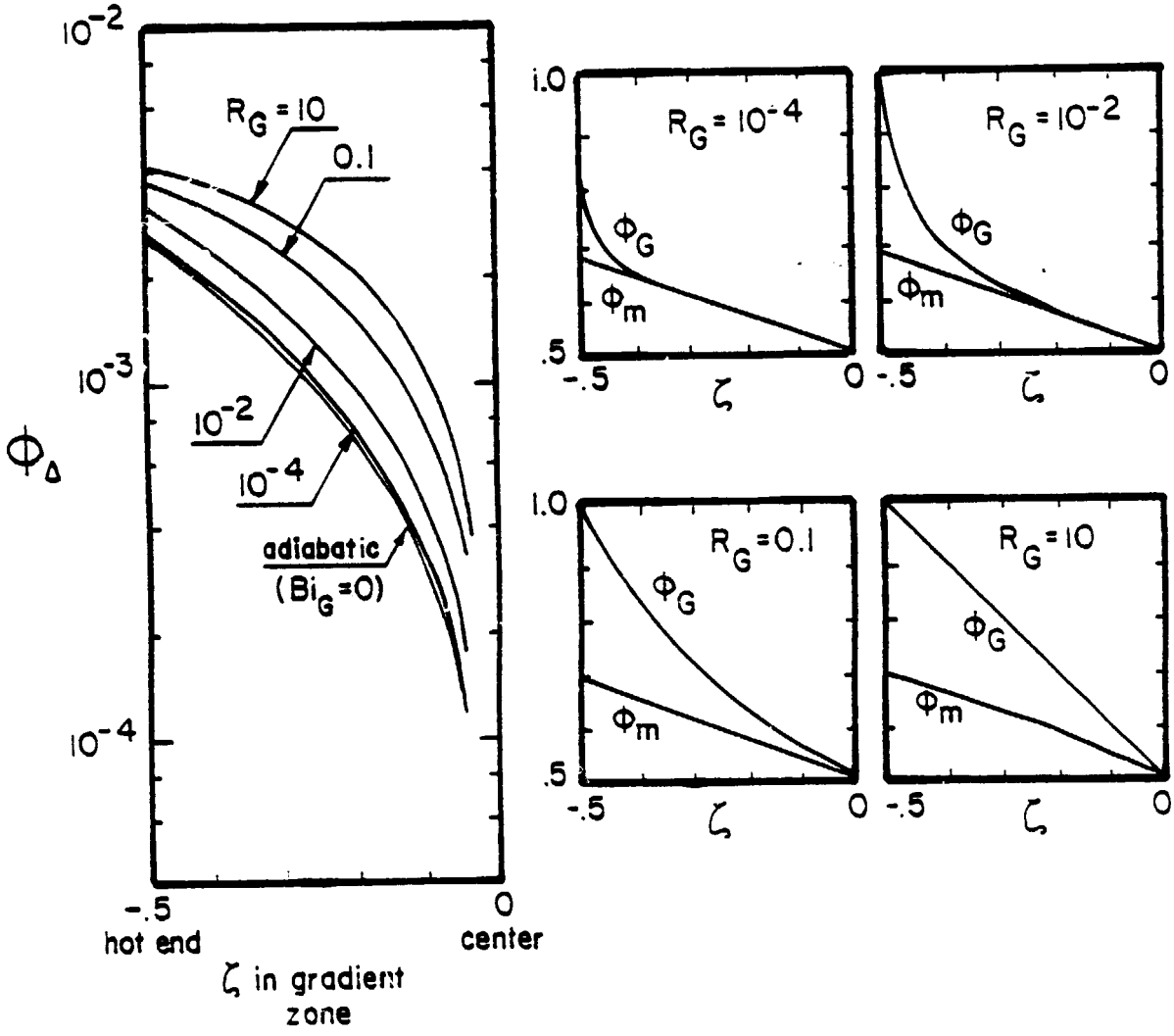

Fig. 7.17: ϕ_Δ, ϕ_m and ϕ_G in a diabatic gradient zone with a crucible. The other parameters are the same as those used in Figure 7.15b.

7.4.2 Analytical Approximation for the Effect of Heat Transfer In the Gradient Zone

The effect of radial heat exchange between the furnace and the charge on the value of Φ_Δ at a particular axial location is described by eq. [7.4]. Analytical expressions for the effects of radial temperature gradients created in the hot and cold zones and at the growth interface have been developed using eq. [7.4] in sections 7.2 and 7.3 respectively. The present section considers a simple model of heat transfer to or from the charge in the gradient zone in order to analytically approximate its effect on Φ_Δ.

The present model considers that the primary effect of heat transfer between the gradient zone annulus and the charge is attributable to thermal conditions near the axial location of interest. This assumption is qualitatively justified by the high rate of attenuation of the effects of radial heat transfer distant from the location of interest; c.f., eq. [7.4]. Accordingly, a linearized description for $d^2\Phi_m/d\zeta^2$ about the location of interest, ζ, is employed:

$$\frac{d^2\Phi_m(x)}{dx^2} = \frac{d^2\Phi_m(\zeta)}{d\zeta^2} + \frac{d}{dx}\left[\frac{d^2\Phi_m(x)}{dx^2}\right]_{x=\zeta} \cdot (x-\zeta) \qquad [7.36]$$

Substituting eq. [7.36] into eq. [7.7] yields:

$$\Phi_\Delta(\zeta) = -\frac{1}{66.2}\,\frac{d^2\Phi_m(\zeta)}{d\zeta^2} \qquad [7.37]$$

Next, eq. [7.16] is used to approximate $d^2\Phi_m/d\zeta^2$; this approximation assumes that $d^2\theta_m/d\zeta^2$ of the moving fin model accurately represents $d^2\Phi_m/d\zeta^2$ of the concentric fin model and that $Bi^{**}_{loc}(\Phi_{f,loc} - \Phi_m)$ varies

linearly near the location of interest. Subsituting eq. [7.16] into [7.37] yields:

$$\phi_\Delta(\zeta) = \frac{Bi^{**}_{loc}\left[\phi_{f,loc} - \phi_m(\zeta)\right]}{14.55} \qquad [7.38]$$

(Within the gradient zone, ϕ_f becomes ϕ_G.) According to eq. [7.38], the value of ϕ_Δ at a certain location, ζ, depends only on the local Biot number and the local temperature difference between the furnace and the charge.

Equation [7.38] is expected to be a good approximation of ϕ_Δ when $d^2\phi_m/d\zeta^2$ is approximately linear in the vicinity of the axial location of interest. Linearity of $d^2\phi_m/d\zeta^2$ is not expected, however, near the ends of the gradient zone (see section 7.2) or at the interface (see section 7.3). In these regions, eq. [7.38] should be interpreted as an order of magnitude estimation of the effect of heat exchange in the gradient zone on the value of ϕ_Δ which would exist in the absence of such heat exchange (i.e., due to the attenuation and interface effects).

7.4.3 Constant Interface Shape in the Gradient Zone

Equation [7.38] suggests, in accordance with its limitations discussed above, that ϕ_Δ may be maintained at a constant value over a portion of the gradient zone if the product $Bi_G^{**}(\phi_G - \phi_m)$ is constant over a sufficiently long region near the center of the gradient zone, i.e., not near the ends of the gradient zone. The following set of "design rules" illustrates how the heat transfer in the gradient zone can be "tailored" so that these conditions may be approximately achieved for a system in which the interface disturbance is not present:

(1) Calculate $d\theta_m/d\zeta$ in the gradient zone, assuming that $Bi_G = 0$, by using the results of the moving fin model. A symmetric system is presently used to demonstrate this procedure; consequenty, eq. [5.8] provides the required value of $d\theta_m/d\zeta$.

(2) Allow R_G to be sufficiently large so that ϕ_G is linear.

(3) Alter the end temperatures of the gradient zone annulus so that $d\phi_G/d\zeta = d\theta_m/d\zeta$. In this way, $\phi_G - \phi_m$ is constant in the gradient zone, negecting the effects of the crucible near the ends of the gradient zone. In the present development, it is arbitrarily chosen to maintain $\phi_G(-\lambda_G/2) = 1$ while altering $\phi_G(\lambda_G/2)$. In this case:

$$\phi_G(\lambda_G/2) = 1 + \lambda_G \frac{d\theta_m}{d\zeta} \qquad [7.39]$$

$$(\phi_G - \phi_m) = \frac{1}{2}\left(1 + \lambda_G \frac{d\theta_m}{d\zeta}\right) \qquad [7.40]$$

(4) The desired value of ϕ_Δ determines the required value of Bi_G^{**} by substituting eq. [7.40] into eq. [7.38]:

$$Bi_G^{**} = \frac{29.1\,\phi_\Delta}{1 + \lambda_G (d\theta_m/d\zeta)} \qquad [7.41]$$

A non-zero value of Bi_G^{**} leads to a non-symmetric system and non-constant ($\phi_G - \phi_m$), thus contradicting the assumptions of steps (1) and (3) above. These effects are shown, however, to be of secondary importance in the results which follow.

(5) The desired radius of curvature of the interface, N_i, is next used to eliminate ϕ_Δ from eq. [7.41]. Using eq. [G.6]

$$Bi_G^{**} = -\frac{29.1}{16 N_i} \frac{d\theta_m/d\zeta}{1+\lambda_G(d\theta_m/d\zeta)} \qquad [7.42]$$

Using eq. [5.8] to eliminate $d\theta_m/d\zeta$:

$$Bi_G^{**} = -\frac{29.1}{16 N_i} \left(Bi_H^{**}\right)^{1/2} \qquad [7.43]$$

Three test cases are employed to demonstrate the procedure described above. The parameters defining the systems and the results of the calculations of steps (1) through (5) are shown in Table 7.5. Figures 7.18, 7.19, and 7.20 plot the resultant distributions of temperature and isotherm curvature calculated by the concentric fin model: part (a) of each figure plots the distribution of ϕ_Δ in the gradient zone while part (b) shows the distribution of ϕ_G and ϕ_m and the inverse radius of curvature, N^{-1}, of isotherms in the gradient zone. The desired constant radius of curvature chosen for use in eq. [7.43] is $N_i = 20$; therefore $N_i^{-1} = 0.05$.

Figure 7.18 considers a system without a crucible and with a gradient zone length $\lambda_G = 1.0$. It is seen that the distribution of ϕ_Δ and N tend to flatten out near the center of the gradient zone, approximating the desired values of $\phi_\Delta = 0.00127$ and $N_i^{-1} = 0.05$. It is expected that the distributions of ϕ_Δ and N will be yet more flat when the influence from the ends of the gradient zone are more diminished at its center. This may be accomplished by increasing the length of the gradient zone to $\lambda_G = 2.0$ (Fig. 7.19). The curves for ϕ_Δ and N are quite flat in a large portion of the center of the gradient zone in this case. Note that the required value of ϕ_Δ, 0.000903, for case 2 (see Table 7.5) is larger than actually

	Case		
	1	2	3
Figure	7.18	7.19	7.20
δ	1.0	1.0	1.5
λ_G	1.0	1.0	2.0
$Bi_H = Bi_C$	0.5	0.5	0.5
$Bi_H^{**} = Bi_C^{**}$	0.471	0.471	0.291
$d\theta_m/d\zeta$ (eq. [5.8])	-0.407	-0.289	-0.259
$\Phi_G(\lambda_G/2)$ (eq. [7.39])	0.393	0.422	0.481
$(\Phi_G - \Phi_m)$ (eq. [7.40])	0.297	0.211	0.241
Bi_G^{**} (eq. [7.43])	0.0625	0.0625	0.0491
Bi_G	0.0625	0.0625	0.0735
Φ_Δ	0.00127	0.000903	0.000811

Symmetric system except $\Phi_G(\lambda_G/2) \neq 0$

$\lambda_H = \lambda_C = \zeta_\infty$

Desired value of N_i is 20

Table 7.5: Description of the systems used in Figures 7.18, 7.19, and 7.20.

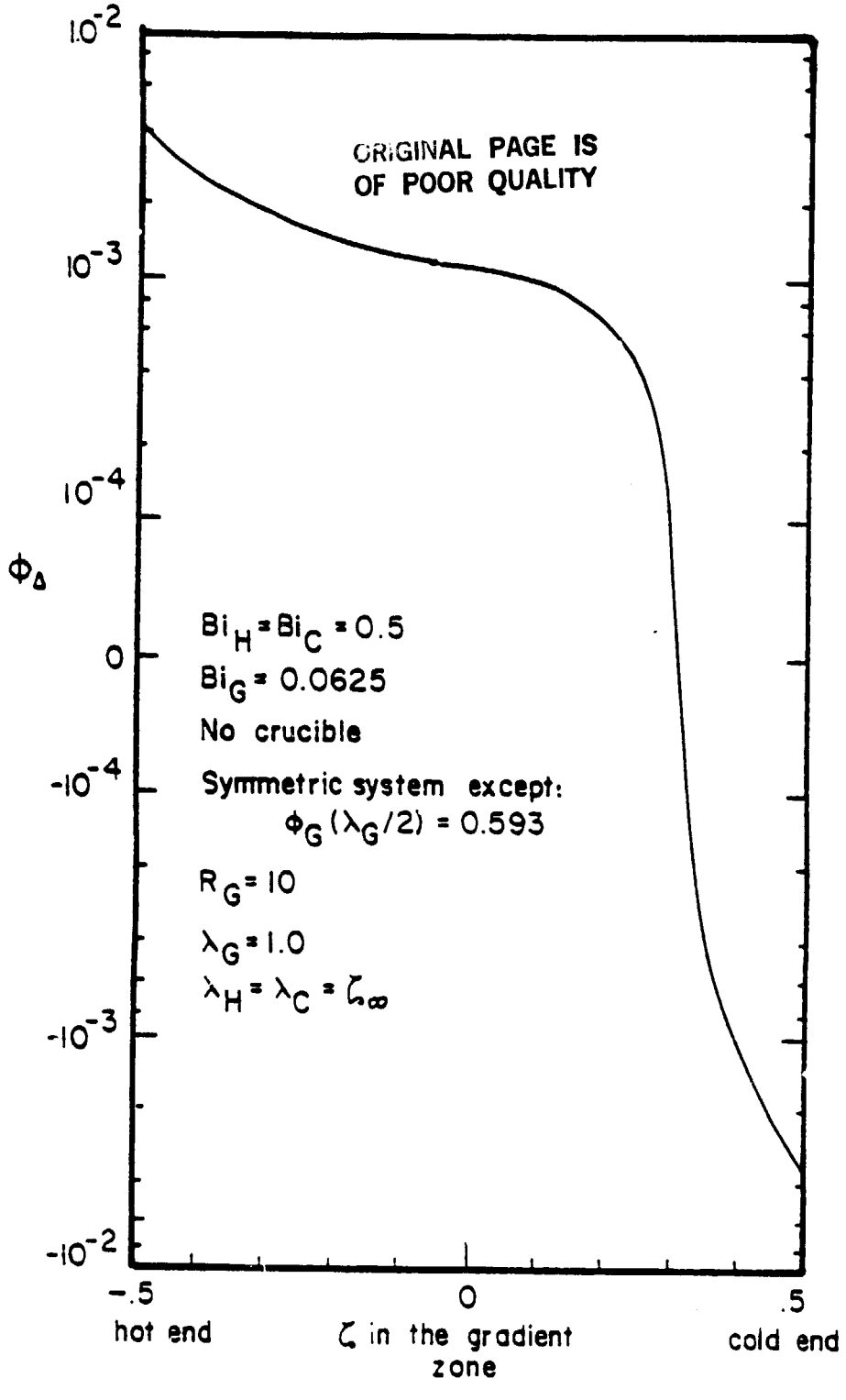

Fig. 7.18a: Demonstration of the procedure used to obtain an approximately constant isotherm shape in the gradient zone. No crucible, symmetric system and $\lambda_G = 1.0$.

Distribution of Φ_Δ.

$Bi_H = Bi_C = 0.5$

$Bi_G = 0.0625$

No crucible

Symmetric system except:

$\Phi_G(\lambda_G/2) = 0.593$

$R_G = 10$

$\lambda_G = 1.0$

$\lambda_H = \lambda_C = \zeta_\infty$

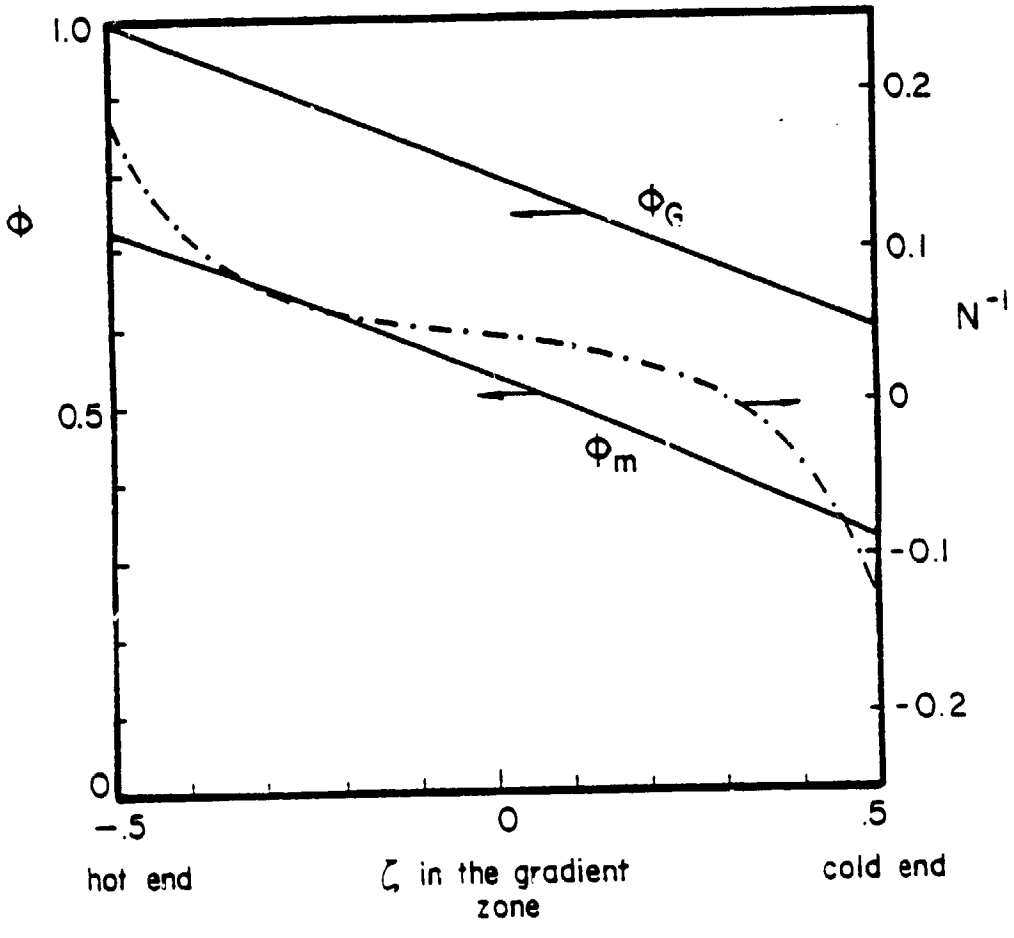

Fig. 7.18b: Demonstration of the procedure used to obtain an approximately constant isotherm shape in the gradient zone. No crucible, symmetric system and $\lambda_G = 1.0$.

Distribution of Φ_m, Φ_G and N.

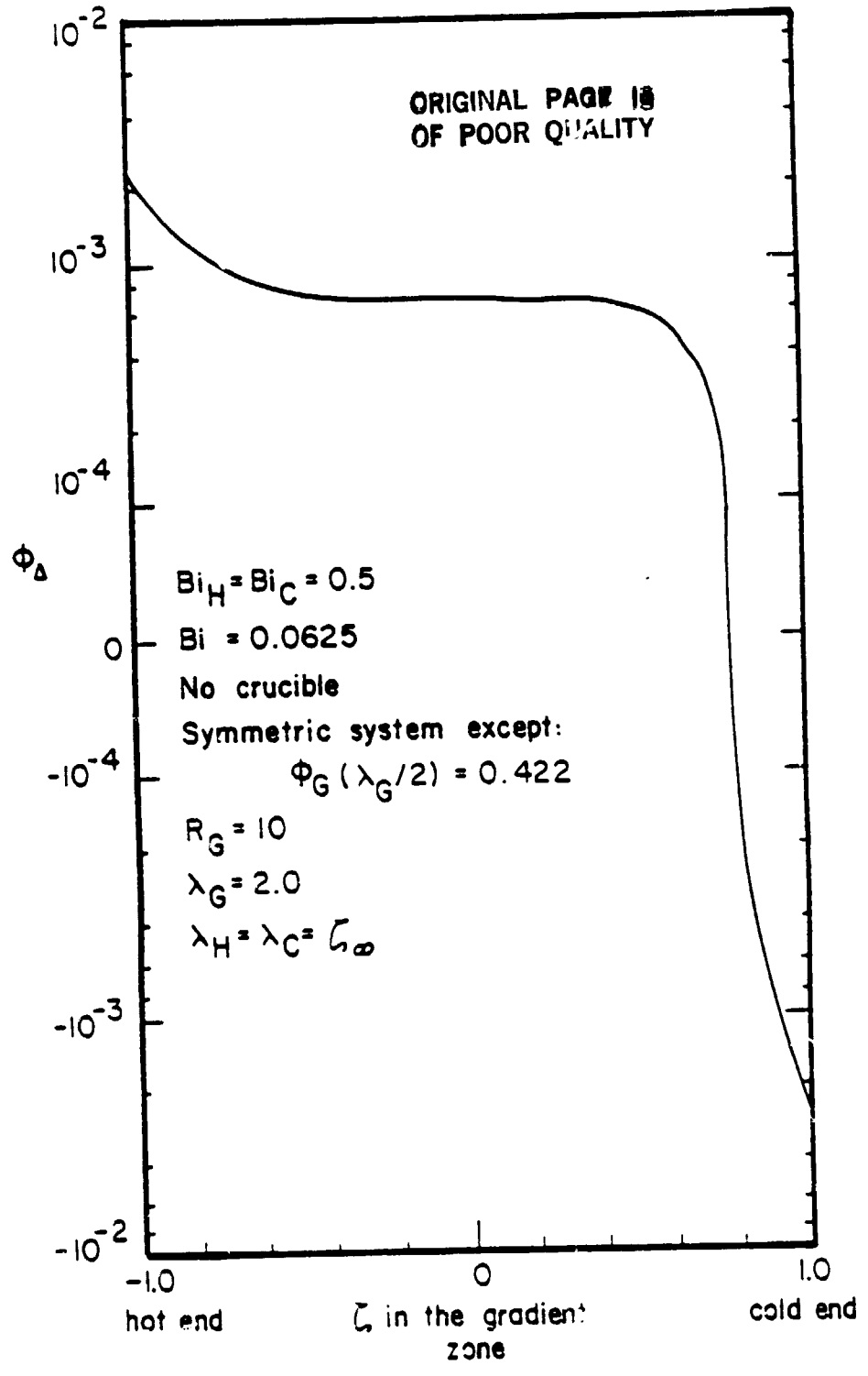

Fig. 7.19a: Analogous to Figure 7.18a except the gradient zone is longer; i.e., $\lambda_G = 2.0$.

Distribution of ϕ_Δ.

$Bi_H = Bi_C = 0.5$

$Bi_G = 0.0625$

No crucible

Symmetric system except:

$\Phi_G(\lambda_G/2) = 0.422$

$R_G = 10$

$\lambda_G = 2.0$

$\lambda_H = \lambda_C = \zeta_\infty$

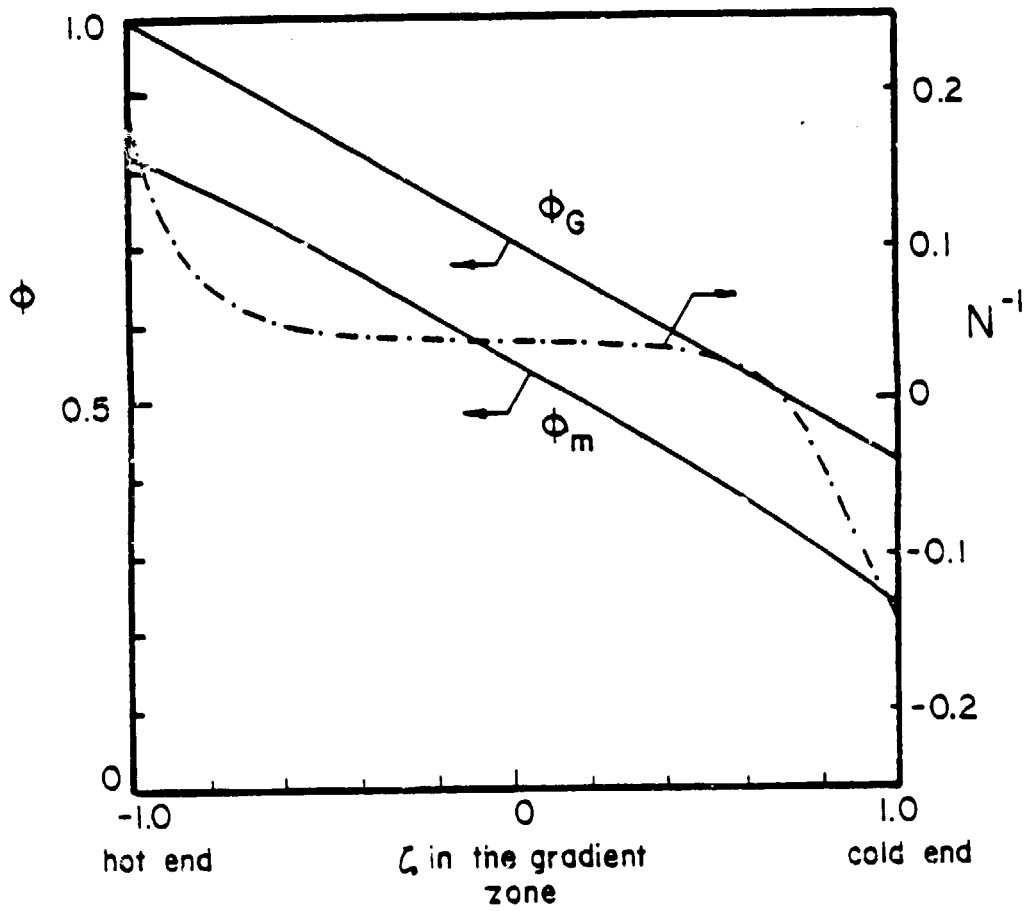

Fig. 7.19b: Analogous to Figure 7.18b except the gradient zone is longer; i.e., $\lambda_G = 2.0$.

Distribution of ϕ_m, ϕ_G and N.

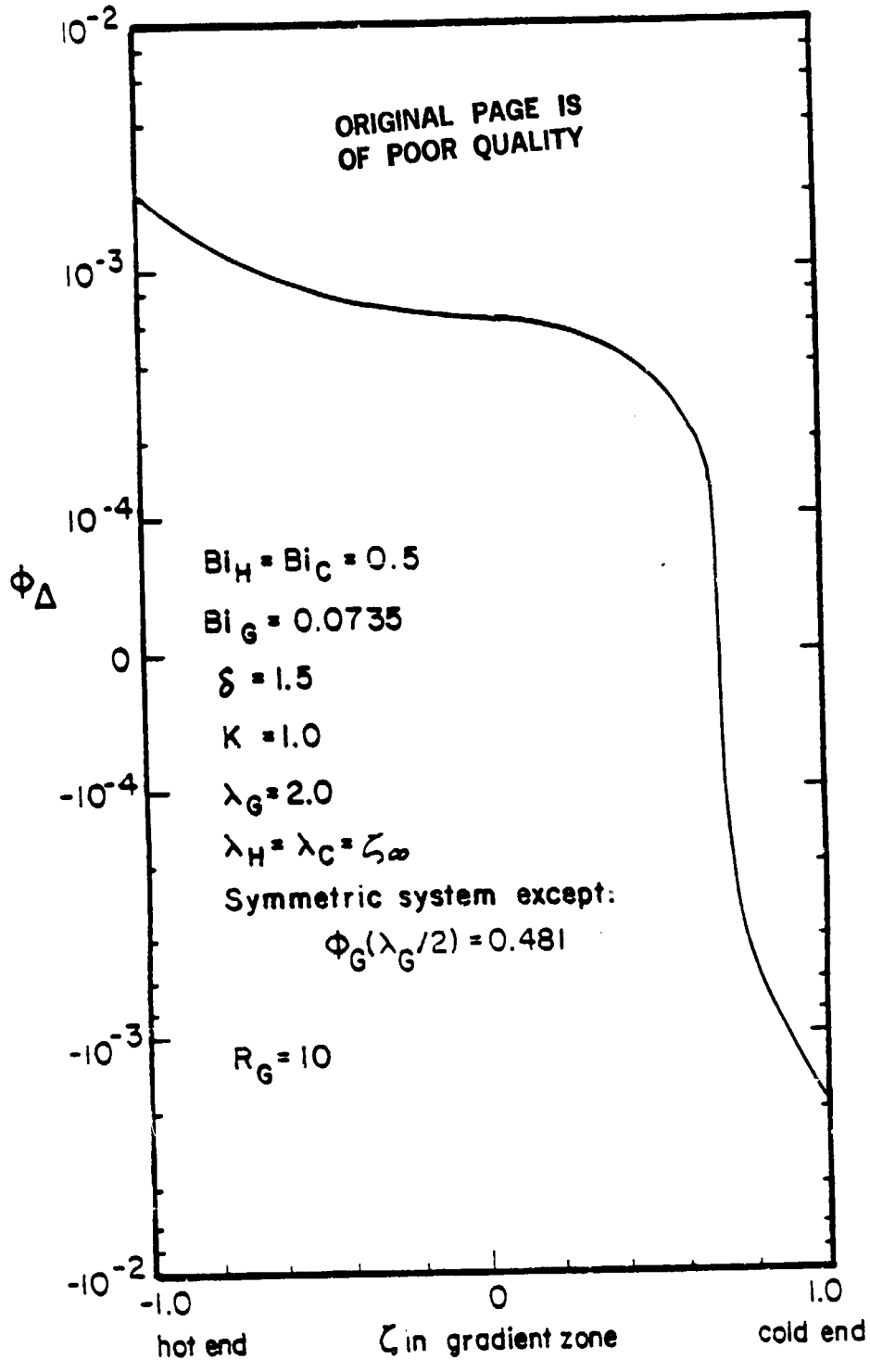

Fig. 7.20a: Analogous to Figure 7.19a except a crucible is present; i.e., $\delta = 1.5$.

Distribution of Φ_Δ.

$Bi_H = Bi_C = 0.5$

$Bi = 0.0735$

$\delta = 1.5 \quad K = 1.0$

Symmetric system except:

$\Phi_G(\lambda_G/2) = 0.481$

$R_G = 10$

$\lambda_G = 2.0$

$\lambda_H = \lambda_C = \zeta_\infty$

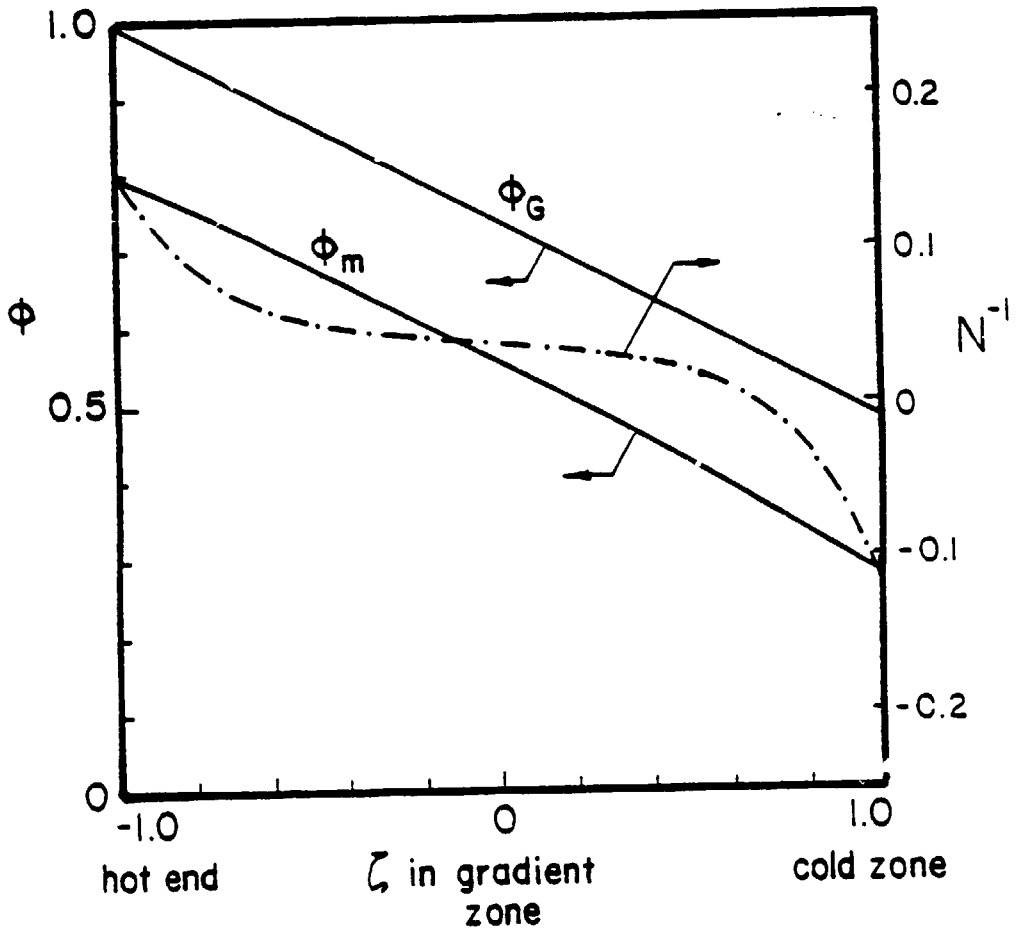

Fig. 7.20b: Analogous to Figure 7.19b except a crucible is present; i.e., $\delta = 1.5$.

Distribution of Φ_m, Φ_G and N.

(-3)

present as shown in Fig. 7.19. This is due to heat transfer to the charge in the gradient zone, not considered in eq. [7.40], which causes $\phi_\Delta - \phi_M$ to be slightly smaller than the value predicted for a symmetric system. Reduced heat transfer to the charge, and therefore a reduced value of ϕ_Δ results. The value of ϕ_Δ can be adjusted upward by an appropriate alteration in Bi_G.

Figure 7.20, which considers a system similar to that of Fig. 7.19 except $\delta = 1.5$, demonstrates that the presence of a crucible is adequately accounted for in this procedure.

The procedure outlined i this section is not intended as a generalized design method leading to optimized heat transfer for Bridgman crystal growth. Systems of pra'ical interest do not behave as those considered in Figs. 7.18 to 7.20 due to the generation of radial temperature variations at the growth interface (c.f., section 7.3). Its intent, rather is to accentuate three important features concerning the radial temperature distribution in the charge:

(1) Heat transfer in the gradient zone is a useful tool for altering the interface shape in the gradient zone.

(2) Where appropriate, results from one-dimensional models, in conjunction with the Green's function approach, can be used to help predict radial temperature variations in the charge. In the model developed in this section, eq. [7.38] is seen to provide at least order of magnitude accuracy.

(3) Generation of radial temperature variations at the interface ($R_K \neq 1$ and/or $Pe_S R_H \neq 0$) is detrimental for achieving a region about the interface which exhibits a relatively constant isotherm curvature.

8. FURNACE DESIGN CONSIDERATIONS

8.1 AXIAL TEMPERATURE DISTRIBUTION

The principal objectives of the thermal design of a Bridgman growth system regarding the axial temperature distribution of the charge are (1) to obtain a sufficiently large axial temperature gradient in the melt at the growth interface and (2) to control the location of the interface. The thermal parameters affecting the attainment of these objectives may be classified as fixed, i.e., the thermal properties of the charge, or variable, i.e., the furnace process parameters such as the lowering rate, diameter of the charge, diameter and thermal conductivity of the crucible, gradient zone length, furnace heat transfer coefficients and furnace temperatures.

8.1.1 Thermal Properties of the Charge

The thermal properties of the charge are fixed parameters and therefore constrain the thermal behavior of the growth system. The most important of the thermal properties of the charge is its thermal conductivity. A small thermal conductivity leads to a large Biot number; a Bridgman system for the growth of CdTe, for example, can have a Biot number in excess of unity. In such cases, satisfying the constitutional supercooling requirement may not be difficult. Additionally, since the "infinite" charge length is smaller when the Biot number is larger, a charge with a small thermal conductivity exhibits decreased thermal transients associated with growth near the ends of the charge and therefore tends to stabilize the growth interface. Biot numbers are smaller, on the other hand, when the thermal conductivity of the charge is relatively large (e.g., germanium). In this case, it is important to verify that the axial

temperature gradient at the growth interface is sufficiently large; if not, efforts to increase the Biot number by augmenting the heat transfer coefficients may be necessary. Further, a longer charge and furnace is necessary for the growth of an equivalent length of crystal under quasi-steady thermal conditions when the thermal conductivity is relatively large.

Related to the magnitude of the thermal conductivity is the change in thermal conductivity between the melt and the crystal at the growth interface (denoted by the symbol R_K). When the melt conductivity is greater than that of the crystal (i.e., $R_K > 1$) the axial gradient in the liquid at the interface is adversely affected, becoming less than that on the solid side of the interface. The magnitude of this effect may be significant (c.f., section 5.3) and is a potential problem for the growth of semiconductors which typically have values of R_K greater than unity. When R_K is less than unity, as is the case for metals, satisfying the constitutional supercooling requirement is more easily effected as a consequence of this effect.

Other thermal properties of the charge which affect its axial temperature distribution are the thermal diffusivity, α , mass density, ρ , and latent heat of solidification, ΔH_{sl}. The thermal diffusivity is a factor in the Peclet number which accounts for the effect of convection of sensible heat due to the motion of the charge. The product of ρ and ΔH_{sl} is contained in the product of nondimensional parameters $Pe_S R_H$ which accounts for the effect of the liberation of latent heat at the growth interface. Additionally, the convection and latent heat effects are proportional to the lowering rate, V. The significance of these heat

flows, however, depends upon their relative magnitude compared to the primary heat flow in the system, i.e., the heat flow between the furnace and the charge in the hot and cold zones. These comparisons are made in eqs. [5.6] and [5.12] where $Bi^{1/2}$ indicates the importance of the furnace-to-charge heat transfer. The effects of the thermal properties α, ρ, and ΔH_{sl} therefore depend on the prevailing values of Bi and V; typical values of these parameters for semiconductor growth systems produce small convection and latent heat effects. It may be concluded, therefore, that these thermal properties are of secondary importance to the axial temperature distribution of the charge compared to the thermal conductivity of the charge.

8.1.2 Furnace Process Parameters

A number of furnace design parameters can be used to alter the axial temperature distribution of the charge. The most obvious of these are the hot and cold zone furnace temperatures. An increase in the hot and cold zone furnace temperature difference results in a roughly proportional increase of the axial temerature gradient within the charge. On the other hand, lowering one or both of the furnace temperatures moves the growth interface toward the hot zone while an increase moves the growth interface toward the cold zone. Furthermore, alterations of the axial gradient and interface location can be made independently of each other by the proper choice of furnace temperatures; for example, the axial gradients can be made to increase while maintaining the interface in the same location or vice-versa. Typically, temperature limits in the hot and cold zone furnace constrain the application of these techniques. The heat pipes used in the experimental system described in section 2.2.1 may be used only between the

temperatures of 500 °C and 1100 °C. Furthermore, the hot zone furnace temperature may be limited by the development of excessive vapor pressure of one of the constituent elements in the melt or by the mechanical properties of the crucible at elevated temperatures.

The most important of the dimensionless parameters regarding the axial temperature distribution of the charge are the Biot numbers of the hot and cold zones. The Biot numbers reflect the thermal coupling between the furnace and the charge; eq. [5.9] indicates that as the Biot numbers increase, so do the axial temperature gradients in the gradient zone. The effect of the thermal conductivity of the charge on Bi has been discussed in section 8.1.1. The furnace process parameters which affect the Biot numbers are the furnace to charge heat transfer coefficients, h, charge diameter, D, and the thermal conductivity and thickness of the crucible, K and δ through their effect on the effective Biot number, Bi^*. It must be noted, however, that the internal radial thermal resistance of the charge, accounted for by Bi^{**}, limits the degree to which axial gradients may be increased through augmentation of the Biot number. As shown by eq. [4.14], Bi^{**} can not exceed the valued of 8; changes in h, K and δ have little effect on increasing Bi^{**} when it is close to this maximum value.

The value of the furnace to charge heat transfer coefficient, h, includes both radiative and conductive components. The radiative component may be minimized by employing reflecting surfaces between the inner furnace and outer crucible surfaces; it may be increased by utilizing surfaces of large emissivity. The magnitude of radiation heat transfer is, however, limited to that which would occur between black surfaces. Additional amounts of heat transfer may be obtained by conduction heat transfer across the furnace cavity gap. Appendix C indicates that the conductive part of

the gap heat transfer can be as large as the radiative part by using an interjacent gas of high thermal conductivity, such as helium, and a gap width of the order of one to three millimeters. Higher conduction heat transfer coefficients may, of course, be obtained by further decreasing the gap width. Small gap widths accentuate, however, the error in misalignment of the axes of the charge and furnace cavity which lead to non-radially symmetric heat transfer coefficients and interface shape. (The radiation component to the gap heat transfer is less sensitive to the gap width, especially for gap widths which are small compared to the furnace cavity diameter.

The thermal coupling between the furnace and the charge, is in most cases adversely affected by the crucible; i.e., the effective Biot number, Bi^* is usually less than the Biot number, Bi (see section 4.2.2). In order to maintain a large value of Bi^*, it is desirable to use a crucible which has a small thickness compared to the charge diameter; i.e., δ should be as close to unity as possible while maintaining structural integrity. The use of crucibles which have a very high or very small thermal conductivity compared to that of the charge should also be avoided since they tend to cause a significant reduction in Bi^*. Equation [4.7] may be used to reveal which among several potential crucible materials will yield the largest effective Biot number.

An increase in charge diameter, D, tends to increase the dimensionless axial gradient in the gradient zone through its effect on the Biot number. As section 5.6 demonstrates, the corresponding effect on the dimensional axial gradient depends on the prevailing values of Bi, K and δ . Unless accompanied by a decrease in δ , an increase in D causes a decrease in the

axial temperature gradient at the interface. A decrease in δ , however, does not guarantee an increased axial gradient; such cases should be evaluated individually.

The length of the gradient zone, λ_G , has an appreciable effect on the axial temperature gradients at the interface. For example, Fig. 5.3 demonstrates that the axial gradient may always be increased by decreasing λ_G. The effect is most significant when the hot and cold zone Biot numbers are large (greater than about 0.1). The absence of a gradient zone, (i.e., $\lambda_G = 0$), however, limits the extent of this effect; if the axial temperature gradient is not sufficiently large when $\lambda_G = 0$, other methods to increase the axial gradient must be employed. The gradient zone length additionally affects the distribution of radial temperature varitions near the growth interface. Changes in λ_G must therefore be evaluated on the basis of its effect on the interface shape as well as on the axial temperature gradient at the interface.

8.2 RADIAL TEMPERATURE VARIATIONS NEAR THE GROWTH INTERFACE

Radial temperature variations within the charge have been shown in Chapter 7 to attenuate rapidly with axial distance from the location at which they are generated. This behavior permits the formulation of a thermal design procedure leading to a satisfactory interface shape for systems in which radial temperature variations created at the interface are not present. In summary:

> The interface should be located in a gradient zone which is made approximately adiabatic through the use of a thermal insulating material placed between the hot and cold zones and

radiation shields in the furnace cavity gap. The gradient zone should be sufficiently long so that radial temperature gradients generated in the hot and cold zones have largely attenuated at the interface location; this length is approximately one to two charge diameters and depends on the effect of the crucible in reducing the rate of attenuation of the radial temperature gradients created in the furnace zones (see section 7.2.2). The exact location of the interface within the gradient zone is chosen so that the shape of the interface is slightly curved toward the solid. Additionally, small amounts of heat transfer to the charge in the gradient zone, as described in sections 7.4.2 and 7.4.3, can be used alter the interface shape or to maintain a large axial region of nearly constant isotherm curvature.

The thermal design is complete at this stage if the axial temperature gradient in the melt at the interface is sufficiently large to satisfy the constitutional supercooling requirement. If the axial gradient is not sufficiently large, however, techniques to increase its value, as described in section 8.1, can be evaluated while attempting to maintain satisfactory interface shape.

Radial temperature variations generated at the interface are, however, the dominant factor with regard to the interface shape. The procedure outlined above, therefore, does not lead to desirable interface shapes unless the interface effect can be eliminated. This issue is of particular importance for the growth of semiconductor materials which have values of R_K greater than unity; for such materials, the interface effect tends to

produce an interface shape which is curved in the adverse direction, i.e., toward the melt.

8.2.1 Counteracting the Effects of Radial Temperature Variations Generated at the Growth Interface

The analysis of section 7.1 suggests that heat transfer from the furnace to the charge tends to produce isotherm shapes which are concave toward the solid. Such heat transfer in the gradient zone thus serves to make the interface shape more favorable if it is originally concave toward the melt. The gradient zone, in such a case, resembles somewhat an extension of the hot zone furnace. The potential for completely eliminating an adverse interface curvature may be estimated by comparing the value of ϕ_Δ produced at the interface due to the interface effect (eq. [7.30]) to a representative value of ϕ_Δ caused by heat exchange with the furnace at the prevailing Biot numbers. The value of ϕ_Δ at the end of an adiabatic gradient zone (see section 7.2) may be used to estimate this latter value of ϕ_Δ. If radial temperature gradients caused by heat transfer in the furnace zones are of comparable magnitude, or larger, than those generated due to the interface effect, additional heat transfer to the charge in the gradient zone may prove useful in reversing an adverse interface curvature. If, on the other hand, radial temperature gradients caused by heat transfer to the charge are less than those generated at the interface, this technique can not be expected to change the direction of the shape of the interface.

A decrease in the value of δ likewise decreases the magnitude of the radial temperature gradients generated at the interface, as shown in Fig. 7.12. The value of δ can be decreased by either an increase in the charge diameter or by a decrease in the thickness of the crucible. A

decrease in δ, while not eliminating the interface effect, may be useful in combination with heat transfer to the charge as described in the previous paragraph.

The ideal method of dealing with the interface effect is to eliminate it. If this is possible, the design procedure for obtaining the desired interface shape, described in section 8.2, becomes applicable. The cause of the interface effect is the change in the axial temperature gradient within the charge at the growth interface which is not present in the crucible. Efforts to eliminate the interface effect therefore must either (1) remove the change in axial gradient within the charge at the interface or (2) produce an equivalent change in axial gradient within the crucible.

Equation [7.26] suggests that the slope change at the interface disappears for an appropriate value of the lowering rate, V, when $R_K < 1$. The efficacy of this technique depends, however, on the interplay between the value of V required to eliminate the slope change at the interface and the effect of V on the constitutional supercooling requirement. Further, this technique is not applicable when $R_K > 1$.

Since the electron potentials are not equal in the solid and liquid portions of the charge, the passage of an electric current across the growth interface produces or absorbs heat (depending on the direction of the current) by virtue of the Peltier effect. Such heat can be used to eliminate the change in axial temperature gradient at the interface caused by the change in thermal conductivity and the liberation of latent heat. Rewriting the heat balance at the interface in order to include the Peltier heat yields:

$$(R_K - 1) = Pe_s R_H + \frac{Se\, T_i\, I''D}{k_s (T_{f,H} - T_{f,c})} \qquad [8.1]$$

where: $G_L = G_S$ in order to eliminate the slope change at the interface

Se = Seebeck coefficient

I" = current per unit cross sectional area

SeT_iI'' = rate of generation of Peltier heat per unit cross sectional area

T_i = absolulte melting temperature

Using germanium as an example (Se = 70μV/K, T_i = 1211°K), eq. [8.1] shows that the required current density is in excess of 200 amps/cm^2 for typical operating conditions. Such large current densities may be difficult to attain experimentally and may also produce significant Joule heating effects. Although each case should be examined individually, it appears that Peltier heating is not a viable method for eliminating the slope change at the interface.

Peltier heating/cooling has, however, greater potential for modifying the interface shape in small amounts. For example, a flat interface shape may be made slighlty concave toward the solid by the application of a small amount of Peltier cooling. This technique yields a similar result as that of transferring small amounts of heat to the charge in the gradient zone as described in section 7.4.3.

The interface effect may also be eliminated by producing a slope change in the crucible at the interface which is equivalent to that in the charge. This may be done by adding the appropriate amount of heat to the crucible in a very narrow region near the axial location of the interface. The remainder of the gradient zone may be adiabatic if desired. A thin

crucible, being to a greater extent thermally one-dimensional than a thicker crucible, is more desirable in this respect.

9. CONCLUSIONS AND RECOMMENDATIONS

The objectives of this analysis are to determine the primary thermal behavior of the vertical Bridgman crystal growth method and, where possible, to develop simplified analytical results to indicate quantitatively the relationship between the thermal parameters of the system and its thermal response. The purpose of these objectives are (1) to aid in both the preliminary thermal design of a Bridgman growth system, (2) to better interpret experimental results of existing systems in order to improve their design and (3) in a more general sense, to critically evaluate the capabilities of the Bridgman technique. The major efforts involved in attaining these objectives has been the development of appropriate simplified thermal models of the Bridgman growth system. The major findings of this study are reviewed, and possible directions for future research are outlined, in this chapter.

9.1 CONCLUSIONS

A one-dimensional thermal model was developed in order to determine the axial temperature distribution within the charge. Approximations for the radial thermal resistance offered by the crucible and by the charge itself are incorporated in a straightforward manner into the one-dimensional model through the definition of the "effective" Biot number. In general, these radial resistances decrease the effective thermal coupling between the furnace and the charge, leading to reduced effective Biot numbers and axial temperature gradients at the growth interface. The relationship between the crucible thickness and thermal conductivity and the effective Biot number is analytically described by eq. [4.7]. This relationship demonstrates that the ratio of thermal conductivity of the

crucible to that of the charge, K, should be between 0.1 and 1.0 in order to prevent severe reduction of the effective Biot number. Equation [4.14] incorporates the effect of the radial thermal resistance within the charge and indicates that axial gradients are limited since the effective Biot number can not exceed the value of 8. Efforts to increase the heat transfer coefficient between the furnace and crucible therefore does not increase axial temperature gradients in systems which already have an effective Biot number which approaches this value.

The axial temperature distribution within the charge is easily obtained from the one-dimensional model by computer. Analytical solution, however, yields several important results. Criteria are developed which indicate when the effects of axial convection of sensible heat, generation of latent heat and length of the charge can be neglected. Additionally, analytical expressions for the axial temperature gradient in the melt at the growth interface (required for the constitutional supercooling requirement) and the axial location of the interface are developed. (When the axial convection of sensible heat is sufficiently small, these analytical results reduce into yet more simple forms.) These expressions assume a charge length which satisfies the infinite length criteria but includes the effects of: hot and cold zone effective Biot numbers, unequal melt and crystal thermal conductivity, axial convection of sensible heat, generation of latent heat, length of an adiabatic gradient zone, and interface position within the gradient zone. The effects of the charge diameter and thermal properties are included by virtue of the non-dimensional formulation of the thermal model. Such results indicate that the principle factors affecting the axial temperature gradient at the

interface are: level of the effective Biot numbers, unequal melt and crystal thermal conductivity, gradient zone length and generation of latent heat.

Two-dimensional thermal modeling is utilized to predict the shape of the growth interface. The two-dimensional thermal models developed here are extensions of the one-dimensional model; i.e., the charge is considered as two radially concentric fins, the crucible is a third fin and, in the gradient zone, the furnace is considered to be a fourth annular fin. This approach is taken, rather than a finite difference or finite element computer formulation, for the potential to develop analytical results.

The equations describing the temperature distributions of the concentric fins indicates that radial temperature variations within the charge are created by heat exchange between the charge and its surroundings (see eq. [7.2]). Heat transfer to the charge leads to interface shapes which are concave toward the solid, and heat transfer from the charge tends to produce an interface shape which is concave toward the liquid. The effect of heat transfer to the charge at a particular axial location dies out rapidly with distance from that location. Thermal conditions as little as one charge diameter from the interface have only a very small effect on its shape. The design of a Bridgman apparatus for the proper interface shape may therefore be interpreted as providing the proper amount and distribution of heat exchange to or from the charge in the vicinity of the interface.

The two-dimensional results identify for the first time a potentially serious problem for the satisfactory growth of materials, such as semiconductors, which have a thermal conductivity of the melt which is greater than that of the solid. In the presence of a crucible, inherent to

the Bridgman technique, such conditions lead to heat transfer from the charge to the crucible. This is the dominant effect on the shape of the interface since it occurs at the interface itself. Further, the shape of the interface produced through this effect is curved in the undesirable direction, i.e, toward the liquid.

9.2 RECOMMENDATIONS FOR FURTHER RESEARCH

The results of the one- and two-dimensional models presented in this work compare well to published analytical results from more accurate computer models. Published experimental results are, however, few and not suitable for the direct verification of the conclusions presented here. Such verification is considered necessary and is, in part, the motivation for the experimental program currently in progress.

The numerical accuracy of the simple thermal models of this work is expected to be sufficient for initial furnace design as well as to indicate the expected parametric thermal behavior. Increased numerical accuracy obtainable from a two-dimensional finite difference or finite element computer model will, however, be required for final system design and for quantitative comparison with experimental results. Effects such as thermal conductivity change and/or generation of latent heat at the interface in the presence of a crucible, presently not included by computer models described in the literature, must be included in any new computer model. Modeling assumptions used in the present work, but anticipated to have a minor effect in actual growth systems, can also be relaxed; these include temperature dependent thermal properties and heat transfer coefficients and temperature uniformity of the hot and cold zone furnaces. Finally, the furnace boundary conditions should be flexible, especially in the gradient

zone, in order to study the effect of different distributions of heat exchange between the furnace and the charge on the shape of the growth interface.

The two-dimensional concentric fin model assumes that the axial location of the growth interface is the same within both the inner and outer charge fins. The error in predicted radial temperature variations obtained through the use of this assumption is expected to increase with interface curvature but presently is not known quantitatively. A two-dimensional computer model as described above may be used to determine this error.

The accuracy of a computer model of Bridgman growth as described above will be compromised by thermal property data of questionable reliability. Unfortunately, the thermal properties of many semiconductors, especially those of the liquid, are not accurately known. In such cases, data of increased reliability must be found by experimental means.

Adverse interface curvature is expected for the growth of semiconductor materials due to radial temperature gradients created at the interface. Section 8.2.1 offers several methods to counteract this effect. Detailed evaluation of these (and any other) methods must take place in order to solve this potentially serious problem inherent to the Bridgman growth technique.

The technique presently considered most promising for counteracting the interface effect is locally heating the crucible near the interface in conjunction with a thin crucible. Analysis of these conditions is required to examine the potential of this method. The relationship between the thickness of the crucible and the amount and distribution of heat transfer

to the surface of the crucible to the shape of the growth interface will require the solution of an appropriate two-dimensional thermal model of the interface region.

This work considers furnace boundary conditions as an independent variable which, in combination with the other system parameters, determines the interface shape. It would be useful, however, to be able to solve the inverse problem: i.e., what must the furnace boundary conditions be in order to produce a desired interface shape? There may be multiple solutions or no solution at all. In the first case, such results would provide a direct indication of the thermal design required for satisfactory interface shape; in the second case, the knowledge that no set of furnace boundary conditions exist which can produce the desired interface shape indicates that other parameters of the growth system require alteration. The ability to make such conclusions will require the computer solution of the appropriately modeled inverse heat transfer problem.

REFERENCES

1. Brice, J. C., "The Growth of Crystals from Liquids", North-Holland Publishing Co., Amsterdam, London-American Elsevier Publishing Co. Inc., N.Y., (1973).

2. Gilman, J. J., (ed.), "The Art and Science of Growing Crystals", Wiley, N.Y., (1963).

3. Gatos, H. C., "Crystal Growth: Available Methods", Proc. Third Int. Summer School for Cryst. Growth, Univ. of New Hampshire, (1977).

4. Flemings, M. C., "Solidification Processing", McGraw-Hill, New York, (1974).

5. Jackson, K. A., and Hunt, J. D., Acta Met. 13, 1212 (1965).

6. Schaefer, R. J., and Glicksman, M. E., Met. Trans. 1, 1973 (1970).

7. Sharp, R. M., and Hellawell, A., J. Crystal Growth 6, 334 (1970).

8. Tiller, W. A., Jackson, K. A., Rutter, J. W., and Chalmers, B., Acta Met. 1, 428 (1953).

9. Riquet, J. P., and Durand, F., J. Crystal Growth 33, 303 (1976).

10. Clyne, T. W., J. Crystal Growth 50, 691 (1980).

11. Clyne, T. W., J. Crystal Growth 50, 684 (1980).

12. Coriell, S. R., and Sekerka, R. F., J. Crystal Growth 46, 479 (1979).

13. Coriell, S. R., Boisvert, R. F., Rehm, R. G., and Sekerka, R. F., J. Crystal Growth 54, 167 (1981).

14. Chang, C. J., "A Study of Natural Convection and Its Effects on Melt Crystal Growth", Ph.D. Thesis, Massachusetts Institute of Technology, Dept. of Chem. Eng., Sept. 1982.

15. Chang and Brown, in preparation for J. Crystal Growth.

16. Stockbarger, D., C., Review of Scientific Instr. 7, 133 (1936).

17. Chang, C. E., and Wilcox, W. R., J. Crystal Growth 21, 135 (1974).

18. Davis, K. G., Can. Met. Quart. 11, (2) 317 (1972).

19. Bartholemew, D. M. L., and Hellawell, A., J. Crystal Growth 50, 453 (1980).

20. Vetter, J., Fruehauf, J., and Schneider, H. G., Crystal Res. and Tech. 16, (12) 1401 (1981).

21. Fu, T.-W., and Wilcox, W. R., J. Crystal Growth 51, 557 (1981).

22. Sukanek, P. C., J. Crystal Growth 58, 208 (1982).

23. Sukanek, P. C., J. Crystal Growth 58, 219 (1982).

24. Sen, S., and Wilcox, W. R., J. Crystal Growth 28, 36 (1975).

25. El-Mahallawy, N. A., and Farag, M. M., J. Crystal Growth 44, 251 (1978).

26. Fu, T.-W., and Wilcox, W. R., J. Crystal Growth 48, 416 (1980).

27. Domanski, R., Fiszdon, J. F., Styczek, A., ASME paper no. 81-WA/HT-39, (1981).

28. Jones, C. L., Capper, P., and Gosney, J. J., J. Crystal Growth 56, 581 (1982).

29. Carslaw, H. S., and Jaeger, J. C., "Conduction of Heat in Solids", 2nd ed., Oxford University Press, Amen House, London (1959).

30. Rohsenow, W. M., and Choi, H. Y., "Heat, Mass and Momentum Transfer", Prentice-Hall, 1st ed., Englewood Cliffs, New Jersey (1961).

31. Arpaci, V. S., "Conduction of Heat in Solids", 1st ed., Addison-Wesley, Reading, Massachusetts (1966).

32. CRC Handbook of Chemistry and Physics, The Chemical Rubber Company, Cleveland, Ohio, 51st ed. (1970-1971).

33. Eckart, E. R. G., and Drake, R. M., "Analysis of Heat and Mass Transfer", 1st ed., Mcgraw-Hill, New York (1972).

34. Devienne, F. M., "Low Density Heat Transfer", in Advances in Heat Transfer, v.2, Academic Press, New York, 1965.

35. Kraus, A. D., "Analysis and Evaluation of Extended Surface Thermal Systems", 1st ed., Hemisphere Publishing Corp., Washington D. C. (1982).

36. Boyce, W. E., and DiPrima, R. C., "Elementary Differential Equations and Boundary Value Problems", 2nd ed., Wiley, N.Y, (1969).

37. Ogata, K., "Modern Control Engineering", Prentice-Hall, Englewood Cliffs, N.J., (1970).

APPENDIX A

DERIVATION OF EQUATION 4.11

This appendix presents the derivation of eq. [4.11].

In nondimensional form, the heat conduction equation in the charge is given by eq. [4.12]. Integrate each term in eq. [4.12] according to the formula:

$$\theta_m(\zeta) = \frac{\int_0^{D/2} \theta(r,z)\, 2\pi r\, dr}{\frac{1}{4}\pi D^2} = 8\int_0^{1/2} \theta(\rho,\zeta)\,\rho\, d\rho \qquad [A.1]$$

(Subscript "m" in eq. [A.1] denotes an area-averaged quantity.) Equation [4.12] becomes:

$$\frac{d^2\theta_m}{d\zeta^2} - Pe\,\frac{d\theta_m}{d\zeta} + 4\left.\frac{\partial\theta}{\partial\rho}\right|_{\rho=1/2} = 0 \qquad [A.2]$$

The boundary condition at the surface of the charge is, in nondimensional form:

$$\left(\frac{\partial\theta}{\partial\rho}\right)_{\rho=1/2} = Bi\,(\theta_f - \theta_s) \qquad [A.3]$$

where θ_s is the surface temperature of the charge. Substituting eq. [A.3] into eq. [A.2] yields:

$$\frac{d^2\theta_m}{d\zeta^2} - Pe\,\frac{d\theta_m}{d\zeta} + 4Bi\left[(\theta_f - \theta_m) - (\theta_s - \theta_m)\right] = 0 \qquad [A.4]$$

The crucible effect (section 4.2.2) is included by using the effective Biot and Peclet numbers in eq. [A.4] resulting in eq. [4.11].

APPENDIX B

ANALYTICAL SOLUTION OF THE ONE-DIMENSIONAL MODEL: INFINITE CHARGE LENGTH

According to the moving fin model described in Chapter 4, eq. [4.17] gives the axial temperature distribution in each of the four regions listed below:

1. Hot zone.
2. Liquid part of the gradient zone.
3. Solid part of the gradient zone.
4. Cold zone.

The solution of eq. [4.17] for each zone is:

$$\theta_{m,n} = A_n e^{w^+_{m,n}\zeta} + B_n e^{w^-_{m,n}\zeta} + [1] \qquad [B.1]$$

where: n = 1, 2, 3, 4

(The subscript "n" denotes the zone number according to the list above). The constant term, 1.0, in eq. [B.1] is the particular solution for the hot zone and is zero for the other zones. The characteristic roots, $w^{\pm}_m$, are given by:

$$w^{\pm}_{m,n} = \frac{Pe^*_n}{2}\left\{1 \pm \left[1 + 16\frac{Bi^{**}_n}{(Pe^*_n)^2}\right]^{1/2}\right\} \qquad [B.1]$$

Since the moving fin model assumes that $Bi_G = 0$, the characteristic roots in the gradient zone can be simplified:

$$
\begin{aligned}
W^{+}_{m,2} &= Pe^{*}_{2} \\
W^{-}_{m,2} &= 0 \\
W^{+}_{m,3} &= Pe^{*}_{3} \\
W^{-}_{m,3} &= 0
\end{aligned}
\qquad \text{[B.3]}
$$

There are eight unknown coefficients in eq. [B.1], two for each of the four zones. For the results given in this appendix, it is assumed that the length of charge in the hot and cold zones is infinite; under these conditions, $B_1 = A_4 = 0$. Boundary conditions between adjacent zones, given by eqs. [4.18], [4.19] and [4.20], are used to calculate the remaining coefficients. The boundary condition of equality of temperature between adjacent zones, eq. [4.18] yields:

$$
\begin{aligned}
A_1 e^{-W^{+}_{m,1}\mu} + 1 &= A_2 e^{-W^{+}_{m,2}\mu} + B_2 \\
A_2 e^{W^{+}_{m,2}\zeta_i} + B_2 &= A_3 e^{W^{+}_{m,3}\zeta_i} + B_3 \\
A_3 e^{W^{+}_{m,3}\mu} + B_3 &= B_4 e^{W^{-}_{m,4}\mu}
\end{aligned}
\qquad \text{[B.4]}
$$

where: $\mu = \lambda_G/2$

ζ_i = axial location of the growth interface

At the ends of the gradient zone, the boundary conditions of equality of heat flux between adjacent zones, eq. [4.19], gives:

$$
\begin{aligned}
W^{+}_{m,1} A_1 e^{-W^{+}_{m,1}\mu} &= W^{+}_{m,2} A_2 e^{-W^{+}_{m,2}\mu} \\
W^{+}_{m,3} A_3 e^{W^{+}_{m,3}\mu} &= W^{-}_{m,4} B_4 e^{W^{-}_{m,4}\mu}
\end{aligned}
\qquad \text{[B.5]}
$$

The flux boundary condition at the interface, eq. [4.20], yields:

$$w^+_{m,2} A_2 e^{w^+_{m,2}\zeta_i} = \frac{1}{R^*_K}\left[w^+_{m,3} A_3 e^{w^+_{m,3}\zeta_i} + Pe_s R^*_H\right] \qquad [B.6]$$

where:

$$R^*_K = \frac{R_K + K_s(\delta^2-1)}{1 + K_s(\delta^2-1)}$$

$$R^*_H = \frac{R_H}{1 + K_s(\delta^2-1)}$$

Eqs. [B.4], [B.5], and [B.6] present six linear equations in the six unknown coefficients A_1, A_2, B_2, A_3, B_3, and B_4. After solving for these coefficients, the axial gradient in the liquid near the interface, G_L, and the nondimensional interface temperature are given by:

$$G_L = \frac{Pe_s R^*_H + \dfrac{w^+_{m,3}}{1+\left(\dfrac{w^+_{m,3}}{w^-_{m,4}}-1\right)\exp\left[+w^+_{m,3}(\mu-\zeta_i)\right]}}{R^*_K - \dfrac{w^+_{m,3}}{w^+_{m,2}}\dfrac{1+\left(\dfrac{w^+_{m,2}}{w^+_{m,1}}-1\right)\exp\left[-w^+_{m,2}(\mu+\zeta_i)\right]}{1+\left(\dfrac{w^+_{m,3}}{w^-_{m,4}}-1\right)\exp\left[w^+_{m,3}(\mu\ \ \zeta_i)\right]}} \qquad [B.7]$$

$$1-\theta_i = -G_L \cdot \frac{1+\left(\dfrac{w^+_{m,2}}{w^+_{m,1}}-1\right)\exp\left[-w^+_{m,2}(\mu+\zeta_i)\right]}{w^+_{m,2}} \qquad [B.8]$$

(Section 4.4.3 explains that the axial gradient at the interface calculated from the one-dimensional model must be interpreted as the average of the

charge and crucible axial gradients. G_L denotes this average value.) Note that eq. [B.8] requires an iterative solution if it is desired to determine ζ_i given θ_i.

For small Pe^*, eq. [5.6] holds and $w^+_{\bar{m},1}$ and $w^-_{\bar{m},4}$ can be approximated by eq. [5.7]. This leads to a simplified form of the above expressions:

$$G_L = \frac{-2 + \left[(Bi_c^{**})^{-1/2} + \lambda_G - 2\zeta_i\right] Pe_s R_H^*}{R_K^* \left[(Bi_c^{**})^{-1/2} + \lambda_G - 2\zeta_i\right] + \left[(Bi_H^{**})^{-1/2} + \lambda_G + 2\zeta_i\right]} \qquad [B.9]$$

$$1 - \theta_i = \frac{1 - \frac{1}{2} Pe_s R_H^* \left[(Bi_c^{**})^{-1/2} + \lambda_G - 2\zeta_i\right]}{1 + R_K^* \dfrac{\left[(Bi_c^{**})^{-1/2} + \lambda_G - 2\zeta_i\right]}{\left[(Bi_H^{**})^{-1/2} + \lambda_G + 2\zeta_i\right]}} \qquad [B.10]$$

The assumptions that $Bi_G = 0$ and $\lambda_H = \lambda_c = \infty$ yield relatively simple analytical results. When it is desired to relax these assumptions, the preceding development can be appropriately modified. When $Bi_G \neq 0$, for example, $w_{m,2}$ and $w_{m,3}$ are no longer described by eq. [B.3]. Additionally, a particular solution must be included in eq. [B.1] for the gradient zone regions; the form of the particular solution depends on the temperature distribution in the gradient zone annulus. When λ_H and/or λ_c is not infinity, the coefficients B_1 and/or A_4 is not zero. Additional boundary conditions at the ends of the charge must then be employed. In these cases it is more convenient to determine the coefficients A_n and B_n by computer. This has been the procedure used to determine the results presented in section 5.5 for finite charge length.

APPENDIX C

CALCULATION OF HEAT TRANSFER COEFFICIENTS

Heat transfer between the furnace walls and the outer crucible surface occurs by conduction and radiation across the annular gap which separates them. The gap width is here considered sufficiently small so that natural convective flow of the gas in the gap does not occur. The magnitude of the conduction and radiation heat transfer is here described by heat transfer coefficients, h_c and h_r respectively. Since the conduction and radiation heat transfer occurs in parallel, the overall h is simply the sum of h_c and h_r:

$$q''_D = (h_c + h_r)(T_f - T_m) = h(T_f - T_m) \qquad [C.1]$$

C.1 SAMPLE HEAT TRANSFER COEFFICIENTS

For an annular gap whose width is small compared to the diameter, the conduction heat transfer coefficient can be approximated by:

$$h_c = \frac{k_{gas}}{t_{gap}} \qquad [C.2]$$

Table C.1 gives heat transfer coefficients across a 1 mm gap for air and helium at a number of temperatures. (Helium has a high thermal conductivity compared to most gases.) For different gap widths, eq. [C.2] can be used to adjust the sample values given in the table.

Radiation heat transfer across the gap, as shown in Fig. C.1, is described by the following equations assuming that the surfaces are grey:

$$q''_r(f \text{ to } cr) = \sigma(T_f^4 - T_c^4)\, \mathcal{F}_{f,cr} \qquad [C.4]$$

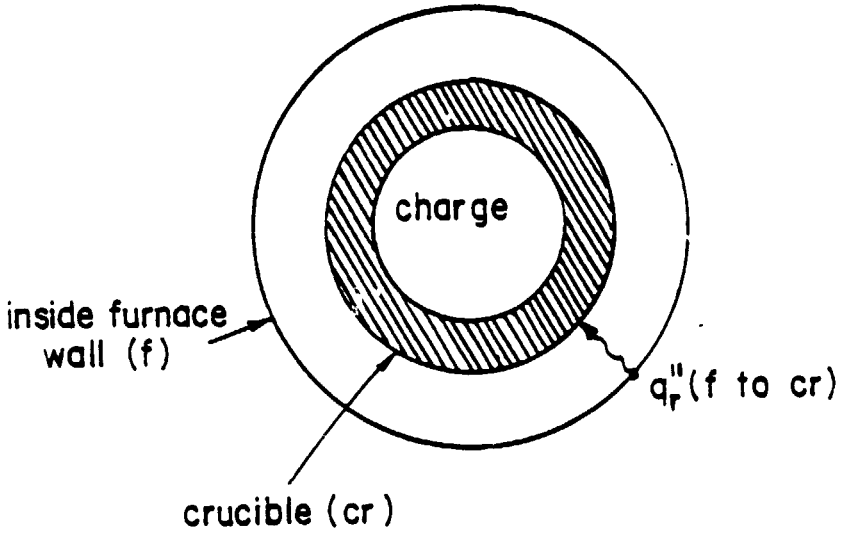

Fig. C.1: Geometry used to describe radiation heat transfer between the furnace and the outer crucible surface.

Temperature (°C)	Helium		Air	
	k_{gap} [32]	h_c	k_{gap} [33]	h_c
500	0.00299	299	0.000564	56.4
700	0.0035	355	0.000663	66.3
900	0.00409	409	0.000769	76.9
1100	0.00462	462	0.000876	87.6

h_c measured in W/m^2-K

k_{gap} measured in W/cm-K

t_{gap} = 1 mm

Table C.1: Conduction heat transfer coefficients across a 1 mm thick gas layer.

$$\mathcal{F}_{f,cr} = \frac{1}{1 + \left(\frac{1}{\epsilon_{cr}} - 1\right) + \frac{D_{cr}^2}{D_f^2}\left(\frac{1}{\epsilon_f} - 1\right)} \qquad [C.4]$$

where: q_f''(f to cr) = radiation heat flux from the furnace to the outer crucible surface (c.f., Fig. C.1) per unit surface area of the crucible

σ = 5.729×10^{-8} W/m^2-K^4

D = diameter

ϵ = surface emissivity

T_f = furnace temperature

T_{cr} = crucible temperature

If the gap width is small compared to the diameter of the charge (i.e., $D_f \cong D_{cr}$), eq. [C.4] becomes:

$$\mathcal{F}_{f,cr} = \frac{1}{\frac{1}{\epsilon_f} + \frac{1}{\epsilon_{cr}} - 1} \qquad [C.5]$$

Further, if the surfaces are black, $\epsilon_f = \epsilon_{cr} = 1$; in this case, the radiation heat transfer is maximized as $\mathcal{F}_{f,cr} = 1$.

When T_f is not extremely different from T_{cr}, eq. [C.3] can be conveniently approximated in order to yield a radiation heat transfer coefficient in simpl form [30]:

$$q''_r(f \text{ to } cr) = h_r(T_f - T_{cr}) \qquad [C.6]$$

$$h_r \simeq 4\,\mathcal{F}_{f,cr}\,\sigma\,\bar{T}^3 \qquad [C.7]$$

where: $\bar{T} = (T_f + T_{cr})/2$

Equation [C.7] shows that the radiation heat transfer coefficient increases as the absolute temperature cubed. Table C.2 lists sample values of the radiation heat transfer coefficient for various $\bar{T}$, calculated according to eq. [C.7] and assuming that $\mathcal{F}_{f,cr} = 1$.

C.2 RAREFIED GAS CONDUCTION

The values listed in Table C.1 for the conduction heat transfer coefficient assume that the pressure of the gas in the gap is sufficiently large so that the gas can be considered as a continuum. As the gas pressure decreases to a sufficiently low value, however, the gas no longer behaves as a continuum and the conduction heat transfer across the gap

T(C)	h_r (W/m^2-K)
500	106
700	211
900	370
1100	593

Table C.2: Radiation heat transfer coefficients between black surfaces which are separated by a narrow annular gap.

decreases. Devienne [34] distinguishes the following limiting regimes for conduction heat transfer in a gas:

$$\frac{L_{mfp}}{t_{gap}} < 0.001 \qquad \text{continuum regime} \qquad [C.8a]$$

$$\frac{L_{mfp}}{t_{gap}} > 10 \qquad \text{free molecule regime} \qquad [C.8b]$$

where: L_{mfp} = mean free path length of a molecule of the gas

In the free molecule regime, a gas molecule has little probability of colliding with other gas molecules between collisions with the furnace and crucible walls; in the continuum regime, this probability is very high.

The mean free path length of a gas molecule, L_{mfp}, is given by [30]:

$$L_{mfp} = 0.707/\sigma n \qquad [C.9]$$

where:

$\sigma = \pi d^2$

d = "effective" diameter of the gas molecule

n = number of molecules per unit volume

The ideal gas law may be used to express the molecule density of the gas, n:

$$n = \frac{pN}{R_u T} \qquad [C.10]$$

where: N = Avagadro's number, 6.02×10^{23}/gm-mole

R_u = universal gas constant

T = temperature

p = pressure

Subsituting eq. [C.10] into [C.9] the mean free path length becomes:

$$L_{mfp} = \frac{0.707\, R_u T}{\sigma p N} \qquad [C.11]$$

Helium and air are again used as typical examples. Their effective diameters, d, are [30]:

He: $d = 2.18 \times 10^{-8}$ cm [C.12a]

Air: $d = 3.72 \times 10^{-8}$ cm [C.12b]

Using these values, eq. [C.11] gives the mean free path length at a temperature of 900 °C as:

He: $L_{mfp} = \frac{0.0477}{p(\text{torr})}$ (cm) [C.13a]

$$\text{Air:}\quad L_{mfp} = \frac{0.0164}{p(\text{torr})}\ \text{cm} \qquad \text{[C.13b]}$$

Equations [C.13] can be used in eqs. [C.8] in order to determine the pressure limits for the continuum and free molecule regimes.

In the free molecule regime, the conduction heat transfer coefficient is given by Devienne [34]:

$$h_c = \frac{1}{2}(\gamma+1)c_v \frac{P}{\left(\frac{2\pi R_u T}{M}\right)^{1/2}}\ a \qquad \text{[C.14]}$$

where: $\gamma = c_p/c_v$

c_p = specific heat at constant pressure

c_v = specific heat at constant volume

M = molecular weight of the gas

a = accomodation coefficient

The parameter a in eq. [C.14] depends on the effectiveness of energy transfer during collisions between a gas molecule and the walls of the furnace and crucible. If this energy transfer is complete, the value of a is equal to unity and heat transfer is maximized. A value of unity is presently used so that eq. [C.14] will give an upper limit for the free molecule conduction heat transfer coefficient. A reasonable approximation to the temperature T in eq. [C.14] is the mean value of the furnace and crucible surface temperatures. Evaluating eq. [C.14] at T=900 °C, for helium and air:

at 900 °C

$$\text{He:}\quad h_c(\text{W/m}^2\text{-K}) = 47.6\ p(\text{torr}) \qquad \text{[C.15a]}$$

$$\text{Air:}\quad h_c(\text{W/m}^2\text{-K}) = 34.6\ p(\text{torr}) \qquad \text{[C.15b]}$$

At pressures required so that conduction heat transfer across the gap is in the free molecule regime, eq. [C.15] shows that the conduction heat transfer coefficient is much smaller than the radiation heat transfer coefficients given in Table C.2. Conduction heat transfer is, in this case, essentially eliminated.

C.3 TEMPERATURE DEPENDENCE OF THE HEAT TRANSFER COEFFICIENT

The thermal models developed in Chapters 4 and 6 assume that the Biot number is not a function of position within the hot, gradient and cold zones. The temperature dependence of the conductive and radiative heat transfer coefficients, as indicated in Tables C.1 and C.2, affects the use of these models as follows:

(1) The temperature distribution in the system is not known a priori. Since the heat transfer coefficients are temperature dependent, the Biot numbers are also not initially known. An estimate of the temperature levels must be made in order to calculate an initial estimate of the heat transfer coefficients. From the resulting temperature response of the system the accuracy of the initial estimate can be checked. New estimates can be made for the heat transfer coefficients and the precedure is repeated until the desired level of accuracy is obtained.

(2) Since the temperatures are not spatially uniform within the system, the heat transfer coefficients are also not spatially uniform. A reasonable estimate of a single

"average" heat transfer coefficient for each zone must be made.

APPENDIX D

END BOUNDARY CONDITIONS AND INFINITE FURNACE LENGTH

D.1 END BOUNDARY CONDITION

When the length of the charge in the hot and/or cold zone is not infinite (see section 5.5), boundary conditions at the end of the charge must be included in the thermal model of the charge. The hot end of the charge, for example, receives heat from the hot zone furnace by radiation and convection (Fig. D.1). A heat transfer coefficient describing the heat transfer between the hot end of the charge and the hot zone furnace can be approximated in order to calculate a Biot number for use in the hot end boundary condition. If $\lambda_H > \zeta_{\infty,H}$, the magnitude of this Biot number has little effect on conditions near the interface; on the other hand, if $\lambda_H < \zeta_{\infty,H}$, the value of the hot end Biot number is required in order to completely specify the thermal model of the charge at the hot end.

The cold end of the charge is attached to the lowering rod and, hence, the cold end boundary condition is more complicated. A simple thermal model for this case, shown in Fig. D.2, is presently used in order to calculate an approximate Biot number for the cold end boundary condition. A pull rod of thermal conductivity k_p, diameter D_p, cross sectional area A_p and length L_p, is attached to the cold end of the charge; the heat transfer between the furnace and the pull rod is described by a heat transfer coefficient, h_p. The pull rod and charge are assumed to be in perfect thermal contact, the cold zone heat pipe is assumed to be infinitely long, and radial temperature gradients are neglected. Motion of the system is neglected (i.e., Pe is assumed negligible).

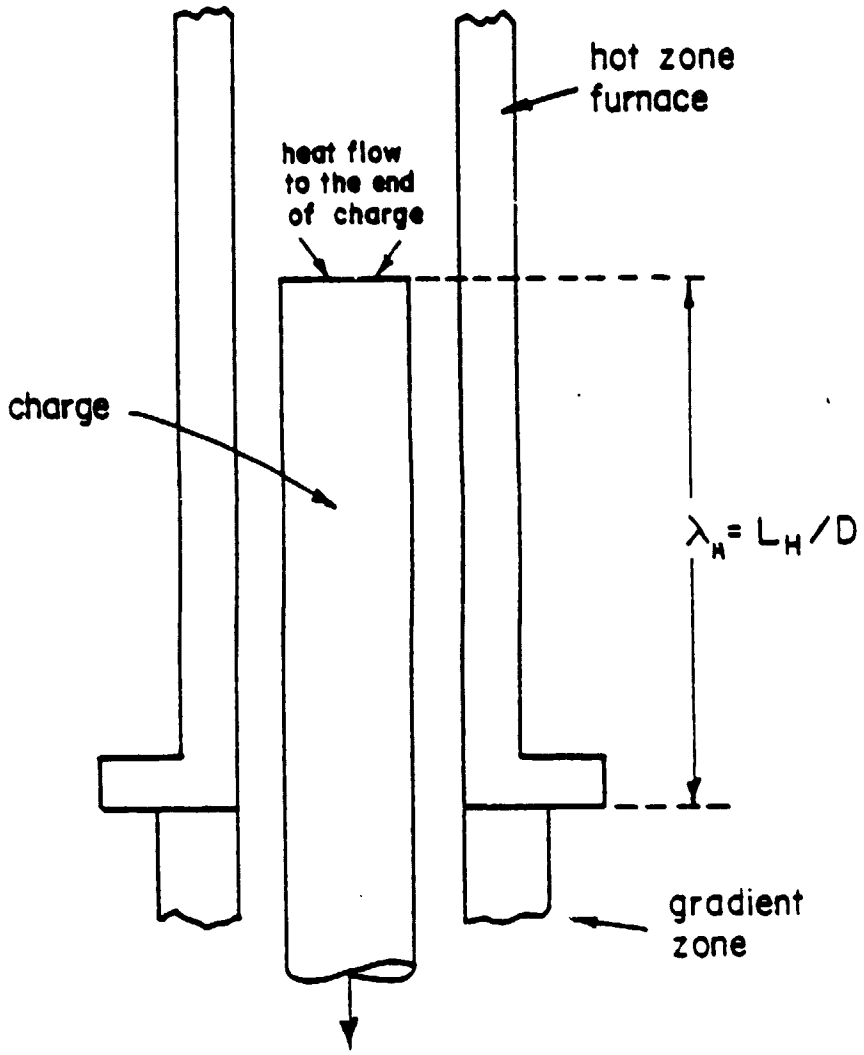

Fig. D.1: Schematic of the heat transfer at the hot end of the charge.

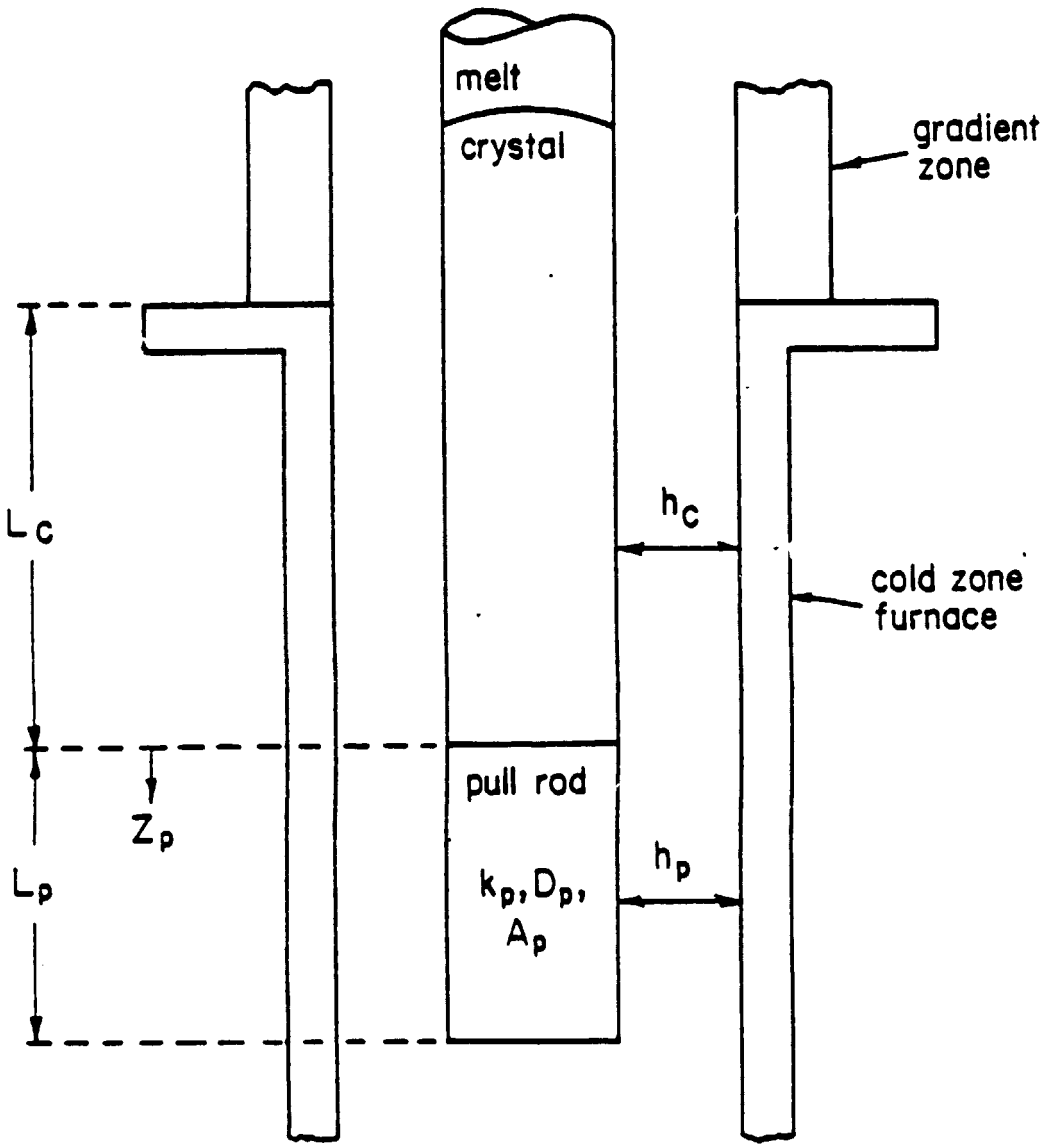

Fig. D.2: Schematic of the cold end of the charge which communicates thermally with the cold zone furnace through the pull rod.

The cold end of the charge experiences a heat loss to the pull rod which may be used in order to define a heat transfer coefficient for the cold end of the charge, h_{cp}:

$$h_{cp} A \left[T_m(z_p=0) - T_{F,c}\right] = -k_{loc} A \frac{dT_m(z_p=0)}{dz} = -k_p A_p \frac{dT_p(z_p=0)}{z_p} \qquad [D.1]$$

where: z_p = axial distance from the charge/pull rod boundary, see Fig. D.2

(The subscript "cp" denotes the charge/pull rod boundary.) Nondimensionalizing eq. [D.1] defines a cold end Biot number for the cold end boundary condition:

$$Bi_{cp} \left[\theta_m(z_p=0) - \theta_{F,c}\right] = -\frac{d\theta_m(z_p=0)}{dz} \qquad [D.2a]$$

$$Bi_{cp} \equiv \frac{h_{cp} D}{k_{loc}} = -\frac{k_p}{k_s} \frac{A_p}{A} \frac{d\theta_p(\zeta_p=0)}{d\zeta_p} \frac{1}{\theta_p(\zeta_p=0)} \qquad [D.2b]$$

The thermal conditions at the ends of the pull rod are described by the "transmission" matrix developed by Kraus [35]. In nondimensional form, the transmission matrix equation for the pull rod is:

$$\begin{bmatrix} \theta_p(\zeta_p=0) \\ \hline \frac{d\theta_p(\zeta_p=0)}{d\zeta_p} \end{bmatrix} = \begin{bmatrix} \cosh(w_p\lambda_p) & -\frac{1}{w_p}\sinh(w_p\lambda_p) \\ \hline -w_p \sinh(w_p\lambda_p) & \cosh(w_p\lambda_p) \end{bmatrix} \begin{bmatrix} \theta_p(\zeta_p=\lambda_p) \\ \hline \frac{d\theta_p(\zeta_p=\lambda_p)}{d\zeta_p} \end{bmatrix} \qquad [D.3]$$

where: ζ_p = nondimensional axial coordinate, based on diameter D_p, z_p/D_p.

$w_p = 2\sqrt{Bi_p^{**}}$

Bi_p^{**} = effective Biot number for the pull rod.

Bi_p = Biot number for the pull rod used to calculate Bi_p^{**}; $Bi_p = h_p D_p / k_p$.

The transmission matrix relates the temperature and the gradient in temperature at one end of the pull rod to these conditions at the other end. Equation [D.3] may be used to develop an expression for the axial gradient of temperature in the pull rod at the charge/pull rod boundary:

$$\frac{d\theta_p(\zeta_p=0)}{d\zeta_p} = w_p\left[-\theta_p(\zeta_p=0)\coth(w_p\lambda_p) + \theta_p(\zeta_p=\lambda_p)\operatorname{csch}(w_p\lambda_p)\right] \quad [D.4]$$

If the pull rod is very long, the second term within the brackets of eq. [D.4] becomes negligible; eq. [D.4] then takes the form:

$$\frac{d\theta_p(\zeta_p=0)}{d\zeta_p} = -w_p\theta_p(\zeta_p=0) \quad [D.5]$$

Substituting eq. [D.5] into eq. [D.2]:

$$Bi_{cp} = 2\,\frac{k_p}{k_{loc}}\,\frac{A_p}{A}\sqrt{Bi_p^{**}} \quad [D.6]$$

Bi_{cp} given by eq. [D.6] can be used as an approximation for the cold end boundary condition of the charge, i.e., eq. [D.2b].

Equation [D.6] gives the Biot number for the cold end boundary condition for an infinite length pull rod of uniform properties and cross section. The transmission matrix concept [35] can also be conveniently

employed to approximate the end Biot number for pull rods of varying composition and cross section. Equation [D.6] also applies for extensions at the hot end of the charge.

The charge would appear infinitely long at on of its ends if it was attached to an extension at that end which has the same thermal properties, cross sectional area and heat transfer coefficient as the charge itself. In this case, eq. [D.6] indicates that the end Biot number is twice the square root of the local charge Biot number: $2\sqrt{Bi^{**}_{loc}}$. This leads to the conclusion, reported by Chang and Wilcox [17], that the charge appears infinitely long if the end Biot number is $2\sqrt{Bi^{**}_{loc}}$. Hence, eq. [D.6] indicates the manner in which the end Biot number may be adjusted, by the proper choice of k_p, A_p and/or Bi_p^{**}, in order to approximate infinite length conditions with an extenstion attached to the end of the charge:

$$h_{loc} A \sqrt{Bi^{**}_{loc}} = k_p A_p \sqrt{Bi^{**}_p} \qquad [D.7]$$

D.2 INFINITE FURNACE LENGTH

An assumption in the thermal model of the Bridgman system is that the furnace temperature boundary condition is of infinite extent in both the hot and cold ends (section 2.2.2). The actual case of finite furnace length is illustrated in Fig. D.3 for the cold zone furnace. The part of the charge not within the furnace experiences different boundary conditions than that part of the charge within the furnace. The following brief analysis explains under what conditions the furnace boundary conditions may be considered infinite in extent, thereby making unnecessary the inclusion of the thermal conditions outside of the furnace in the thermal models.

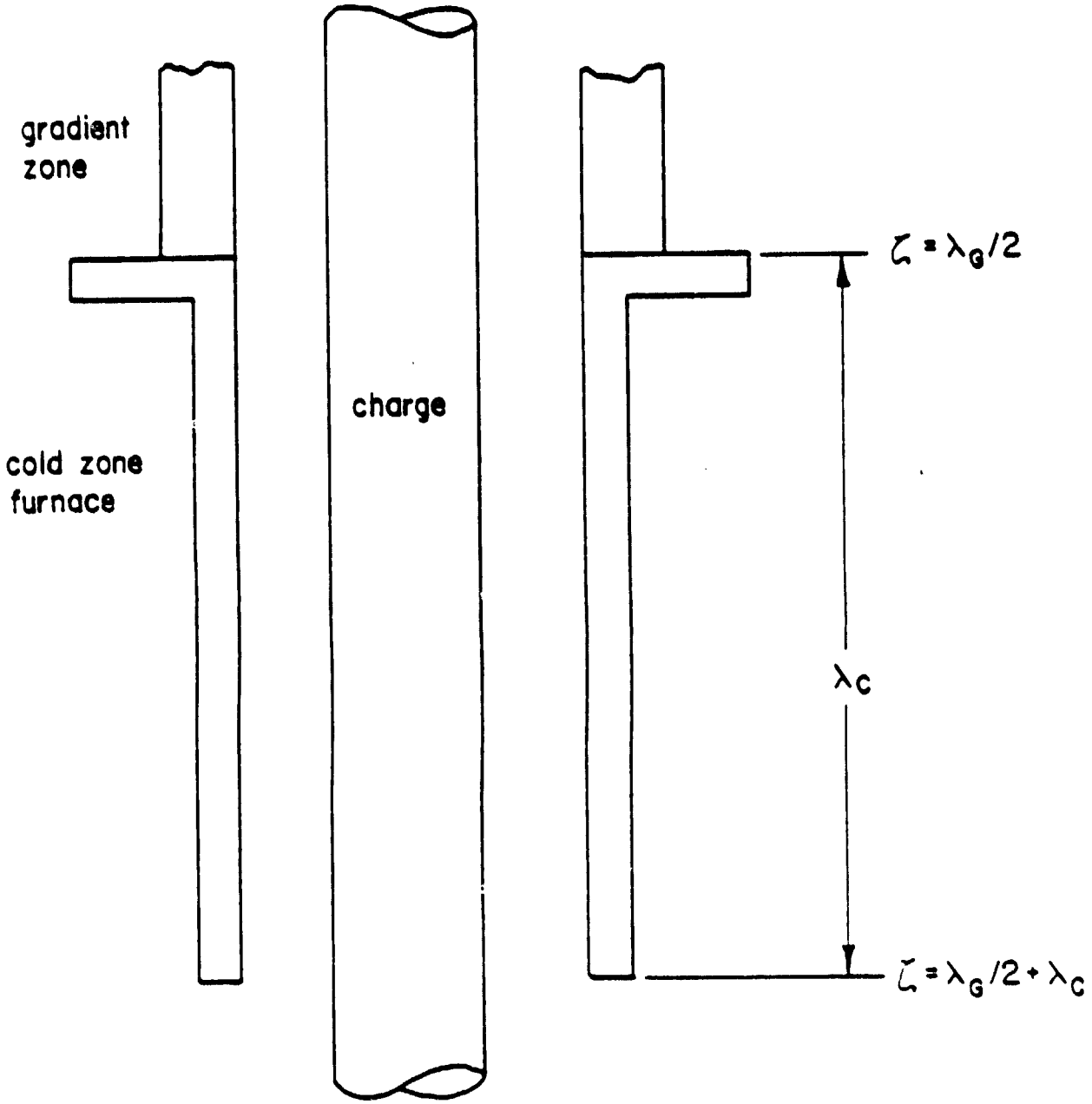

Fig. D.3: Schematic of a finite length furnace in the cold zone.

The analogous expression to eq. [D.4] for the charge within the cold zone of Fig. [D.3] is:

$$\frac{d\theta_m(\lambda_c/2)}{d\zeta} = w_{m,c}\left[-\theta_m(\zeta=\tfrac{\lambda_c}{2})\coth(w_{m,c}\lambda_c) + \theta_m(\zeta=\tfrac{\lambda_c}{2}+\lambda_c)\operatorname{csch}(w_{m,c}\lambda_c)\right] \qquad [D.8]$$

where: $w_{m,c} = 2\sqrt{Bi_c^{**}}$

Equation [D.8] indicates that the thermal conditions at the hot end of the cold zone (i.e., at $\zeta = \lambda_c/2$) are little affected by the conditions at the end of the cold zone furnace if:

$$\operatorname{csch}(w_{m,c}\lambda_c) \ll 1 \qquad [D.9]$$

Equation [D.9] is analogous to the infinite charge length criteria developed in section 5.5. Therefore, if the length of the furnace satisfies eq. [5.14], the furnace length can be considered infinite. This conclusion is valid for either the hot or cold zone furnace.

APPENDIX E

TRANSIENT THERMAL BEHAVIOR

The dimensionless form of eq. [4.1] for the one-dimensional thermal model of the charge is:

$$\frac{\partial^2\theta_m}{\partial\zeta^2} - Pe\frac{\partial\theta_m}{\partial\zeta} + 4Bi(\theta_f - \theta_m) - Pe\frac{\partial\theta}{\partial\tau} = 0 \qquad [E.1]$$

where: $\tau = t/(D/V)$

The nondimensional time, τ, in eq. [E.1] is measured with reference to the time required for the charge to be lowered a distance equal to one charge diameter.

The axial coordinate in the present work, ζ, is measured with respect to a stationary reference frame (i.e., the center of the gradient zone); the transient term of eq. [E.1] therefore accounts for changes in the charge temperature with time at a given location within the furnace (i.e., not the changes in temperature of a material portion of the charge). The quasi-steady assumption in the thermal model of section 2.2.2 implies that the transient term of eq. [E.1] is negligible.

E.1 THERMAL TRANSIENTS CAUSED BY NON-INFINITE CHARGE LENGTH

Temperature transients do not occur when the charge length is infinite; therefore, when the length of charge within the hot and cold zones satisfies the infinite length criteria, eq. [5.14], the quasi-steady state assumption is valid.

When the charge length can not be considered infinite, temperature transients in the charge occur. Results obtained from a quasi-steady model

may still, however, provide information which is useful in a qualitative sense. For example, the curves of Fig. 5.8 indicate that the axial position of the interface moves from the cold to the hot furnace as the charge is lowered. Riquet and Durand [9] and Sukanek [22,23] also neglect transient heat transfer in their studies of the dependence of the growth rate on the axial position of the charge.

Large Biot numbers decrease the infinite charge length criteria, eq. [5.14]; a larger portion of the charge is solidified under quasi-steady conditions as the Biot number increases. An alternative to larger Biot numbers for making the charge appear infinitely long is to increase the apparent length of the charge at both the hot and cold ends by the addition of extensions to the crucible. (See Appendix D.) This is normally accomplished at the cold end of the charge through its thermal communication with the pull rod.

E.2 TEMPERATURE TRANSIENTS CAUSED BY CHANGES IN OPERATIONAL PARAMETERS

Section E.1 discusses temperature transients caused by the steady motion of a finite length charge through the furnace. When a sudden change in one of the furnace operational parameters (e.g., lowering rate, hot and cold zone temperatures) occurs, the coefficients of eq. [E.1] (i.e., Pe and θ_f) likewise change and temperature transients occur. The neglect of the transient term under these circumstances would indicate a sudden shift from the quasi-steady temperature field in the charge before the change to the new quasi-steady state after the change.

Fu and Wilcox [21] have studied the transient interface position after a sudden change in the lowering rate for a charge of infinite length. Their results indicate that the interface changes with time from its

initial to final quasi-steady position in an exponential fashion:

$$\frac{\zeta_{i,2} - \zeta_i(t)}{\zeta_{i,2} - \zeta_{i,1}} = \exp\left(-\frac{t}{\beta}\right) \qquad [E.2]$$

where: $\zeta_{i,1}$ = quasi-steady interface position after change in lowering rate

$\zeta_{i,2}$ = quasi-steady interface position before change in lowering rate

The time constant of the exponential function in eq. [E.2], β, is shown to decrease for larger Biot numbers, smaller gradient zone length, L_G, and smaller latent heat factor, R_H. They suggest that the time constant is similar for transients caused by a sudden change in furnace temperature.

APPENDIX E

DEVELOPMENT OF THE FIN EQUATIONS FOR THE TWO-DIMENSIONAL THERMAL MODEL

With the assumptions of Sections 2.2 and 6.2, each of the concentrically located fins (i.e., inner charge, outer charge, crucible, gradient zone annulus) can be considered as a moving thin fin. According to Carslaw and Jaegar [29], the axial temperature distribution for the fins in the hot and cold zones is given by the following equations:

$$k_{loc} A_{in} \frac{d^2 T_{in}}{dz^2} - A_{in} V \rho c_p \frac{dT_{in}}{dz} + \frac{T_{out} - T_{in}}{R_{in,out}} = 0 \qquad [F.1a]$$

$$k_{loc} A_{out} \frac{d^2 T_{out}}{dz^2} - A_{out} V \rho c_p \frac{dT_{out}}{dz} + \frac{T_{in} - T_{out}}{R_{in,out}} + \frac{T_{cr} - T_{out}}{R_{out,cr}} = 0 \qquad [F.1b]$$

$$k_{cr} A_{cr} \frac{d^2 T_{cr}}{dz^2} - A_{cr} V \rho_{cr} c_{p,cr} \frac{dT_{cr}}{dz} + \frac{T_{out} - T_{cr}}{R_{out,cr}} + \frac{T_f - T_{cr}}{R_{cr,f}} = 0 \qquad [F.1c]$$

where: A = cross sectional area of a fin

R = thermal resistance per unit length between fins

subscripts:

loc = local charge phase, liquid or solid

in = inner charge fin

out = outer charge fin

cr = crucible

f = hot or cold zone furnace

When considering the fins within the gradient zone, T_f and $R_{cr,f}$ in eq. [F.1c] change to T_G and $R_{cr,G}$, where the subscript "G" denotes the

gradient zone annulus. Further, there is an additional equation representing the gradient zone annulus:

$$k_G A_G \frac{d^2T_G}{dz^2} + \frac{T_{cr} - T_G}{R_{cr,G}} = 0 \qquad [F.1d]$$

The radial geometry of the concentric fins shown in Fig. 6.2 specifies the cross section areas and thermal resistances in eqs. [F.1]. The cross section areas A_{in} and A_{out} are chosen equal; therefore, $D_{in} = D/\sqrt{2}$. The radial locations for the representative temperatures of the fins are $D_1/2$, $D_2/2$ and $D_3/2$ for the inner and outer charge fins and crucible fin respectively; they are chosen so that there is an equal area within the fin to either side:

$$D_1 = D/2 \qquad [F.2a]$$

$$D_2 = \sqrt{3/4}\, D \qquad [F.2b]$$

$$D_3 = \sqrt{(\delta^2+1)/2}\, D \qquad [F.2c]$$

The thermal resistances can then be expressed as (Rohsenow and Choi [26]):

$$R_{in,out} = \frac{\ln\sqrt{3}}{2\pi k_{loc}} \qquad [F.3a]$$

$$R_{out,cr} = \frac{\ln\sqrt{\frac{4}{3}}}{2\pi k_{loc}} + \frac{\ln\left(\frac{\delta^2+1}{2}\right)^{1/2}}{2\pi k_{cr}} \qquad [F.3b]$$

$$R_{cr,f} = R_{cr,G} = \frac{\ln\left(\frac{2}{1+\delta^{-2}}\right)^{1/2}}{2\pi k_{cr}} + \frac{1}{h_{loc}\pi D_{cr}} \qquad [F.3c]$$

where: $\delta = D_{cr}/D$

h = heat transfer coefficient from furnace or gradient zone annulus to the surface of the crucible based on the crucible outer surface area

Substituting eqs. [F.2] into eqs. into eqs. [F.1] and non-dimensionalizing results in eqs. [6.1] and [6.2].

APPENDIX G

EXPRESSION FOR APPROXIMATE INTERFACE CURVATURE

This appendix employs simple approximations in order to develop a useful relation between isotherm curvature and the axial and radial temperature gradients obtained from the one- and two-dimensional thermal models.

An isotherm within the charge is assumed to be spherical; its curvature can then be represented by a single number -- its radius. The axial distance between the locations of an isotherm at the center and the surface of the charge is denoted by Z_ϕ. The assumed isotherm geometry, shown in Fig. G.1, yields the following relation between Z_ϕ and the isotherm curvature:

$$\frac{Z_\phi}{D} \equiv \zeta_\phi = -\frac{N-(N^2-1)^{1/2}}{2} \simeq -\frac{1}{4N} \quad (\text{for } |N| \geq 3) \qquad [G.1]$$

where N is the radius of curvature of the isotherm in number of charge radii. (The reciprocal of N is the curvature.) Eq. [G.1] gives a positive value of N when the isotherm is curved as shown in Fig. G.1. If the axial gradient does not vary greatly over the cross section:

$$\zeta_\phi \simeq \frac{\phi_{sc}}{d\phi_m/d\zeta} \qquad [G.2]$$

where: $\phi_{sc} \equiv \phi(\varphi = 1/2) - \phi(\varphi = 0)$

Substituting eq. [G.2] into [G.1]:

$$N \simeq -\frac{1}{4}\frac{d\phi_m/d\zeta}{\phi_{sc}} \qquad [G.3]$$

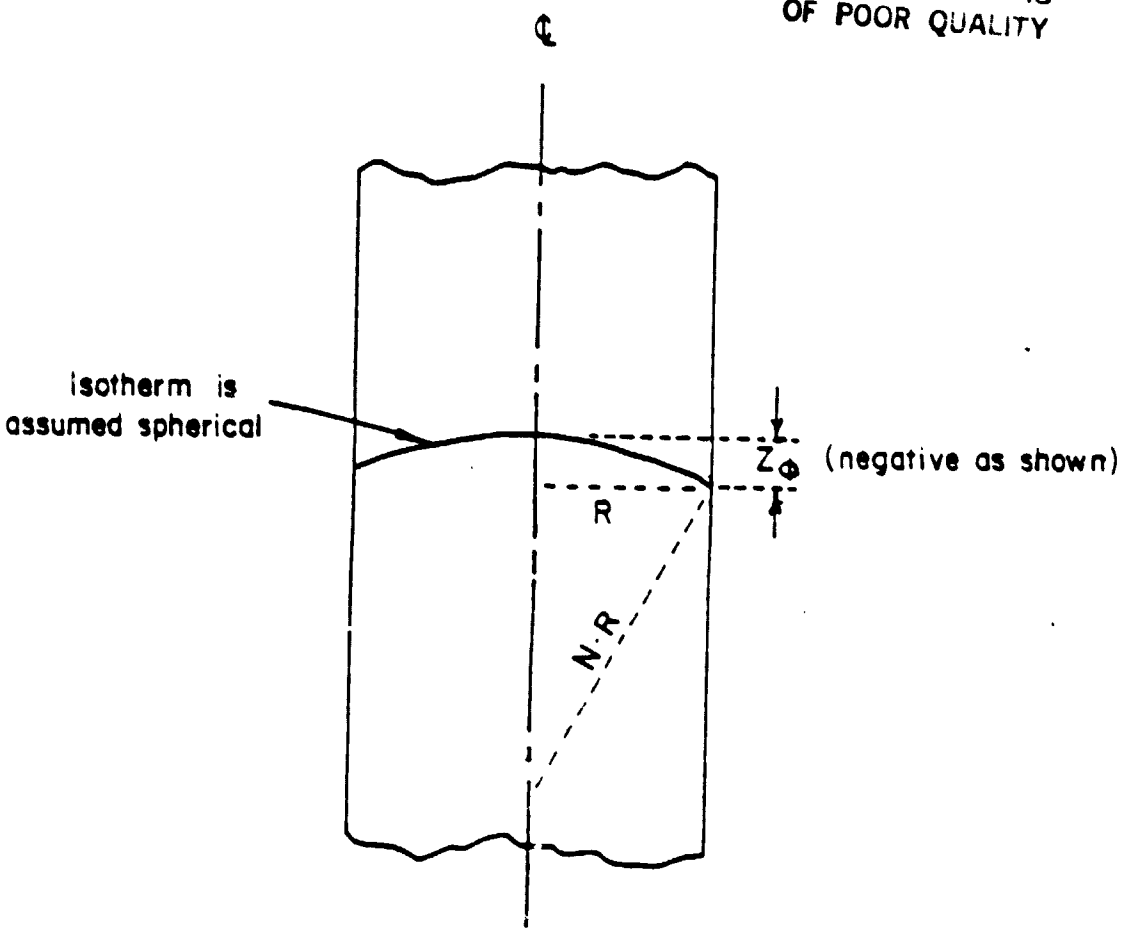

Fig. G.1: Assumed geometry used to calculate an approximate isotherm curvature. N is positive for the isotherm curvature shown above.

For the purpose of relating ϕ_{sc} to ϕ_{Δ}, the heat conduction equation within the charge is used:

$$\frac{1}{\rho}\frac{\partial}{\partial \rho}\left(\rho \frac{\partial \phi}{\partial \rho}\right) + \frac{\partial^2 \phi}{\partial \zeta^2} - Pe \frac{\partial \phi}{\partial \zeta} = 0 \qquad [G.4]$$

If the Pe term is neglected and if it is assumed that $\partial^2\phi/\partial\zeta^2$ is not a function of ρ, the resulting temperature distribution in the radial direction is parabolic. In this case, it is easily shown that:

$$\phi_{\Delta} = \frac{1}{4}\phi_{sc} \qquad [G.5]$$

Using eq. [G.5] in eq. [G.3]:

$$N \simeq -\frac{1}{16}\frac{d\phi_m/d\zeta}{\phi_{\Delta}} \qquad [G.6]$$

Equation [G.6] indicates that isotherm curvature is small (i.e., large N) when the axial temperature gradient is large as well as when the radial temperature gradients are small.